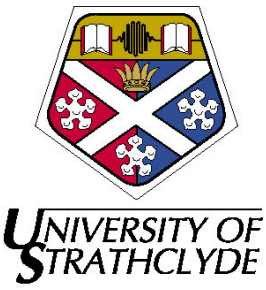

University of Strathclyde

Department of Electronic and Electrical Engineering

Cellular MIMO Networks (CeMNets)

The Channel Modelling, Decomposition and Information Theoretic Perspectives

by

Muhammad Zeeshan Shakir

A thesis presented in fulfilment of the requirements for the degree of Doctor of Philosophy

2010

(This page intentionally left blank)

CONTENTS

List of Figures

List of Tables

List of Symbols

ν ..... Number of clusters, 180
κ ..... Number of scatterers, 180
Γ_i^p ..... p^{th} Permutation distance of i^{th} row, 189
$\boldsymbol{\mathcal{Q}}_N$ ..... $n^2 \times \left(n^2 - n\right)$ Partial permutation matrix, 160
$\boldsymbol{\mathcal{P}}_M$ ..... $m^2 \times m$ Permutation matrix with 1 at $\left((i-1)m+i\right)^{\text{th}}$ position, 159
$\boldsymbol{\mathcal{P}}_N$ ..... $n^2 \times n$ Permutation matrix with 1 at $\left((i-1)n+i\right)^{\text{th}}$ position, 159
1_K ..... $1 \times K$ vector, $1_K \triangleq \left(1, \cdots, 1\right)$, 72
$\boldsymbol{\Omega}_{N,1}$ ..... $N \times N$ circulant channel slow gain matrix $\boldsymbol{\Omega}_{N,1} \triangleq \boldsymbol{\Omega}$, 72
$\mathbf{G}^c$ ..... $N \times M$ Circulant systematic matrix, 188
$\widetilde{\boldsymbol{\mathcal{P}}}_{N,K}$ ..... $NK \times NK$ Permutation Matrix, 89
Δ ..... Absolute gain, $\Delta \triangleq \overline{\mathrm{C}}_{\mathrm{opt}} - \mathrm{C}_{\mathrm{opt}}$, 163
$\approx$ ..... Almost equal to, 130
$a.s.$ ..... Almost surely, 112
$\mathsf{mmse}_{\mathrm{avg}}$ ..... Arithmetic mean MMSE, 96
$\simeq$ ..... Asymptotically equivalent, 116
B_j ..... Basestations located in N^{th} cell for $j = 1,2,\cdots,N$, 67
ζ ..... BER Relative Reduction Ratio, 214
p_e ..... Bit Error Rate, 214
$\mathrm{C}_{\mathrm{cell}}$ ..... Cell optimum joint decoding capacity, 103
$\widehat{\gamma}$ ..... Cell SNR, $\widehat{\gamma} = K\gamma$ where K is the number of users per cell, 105
$\boldsymbol{\Omega}_{N,K}$ ..... C-GCMAC channel slow gain matrix with N cells and K users per cell, 71
$\mathbf{G}_{N,K}$ ..... C-GCMAC fading channel matrix with N cells and K users per cell, 71
Ω ..... Channel slow gain, 67, 179
$\boldsymbol{\mathcal{S}}$ ..... circular permutation operator, 86
$\mathrm{cl}\{\cdot\}$ ..... Closure, 99
$\left(\mathrm{c.c.s}\right)$ ..... Complex Circularly Symmetric, 18
$\left(\cdot\right)^*$ ..... Complex conjugate, 63
$\mathcal{H}\left(\cdot|\cdot\right)$ ..... Conditional entropy, 39
β ..... Constant $\beta \triangleq M / N$, ratio of transmitting antenna to receiving antenna, 107
e ..... Constant $e \triangleq \exp\left(1\right)$, 39
$\mathrm{co}\{\cdot\}$ ..... Convex hull, 99

$\det(\cdot)$ ..... Determinant, 34

$\mathrm{diag}(\cdot)$ ..... Diagonal matirx, 97

$\mathbf{\Sigma}$ .....Diagonal matrix obtained via SVD, 21

$\mathcal{G}$ .....Diversity Gain, 13

$\in$ .....Element of, 24

$F_{\boldsymbol{A}}^{N}$ .....Empirical eigenvalue distribution, 111

$\mathcal{H}(\cdot)$ ..... Entropy, 39

$\mathbb{E}[\cdot]$ ..... Expectation, 17

f_c ..... frequency, 76

$\|\cdot\|$ .....Frobenius norm, 95

$\Gamma_{(\mathcal{P},\mathcal{Q})}$ .....Gamma Capacity, 161

$\mathcal{N}(0,\sigma_z^2)$ .....Gaussian distribution with mean μ and variance σ_z^2, 24

$\bar{\lambda}$ ..... Geometric mean of non-zero singular values of $\mathbf{H}$, 23

$(\circ)$ .....Hadamard Operator, 69

$(\cdot)^H$ ..... Hermitian transpose, 17

Υ_h .....Horizontal Flip Operator, 278

$\mathbf{\Phi}$ ..... Input covariance matrix, 39

$\otimes$ ..... Kronecker product, 72

$p_{\boldsymbol{A}}$ .....Limiting eigenvalue density, 112

$F_{\boldsymbol{A}}$ .....Limiting eigenvalue distribution, 112

$\langle \lambda_M \rangle$ .....Mean power distribution of M^{th} eigenvalue, 152

mmse_k ..... MMSE of the filtered symbol, 96

T_j ..... Mobile terminals located in N^{th} cell for $j = 1,2,\cdots,N$, 67

λ_M ..... M^{th} eigenvalue of Wishart matrix, 21

$\mathcal{R}$ ..... Multiplexing Gain, 14

$\mathbb{R}^N$ ..... N Dimensional real vector space, 21

$\exp(\cdot)$ .....Natural exponential, 233

α .....Noise to Signal Ratio, 191

$(\cdot)^T$ .....Non-Hermitian Transpose, 63

L .....Number of Eigenmodes or Rank of channel matrix $\mathbf{H}$, 44

K ..... Number of users per cell, 67

$\mathbf{C}_{\text{opt}}$ ..... Optimum decoding capacity, 107

Glossary

AF ..... Amplify and Forward, 62
APA ..... Adaptive Power Allocation, 42

BC ..... Broadcast Channel, 61
BCCH ..... Broadcast Control Channel, 269
BER ..... Bit Error Rate, 20
BS ..... Base Station, 64

CCCH ..... Command Control Channel, 269
CCDF ..... Complementary Cumulative Distribution Function, 138
CDF ..... Complimentary Distribution Function, 43
CeMNets ..... Cellular MIMO Networks, 58
CF ..... Compression and Forward, 62
C-GCMAC ..... Circular-Gaussian Cellular Multiple Access Channel, 55
CH ..... Channel Number, 74
CID ..... Cell ID, 274
CSI ..... Channel State Information, 16
CSIR ..... Channel State Information Receiver, 20
CSIT ..... Channel State Information Transmitter, 20

DF ..... Decode and Forward, 62
DFE ..... Decision Feedback Equalizer, 207
DFT ..... Discrete Fourier Transform, 115
DPC ..... Dirty Paper Coding, 207

EMTS ..... Eigenmode Transmission System, 11
EPA ..... Equal Power Allocation, 41

FDMA ..... Frequency Division Multiple Access, 105
FTD ..... Field Test Display, 73

GCMAC ..... Gaussian Cellular Multiple Access Channel, 54
GDFE ..... Generalized Decision Feedback Equalizer, 194
GMD ..... Geometric Mean Decomposition, 11
GSM ..... Global System for Mobile Communication, 75

HPC ..... Hadamard Permuted Channel, 187

IE ..... Identical Eigenmode, 42
IETS ..... Identical Eigenmode Transmission System, 11
IMSE ..... Identical Mean Square Error, 205

LAC ..... Local Area Code, 274
LDPC ..... Low Density Parity Check, 43

MAC ..... Multiple Access Channel, 62
MCC ..... Mobile Country Code, 274

MCP .....Multi Cell Processing, 61
MIMO ..... Multiple Input Multiple Output, 11
MMSE .....Minimum Mean Square Error, 95
MNC .....Mobile Network Code, 274
MSE .....Mean Square Error, 192
MSE .....Mean Square Error, 34
MT ..... Mobile Terminal, 67

OSTBC .....Orthogonal Space Time Block Codes, 16

Pdf ..... Probability Density Function, 51

QAM .....Quadrature Amplitude Modulation, 37
QPSK .....Quadrature Phase Shift Keying, 36

RMT .....Random Matrix Theory, 111
RxL ..... Received Signal Strength, 74

SINR ..... Signal to Interference and Noise Ratio, 95
SISO .....Single Input Single Output, 26
SNRs .....Signal to Noise Ratios, 20
SVD ..... Singular Value Decomposition, 20

TDD .....Time Division Duplex, 16
TDMA ..... Time Division Multiple Access, 94
TxPwr .....Transmitted Signal Power, 77

UMTS .....Universal Mobile Telecommunication System, 75

V-BLAST ..... Vertical Bell Labs Layered Space Time, 11

WiMax .....Worldwide Interoperability for Microwave Access, 5
WLANs ..... Wireless Local Area Networks, 16
WMAN ..... Wireless Metropolitan Area Network, 4

ZF ..... Zero Forcing, 35
ZF-DPC ..... Zero Forcing Dirty Paper Coding, 191

Declaration

This thesis is the result of the author's original research. It has been composed by the author and has not been previously submitted for examination which has lead to the award of a degree.

_____

M Zeeshan Shakir

09 April 2010

Acknowledgments

"If I have seen farther than others, it is because I was standing on the shoulders of giants"

Sir Isaac Newton (15 February 1676)

First and foremost, I want to thank my PhD supervisor Professor Tariq S. Durrani at Centre of Excellence for Signal and Image Processing (CeSIP) at the University of Strathclyde, Glasgow. Although I cannot claim a foresight of any magnitude near to the revolutionary soul, but my mentor corroborated to no degree less than the folks who facilitated Sir Newton's enlightening itinerary through the realms of knowledge. Professor Durrani's constant support has been as entertaining and edifying as anyone can ever wish for. He smoothed the processes with deftness and explained my queries with patience in his signatured pedagogical approach.

I thank CeSIP for providing me the scholarship funding and more importantly, a fantastic place to study with friendly, vibrant and highly skilled personals. I thank my colleagues from the Dept of Electronic and Electrical Engineering (EEE) at CeSIP. I thank my industry sponsor Picsel Technologies Ltd. Glasgow, for providing additional financial support. I would like to extend my sincere appreciation and thanks to Dr. Lykourgos Petropoulakis for his immeasurable support during Postgraduate studies at the University of Strathclyde.

I will consider myself futile if I do not thank my parents Ishrat and Shakir. A mere thank to both is acutely short to express my appreciation and gratitude against their unconditional support and love throughout my educational life. My dreams would never have come true without the continuous support of my siblings Salman, Saima, Mansoor and Uzma. I especially thank Khan's family: Mr and Mrs Feroze, Khurrum, Khizer, Amrah, Farrukh and Nazish for keeping me motivated in completing my studies. Special thanks must go to all my helpful friends and relatives for their uninterrupted support through difficult times and challenges of completing this thesis.

Last but by no mean least I thank to my wife Benish for her whole hearted support, endless love and her steady believe in me. I could not have completed my studies without her motivational lifts and sincere prayers. I especially thank my son Rayyan who has been the greatest source of inspiration for me, which made the completion of this study possible and worthwhile.

Above all I thank my creator for the abilities He has ensured me with.

Summary

Considerable attention has been paid in recent years to the design of Multiple-Input Multiple-Output (MIMO) EigenMode Transmission Systems (EMTS). MIMO systems are envisioned to meet the challenges of the future generation of cellular networks. MIMO systems require more than one transmit antenna which is impractical for an ever decreasing size of the mobile devices. However, a virtual MIMO environment can be generated when two or more users intend to transmit information independent of each other, with perfect symbol and frame synchronism across the same channel to the receiver in the presence of AWGN. Towards this end, numerous cellular models have been formulated and analyzed to identify the associated issues. One such model that captures the essence of the uplink of a Cellular MIMO Networks (CeMNets) is a Gaussian Cellular Multiple Access Channel (GCMAC). The classical GCMAC was first formulated by Wyner to model the uplink of a cellular network and provide a meaningful insight to the multiple access channel's behaviour [29]. The Circular version of Wyner GCMAC referred to as Circular-GCMAC (C-GCMAC) is the main focus of this research where Base Stations (BSs) are arranged in circular fashion. The Wyner C-GCMAC comprises of N contiguous cells, each containing a BS and K users each with single transmit antenna. The received signal at the given BS is the sum of the local user's signals plus $\Omega \in (0,1)$ (channel's slow gain) times the sum of the adjacent cell user's signals, plus Gaussian noise. The resultant channel matrix (**H**) is the Hadamard product of the channel fading matrix (**G**) and channel slow gain matrix ($\boldsymbol{\Omega}$).

We proposed an empirical formation of channel slow gain matrix by exploiting the appropriate propagation model to approximate $\boldsymbol{\Omega}$. The empirical approximation is based on the results of the measurements carried out in Glasgow city centre around the BSs, using network monitoring software referred to as Net-Monitor. Experimental trials revealed that the channel slow gain among the Mobile Terminals (MTs) and BS of interest is variable across the cell which is contrary to Wyner's original assumption [27] and [29]. Based on the fact that the channels slow gain offered by MTs in adjacent cells is variable across the cell (depending on the location of MTs), we split each cell into three zones. Namely, zone #1: where the interfering MTs are offering high level of interference; zone #2: where the interfering MTs are offering medium level of interference; and zone #3 where the interfering MTs are offering low level of interference. Therefore, the proposed channel model reflects a closer version of realistic CeMNets model where inter-cell interference levels (channel's slow gain) between the MTs and BS of interest are variable across the cell.

This research presents an in-depth information theoretic analysis for Wyner C-GCMAC incorporating the variable inter-cell interfering levels. The performance analysis

includes analytical presentation of capacity over multi-user and single user decoding strategies with and without intra-cell Time Division Multiple Access (TDMA). The analysis also includes illustrations to demonstrate the reliance of channel capacity on inter-cell interference levels. It has been discussed that the cell optimum decoding strategy is optimal at low levels of inter-cell interferences while at high level of inter-cell interferences it suffers from interference limited behaviour and offers the lowest capacity of multi-user decoding schemes. Multi-user decoding strategy is advantageous over single user decoding at all levels of interferences since the single user decoding is intra-cell interference limited. It has been also shown that optimal performance is attainable using intra-cell TDMA. We derive the capacity when two or more MTs experience fading with different means i.e. they offer variable level of inter-cell interference to the BS of interest. By exploiting the inter-cell interference among the MTs and BS of interest in each of the adjacent cells separately, a significant improvement in cell optimum joint decoding capacity is possible. The performance of proposed version of Wyner cellular model is analyzed and compared when the level of inter-cell interference is equal among the MTs and BS of interest. Later, the information theory perspective of Wyner C-GCMAC is extended to derive a new upper bound referred to as Hadamard upper bound on optimum joint decoding capacity of Wyner C-GCMAC. New results have been shown and compared with the capacity offered using the well known Jensen's inequality. Furthermore, the improvement in optimum joint decoding capacity is the original application of Hadamard inequality over Wyner's Hadamard channel. It is recognized that the significant gain in capacity can be achieved over the capacity obtained with Jensen's inequality.

Another key contribution of this research is the simulation perspectives of transmission schemes over uncorrelated and correlated Wyner circular cellular setup by exploiting the recently introduced, Geometrical Mean Decomposition (GMD). The system based on such decomposition technique is referred to as MIMO Identical Eigenmode Transmission Systems (IETS). The transmission design has two implementation forms. One is the combination of GMD with linear precoder and a Minimum Mean Squared Error Vertical Bell Laboratories Layered Space Time (V-BLAST - MMSE) detector, which is referred to as GMD V-BLAST, and the other comprises of a Dirty Paper Zero Forcing Coder (DP-ZFC) which is referred to as GMD DP-ZFC. Hence, by exploiting either the sequential signal cancellation or the DP-ZFC, we can regard the Wyner C-GCMAC as identical, parallel and independent pipes for data transmission. This non-linear decomposition technique brings about much more convenience in coding/decoding and modulation/demodulation processes. In order to demonstrate the effectiveness of transmission strategy, various simulation scenarios are created in MATLAB®. Comparative performance analysis, discussions and numerical examples are included at various points of this thesis to illustrate the contribution.

Chapter 1

Introduction

1.1 Preface

The main objective of wireless communication networks is to provide the user access to the global network at any time, regardless of the user's location or mobility requirements. To some degree this has been achieved through the development and implementation of terrestrial cellular communication systems. Cellular networks operate by dividing a large service coverage area into a number of smaller zones or cells, each of which has its own set of resource or channels, which can be accessed by users of the networks. Initial cellular concepts were discussed within Bell Laboratories in late 1940's [16]. However, it was not until the 1970's that technology had developed sufficiently to allow the commercial implementation of cellular systems to be investigated. These investigations led to one of the most outstanding technological and commercially successfully inventions of the last two decades – mobile cell phone. Since its introduction in the 1980's, the mobile cell phone has undergone a dramatic reduction in size and a dramatic increase in the variety of the supported services. Nowadays in addition to standard voice calls, mobile cell phones are capable of providing a multitude of services, such as photography, streaming video, music, email, and broadband connectivity. Such developments have enjoyed widespread public approval and popularity, fuelling an ever increasing demand for these services. Like the discovery of the telephone by Alexander Graham Bell in the 1870s, cellular networks have become so deeply ingrained into the fabric of modern society that for many urban dwellers it is difficult to imagine day to day life without the convenience of a mobile cell phone.

The evolution of mobile communications can be categorized into a number of generations of development. First generation systems, introduced in the early 1980s, were based on analogue technology and paved the way for cellular

networks, providing voice communications to the mobile user. Second generation systems were introduced in the late 1980's and employed digital transmission offering higher spectrum efficiency, digital voice telephony; low rate digital services and advanced roaming capabilities. The birth of a new millennium saw the introduction of third generation system, which provides a multitude of high speed multimedia applications such as video telephony and web browsing.

The use of multiple antennas at both the transmitter and the receiver side, to form a Multiple Input Multiple Output (MIMO) communication system, is an emerging technology that makes both reliable and high data rate wireless networks a reality [1] and [8]. Compared with the conventional Single Input Single Output (SISO) system, MIMO system creates multiple spatial dimensions that can be exploited to improve the performance of the wireless communication systems. Moreover, such performance improvement comes from the diversity gain and the multiplexing gain introduced by MIMO systems, which will be illustrated in next Chapter 2. Due to the promising advantages brought by MIMO communication system, MIMO technology is being adopted by international standards organizations, such as high-speed packet data mode of third generation cellular systems, high-speed Wireless Local Area Networks (WLAN, IEEE 802.11n) and high-speed Wireless Metropolitan Area Network (WMAN, IEEE802.16) [13] and [16].

A key technology that that has been identified to potentially overcome the limitations of conventional cellular network in terms of throughput and coverage is cooperation [8] and [127]. The cooperation in cellular network may be deployed at either the base station (BS) or at the mobile terminal (MT). The cooperation at the BS level is referred to as distributed antenna systems, which prescribes joint encoding/decoding of the transmitted/received signals at the BS via high capacity backhaul connecting the BSs (see [97] and [98] for recent survey on BS cooperation). Cooperation at the MT level in the context of cellular network has been studied under different names such as mesh, hybrid, or multi-hop network, and is based on specific forms of relaying by the MTs (see e.g. [99]). By exploiting the cooperation at both sides of the transmission link, the conventional cellular system can be transformed into Cellular MIMO Network (CeMNet).

The development of modern CeMNets would not have been possible without significant advancements made in information theory. Information theory originally conceived in the late 1940's by Claude E. Shannon [16] and [12] provides a fundamental limit on the coded performance of a communication system and succinctly identifies the impact of design parameters and constraints on systems performance. In addition to this, information theory suggests means of achieving these fundamental limits on communication [1]. The ever increasing demand for mobile cellular communication services has lead to intensive effort by researchers to determine the information theoretic limitation of these systems.

In the last few years, the recovery of communication services to regional, rural and remote users on an equitable basis compared with their counterparts in metropolitan and large urban centres has been a controversial topic in the UK. It is recognized that the future of CeMNets is heading toward the seamless integration of realistic cellular channel modelling by using latest channel modelling and transmission design techniques [141], [142] and [144].

1.2 Thesis Motivation

Wireless communication has been playing a critical and important role in the Information Age. From mobile phone to cordless home apparatus, from WLAN to WiMax, wireless communications has been experiencing explosive growth and penetrating into every aspect of human life. To meet these objectives, fundamental changes in system configuration and signal processing techniques are required to enable new and effective ways of signal transmission, reception and modelling. The MIMO architecture satisfies many of these demands [1], [8], [13] and [16].

Performance of SVD based MIMO transceiver is limited by the weakest singular value of the channel matrix [17] and [18]. Intelligent bit allocation mechanism is required in order to match the capacity of the sub-channels. Therefore, the complexity in transceiver design due to high condition number cannot be ignored [1]. On the contrary, allocating the equal power across the sub-channels would degrades the over all system performance. A fundamental trade off is always required to be made between the capacity and the BER performance when dealing

with such linear decomposition technique. We analyzed MIMO transceiver design by exploiting recently introduced decomposition technique which is referred to as Geometric Mean Decomposition (GMD) [3]. This motivates research on improving the performance of the multi antenna communication system by the formation of Identical Eigenmodes over the wireless communication channel.

To exploit the factual benefits of the multiple antennas in CeMNets, it is necessary to propose models which are much closer to the realistic cellular scenario. The focus of this thesis is to evaluate the performance of cellular networks when every mobile user in the adjacent cells are offering variable level of channel slow gain to the base station of interest which is contrary to the Wyner's original assumption [29] (equal channel slow gain among the mobile terminals and the base stations). We proposed the empirical models based on the results of experimental trials carried out in Glasgow city center. This incorporates the strategies and scenarios to evaluate the system performance which are closer to the realistic cellular network.

Information theoretic analysis based on the realistic scenario for CeMNets is extremely important to meet the data rate requirements of the future generation of cellular communications [18]. Another direction of this research is the information theory analysis of the multi antenna/multi-user cellular communication systems based on realistic channel modelling. A part of this thesis is devoted to perform the Information theoretic analysis of such systems by employing various decoding strategies under realistic scenarios. This involves the derivation of capacity expressions which are not constrained by the Wyner's original assumption [29]. Moreover, it is extremely important to establish the impact of variable channel slow gain among the mobile terminals and the base stations on the practical decoding schemes, spectral efficiency and the diversity of the CeMNets.

1.3 Original Contributions

1. An Empirical channel model for cellular Multiple Access Channels (MACs) has been proposed for single user and the multi-user setups. The proposed model is close to the realistic cellular setup as it assumed every user is offering variable levels of channel slow gain to the base station of interest which is contrary to the Wyner's original assumption. The proposed modeling is based on the results of the experimental trials carried out in Glasgow city center.

2. Based on the results of the experimental trials the adjacent cells in Wyner like cellular models are split into three zones depending on the distance between the mobile terminals and the base station of interest. The proposed single user and the multi-user channel model incorporate the fact that each user is offering slow gains by different means.

3. Information theoretic analysis over the proposed empirical channel model has been performed by deriving the capacity expressions which incorporate the variable channel slow gain offering by the mobile users in each of the adjacent cells across the three zones.

4. A novel upper bound on the joint optimum decoding capacity has been proposed by exploiting the Hadamard inequality. It is recognized that the use of the Hadamard inequality to find the deterministic gain in optimum capacity is the unique application in wireless communications. The new upper bound will be useful to derive the closed form analytical expression for the joint optimum decoding capacity.

5. A new correlated structure for the typical cellular correlated Wyner like channels has been introduced by exploiting the circular arrangement of the base stations. The new channel model is referred to as Hadamard Permuted Channel (HPC).

6. The transmission designs have been presented to show the impact of variable channel slow gain on the diversity of the CeMNets. Moreover, an unusual behaviour of the Bit Error Rate (BER) over the correlated channels has been reported for the first time for Wyner like channel models. It is recognized that the degradation in BER performance is due to the ill-conditioned channel matrix (low rank problem). A simple channel regularization technique has also been introduced to avoid such abrupt change in the BER performance of cellular networks.

1.4 List of Publications

Conference Papers

1. M. Z. Shakir, T. S. Durrani, and M-Slim Alouini, "New upper bound on the optimum joint decoding capacity of Wyner Circular-GCMAC by exploiting Hadamard inequality," ITW'10*, Dublin, Sep.* 2010, *[to be submitted]*.

2. M. Z. Shakir, and T. S. Durrani, "Information theoretic analysis of Wyner Circular-GCMAC (C-GCMAC) with variable inter-cell interfering gain," *ISWCS'10, York*, Sep. 2010 *[to be submitted]*.

3. M. Z. Shakir, and T. S. Durrani, "Identical eigenmode transmission systems (IETS) – A channel decomposition perspective," *in Proc. 15th EUSIPCO'07*, Poznan, pp. 916-920, Sep. 2007.

Journal Paper

1. M. Z. Shakir, and T. S. Durrani, "On the upper bound of optimum joint decoding capacity of Wyner GCMAC by exploiting Hadamard inequality," *in IEEE Trans. on Info. Theory*, *[to be submitted]*.

1.5 Thesis Organization

The research presented in this thesis is organized into six chapters. The following is a brief description of each of the chapter.

Chapter 2: MIMO Identical Eigenmode Transmission Systems (IETS)

This Chapter first presents a review on the MIMO communication systems and its associated advantages in Section 2.2. Later, this Chapter deals with MIMO channel decomposition perspectives. The Chapter contains a detailed comparative study based on MIMO transmission design (see Section 2.4). The comparison is based on MIMO transceiver design by exploiting recently introduced decomposition technique referred to as Geometric Mean Decomposition (GMD) with Singular Value Decomposition (SVD) based transceiver design (see Section 2.8.2). The GMD is also employed over Wyner cellular multi-antenna/multi-user scenarios later, in Chapter 5. Later, the Chapter also includes a detailed comparison of capacities offered by the MIMO systems with bit loading or without bit loading mechanisms, and compares these with the capacities offered when GMD is employed (see Section 2.10).

Chapter 3: The Circular Gaussian Cellular MAC (C-GCMAC)

This Chapter begins with an introduction on the cellular MIMO Networks (CeMNets) and then presents a comprehensive review on latest trends and technologies employed in current infrastructure to achieve the benefits of the multiple antenna communication systems (see Section 3.2 – 3.4). In one of the first papers to analyze cellular systems using information theoretic approach Wyner [29] introduced a simple, yet tractable model, known as Gaussian Cellular Multiple Access Channel (GCMAC). As the name suggests, the GCMAC falls under the framework of the classical Gaussian MAC. We introduced Wyner GCMAC model in Section 3.5. Later in this Section, we introduced circular version of GCMAC known as C-GCMAC. This Chapter presents the trials methodology and experimental setup to derive the mathematical model for a single user and the multi-user scenarios.

Chapter 4: Information Theoretic Analysis

This chapter begins with the fundamental information theoretic principles of the multi-user/multi-antenna communication systems. In particular, two figures of merit, capacity and Minimum Mean Square Error (MMSE) commonly employed in the analysis of such systems are introduced. This Chapter established an in-depth information theoretical analysis for the Wyner C-GCMAC incorporating variable intra-cell interference gain. The information theory analysis in this Chapter is based on the empirical model we proposed in Chapter 3. A novel upper bound on optimum joint decoding capacity for Wyner C-GCMAC is derived by exploiting the Hadamard inequality (see Section 4.8). The new upper bound is the original application of the Hadamard inequality in wireless communications. Several simulation scenarios are included in this Chapter to determine the information theory limitations of the Wyner C-GCMAC.

Chapter 5: Transmission Design of Wyner C-GCMAC

This chapter begins with introducing the correlated structure for the Wyner circular cellular setup (see Section 5.2). The correlated and uncorrelated structures are studied with the eigenvalue distribution perspectives (see Section 5.3). At several point in the Chapter, we developed the important properties of the Hadamard product which has an unidentified importance in the multi-user/multi-antenna cellular communication. In this Chapter, we present the transmission schemes by employing V-BLAST decoder and ZF-DPC over the Wyner cellular setups (see Section 5.5). Moreover, an abrupt change in the BER performance of V-BLAST and ZF-DPC transmission schemes over the correlated scenarios is reported in this Chapter (see Section 5.6.4).

Chapter 6: Conclusion and Future Work

The conclusions and recommendations for the future work are included in this Chapter.

Chapter 2

MIMO Identical Eigenmode Transmission Systems (IETS)

2.1 Introduction

In the past few years considerable attention has been given to the design of Multiple-Input Multiple-Output (MIMO) EigenMode Transmission Systems (EMTS). This Chapter presents an in-depth analysis of a MIMO eigenmode transmission strategy. The decomposition technique referred to as Geometric Mean Decomposition (GMD) is employed for the formation of eigenmodes over MIMO flat-fading channels [72]. Exploiting the GMD technique, identical, parallel and independent transmission pipes are created for data transmission at higher rate. The system based on such decomposition techniques are referred to as MIMO Identical Eigenmode Transmission system (IETS). The comparative analysis of the MIMO non-linear and linear transceiver design exploiting the GMD and the Singular Value Decomposition (SVD) respectively for variable constellation is investigated in detail in this Chapter. The transmission strategy is tested in combination with the Vertical Bell Labs Layered Space Time (V-BLAST) decoding scheme using different number of antennas on both sides of the communication link. The investigation study is based on the Bit Error Rate (BER) and sum-rate analysis employing the equal power allocation and adaptive power allocation transmission strategies. The Chapter is organized as follows; § 2.2, presents a review on emergence of MIMO systems and its associated benefits. Later, a sub Section 2.2.2 review the two implementation approaches-V-BLAST and Space Time Block Coding (STBC), § 2.3 presents the linear MIMO channel model; § 2.4 presents a review on MIMO channel decomposition perspectives; § 2.5 presents a review on the SVD and § 2.6, presents the GMD; this Section reviews the optimization problem of GMD as well, § 2.7

presents the transmission design over the MIMO channel by exploiting GMD and SVD, this Section introduces the concept of formation of identical, parallel and independent pipes (identical scalar sub-channels) for data transmission over the MIMO channel; § 2.8 presents BER simulations results with comparative investigations; § 2.9 reviews the mutual information of the MIMO channel and § 2.10 presents the capacity advantages of employing GMD over the MIMO channel; The capacity analysis has been performed and compared with Equal Power Allocation (EPA) and Adaptive Power Allocation (APA) schemes, simulations analysis is included in this Section to support the investigations, conclusions to the Chapter are given in § 2.11.

2.2 Literature Review

2.2.1 Multiple Antenna Wireless Communication Systems

The expansion in wireless communications in recent years encounters severe technical challenges such as demand of transmitting speech, data and video at high rates in an environment rich of scattering [1] and [8]. MIMO wireless link are an important recent development in wireless communication systems because of their significant potential in meeting these future challenges caused by fading channels together with power and bandwidth limitations [6].

There are great deals of published research work regarding multipath channels but the majority of the work focuses on mitigating or removing the multipath component of the wireless channels [1]. The major aim behind this approach was to reduce the complex multipath channel to a simple single user channel to which well known results for non fading channels may be applied.

Towards the end of 1990's it was recognized that the diversity is inherent in multipath and fading channels that allowed for multiplexing of wireless transmission. This promoted the concept of exploiting the multipath channel rather than attempting to mitigate its effect. Initial results from Teletar [13] showed that it was theoretically possible to exploit the multipath channels and thereby increase the information capacity of the wireless link through receive and transmit diversity using the multiple

receivers and the multiple transmitters [13]. The outcome of the idea first time proposed was that a group of cross correlated channels could be combined and considered as a single channel, with Multiple Input and Multiple Output (MIMO).

Raleigh and Coiffi [9] proposed signal processing techniques based upon the SVD theorem to construct the multiple antenna coding systems that benefit from inherent properties of severe multipath channels. It was shown that with M transmit elements and N receives elements, the wireless channel could be decomposed into L parallel channels where L was the rank of the channel transfer matrix $\mathbf{H}$. By definition, $L \leq \min(N, M)$ and therefore the full rank case may be considered as optimal in terms of channel capacity [1] and [9].

The results of Raleigh and Coiffi were given a formal ground with the work of Foschini and Gans [6]. Foschini and Gans provided an intuitive insight into the MIMO channel, predicting that under rich scattering the MIMO channel would achieve a linear growth in channel capacity, proportional to $L = \min(N, M)$ [6]. Later, it was analytically supported and proved by Telatar for the flat fading environment [13]. The mathematical condition of the rich scattering of Foschini and Gans was that the transfer matrix $\mathbf{H}$ had entries from an i.i.d. Gaussian collection with zero mean independent real and imaginary part each with variance ½ [6] and [7].

In addition to the capacity advantage, communication over the multi-antenna channels presents two main practical advantages with respect to traditional communication over single antenna channels. These gains are usually referred to as diversity and multiplexing gains. An overview on the potential benefits of MIMO channels can be found in [18].

A MIMO communication system is said to have diversity gain $\mathcal{G}$ if, in the high SNR regime, the average error probability decays as $SNR^{-\mathcal{G}}$. Loosely speaking, the diversity gain can be viewed as an enhancement of reliability due to the reception (or transmission) of replicas of the same information that have experienced different fading paths. The diversity gain is based on the assumption that at least one of these fading paths will not be in a bad fade state. Traditionally, diversity has been

exploited in the time or frequency domains; however, the presence of the additional space dimension (due to the use of multiple antennas) yields another source of diversity. Notice that spatial diversity gain is not exclusive of MIMO systems, as it can also be extracted from Multiple Input Single Output (MISO) or Single Input Multiple Output (SIMO) architectures [6] and [13].

A MIMO system is said to achieve multiplexing gain $\mathcal{R}$ if, in the high SNR regime, its achievable rates scale as $\mathcal{R}\log\left(SNR\right)$ [1]. In other words, multiplexing gain is the increase of rate that can be attained through the use of multiple antennas at both sides of the communication link, with respect to the rate achievable with a single antenna system, without utilizing additional power. Notice that, as opposed to the diversity gain, the multiplexing gain can only be obtained with the simultaneous presence of multiple antennas at the transmitter and the receiver ends. The designers of MIMO communication systems have focused their efforts in trying to obtain transceivers architectures which achieve either the maximum multiplexing gain [7], or the maximum diversity gain [19]. In [20], Zheng and Tse proved that both gains can be achieved but that; actually, there is a fundamental trade-off between how much of each gain can be extracted. Precisely, for i.i.d. Rayleigh flat-fading MIMO channels with coherence time τ, they proved that the optimal diversity gain achievable by any coding scheme of block length τ and multiplexing gain $\mathcal{R}$ is $\left(M-\mathcal{R}\right)\left(N-\mathcal{R}\right)$ as long as $\tau \geq M+N-1$. Their appealing interpretation for this result was that out of the total resource of M transmit and N receive antennas, it is as though $\mathcal{R}$ transmit and $\mathcal{R}$ receive antennas were used for multiplexing and the remaining $\left(M-\mathcal{R}\right)$ transmit and $\left(N-\mathcal{R}\right)$ receive antennas provided the diversity [8] and [127].

2.2.2 Two Implementation Approaches for MIMO

The MIMO EigenMode Transmission System (EMTS) has a significant potential to increase the capacity linearly with the number of spatial channels [1], [8]. The same has been illustrated in [7] for the Bell Labs Layered Space Time (BLAST)

architecture. Since then, many transmission strategies have been proposed [1], [5], [8], [14], [15] and [127]. Among the two most important and well known approaches, one is the space time coding method that attempts to improve the communication reliability by the coding and the diversity gain which is achieved by appropriate coding design [1]. The other is the spatial multiplexing method which transmits data over spatial sub-channels, often in conjunction with an outer channel code, e.g., the BLAST architecture which focuses on maximizing the channel throughput [6] and [8].

Foschini and Gans proposed different variations of such space time architecture have been proposed under the general framework of BLAST architecture [7]. One version of BLAST that attempts to achieve higher data rate is Vertical BLAST (V-BLAST) scheme. This architecture breaks the original data streams in to sub streams to be transmitted on individual antennas [1], [7] and [8]. At the receiver side, the decomposition algorithm can be exploited in combination with the V-BLAST decoding. The decoding algorithm is based on sequential nulling and cancellation in order to decode the transmitted information symbols [1], [7] and [8]. The nulling step can be implemented by either using Zero Forcing (ZF) or Minimum Mean Squared Error (MMSE) criterion [1] and [75]. The main drawback of the V-BLAST detection algorithm lies in the computational complexity, as it requires multiple calculations of the pseudo inverse of the channel matrix $\mathbf{H}$ in ZF case [1] or of the extended channel matrix $\mathbf{H}$ in the MMSE case. Thus, several schemes with reduced complexity have been proposed, for example, [1], [73] and [74].

A pioneering work in the area of space time coding for the MIMO channel has been done by Tarokh [19] in which two code design criteria have been proposed for flat fading channels with coherent receivers, and high performance space time trellis codes have been designed [19]. However, these codes suffer from rather high decoding complexity. In the same year, Alamouti proposed his celebrated space time block coding for two transmit and multiple receive antenna [10]. This contribution is considered as major breakthrough in space time block coding. The maximum likelihood decoder for Alamouti's code had very low complexity. Inspired by this work Tarokh generalized Alamouti's code to the multiple transmits antennas exploiting the theories of orthogonal design. The codes developed by Tarokh [19] are

known as Orthogonal Space Time Block Codes (OSTBC) and are able to provide high performance at very low decoding complexity [19]. Recently some other design of OSTBCs has also been developed [1] and [8]. These codes provide full diversity with linear processing maximum likelihood detector. However, they suffer from having a limited transmission rate and thus do not achieve full capacity in the MIMO channels [19].

Both design schemes assumed that the Channel State Information (CSI) is available only at the receiver. By transmitting through parallel, spatial sub-channels and exploiting the CSI at the receiver, spatial multiplexing systems can provide high data rates [8]. However, if the communication environment is slowly time varying, such as indoor communication via WLANs, the availability of the CSI is also possible at the transmitter, using feedback or the reciprocal technique when Time Division Duplex (TDD) is used [1]. With the CSI available at the transmitter as well, channel capacity can be achieved by exploiting a simple linear transformation at the transmitter. The linear decomposition techniques can be employed at the receiver to convert the MIMO EMTS channel into the set of parallel and independent scalar sub-channels [143].

The importance of MIMO communication channels lies in the fact that they are able to provide a significant increase in capacity over SISO channels [1], [8] and [127]. One simple example of spatial multiplexing is when the input is de-multiplexed in to M separate streams, using a serial to parallel converter, and each stream is transmitted from an independent antenna, the resultant throughput is M symbols per channel use for the MIMO channel with M transmit antennas. This M fold increase in throughput will generally come at the cost of lower diversity gain compared to space time coding [19] and [20]. Therefore, space time multiplexing is better choice for high rate systems operating at relatively high SNRs while space time coding is more appropriate for transmitting at relatively low rates and low SNRs [19] and [20].

2.3 Gaussian Linear Vector MIMO Channel

Although the MIMO channels arise in many different communication scenarios such as wire line systems or frequency selective single antenna systems [127], our work will focus on multi-antenna/multi-user wireless communication networks. As commented above, in its most general form, the MIMO channel is characterized by its transition probability density function, which is given by $p\left(\boldsymbol{y} \mid \boldsymbol{x}\right)$, and which describes the probability of receiving the vector $\boldsymbol{y}$ conditioned on the fact that the transmitting vector $\boldsymbol{x}$ was actually transmitted. However, dealing with such a generic type of channel is usually very difficult, and often even unnecessary.

One of the most important and simplest MIMO channels is the linear MIMO channel (also termed Gaussian linear vector channel). As its name suggests, in this case the output of the channel $\boldsymbol{y}$ is a linear function of the input $\boldsymbol{x}$. In addition, to thermal noise and other undesired effects that are present in the receiving radio-frequency front-ends, a noise term $\boldsymbol{z}$ is also included.

Most of the information theoretic literature that deals with multi-user/multi-antenna communication networks can be described by the following symbol synchronous, discrete time channel model [21], the resulting input output relation is given by

$$\boldsymbol{y}\left[i\right]=\mathbf{H}\left[i\right]\boldsymbol{x}\left[i\right]+\boldsymbol{z}\left[i\right] \tag{2-1}$$

where, at discrete time i $\boldsymbol{x}\left[i\right]=\left(\boldsymbol{x}_1\left[i\right],\boldsymbol{x}_2\left[i\right],\cdots,\boldsymbol{x}_M\left[i\right]\right)^T$ is an $M\times 1$ dimensional vector complex input symbols with zero mean and covariance

$$\boldsymbol{\Phi} \triangleq \mathbb{E}\left[\boldsymbol{x}\left[i\right]\boldsymbol{x}^H\left[i\right]\right] \qquad \forall\ i=1,2,\cdots, \tag{2-2}$$

$\mathbf{H}$ is a $N\times M$ complex channel matrix that represents the linear response of the channel, such that its element $h_{i,j}$ denotes the channel path gain (transfer functions) between i^{th} transmitter and j^{th} receiver. We assumed that the channel is Rayleigh

flat fading, the gains and $h_{i,j}$ are Independent Identically Distributed $\left(\text{i.i.d}\right)$ zero mean Complex Circularly Symmetric $\left(\text{c.c.s}\right)$ random variables with unit variance, i.e., the real and imaginary parts each has ½ variance [1], [6] and [8]. This is the case we will consider henceforth, unless stated otherwise. This is the simplest channel possible model; it assumes heavy multipath. It becomes clear from mathematical formulation that the existence of many multipath components in wireless channel, which is usually considered as a drawback, becomes a major advantage in multiple antenna systems[1]. As in vast majority of cases (and in this dissertation in particular), $\boldsymbol{z}\left[i\right]=\left(\boldsymbol{z}_1\left[i\right],\boldsymbol{z}_2\left[i\right],\cdots,\boldsymbol{z}_N\left[i\right]\right)^T$ is a $N\times 1$ vector of i.i.d zero mean c.c.s Gaussian[2] noise samples with variance σ^2, and $\boldsymbol{y}\left[i\right]=\left(\boldsymbol{y}_1\left[i\right],\boldsymbol{y}_1\left[i\right],\cdots,\boldsymbol{y}_N\left[i\right]\right)^T$ is a $N\times 1$ vector representing the channel output. Assuming the channel is memory-less (and without feedback) the channel output at time i doesn't depend on past output symbols [22], and therefore, for brevity of notation the time index i can be dropped.

[1] Multiple antenna systems are also referred to as Multiple Input Multiple Output (MIMO) system in wireless communication text and are used interchangeably throughout this thesis.

[2] In this thesis complex random variable $Z=X+\text{i}\,Y$ is a c.c.s. Gaussian distributed denoted by $Z\sim\mathcal{CN}\left(\mu,\sigma^2\right)$, if X and Y are real independent Gaussian random variable with same variance i.e. $X\sim\mathcal{N}\left(\mu,\frac{1}{2}\sigma^2\right)$, $Y\sim\mathcal{N}\left(\mu,\frac{1}{2}\sigma^2\right)$ and $\mu=\mu X+\text{i}\mu Y$.

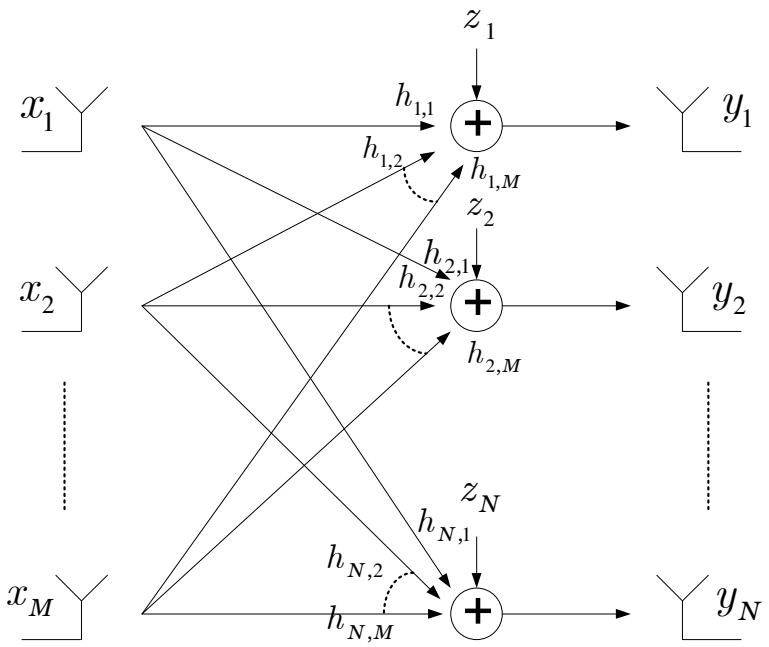

Figure 2-1: Graphical Interpretation of Gaussian linear vector memory less channel.

The model described by (2-1), can be rewritten as

$$\boldsymbol{y}=\mathbf{H}\boldsymbol{x}+\boldsymbol{z} \tag{2-3}$$

This model is referred to as Gaussian linear vector channel. The graphical interpretation of Gaussian linear vector channel is shown in Figure 2-1 where $h_{N,M}$ element denotes the fading coefficient between the N^{th} transmitting and M^{th} receiving antennas.

2.4 MIMO Channel Decomposition Perspectives

MIMO technology constitutes a breakthrough in the design of wireless communication systems, is and already at the core of several wireless standards. Exploiting multi path scattering, MIMO techniques deliver significant performance enhancements interms of data transmission rate and interference reduction [127]. The design of the MIMO EMTS transceiver includes precoding at the transmitter and

employing an equalizer at the receiver [73]. Several designs have been proposed based on conventional decomposition techniques and using a variety of criteria, including maximum Signal to Noise Ratio (SNR), Minimum Mean Squared Error (MMSE) and BER based criteria [71] and [73].

In general, MIMO transmission has been designed using linear transformation referred to as SVD when Channel State Information at Transmitter (CSIT) and Channel State Information at Receiver (CSIR) are available. The SVD decomposes the MIMO EMTS flat fading channel into the multiple parallel sub-channels. The waterfilling algorithm is used to achieve the capacity of each sub-channel [75]. The non-zero singular values of the diagonal matrix represent the SNRs of the sub-channels formed by SVD. However, due to very high variations in the SNRs of the sub-channels and high condition number, this apparently simple decomposition scheme requires a very intelligent and adaptive bit allocation in order to match the capacity of each sub-channel and achieve the prescribed BER [75]. Bit allocation among the eigenmodes of the MIMO EMTS not only increases the coding/decoding complexity but also inherently capacity loss because of finite constellation granularity [26]. Alternatively, assignment of equal power to the sub-channels, results in the same constellation among all eigenmodes. However, more transmitting power could be allocated to the channel having a poorer SNR i.e. the eigenmode having lowest SNR. A fundamental trade off is always required to be made between the capacity and the BER performance when dealing with such linear decomposition technique.

In [2], a new nonlinear decomposition scheme referred to as the Geometrical Mean Decomposition (GMD) is proposed which decomposes the MIMO channel into multiple identical and parallel independent sub channels. This decomposition brings much more convenience in coding/decoding and modulation/demodulation schemes as there is no need of bit allocation mechanism in transmission design. This decomposition assumes CSIT and CSIR are perfectly known unlike the QR decomposition where only CSIR is available.

In the following Section, we first review the SVD and then present the GMD. The MIMO system based on such decomposition is investigated later in § 2.7.

2.5 Singular Value Decomposition (SVD)

The SVD of a channel matrix $\mathbf{H} \in \mathbb{C}^{N \times M}$ with rank M i.e. $N \geq M$ may be expressed as [1] and [8]

$$\mathbf{H} = \mathbf{U} \boldsymbol{\Sigma} \mathbf{V}^H \tag{2-4}$$

where $\mathbf{U} \in \mathbb{C}^{N \times M}$ and $\mathbf{V} \in \mathbb{C}^{M \times M}$ are unitary matrices such that $\mathbf{U}\mathbf{U}^H = \mathbf{V}\mathbf{V}^H = \mathbf{I}_M$ and $\boldsymbol{\Sigma} \in \mathbb{R}^{M \times M}$ is a diagonal matrix with positive real singular values of the channel matrix $\mathbf{H}$, given by $\left\{\lambda_{H,i}\right\}_{i=1}^{M}$ such that $\lambda_{H,1} \geq \lambda_{H,2} \geq \cdots \geq \lambda_{H,M}$

Let us define Θ *as a complex Wishart matrix, which may be expressed as*

$$\Theta = \begin{cases} \mathbf{H}\,\mathbf{H}^H & \text{for } M \leq N \\ \mathbf{H}^H\,\mathbf{H} & \text{for } N < M \end{cases} \tag{2-5}$$

Let $\lambda_1 \geq \lambda_2 \geq \cdots \geq \lambda_M$ *be the singular values of* $\Theta = \mathbf{H}\,\mathbf{H}^H$. *We know that the square root of the singular values (eigenvalues) of* Θ *is equal to the singular values of* $\mathbf{H}$, *i.e.*

$$\lambda_{H,i} = \sqrt{\lambda_i} \text{ for } i = 1,2,\cdots,M \tag{2-6}$$

2.6 Geometric Mean Decomposition (GMD)

Recently, a unique and useful matrix decomposition technique referred to as Geometric Mean Decomposition (GMD) has been proposed by Jiang [2]. For any complex or real matrix $\mathbf{H} \in \mathbb{C}^{N \times M}$ with rank i.e. M, $N \geq M$ and singular values

$\lambda_{H,1} \geq \lambda_{H,2} \geq \cdots \geq \lambda_{H,M} > 0$, there exists an upper triangular matrix $\mathbf{R} \in \mathbb{R}^{M \times M}$, such that the SVD of $\mathbf{R}$ may be expressed as

$$\mathbf{R} = \mathbf{U}_R \boldsymbol{\Sigma} \mathbf{V}_R^H \tag{2-7}$$

where the i^{th} diagonal element of $\mathbf{R}$ equal to r_{ii} such that

$$\prod_{i=1}^{M} r_{ii} = \prod_{i=1}^{M} \lambda_{H,i} \tag{2-8}$$

Here, $\mathbf{U}_R$ and $\mathbf{V}_R$ are the unitary matrices and $\boldsymbol{\Sigma}$ is a diagonal matrix whose elements are equal to the singular values of the matrix $\mathbf{H}$ i.e. $\{\lambda_{H,i}\}_{i=1}^{M}$. After combining (2.4) with (2.7), we have

$$\mathbf{H} = \mathbf{U} \mathbf{U}_R^H \mathbf{R} \mathbf{V}_R \mathbf{V}^H$$

$$\mathbf{H} = \mathbf{Q} \mathbf{R} \mathbf{P}^H \tag{2-9}$$

where $\mathbf{Q} \in \mathbb{C}^{N \times M}$ and $\mathbf{P} \in \mathbb{C}^{M \times M}$ are semi-unitary matrices denoting the linear operations at the receiver and the transmitter respectively and $\mathbf{R} \in \mathbb{R}^{M \times M}$ is an upper triangular matrix with diagonal element r_{ii} that corresponds to the channel gain of the sub-channels. Hence, the channel $\mathbf{H}$ may be decomposed into scalar channels, where the diagonal entries satisfying the condition (2.8) i.e. the diagonal values of matrix $\mathbf{R}$ are completely majorized by the singular values of the channel matrix $\mathbf{H}$ [2]. Assuming the variance of the noise on the M sub-channels is the same, the sub-channel with the smallest r_{ii} has the highest error rate. To decrease the highest error rate leads to the problem of choosing $\mathbf{Q}$ and $\mathbf{P}$ to maximize the minimum of r_{ii}. The optimization problem may be expressed as [2] and [3]

$$\begin{aligned} &\max_{\mathbf{Q},\mathbf{P}} \ \min\left\{r_{ii} : 1 \le i \le M\right\} \\ &\text{subject to} \ \ \mathbf{H} = \mathbf{Q}\mathbf{R}\mathbf{P}^H \\ &\qquad\qquad \mathbf{R} \in \mathbb{R}^{M\times M}, r_{ij} = 0 \,; \forall\, i > j \\ &\qquad\qquad r_{ii} > 0 \,; \forall\ 1 \le i \le M \\ &\qquad\qquad \mathbf{Q}^H\mathbf{Q} = \mathbf{P}^H\mathbf{P} = \mathbf{I}_M \end{aligned} \tag{2-10}$$

The non-zero diagonal elements of $\mathbf{R}$ derived from the optimization (2-10) are all equal to the geometric mean of the non-zero singular values of the channel matrix $\mathbf{H}$ and define in the following lemma.

Lemma 2.6.1: (Identical diagonal entries [2]). *The channel matrix* $\mathbf{H} \in \mathbb{C}^{N\times M}$ *with rank M i.e.* $N \ge M$ *and singular values* $\lambda_{H,1} \ge \lambda_{H,2} \ge \cdots \ge \lambda_{H,M} > 0$ *may be decomposed as*[3]

$$\mathbf{H} = \mathbf{Q}\mathbf{R}\,\mathbf{P}^H, \text{ or equivalently } \mathbf{R} = \mathbf{Q}^H\,\mathbf{H}\,\mathbf{P} \tag{2-11}$$

where the diagonal elements of $\mathbf{R}$ *are given by*

$$r_{ii} = \overline{\lambda} = \left(\prod_{i=1}^{M} \lambda_{H,i}\right)^{1/M} . \quad 1 \le i \le M \tag{2-12}$$

Then $\mathbf{R}$ *is the solution to the* (2.10)*. The decomposition* (2.11) *is referred to as Geometric Mean Decomposition (GMD) since the diagonal elements of are the geometric mean of* $\{\lambda_{H,i}\}_{i=1}^{M}$.

Using (2.6) $\overline{\lambda}$ *in* (2.12) *can also be rewritten as*

$$\overline{\lambda} = \left(\prod_{i=1}^{M} \lambda_i\right)^{1/2M} . \quad 1 \le i \le M \tag{2-13}$$

[3] It is to note that (2.11) is the special case of Generalized Triangular Decomposition (GTD) where the diagonal values of $\mathbf{R}$ (which is geometric mean of the non-zero singular values of $\mathbf{H}$) are majorized by the singular values of the channel matrix $\mathbf{H}$ [3].

Hence, by exploiting the decomposition derived in (2.11), *the channel matrix* $\mathbf{H}$ *can be decomposed into identical, parallel and independent transmission pipes. The same has been shown later in the following Section.*

2.7 Transmission Design over Rayleigh Flat Fading Channel

In this Section, we present transmission design over linear vector MIMO channel by exploiting GMD [143] and [145]. First we review SVD based transmission design to compare the performance of GMD based transmission (to be considered in the next Section). In a TDD channels, the CSI is available at both ends of the communication link within a reasonable accuracy [6] and [9].

We consider a MIMO communication system with M transmitting and N receiving antennas in a frequency flat fading channel. The graphical interpretation of the channel model is shown in Figure 2-2. At the receiver, the overall input output transmission equation becomes

$$\boldsymbol{y} = \mathbf{H}\boldsymbol{s} + \boldsymbol{z} \tag{2-14}$$

where $\boldsymbol{s} \in \mathbb{C}^{M\times 1}$ is the transmitted signal vector such that $\boldsymbol{s} = \mathbf{V}\boldsymbol{x}$, $\boldsymbol{y} \in \mathbb{C}^{N\times 1}$ is the received signal vector, $\mathbf{H} \in \mathbb{C}^{N\times M}$ is the channel matrix with the $h_{n,m}$ element denoting the fading coefficient between the n^{th} transmitting and m^{th} receiving antennas. As in (2.1), we again assume $\boldsymbol{z} \sim \mathcal{CN}\left(0, \sigma_z^2 \mathbf{I}_N\right)$ is zero mean complex circularly symmetric Gaussian noise, $\mathbf{I}_N$ is the identity matrix with dimension N. We also define the SNR as

$$\gamma = \frac{\mathbb{E}\left[\boldsymbol{s}^H \boldsymbol{s}\right]}{\sigma_z^2} \tag{2-15}$$

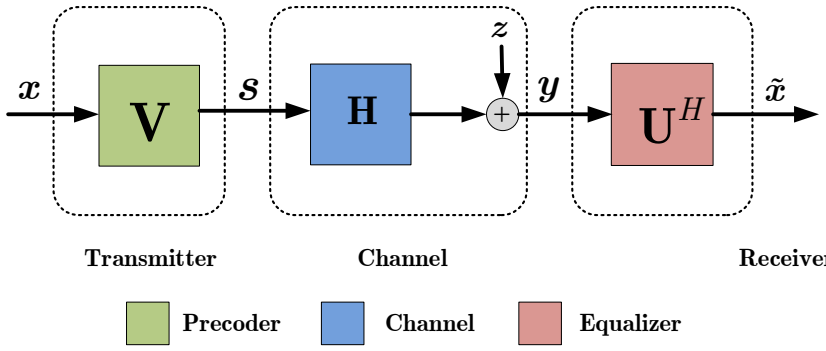

Figure 2-2: Block diagram of SVD based MIMO system showing linear operations at transmitter and receiver by unitary matrices $\mathbf{V}$ and $\mathbf{U}$ respectively.

2.7.1 Transmission Design Using SVD

In order to investigate the geometric mean decomposition technique, we review the linear transformation of the channel matrix $\mathbf{H}$ by employing SVD decomposition of $\mathbf{H}$. The schematic diagram of a MIMO system employing SVD is shown in Figure 2-2. The unitary matrices $\mathbf{U}^H$ and $\mathbf{V}$ are equalizer at the receiver and precoder at the transmitter respectively which decompose the channel $\mathbf{H}$ into parallel, independent non-identical sub-channels. By exploiting SVD, the filtered receive vector $\tilde{\boldsymbol{x}}$, we have [1] and [143]

$$\tilde{\boldsymbol{x}} = \mathbf{U}^H \boldsymbol{y} \tag{2-16}$$

By substituting (2.14) and apply decomposition defined in (2.4), we have

$$= \mathbf{U}^H \mathbf{H} \boldsymbol{s} + \mathbf{U}^H \boldsymbol{z},$$

$$= \mathbf{U}^H \mathbf{U} \boldsymbol{\Sigma} \mathbf{V}^H \boldsymbol{s} + \mathbf{U}^H \boldsymbol{z}$$

The M symbols destined for $\mathbf{H}$ are precoded as

$$\boldsymbol{s} = \mathbf{V}\boldsymbol{x} \tag{2-17}$$

$$= \underbrace{\mathbf{U}^H \mathbf{U}}_{\mathbf{I}_M} \boldsymbol{\Sigma} \underbrace{\mathbf{V}^H \boldsymbol{V}}_{\mathbf{I}_M} \boldsymbol{x} + \mathbf{U}^H \boldsymbol{z}$$

$$\tilde{\boldsymbol{x}} = \boldsymbol{\Sigma}\, \boldsymbol{x} + \tilde{\boldsymbol{z}} \tag{2-18}$$

In matrix notation, the resultant system can be expressed as

$$\begin{pmatrix} \tilde{x}_1 \\ \tilde{x}_2 \\ \vdots \\ \tilde{x}_M \end{pmatrix} = \begin{pmatrix} \sqrt{\lambda_1} & \cdots & \cdots & \mathbf{0} \\ \vdots & \sqrt{\lambda_2} & & \vdots \\ \vdots & & \ddots & \vdots \\ \mathbf{0} & \cdots & \cdots & \sqrt{\lambda_M} \end{pmatrix} \begin{pmatrix} x_1 \\ x_2 \\ \vdots \\ x_M \end{pmatrix} + \begin{pmatrix} \tilde{z}_1 \\ \tilde{z}_2 \\ \vdots \\ \tilde{z}_M \end{pmatrix} \tag{2-19}$$

The MIMO EMTS defined in (2.4) is now decompose into parallel, independent and non-identical sub-channels, each representing a SISO system given by

$$\tilde{x}_i = \sqrt{\lambda_i}\, x_i + \tilde{z}_i \qquad 1 \le i \le M \tag{2-20}$$

where λ_i denotes the singular values of a Wishart matrix Θ as defined in (2.5). Hence, the original MIMO system has now become an equivalent system having a set of parallel sub-channels with gain $\lambda_{H,i} = \sqrt{\lambda_i}$ as shown in Figure 2-3 . It is obvious that the information can only be transmitted over those equivalent channels with non zero singular values [1]. It is very important to note that if the number of transmission layers exceeds the number of strong singular values, the performance of the MIMO system degrades. However, the number of sub-channels depends on the minimum of $\left(N, M\right)$ without exceeding the rank of channel matrix $\mathbf{H}$. The singular values are sorted in decreasing order of values and the equivalent parallel sub-channels have unequal gain. Therefore, the complexity in the design of linear transceiver based on SVD is due to large variations among the singular values of the channel matrix $\mathbf{H}$ [16] and [26]. A practical implementation of such a system has been reported in [14] for reference.

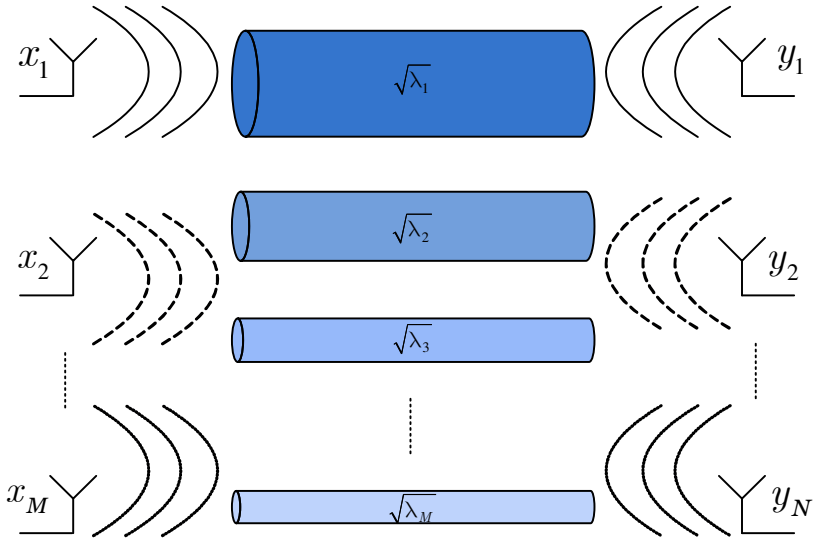

Figure 2-3: Graphical interpretation of MIMO system employing SVD to decompose wireless channel $\mathbf{H}$ into $L = M$ unequal parallel sub-channels such that $\lambda_1 \geq \lambda_2 \geq \cdots \geq \lambda_M$ are the ordered gains of the SISO sub-channels.

Since the different sub-channels of the SVD system have different gains, the use of different constellation sizes for each channel is capable of achieving its capacity [1]. However, to implement this, we need to know the SNR of each sub-channel. The waterfilling method[4] is the ideal power control strategy for SVD based MIMO systems, but it requires information about the noise at the transmitter side. Once the total available power, estimates of noise and gains of parallel sub-channels are known, Teletar [13] showed that the optimum power of the i^{th} sub-channel is

$$\gamma_i = \left(0, \mu - \frac{\sigma_z^2}{\lambda_{H,i}^2}\right)$$
$$= \left(\mu - \frac{\sigma_z^2}{\lambda_{H,i}^2}\right)^+ \tag{2-21}$$

[4] This is to note that waterfilling algorithm is well known power allocation scheme in multiple antenna communication literature; however the derivation is not available easily. The author's derivation is included in Appendix A for reference.

The waterfilling parameter μ is determined by the constraint of the total power P_t, such that

$$P_t = \sum_{i=1}^{M} \gamma_i \tag{2-22}$$

The value of the parameter μ can be found by an iterative loop allocating power to all good sub-channels. Another version of power control strategy is referred to as truncated waterfilling power control. This is same as original waterfilling strategy except that it does not allocate any power to sub-channels with an SNR below a given threshold which is set using the minimum SNR required for transmission with a desired performance. Any sub-channel whose SNR falls below the threshold is not used in the transmission and its power is redistributed among the other sub-channels [1].

2.7.2 Transmission Design Using GMD - Formation of Parallel, Identical and Independent Pipe

The scheme of a general MIMO EMTS communication system with non-linear transceiver design based on GMD is shown in Figure 2-4. The semi-unitary matrices $\mathbf{P}$ and $\mathbf{Q}^H$ are linear precoder at the transmitter and linear equalizer at the receiver respectively.

To design the transmission scheme, we first calculate the GMD of channel matrix $\mathbf{H}$ as defined in (2.11). Next, we encode the information symbols $\boldsymbol{x}$ via the linear precoder $\mathbf{P}$, such that the transmitted vector is given by [143]

$$\boldsymbol{s} = \mathbf{P}\boldsymbol{x} \tag{2-23}$$

where $\mathbf{P} \in \mathbb{C}^{M \times M}$ is a semi-unitary matrix denoting the linear operation at the transmitter (precoder) and $\boldsymbol{x} \in \mathbb{C}^{M \times 1}$ is the data vector that contains the M symbols to be transmitted (zero mean, normalized and uncorrelated that is, $\mathbb{E}\left[\boldsymbol{x}\,\boldsymbol{x}^H\right] = \mathbf{I}_M$ drawn from a set of constellations.

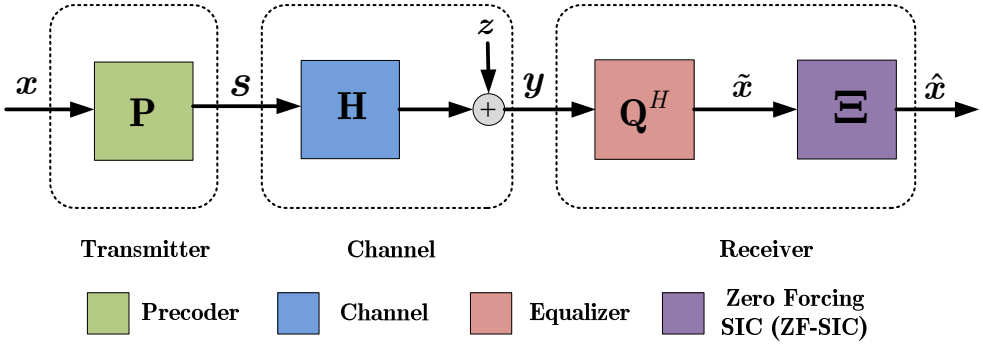

Figure 2-4: Block diagram of MIMO Identical Eigenmode Transmission System (IETS) showing the application of GMD to perform linear operations at transmitter and receiver by unitary matrices $\mathbf{P}$ and $\mathbf{Q}$ respectively.

At the receiver side, the decomposition algorithm is exploited in combination with a receiver interface, referred to as V-BLAST decoding. The decoding algorithm is based on sequential nulling and cancellation in order to decode the transmitted information symbols $\boldsymbol{s}$ [1], [7] and [8]. The nulling step is implemented by using zero forcing (ZF) criterion [1] and [75]. A detailed review on the complexity of the V-BLAST detection algorithm is already discussed in earlier sub Section 2.2.2 [1]. Thus, we consider GMD scheme in order to design a reduced complexity version of V-BLAST detection scheme. The estimated data vector at the receiver is given by [127] and [143]

$$\tilde{\boldsymbol{x}} = \mathbf{Q}^H \boldsymbol{y} \tag{2-24}$$

where $\mathbf{Q} \in \mathbb{C}^{N \times M}$ is the receiver matrix (equalizer) and $\boldsymbol{y} = \mathbf{H}\boldsymbol{s} + \boldsymbol{z}$ as seen from the Figure 2-4, the resultant output at the equalizer becomes

$$\tilde{\boldsymbol{x}} = \mathbf{Q}^H \mathbf{H}\, \boldsymbol{s} + \mathbf{Q}^H \boldsymbol{z},$$

Restating (2.24) by employing GMD (2.11), the resulting vector becomes

$$\tilde{\boldsymbol{x}} = \mathbf{Q}^H \mathbf{Q}\, \mathbf{R}\, \mathbf{P}^H \boldsymbol{s} + \tilde{\boldsymbol{z}},$$

also substituting $\boldsymbol{s} = \mathbf{P}\boldsymbol{x}$ in above, we have

$$\tilde{\boldsymbol{x}} = \mathbf{Q}^H \mathbf{Q}\mathbf{R}\mathbf{P}^H \mathbf{P}\boldsymbol{x} + \tilde{\boldsymbol{z}} \tag{2-25}$$

knowing $\mathbf{Q}\mathbf{Q}^H = \mathbf{I}$ & $\mathbf{P}\mathbf{P}^H = \mathbf{I}$, (2.25) becomes

$$\tilde{\boldsymbol{x}} = \mathbf{R}\ \boldsymbol{x} + \tilde{\boldsymbol{z}} \tag{2-26}$$

also in component wise notation, (2.26) becomes

$$\begin{pmatrix} \tilde{x}_1 \\ \tilde{x}_2 \\ \vdots \\ \tilde{x}_M \end{pmatrix} = \begin{pmatrix} \overline{\lambda} & r_{1,2} & \cdots & r_{1,M} \\ \vdots & \overline{\lambda} & & \vdots \\ \vdots & & \ddots & \vdots \\ \mathbf{0} & \cdots & \cdots & \overline{\lambda} \end{pmatrix} \begin{pmatrix} x_1 \\ x_2 \\ \vdots \\ x_M \end{pmatrix} + \begin{pmatrix} \tilde{z}_1 \\ \tilde{z}_2 \\ \vdots \\ \tilde{z}_M \end{pmatrix} \tag{2-27}$$

Due to upper triangular structure of $\mathbf{R}$, the i^{th} element of $\boldsymbol{x}_i$ is given by

$$\tilde{x}(i) = \mathbf{R}(i,i)\boldsymbol{x}(i) + \sum_{i+1}^{M} \mathbf{R}(i+1,i)\ \boldsymbol{x}(i+1) + \tilde{z}(i) \tag{2-28}$$

Ignoring error propagation effects [12] and [14], i.e. $\sum_{i+1}^{M} \mathbf{R}(i+1,i)\ \boldsymbol{x}(i+1) = 0$, we can regard the resulting sub-channels as M identical, parallel and independent sub-channels given by

$$\hat{\boldsymbol{x}}(i) = \overline{\lambda}\, x(i) + \tilde{z}(i) \quad for\ i = 1,2,\cdots,M \tag{2-29}$$

The concept of formation of identical, parallel and independent pipes using GMD is shown in Figure 2-5. The main advantage of this combined strategy comes with the complexity reduction, as it requires only a fraction of computational effort as compared to the original V-BLAST algorithm [7] and [8]. The channel gain of each eigenmode is given by $\overline{\lambda}$. Beam steering techniques on both the transmitter and the receiver sides are achieved by multiplying vector $\mathbf{P}_i$ at the transmitter and matrix $\mathbf{Q}^H$ at the receiver, where $\mathbf{P}_i$ denotes the i^{th} column of $\mathbf{P}$. As a result, an equivalent channel matrix can be expressed as [143]

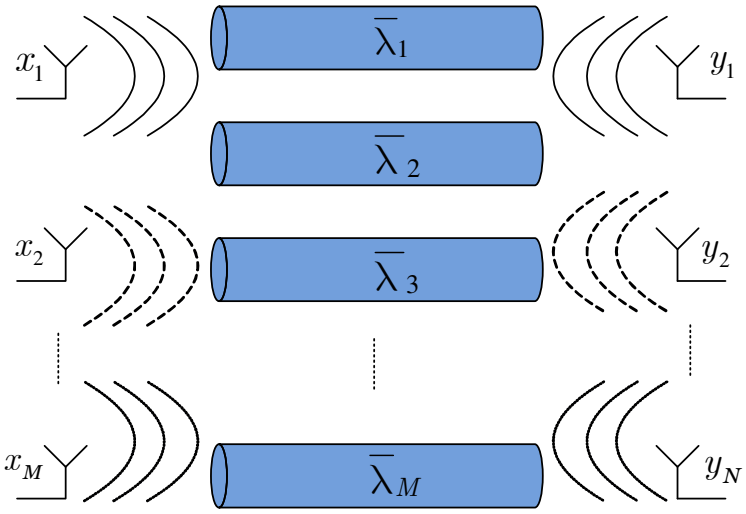

Figure 2-5: Graphical interpretation of MIMO IETS employing GMD to decompose the wireless channel $\mathbf{H}$ into $L = M$ identical, parallel and independent transmission pipes such that $\overline{\lambda}_1 = \overline{\lambda}_2 = \cdots = \overline{\lambda}_M$ are the gain of every SISO sub-channel given by (2.12).

$$\mathbf{Q}^H \mathbf{H} \mathbf{P}_i = \left(0, \cdots, \overline{\lambda}, \cdots, 0\right)^T \tag{2-30}$$

In MIMO systems, data transmission over the equivalent channel given by (2.30) is referred to as identical eigenmode transmission system (IETS) and the M sub-channels with gains $\overline{\lambda}$ and $\mathbf{P}_i$ are referred to as identical eigenmodes and eigenvectors, respectively [143]. By exploiting the triangular structure of matrix $\mathbf{R}$, a simple zero forcing algorithms can be applied to decode $\boldsymbol{x}$.

The zero forcing block in Figure 2-6 performs the following zero forcing algorithm to decode $\boldsymbol{x}$ from $\tilde{\boldsymbol{x}}$ [72]

$$\begin{aligned}
&\text{for } i = M:-1:1; \\
&\quad \hat{x}\left(i\right) \leftarrow C\left[\left(r\left(i,i\right)\right)^{-1} \tilde{x}_i\left(i\right)\right]; \\
&\quad \tilde{x}_{i-1} \leftarrow \tilde{x}^i - \mathbf{R}_i \hat{x}\left(i\right) \\
&\text{end}
\end{aligned} \tag{2-31}$$

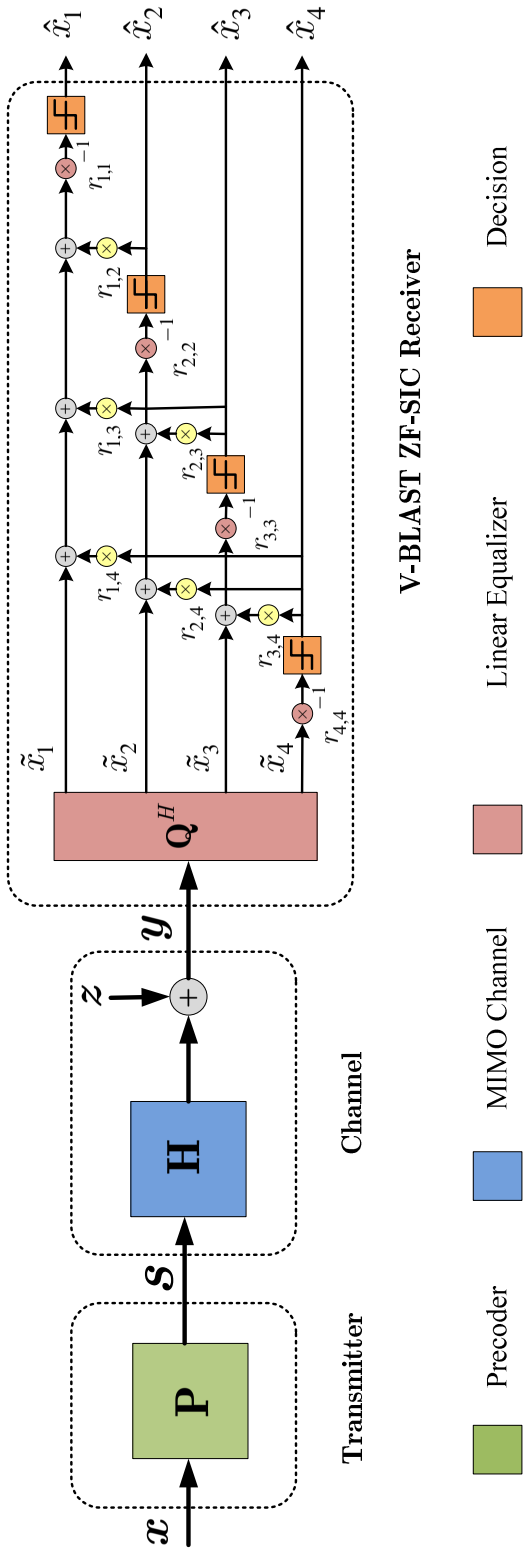

Figure 2-6: Schematic diagram of V-BLAST ZF with GMD transceiver design.

where $C\left[.\right]$ denotes the slicer which maps the symbol to the nearest constellation. As in many analyses of decision feedback systems, we assume there is no error propagation [1], [7], [8], [12] and [14]. That is when decoding i^{th} symbol $x\left(i\right)$, the previous decisions $\hat{x}\left(k\right),\ k = M, M-1, \cdots, i+1$ are assumed to be correct. However, an exact closed form analytical performance evaluation of V-BLAST algorithm for Rayleigh distributed fading has been presented in [146]. The reported analytical analysis is based on considering the impact of error propagation without any approximation or assumption.

According to the above algorithm and using the above assumption $\hat{x}\left(k\right) = x\left(k\right)$ for $k = i+1, \cdots, M$, $\tilde{\boldsymbol{x}}_i \in \mathbb{C}^{i\times 1}$

$$\tilde{\boldsymbol{x}}_i = \tilde{\boldsymbol{x}} - \sum_{k=i+1}^{M} \mathbf{R}_{i,k}\, \hat{\boldsymbol{x}}\left(k\right) \tag{2-32}$$

or equivalently, we have i^{th} element

$$\tilde{\boldsymbol{x}}_i\left(i\right) = \tilde{\boldsymbol{x}}\left(i\right) - \sum_{k=i+1}^{M} \mathbf{R}\left(i,k\right)\hat{\boldsymbol{x}}\left(k\right) \tag{2-33}$$

Now, (2.32) reduces to

$$\tilde{\boldsymbol{x}}_i = \mathbf{R}_{ii}\boldsymbol{x}_i + \tilde{\boldsymbol{z}}_i \tag{2-34}$$

and (2.33) may also reduces to

$$\tilde{\boldsymbol{x}}_i\left(i\right) = \mathbf{R}\left(i,i\right)\, \boldsymbol{x}\left(i\right) + \tilde{\boldsymbol{z}}\left(i\right) \tag{2-35}$$

substituting the above equation (2.35) into the algorithm (2.31)

$$\hat{x}\left(i\right) = C\left[\left(r\left(i,i\right)\right)^{-1}\tilde{x}_i\left(i\right)\right] \tag{2-36}$$

to yield

$$\hat{x}(i) = C\left[\left(r(i,i)\right)^{-1}\left(\tilde{\boldsymbol{x}}(i) - \sum_{k=i+1}^{M} \mathbf{R}(i)_k \, \hat{\boldsymbol{x}}(k)\right)\right] \quad (2\text{-}37)$$

substituting (2.35), we have

$$= C\left[\left(r(i,i)\right)^{-1}\left(\mathbf{R}(i,i)\,\boldsymbol{x}(i) + \tilde{\boldsymbol{z}}(i)\right)\right]$$

$$= C\left[\left(\boldsymbol{x}(i) + \left(r(i,i)\right)^{-1}\tilde{\boldsymbol{z}}(i)\right)\right] \quad (2\text{-}38)$$

It can be seen clearly from (2.38), when the noise $\boldsymbol{z}$ in $\tilde{\boldsymbol{z}} = \mathbf{Q}^H \boldsymbol{z}$ is zero, the estimation is exactly $\boldsymbol{x}(i)$. Therefore, this is a zero forcing decoder. The mean square error (MSE) of system in consideration may be expressed as [11] and [143]

$$\mathrm{MSE}_i = \mathbb{E}\left|\left(\mathbf{R}(i,i)\right)^{-1}\tilde{\boldsymbol{x}}_i(i) - \boldsymbol{x}(i)\right|^2 \quad (2\text{-}39)$$

$$= \mathbb{E}\left|\left(\mathbf{R}(i,i)\right)^{-1}\tilde{\boldsymbol{z}}_i(i)\right|^2$$

$$= \left(\mathbf{R}(i,i)\right)^{-2} \quad (2\text{-}40)$$

$$= \det\left(\mathbf{H}^H\,\mathbf{H}\right)^{-(1/M)} \quad (2\text{-}41)$$

for $i = 1,2,\cdots,M$, where the equality comes from (2.12).

2.7.3 Remarks on Identical Eigenmode Transmission Systems

Several remarks on ZF-V-BLAST based on GMD are now in order:

- The GMD transceiver uses unitary matrices computed from the GMD to convert the channel $\mathbf{H}$ into a triangular matrix $\mathbf{R}$ with identical diagonal elements. Then, the triangular channel matrix $\mathbf{R}$ can be equalized by the Zero Forcing algorithm.
- Due to the identical diagonal elements of $\mathbf{R}$, all symbol streams have identical MSE $\det\left(\mathbf{H}^H\ \mathbf{H}\right)^{-(1/M)}$. The overall system can be viewed as $L = M$ parallel SISO AWGN channels with identical noise variance. The formation of identical, parallel and independent transmission pipes for data transmission is shown in Figure 2-5.
- The drawback of ZF based GMD receiver is that the MSE $\det\left(\mathbf{H}^H\ \mathbf{H}\right)^{-(1/M)}$ becomes very large when one of the singular values of $\mathbf{H}$ is small, and tends to infinity when $\mathbf{H}$ has a null. Since every SISO channel shares the same MSE, this causes a severe degradation in performance. The amplification of the noise results from the zero-forcing design of the ZF-GMD receiver. It can be avoided if the Minimum Mean Square Error (MMSE) estimator is employed. The MMSE V-BLAST with GMD for Wyner like cellular networks [29] is presented later in Chapter 5.

2.8 BER Simulation Results

In this Section, we present some performance results based on BER curves obtained after various simulation scenarios. In all simulation experiments, we assumed that the channel is Rayleigh flat fading. To determine the effectiveness of the GMD based V-BALST detection strategy, the BER performance curves are compared with SVD based decoding strategy. In each scenario, the curves are obtained after averaging 5000 Monte Carlo trials of $\mathbf{H}$.

We consider GMD V-BLAST over Rayleigh flat-fading MIMO channel with $N = M = 1,2,3,4$ transmitting and receiving antennas respectively. In Figure 2-7(a), we present a scenario where M independent symbols, modulated as quadrature phase shift keying (QPSK) are transmitted over the MIMO channel. By employing GMD, we decompose the MIMO channel into $L = M$ identical, parallel and independent sub-channels for data transmission. After observing the BER curves for different number of transmitting and receiving antennas it is demonstrated that the BER curve for $N = M = 4$, GMD V-BLAST performs superior as compared with less number of transmitting and receiving antennas, from moderate to high SNRs. Hence, the diversity gain offered by GMD based scheme is increased with the increase in the number of transmitting and receiving antennas. With the increase in channel dimension, the geometric mean of the non-zero singular values of the channel also increases (increase in sub-channel gains). Therefore, the capacity of the multi-antenna systems employing GMD can be improved by exploiting the number of transmitting and receiving antennas with no extra burden on complexity of transceivers. This phenomenon has been demonstrated in Figure 2-14. Furthermore, it is found that the BER performance of each sub-channel is identical since every channel has identical MSE i.e. $\det\left(\mathbf{H}^H\ \mathbf{H}\right)^{-(1/M)}$.

In order to investigate the efficacy of the GMD based systems, we compare the transmission design with SVD based receiver. Employing SVD over $\mathbf{H}$, we have M parallel and independent unequal sub-channels for symbol transmission. From the BER performance curves it is observed that with the increase in number of

transmitting and receiving antennas, the performance of the SVD based detection is degraded. For higher channel dimension i.e. $\mathbf{H} \in \mathbb{C}^{4\times4}$ the condition number of $\mathbf{H}$ is usually very high that results in ill conditioned sub-channels. Allocating more power to the poor channel degrades the BER performance of the system. To avoid the system degradation, SVD should be used in combination with water filling algorithm which suggests that the binary phase shift keying (BPSK) or QPSK should be used to match the capacity of the worst sub-channels and something like 16-QAM or 64-QAM to the best sub-channels, the same is observed in following simulation scenario.

In Figure 2-7(b), the same simulation scenario is repeated for a different constellation. We present a scenario where M independent symbols, modulated as 16-QAM are transmitted. The performance of GMD based receiver outperforms as compare with the performance of SVD based receiver at higher constellation as well. The degradation in SVD based detection is due to allocating more power to the poor channels, hence the SVD based transceiver doesn't exploit the essence of multi-antenna communication when allocating equal power to every sub-channels.

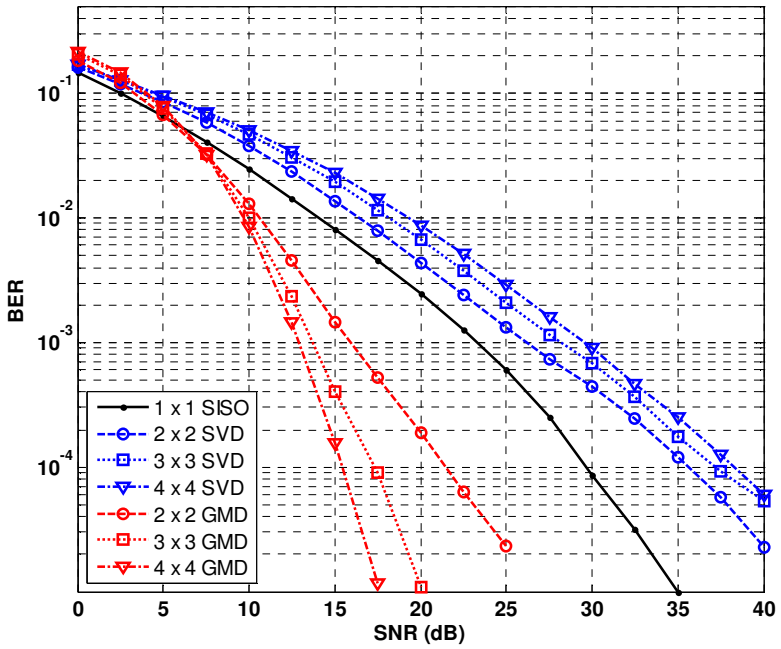

(a) QPSK

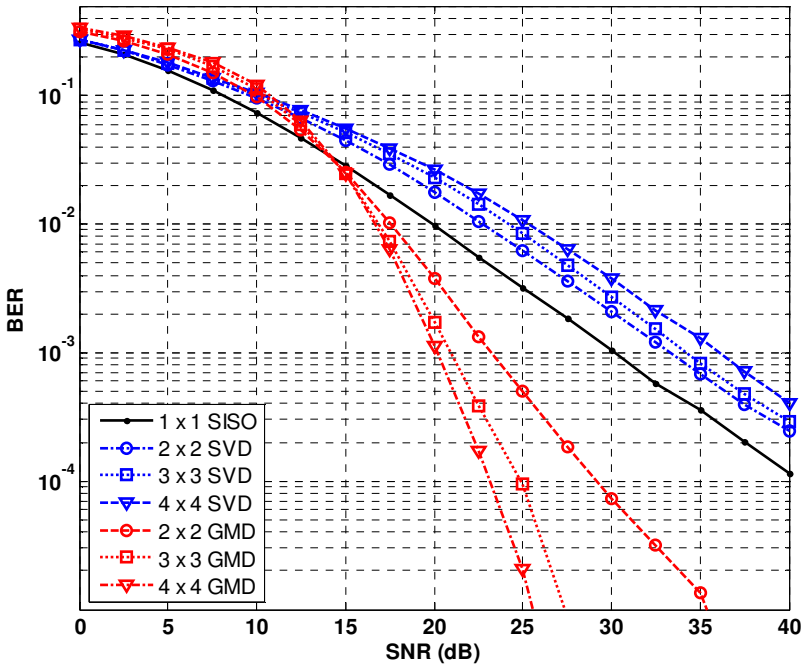

(b) 16-QAM

Figure 2-7: Summary and comparison of BER performance of MIMO wireless system employing SVD and GMD to decompose the wireless channel $\mathbf{H}$ into SISO channels.

2.9 Mutual Information of MIMO Channel

It is well known that capacity crucially depends on the input output mutual information of the channel [22]. In particular, for MIMO memory less channel described by (2.3), the following theorem is used extensively in the literature and forms the basis of the results presented in this thesis.

Theorem 2.9.1: (Input-Output Mutual Information of Linear MIMO Channels [13] and [22]). *For the linear MIMO memory less channel described by* (2.3)*, assume that* $\boldsymbol{x}$, $\mathbf{H}$ *and* $\boldsymbol{z}$ *are independent of each other. Let us assume* $\mathbf{H}$ *is deterministic for instance the first case* $\left(\text{i.e. } \Pr\left(\mathbf{H}[i]=\mathbf{H}\right)=1 \text{ for all } i=1,2,\cdots\right)$. *Assume the receiver has full CSI knowledge. Suppose the input symbols (not necessarily Gaussian) are zero mean with covariance* $\boldsymbol{\Phi}$. *The input output mutual information conditioned on* $\mathbf{H}$ *is*

$$\mathcal{I}(\boldsymbol{x};\boldsymbol{y}\mid\mathbf{H}) \le \log\det\left(\mathbf{I}_N + \frac{1}{\sigma_z^2}\mathbf{H}\boldsymbol{\Phi}\mathbf{H}^H\right) \tag{2-42}$$

with equality when $\boldsymbol{x}$ *is a c.c.s. Gaussian vector.*

Proof of (2.42): From the definition of conditional mutual information [22],

$$\begin{aligned}
&\mathcal{I}(\boldsymbol{x};\boldsymbol{y}\mid\mathbf{H}) = \mathcal{H}(\boldsymbol{y}\mid\mathbf{H}) - \mathcal{H}(\boldsymbol{y}\mid\boldsymbol{x},\mathbf{H})\\
&= \mathcal{H}(\boldsymbol{y}\mid\mathbf{H}) - \mathcal{H}(\boldsymbol{z})\\
&\overset{(a)}{=} \mathcal{H}(\boldsymbol{y}\mid\mathbf{H}) - \log\left((2\pi e)^N \det(\sigma_z^2\mathbf{I}_N)\right)\\
&\overset{(b)}{\le} \log\det(\mathbf{H}\boldsymbol{\Phi}\mathbf{H}^H + \sigma_z^2\mathbf{I}_N)\\
&= \log\det\left(\mathbf{I}_N + \frac{1}{\sigma_z^2}\mathbf{H}\boldsymbol{\Phi}\mathbf{H}^H\right)\\
&= \log\det\left(\mathbf{I}_M + \frac{1}{\sigma_z^2}\boldsymbol{\Phi}\mathbf{H}^H\mathbf{H}\right)
\end{aligned}$$

where $e \triangleq \exp(1)$, line (a) follows from [22] and line (b) follows from [22], i.e. the entropy of $\boldsymbol{y}$ is largest when $\boldsymbol{y}$ is multivariate Gaussian distributed, which only occurs when $\boldsymbol{x}$ is multivariate Gaussian distributed. □

In Theorem 2.9.1, a deterministic channel matrix $\mathbf{H}$ is assumed. In communication scenarios the channel matrix $\mathbf{H}$ is a random matrix[5] with a given density $p(\mathbf{H})$ that models the inherent randomness of the intended application. In general case, when $\mathbf{H}$ is distributed according to some arbitrary density $p(\mathbf{H})$, the input-output mutual information is expectation over all possible realizations of $\mathbf{H}$, i.e. assuming $\boldsymbol{z}$ is c.c.s. Gaussian, (2.42) becomes [22]

$$\mathcal{I}\left(\boldsymbol{x};\boldsymbol{y} \mid \mathbf{H}\right) = \mathbb{E}\left[\log\det\left(\mathbf{I}_N + \frac{1}{\sigma_z^2}\mathbf{H}\boldsymbol{\Phi}\mathbf{H}^H\right)\right] \tag{2-43}$$

$$= \int \log\det\left(\mathbf{I}_N + \frac{1}{\sigma_z^2}\mathbf{H}\boldsymbol{\Phi}\mathbf{H}^H\right) p(\mathbf{H})\, d\,\mathbf{H} \tag{2-44}$$

From (2.44) it is easy to see that when $\Pr\left(\mathbf{H}[i] = \mathbf{H}\right) = 1$ for all $i = 1,2,\cdots$, i.e. the deterministic case, (2.44) reduces to (2.42). For the special case when $\boldsymbol{x}$ is an isotropic signal, i.e. $\boldsymbol{\Phi} = P\,\mathbf{I}_M$ with $\gamma \triangleq P/\sigma_z^2$, then (2.44) becomes

$$\mathcal{I}\left(\boldsymbol{x};\boldsymbol{y} \mid \mathbf{H}\right) = \mathbb{E}\left[\log\det\left(\mathbf{I}_N + \gamma\,\mathbf{H}\mathbf{H}^H\right)\right] \tag{2-45}$$

[5] In this thesis if the channel matrix of (2.1) is random, its statistics are also assumed to be stationary with respect to discrete time i.

2.10 Capacity of MIMO Channel - A Channel Decomposition Perspectives

The most commonly used figure of merit in the analysis of MIMO systems is the total sum-rate constraint [13]. The capacity of the channel $\mathbf{H}$ is given by the sum of the capacities of the M sub-channels (Eigenmodes of the channel) [1] and [18]; and can be expressed as[6]

$$\mathrm{C}\left(\mathbf{H}, \gamma = \frac{P_t}{\sigma_z^2}\right) = \sum_{i=1}^{M} \log_2\left(1 + \frac{P_i}{\sigma_z^2}\lambda_{H,i}^2\right) \tag{2-46}$$

where σ_z^2 is the noise variance, and P_i is the power allocated to the i^{th} mode; we also assume that $\sum_{i=1}^{M} P_i = P_t$ is independent of the number of antennas. This capacity expression can be shown to be equivalent to [1]

$$\mathrm{C}\left(\mathbf{H}, \gamma\right) = \log_2\left(\det\left(\mathbf{I}_N + \frac{\gamma}{M}\mathbf{H}\,\mathbf{\Phi}\,\mathbf{H}^H\right)\right) \tag{2-47}$$

where $\mathbf{I}_N$ is the $N \times N$ identity matrix, γ is the mean signal to noise ratio (SNR) per receive branch, and $\mathbf{\Phi}$ is the correlation matrix of the transmit data (for data at different antenna elements that are uncorrelated, it is a diagonal matrix with entries that describes the power distribution among the antennas). The distribution of power among the different eigenmodes depends on the amount of the CSI at the transmitters.

We now analyze the capacity that can be obtained when the receiver knows the channel perfectly, but no CSI is available at the transmitter. In this case it is optimum to assign equal transmit power to all the transmitting antennas, $P_i = P_t / M$. The capacity offered by Equal Power Allocation (EPA) transmission scheme thus, takes on the now-famous form, [1] and [13]

[6] Information theoretical insights of multiple antennas in cellular wireless systems are presented in details in Chapter 4.

$$\mathbf{C}_{EPA}\left(\mathbf{H},\gamma\right)=\log_2\left(\det\left(\mathbf{I}_N+\frac{\gamma}{M}\mathbf{H}\,\mathbf{H}^H\right)\right) \tag{2-48}$$

The capacity of MIMO system increases linearly with $\min\left(N,M\right)$, irrespective of whether the channel is known at the transmitter or not.

If the transmitter has full CSI, then it can distribute the transmission power in a way that makes the maximum use of the available resources. The problem of assigning the right amount of power to available parallel channels has already been solved in a different context by Shannon, and is known as waterfilling [17]. The capacity obtained with waterfilling power allocation algorithm is referred to as capacity offered by Adaptive Power Allocation (APA) transmission scheme, and may be expressed as [72]

$$\mathbf{C}_{APA}\left(\mathbf{H},\gamma\right)=\sum_{i=1}^{M}\log_2\left(1+\gamma_i\ \lambda_{H,i}^2\right) \tag{2-49}$$

where γ_i is found via waterfilling power allocation algorithm given by (2.21) and $\lambda_{H,i}$ is the singular value of the channel matrix $\mathbf{H}$.

The overall BER performance of the MIMO wireless networks is dominated by worst sub-channels as shown in Section 2.8. Hence, the scheme optimizing the worst sub-channels can result the optimal BER performance. A major advantage over the linear transceiver schemes, the GMD scheme is also optimal in terms of the channel capacity. If the signal power is allocated uniformly to the M sub-channels, then the capacity offered by Identical Eigenmode (IE) transmission scheme can be obtained as [13]

$$\mathbf{C}_{IE}\left(\mathbf{H},\gamma\right)=M\ \log_2\left(1+\frac{\gamma}{M}\ \overline{\lambda}^2\right) \tag{2-50}$$

where $\overline{\lambda}$ is the geometric mean of the positive singular values of channel matrix $\mathbf{H}$ given by (2.12). In case the channel changes; we can compute two different types of capacity.

The ergodic (Shannon) capacity: This is the expected value of the capacity, taken over all the realizations of the channel. This quantity assumes an infinitely long

code that extends over all the different channel realizations. For random ergodic channel matrices, the capacity definitions are easily extended to the ergodic case by performing the expectation of the log det term in (2.48), (2.49) and (2.50) over $\mathbf{H}$.

The outage capacity: This is the minimum capacity that is achieved at a certain fraction of time, e.g., 90% or 95%. We assume that the data are encoded with a near Shannon limit achieving code that extends over a period that is much shorter than the channel coherence time. It has been shown that Low Density Parity Check (LDPC) code with a block length of 10 000 Bits are less than 1 dB away from the Shannon limit [1]. For a data rate of 1 Mbps, such a block can be transmitted within 1 milliseconds. This is much shorter than 10 milliseconds, which is typical coherence time of wireless channels [1].

2.10.1 Capacity Simulation Results

Since the MIMO channel is changing and each channel realization is associated with a (Shannon) capacity value. The capacity thus becomes a random variable, with an associated cumulative distribution function (CDF). It is then of great interest to investigate this distribution function or equivalently the capacity that can be guaranteed for $\%$ of all channel realizations. In this Section, we present the capacity simulation results over the Rayleigh distributed flat fading MIMO channel. The CDF curves are obtained after averaging 5000 Monte Carlo trials of $\mathbf{H}$.

Figure 2-8a and Figure 2-8b presents the CDFs of the channel capacities of $\mathbf{H}\left(N,M\right)=\left(2,2\right)$ independent Rayleigh flat fading channel by exploiting EPA and APA respectively for SNR $\gamma = 10$ dB[7]. The red curves in figures present the capacity offered by IE transmission schemes. The two black curves in Figure 2-8a denotes the channel capacities of the two sub-channels when uniform power is allocated to both channels. On the contrary, the two black curves shown in Figure 2-8b presents the channel capacities of the two sub-channels obtained via SVD plus waterfilling. The red curve is the CDF of each sub-channel capacity obtained via

[7] Independently and identically distributed $\left(\text{i.i.d}\right)$ complex Gaussian channel entries (with variance of each entry one) are assumed in the case of uncorrelated Rayleigh fading channel.

GMD. The $10\,\%$ outage capacity offered by L eigenmodes by exploiting each of the three schemes may be expressed as[8] $\mathrm{C}\left(p(\mathbf{H});\gamma\right)_{EPA,L}^{0.1}$, $\mathrm{C}\left(p(\mathbf{H});\gamma\right)_{APA,L}^{0.1}$ and $\mathrm{C}\left(p(\mathbf{H});\gamma\right)_{IE,L}^{0.1}$. The numerical values for $\gamma = 10$ dB, $\gamma = 0$ dB and $\gamma = -10$ dB are summarized in Table 2-1. It can be seen from the Table 2-1 that waterfilling algorithm is advantageous when CSI at the transmitter is available. The sub-channels can be used according to their capability of contributing towards channel capacity. Employing EPA transmission scheme to such system causes degradation in system performance since the best channel can be underused or the poor channel may be over used i.e. more power may be allocated to the poor channel. The capacity offered by employing IE scheme over MIMO channel is as good as to the capacity offered by the channel when EPA and APA are employed.

Similarly, we repeat the simulation scenarios for $\mathbf{H}\left(N,M\right) = \left(4,4\right)$. Figure 2-9a and Figure 2-9b, shows the CDF curves for $\gamma = 10$ dB when EPA and APA schemes are employed respectively. Again, the red curves in both figures present the CDF when IE scheme is employed. The numerical values of $10\,\%$ outage capacity offered by all three transmission schemes for $\gamma = 10$ dB, $\gamma = 0$ dB and $\gamma = -10$ dB are summarized in Table 2-2. It can be seen that the total capacity offered via GMD is comparable to the total capacity offered via APA and EPA transmission schemes. At lower SNRs, $\gamma = 0$ dB one eigenmode $\left(L = 1\right)$ and $\gamma = -10$ dB two eigenmodes $\left(L = 1,2\right)$ are discarded by waterfilling power allocation process. On the contrary, GMD exploit all four eigenmodes such that each of the eigenmodes offers equal capacity without employing any bit allocation process. Additional figures for $\gamma = 0$ dB and $\gamma = -10$ dB are included in Appendix B.

[8] Probability Capacity < Abscissa means probability that the capacity offered by APA, EPA and IE transmission schemes less than the range of capacity values on the x-axis of the figures.

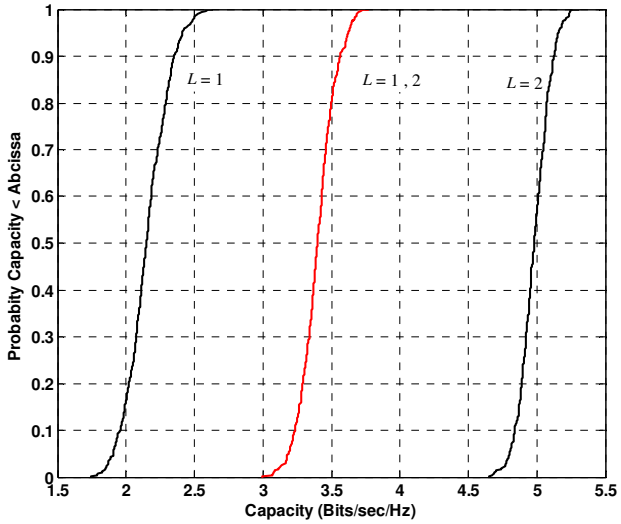

(a) EPA

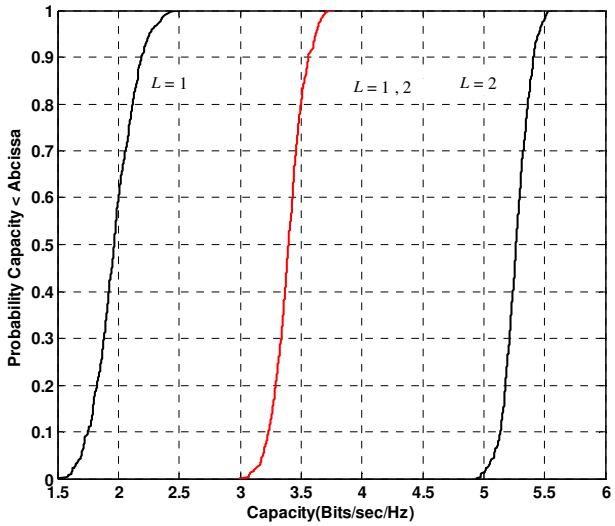

(b) APA

Figure 2-8: Capacity offered by $\mathbf{H}\left(N,M\right)=\left(2,2\right)$ MIMO wireless system with $\gamma = 10$ dB : (a) Equal Power Allocation (EPA); (b) Adaptive Power Allocation (APA) (employing waterfilling scheme to pour desirable power into sub-channels; red curve shows the capacity offered Identical Eigenmode (IE) using GMD.

Table 2-1: Summary of capacity (Bits/sec/Hz) offered by $\left(N,M\right)=\left(2,2\right)$ at various SNR employing EPA, APA and IE transmission schemes.

Eigen Mode No. (L)	$\gamma = 10$ dB		
	$\mathrm{C}\left(p(\mathbf{H});\gamma\right)_{EPA,L}^{0.1}$	$\mathrm{C}\left(p(\mathbf{H});\gamma\right)_{APA,L}^{0.1}$	$\mathrm{C}\left(p(\mathbf{H});\gamma\right)_{IE,L}^{0.1}$
1.	1.96	1.75	3.31
2.	4.84	5.14	3.31
L_1+L_2	6.80	6.89	6.62

Eigen Mode No. (L)	$\gamma = 0$ dB		
	$\mathrm{C}\left(p(\mathbf{H});\gamma\right)_{EPA,L}^{0.1}$	$\mathrm{C}\left(p(\mathbf{H});\gamma\right)_{APA,L}^{0.1}$	$\mathrm{C}\left(p(\mathbf{H});\gamma\right)_{IE,L}^{0.1}$
1.	0.63	0.34	1.41
2.	2.46	3.07	1.41
L_1+L_2	3.09	3.40	2.82

Eigen Mode No. (L)	$\gamma = -10$ dB		
	$\mathrm{C}\left(p(\mathbf{H});\gamma\right)_{EPA,L}^{0.1}$	$\mathrm{C}\left(p(\mathbf{H});\gamma\right)_{APA,L}^{0.1}$	$\mathrm{C}\left(p(\mathbf{H});\gamma\right)_{IE,L}^{0.1}$
1.	0.05	0.00	0.21
2.	0.38	0.66	0.21
L_1+L_2	0.43	0.66	0.42

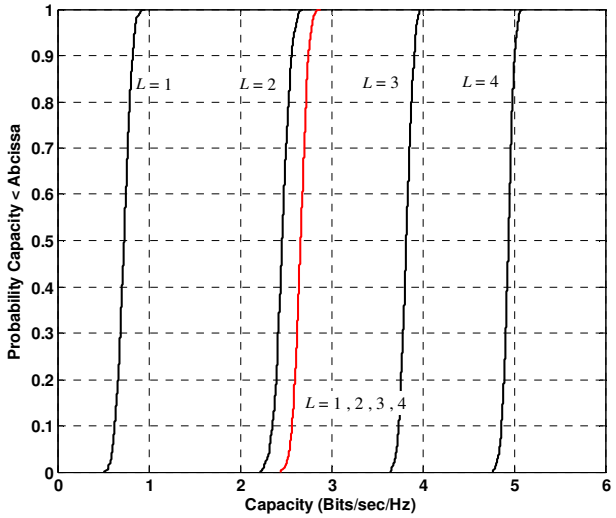

(a) EPA

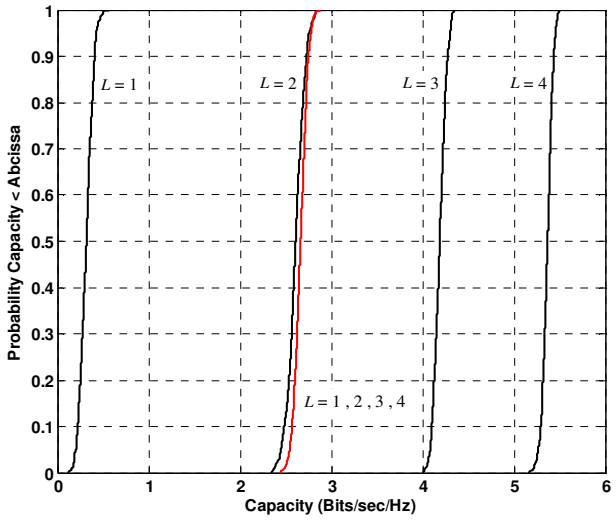

(b) APA

Figure 2-9: Capacity offered by $(N,M)=(4,4)$ MIMO wireless system with $\gamma = 10$ dB : (a) Equal Power Allocation (EPA) (b) Adaptive Power Allocation (APA) (employing waterfilling scheme to pour desirable power into sub-channels); red curve shows the capacity offered Identical Eigenmode (IE) using GMD.

Table 2-2: Summary of capacity (Bits/sec/Hz) offered by $\left(N,M\right)=\left(4,4\right)$ at various SNR employing EPA, APA and IE transmission schemes.

Eigen Mode No. (L)	$\gamma = 10$ dB		
	$\mathrm{C}\left(p(\mathbf{H});\gamma\right)_{EPA,L}^{0.1}$	$\mathrm{C}\left(p(\mathbf{H});\gamma\right)_{APA,L}^{0.1}$	$\mathrm{C}\left(p(\mathbf{H});\gamma\right)_{IE,L}^{0.1}$
1.	0 .62	0 .22	2.8
2.	2.25	2.48	2.8
3.	3.61	4.05	2.8
4.	4.71	5.12	2.8
$L_1+L_2+L_3+L_4$	11.19	11.87	11.2

Eigen Mode No. (L)	$\gamma = 0$ dB		
	$\mathrm{C}\left(p(\mathbf{H});\gamma\right)_{EPA,L}^{0.1}$	$\mathrm{C}\left(p(\mathbf{H});\gamma\right)_{APA,L}^{0.1}$	$\mathrm{C}\left(p(\mathbf{H});\gamma\right)_{IE,L}^{0.1}$
1.	0.20	0.00	1.45
2.	1.0	0.91	1.45
3.	2.0	2.50	1.45
4.	3.0	3.68	1.45
$L_1+L_2+L_3+L_4$	6.0	7.0	5.80

Eigen Mode No. (L)	$\gamma = -10$ dB		
	$\mathrm{C}\left(p(\mathbf{H});\gamma\right)_{EPA,L}^{0.1}$	$\mathrm{C}\left(p(\mathbf{H});\gamma\right)_{APA,L}^{0.1}$	$\mathrm{C}\left(p(\mathbf{H});\gamma\right)_{IE,L}^{0.1}$
1.	0.014	0.00	0.16
2.	0.098	0.00	0. 16
3.	0.26	0.99	0. 16
4.	0.44	1.29	0. 16
$L_1+L_2+L_3+L_4$	0.81	2.28	0.64

The benefits of employing the GMD scheme are significant when the dimension of the channel is large. With the increase in transmitting and receive antennas, the identical eigenmodes offer more capacity with no extra complexity of coding/decoding and modulation/demodulation. The gain of identical eigenmodes with the increase in channel dimension is shown in Figure 2-10. On the contrary, using SVD the condition number $\hbar\left(\mathbf{H}\right)$[9] increases with the increase in channel dimension. The sub-channel capacities via SVD suggests that Binary Phase Shift Keying (BPSK) or Quaternary Phase Shift Keying (QPSK) should be used to match the capacity of weak sub-channels and something like 512-QAM or 1024-QAM to the best sub-channels. The bit allocation mechanism significantly increases the modulation/demodulation complexity. Moreover, exploiting a constellation with size greater than 256-QAM is impractical for current RF circuit design technology [16] and [26]. For the GMD scheme, unlike the SVD, the same constellation with moderate size, say 16-QAM or 64-QAM, can be applied to reap the capacity of the most of the sub-channels.

The capacity gain by waterfilling (compared to the equal power allocation) is rather small when the number of transmit and receive antenna is identical. This is especially true in the limit of large SNRs. When M is larger than N, the benefits of waterfilling become more pronounced (see Figure 2-11). Essentially, waterfilling makes sure that energy is not wasted on eigenmodes that does not carry any significant power. This can be viewed as another trade-off between spatial multiplexing and beamforming gain: waterfilling reduces the number of channel eigenmodes that are used for communications, in order to improve the SNR on the actually employed eigenmodes.

---

[9] $\hbar\left(\mathbf{H}\right) = \frac{\lambda_{H,\max}}{\lambda_{H,\min}}$ where $\lambda_{H,\max}$ and $\lambda_{H,\min}$ are the maximal and minimal singular values of $\mathbf{H}$. The condition number associated with a problem is a measure of that problem's amenability to digital computation, that is, how numerically well-conditioned the problem is. A problem with a low condition number is said to be well-conditioned, while a problem with a high condition number is said to be ill-conditioned. The complexity of transmission design is pronounced when SVD is employed; however much simple transmission design is possible with GMD [90].

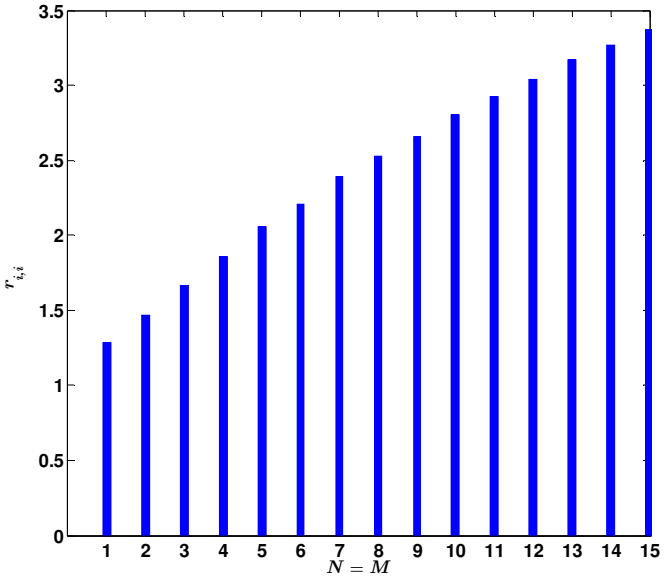

Figure 2-10: Average diagonal value[10] of upper triangular matrix $\mathbf{R}$ with the increase in transmitting N and receiving M antennas. The mean values are obtained over 2000 trials of $\mathbf{H}$.

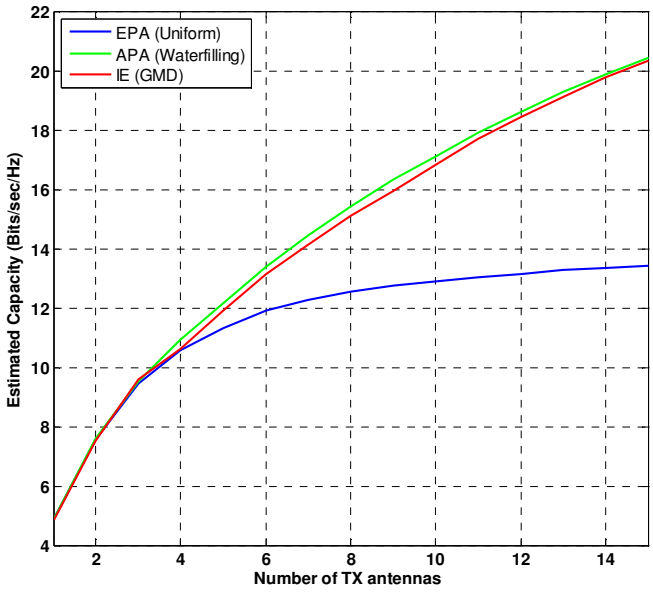

Figure 2-11: Estimated mean capacity with uniform power allocation (2.48); waterfilling (2.49); Identical Eigenmode (2.50); with $N = 5$ and $\gamma = 5$ dB.

[10] Identical Eigenmodes of MIMO channel obtained by employing GMD.

With waterfilling the power is allocated preferably to the eigenmodes that have a good SNR. This is optimum from the point of view of the theoretical capacity. However, it requires that the transmitter can use a Gaussian alphabet. This implies that the constellation size, and thus the peak to average ratio, has to be unlimited. For the case of a finite-modulation alphabet, it might be preferable to use a different power allocation strategy. The capacity per stream is limited by where is the size of the symbol alphabet. It is thus wasteful to assign more energy to one stream that can be actually exploited by the alphabet. In that case 'giving to the poor' principle is preferable [1].

The probability density function (Pdf) of each eigenmode obtained via SVD and GMD is estimated by exploiting a numerical histogram method of Pdf estimation referred to as the Kernel density estimation method[11] [4]. The estimated Pdfs of the eigenmodes of MIMO system with $N = M = 6$ are shown in Figure 2-12. The SVD and GMD are employed to decompose the MIMO channel into independent and parallel sub-channels. From the Pdf curves, it is also observed that the eigenmodes obtained via SVD showing variable behaviour. The eigenmodes $L = 4,5,6$ are the best eigenmodes as compare to $L = 1,2,3$. That is why we need to employ bit allocation process to assign appropriate power to the eigenmodes. On the contrary, since the eigenmodes obtained via GMD are identical, the Pdfs of the eigenmodes are also identical and hence every eigenmode is contributing a wide range of capacities around the mean behaviour of the MIMO channel.

[11] MATLAB command 'ksdensity' is used to compute the density estimate using kernel-smoothing method.

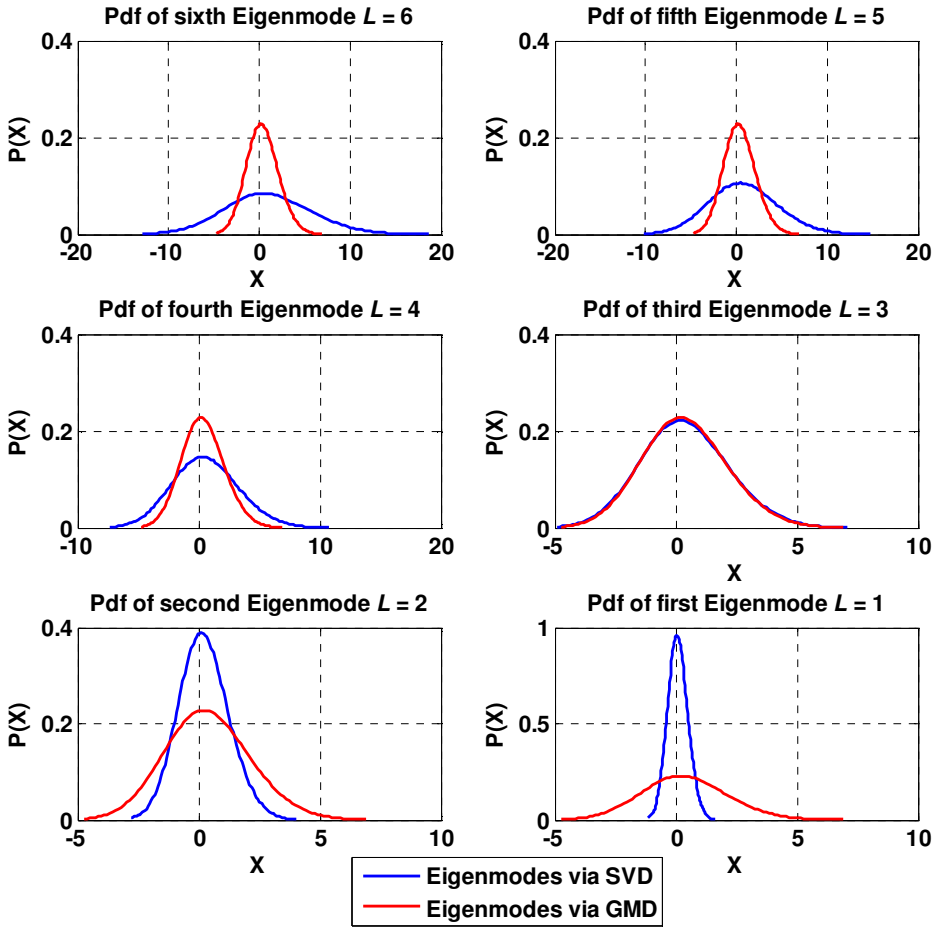

Figure 2-12: The Pdfs of the Eigenmodes of MIMO system $(N,M)=(6,6)$: the red curves shows Pdfs of Eigenmodes obtained via GMD (Identical Eigenmode); the blue curves shows Pdfs obtained via SVD (variable eigenmode with the eigenmode $L=1$ is the weakest eigenmode and $L=6$ is the strongest eigenmode).

2.11 Conclusions

Efficient and less complex non-linear decomposition technique referred to as GMD is used for the formation of identical, parallel and independent sub-channels over Rayleigh flat-fading MIMO wireless networks. The comparison of GMD and SVD based transmission design using BER performance curves has been done. The effectiveness of the strategy is observed for various numbers of transmitting and receiving antennas. It is found that in SVD based transceiver design we cannot use the same constellation among all parallel sub-channels. Therefore, it involves the use of adaptive bit allocation to match the capacity of each sub-channel which increases the complexity. A trade-off is always required to be defined between the capacity and the BER when dealing with SVD based strategy. On the other hand, for GMD technique, the same constellation with moderate size e.g. 16-QAM- or 64-QAM can be used to match the capacity of most of the sub-channels. Results of new MIMO IETS ensure superior performance due to BER and sum-rate in comparison with conventional MIMO transmission system.

Chapter 3
The Circular Gaussian Cellular MAC (C-GCMAC)

3.1 Introduction

MIMO technology provides substantial gains over single antenna communications systems. The cost of deploying multiple antennas at the mobile terminals in a network can be prohibitive, at least for the immediate future. Distributed MIMO is a means of realizing the gains of MIMO with single antenna terminals in a network allowing a gradual migration to a true MIMO network. The approach requires some level of cooperation between the network terminals. The cooperating terminals form a virtual antenna array that leverages the gains of MIMO in a distributed fashion [1]. The concept is applied to the present cellular networks. Toward this end, in the last few decades, numerous papers have been written to analyze various cellular models using information theoretic arguments to gain insight into the implications on performance of the system parameters. For an extensive survey on this literature, the reader is referred to [27] and [28] and references there in. In one of the first papers to exploit the multi-user information theoretic principles, Wyner [29] introduced a simple yet tractable model. This model will be henceforth referred to as the Gaussian Cellular Multiple Access Channel (GCMAC). The model forms the basis of the models considered in later Chapters of this thesis. In this Chapter, we proposed an empirical channel model based on the results of the trials carried out in Glasgow city centre. The proposed empirical model is closer to the realistic cellular scenario. Another important contribution in this chapter is the mathematical modelling of a single user and the multi-user channel based on the results of experimental trials. This model incorporates the variable channel slow gain

among the mobile terminals and the base stations which is contrary to Wyner's assumption [27], [28] and [29].

This Chapter first presents an insight to cellular networks to explain the evolution of cellular networks and current infrastructure in § 3.2. Next, we explain the concept of Cellular MIMO Networks (CeMNets) in § 3.3. Later in § 3.4, we review the strategies and useful concept to create a distributed cellular MIMO systems in present cellular setup. This Section reviews the cooperation technique in cellular networks. Next, we presents the Gaussian multiple access channel in § 3.5. In § 3.6, a relevant background information regarding Wyner's MAC model and circular GCMAC (C-GCMAC) is introduced. This Section also identified the existence of circular arrangement of the base stations in Glasgow city centre; § 3.7 present an Empirical modelling of the channel slow gain matrix. This Section also explains the trial methodology and the experimental setup. In § 3.8, results of the experiments carried out in Glasgow city are presented and discussed. In § 3.9, we present the mathematical models for a single user and the multi-user scenarios which are based on the results of experiments, conclusions to this Chapter are given in § 3.10.

3.2 An Insight to Cellular Networks

Wireless networks may be broadly classified as cellular or ad hoc networks. A cellular network is characterized by centralized communication – multiple users within a cell communicate with a base station that controls all transmission/reception and forwards data to the mobile users. On the contrary, in ad hoc networks, all terminals are on an equal footing – any terminal can act as a sender or receiver of data or as a relay for other transmission. This Section reviews the employment of MIMO technology in wireless cellular networks. Later in Section 3.3, we discuss a new form of technology, known as distributed MIMO and summarize the recent development in this area.

When mobile telephony was introduced in the 1970s, the efficient use of the spectrum (available bandwidth) was important to achieve a large capacity (the capacity here refers to the number of users served) for the whole network. The cellular concept was proposed which allowed the available spectrum to be reused in

different parts of the network. The whole area of the network is divided into small entities known as cells, with a base station (BS) at the centre. The neighbouring BSs in the network are provided with different groups of frequency channels to avoid interference between them. The same group of frequencies are reused at a distance in some other cells to keep the interference at a minimum possible level. When the demand increases for more users, the numbers of BSs are increased by shrinking the cells without requiring the additional radio spectrum [10] and [16].

In addition, the transmit power is kept as low as possible to avoid the interference. This concept of allocating channels to different cells such that interference is kept at a minimum is known as channel reuse or frequency reuse. The reuse scheme attempts to use the spectrum as efficiently as possible in order to provide the maximum possible network level capacity [6] and [13].

There can be many different causes of interference in a cellular network. It may be because of another user in the same cell operating in an adjacent frequency band, other links operating in the same frequency band or a non-cellular system that may be leaking energy in a cellular frequency band. Based on the possible sources, interference in a cellular network can be of two types [26]; one is co-channel interference and the other is adjacent channel interference. Co-channel or inter-cell interference results from the same band of frequencies reused in a nearby cell. In practice, the cells with the same frequency band have to be a certain minimum distance apart to keep the level of interference below a critical level, so that the communication can be reliable [26].

The interference from a frequency band used in the same cell or nearby cell which is adjacent to the desired frequency band is called adjacent channel interference. It arises from non-orthogonal channelization (e.g., CDMA scheme) within a cell (also known as intra-cell interference). In case of orthogonal channelization (e.g., TDMA, FDMA or orthogonal CDMA), it is mainly due to filtering, in which interference leaks from the adjacent frequencies into the pass band. With the advent of more sophisticated hardware design, it is possible to avoid adjacent channel interference [25], [26] and [127].

Different techniques have been proposed to mitigate the effects of interference. In addition to reuse partitioning, power control has also been considered

[8], [25] and [42]. The received signal on a given link is monitored to satisfy a desired Signal to Interference and Noise Ratio (SINR) constraints with the minimum transmit power. This not only helps in reducing the interference but also prolongs the battery life of a mobile unit. Any reduction in the interference will also help in increasing the capacity of the network and its performance. Passive techniques have been developed to mitigate the interference in cellular networks. It includes cell splitting or sectorization, smart (directional) antennas and dynamic resource allocations [24]. With the advent of advanced digital communication systems and signal processing techniques, a form of interference mitigation has been developed known as the multi-user detection [72]. This is about receiver design (say, at the BS) where the desired signal is jointly detected with some or all interference (using the known statistical knowledge about the interference), so that the detected interference is cancelled or nulled out. Depending on the number of interferers and on the type of detector used at the BS, there is trade-off between the complexity and performance of these detectors. A limited form of these detectors can also be used in mobile devices to cancel only the dominant interferers [127].

Due to the presence of co-channel interference, cellular network is a competitive environment where each link of interest between a user and BS has to compete for network resources with other links. To be completely realistic, it is necessary to take account of many issues, and to include many parameters, such as the transmit power and the number of antennas available at each mobile and BS, the propagation environment and its effect on every link in the network, whether the channel and interference conditions are known precisely, and if so, at which end of the link, whether or not there is BS cooperation etc [136] and [137]. The inclusion of all parameters and the precise modelling of all channel conditions can obscure insightful analysis. One way to get around this problem is to ignore the less important parameters and consider only the most important ones, which simplifies the system model. A number of such models have been proposed and used to analyze the cellular networks [93], [94], [95] and [98].

Toward this end, numerous cellular models have been formulated and analyzed using information theoretic principles. One such model that captures the essence of the uplink of a cellular channel is the Cellular Gaussian Multiple Access

Channels (GCMACs). The GCMAC was formulated by Wyner in [29] to model the uplink of a cellular network, and while being somewhat realistic, it nevertheless captures enough of the essential ingredients of a cellular network so that its analysis provides a meaningful insight to the channel's behaviour.

3.3 Cellular MIMO Networks (CeMNets)

In a cellular wireless communication network, the multiple users may communicate at the same time and/or frequency. The more aggressive the reuse of time and frequency resource, the higher the network capacity will be, provided that transmitted signals can be detected reliably. Multiple users may be separated in time (time division) or frequency (frequency division) or code (code division). The spatial dimension in MIMO channels provides an extra dimension to separate users, allowing more aggressive reuse of time and frequency resources, thereby increasing the network capacity [127].

Figure 3-1 shows the schematic of a cell in a MIMO cellular network. A BS equipped with N antenna communicates with K users, each equipped with N antennas. The channel from the base station to the mobile users (downlink) is the Broadcast Channel (BC) while the channel from the users to the base-station (the uplink) is the Multiple Access Channel (MAC). The set of rate-tuples $\left(R_1, R_1, \cdots, R_M\right)$ that can be reliably supported on the downlink or uplink constitutes the capacity rate region for that link. Recently, an important duality has been discovered between the rate regions for the downlink and uplink channels [125], [126], [87] and [88]. This result along with other capacity results for the multi-user MIMO systems will be discussed in Chapter 5.

In order to understand the possible gain from the MIMO technology in the multi-user environment, consider the uplink of a cellular MIMO system where all the users simultaneously transmit independent data streams from each of their transmit antennas, i.e., each user signals with spatial multiplexing. To the BS, the users combined, appear as the multi antenna transmitter with KN antennas. Thus, the effective uplink channel has a dimension of $N \times KN$.

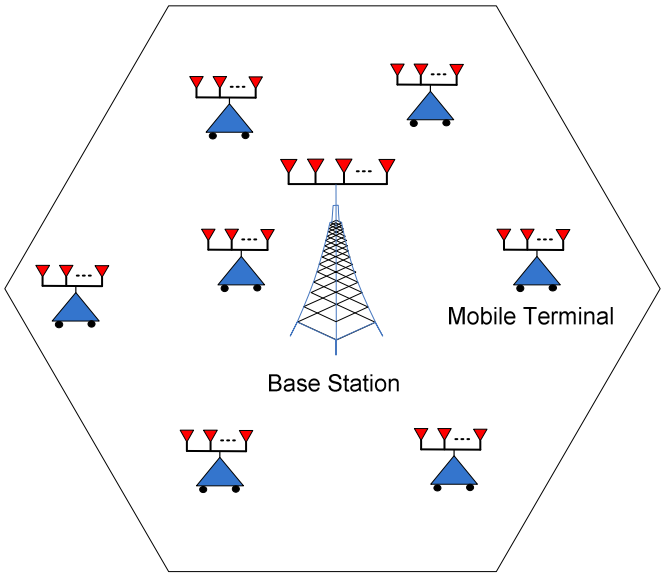

Figure 3-1: CeMNets: A base-station with N antennas communicates with K users, each equipped with N antennas.

This effective channel will have a considerably different structure from the single user MIMO channel due to path loss and shadowing differences between the mobile users. However, with rich scattering and $N > M$, we can expect that the spatial signatures of the mobile users are well separated to allow reliable detection. Using the multi-user zero forcing (ZF) receivers will allow perfect separation of all the data streams at the base station, yielding the multi-user multiplexing gain of KN. A similar thought experiment can be applied for the downlink, where the BS exploits the spatial dimension to beam information intended for particular user towards that user and steers nulls in the directions of the other users, thus completely eliminating interference [1], [54] and [42].

3.4 Cellular Cooperation – State of The Art Technique

One of the most prominent challenges of providing high rate and reliable transmission in aggressive wireless environments is the scarcity of radio resources, which includes but not limited to power, spectrum, and time. Over the last decade, significant work has been done to explore new radio resources [8], [13] and [127]. For an example, MIMO techniques [6] and [13] are extensively discussed to accommodate simultaneous transmissions via different antenna pairs and thus explore resource in space domain as discussed in the review of Chapter 2. The second example is cognitive radio [25], where spectrum of primary users (e.g. TV, microphone) can be occupied by secondary users (e.g. WLAN system subscribers) as long as the transmissions do not affect the primary users. On the other hand, a large amount of work has also been attracted to design efficient scheduling algorithms that best utilize existing radio resources. One of the most influential results in this area is cooperative communication [1], [8], [25] and [26] where the mobile users and the base stations in cellular network cooperate themselves to improve the system performance considerably.

Recent research interests on cooperative communications are mostly derived from extensive results on the MIMO communications. When the multiple antennas are not available at the mobile handset, cooperative communications can imitate the signal processing and coding design developed in the MIMO communications. The approach requires some level of cooperation between network terminals. This can be accomplished through suitably designed protocols [120], [121], [122], [123] and [124]. The cooperating terminals form a virtual antenna array as shown in Figure 3-2. This scheme leverages the gains of the MIMO in a distributed fashion. Substantial performance gains can be realized through this approach. The concept may be applied to both cellular as well as ad hoc wireless networks. Furthermore, by assuming cooperation at the BSs, the geographically dispersed BSs can be considered as a single receiver (in uplink transmission) and a single transmitter in downlink transmission with the multiple antennas. Similarly, the mobile users can also be capable of sharing the messages with each other. The resultant cellular network can be regarded as a *virtual cellular MIMO network* [130] and [141]

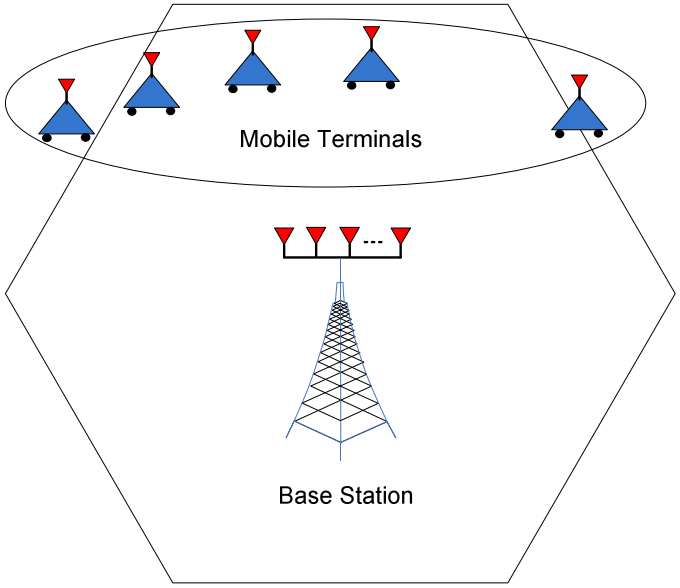

Figure 3-2: Distributed MIMO: multiple users cooperate to form a virtual antenna array that realizes the gain of MIMO in a distributed fashion.

Base station cooperation has been shown to increase the capacity and reduce the BER under the current network infrastructure [1], [8], [70], [106], [107] and [134]. Assuming full base station cooperation in Wyner circular cellular setup, the multiple base stations can be considered as a single base station with multiple geographically dispersed antennas [8]. The uplink from the mobile user to the base station is then modelled as MIMO MAC and the downlink is modelled as MIMO BC [1]. The main idea is to form a virtual MIMO network by exploiting the intra-cell TDMA[1].

Analysis of the Multi Cell Processing (MCP) i.e. BS cooperation has been so far mostly based on the assumption that all the BS in the network are connected to the central processor via links of unlimited capacity [106] and [107]. In this case, the set of BSs effectively act as the multi antenna transmitter (downlink) or receiver (uplink) with the caveat that the antennas are geographically distributed over a large

[1] Note that circular form of arrays is considered among the best array configuration for next generation of Cellular MIMO Networks (CeMNets).

area. Since the assumption of unlimited capacity links to a central processor is quite unrealistic for large networks, more recently, there have been attempts to alleviate this condition by considering alternative models. In [100], a model is studies where only a subset of neighbouring cell is connected to the central processor for joint processing, in [104] and [105] a topological constraint is imposed in that there exist links only between adjacent cells and message passing technique are implemented in order to perform joint decoding in uplink. Moreover, [139] focuses on the uplink and assumes that the links between all the BSs and a central processor has a finite capacity. The reader is referred to [101], [102] and [103] for a different framework which deals with practical aspects of finite capacity backhaul cellular systems incorporating MCP.

Information theoretic analysis of cellular networks by exploiting MT cooperation is a more recent development. Generally, depending on the methods that the relays retransmit the message, cooperative protocols can be divided into three categories: Amplify-and-Forward (AF), where the relays simply retransmit by amplifying the received signal which is noise-corrupted; Decode-and-Forward (DF), where the relays decode the message and retransmit either the same codeword or the another codeword of the message; Compression-and-Forward (CF), where the relays decode the message and retransmit a quantized version of the message. References include [106] and [107] where the uplink of a two hop mesh network is studied with AF cooperation (half-duplex and full-duplex respectively) and [94] (half-duplex) [95] (full-duplex) where DF cooperation is investigated (a comprehensive tutorial on cooperation technique can be found in [108].

3.5 Gaussian Multiple Access Channels (MAC)

The classical Gaussian Multiple Access Channel (MAC) arises when two or more users intend to send information independent of each other, with perfect symbol and frame synchronization, across the same channel to a central receiver in the presence of AWGN. Furthermore, the classical Gaussian MAC assumes each user and the central receiver have a single antenna [27] and [28]. From this point, all channels analyzed in this thesis can be viewed as Gaussian MACs employing M

users each with a single transmit antenna and a central receiver with N receive antennas. Therefore, as depicted in Figure 3-3, an input symbol x_m represents the symbol transmitted by user m. The reason for choosing this model will become clearer in the later chapters. For the purpose of this chapter it suffices to assume a Gaussian MAC of this form. This type of Gaussian MAC is formally defined as follows.

Definition 3.5.1: (Gaussian MAC). *A Gaussian MAC may be modelled as* [96].

$$\boldsymbol{y} = \mathbf{H}\boldsymbol{x} + \boldsymbol{z} \tag{3-1}$$

which defines a scenario with M users (each with a single transmit antenna) where each user intends to send information with perfect symbol and frame synchronism across the same channel to a central receiver with N receiver antennas over complex channel matrix $\mathbf{H} \in \mathbb{C}^{N\times M}$. Furthermore, $\boldsymbol{z} = \left(\boldsymbol{z}_1, \boldsymbol{z}_2, \cdots, \boldsymbol{z}_N\right)^T$ is a $N \times 1$ vector of i.i.d *zero mean* c.c.s *Gaussian noise samples with variance σ^2, and $\boldsymbol{y} = \left(\boldsymbol{y}_1, \boldsymbol{y}_1, \cdots, \boldsymbol{y}_N\right)^T$ is a $N \times 1$ vector representing the channel output. Hence, $\boldsymbol{x} = (x_1, x_2, \cdots, x_M)^T$ are the transmitted symbols, where x_m is the m^{th} user's transmitted symbol. Furthermore, the users are assumed to transmit independent, zero mean complex symbols, each subject to an individual average power constraint, i.e.*

$$\mathbb{E}[x_m x_m^*] \le P_m, \qquad \forall\, m = 1, 2, \cdots, M \tag{3-2}$$

Hence the covariance $\boldsymbol{\Phi}$ is constrained to the set of non-negative matrices with $\Phi_{m,m} \le P_m$ for all $m = 1, 2, \cdots, M$. It is assumed that each user has statistical CSI knowledge, which translates to full CSI if $\mathbf{H}$ is deterministic. Furthermore, it is also assumed that the receiver has access to every user's codebook as well as full knowledge of the CSI.

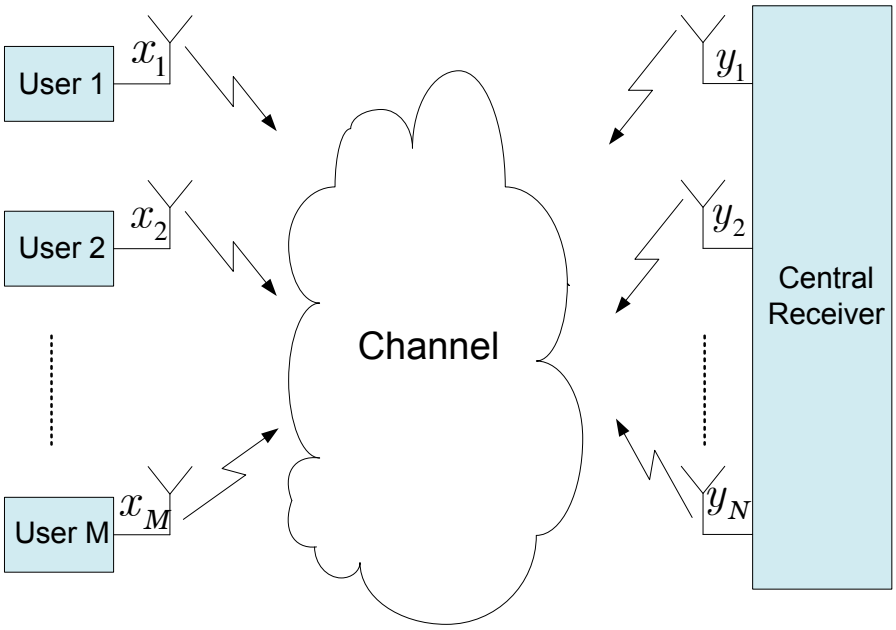

Figure 3-3: Graphical interpretation of Gaussian Multiple access channel (MAC) in Definition 3.5.1. The grey cloud represents the inner working of Gaussian linear vector memory less channel.

3.6 Wyner C-GCMAC Modelling

In [29], Wyner incorporated the fundamental aspects of cellular networks into the framework of the well known Gaussian MAC to form the Gaussian Cellular Multiple Access Channel (GCMAC). The Wyner's insightful model of cellular network used a single parameter to represent the strength of inter-cell interference. Figure 3-4 illustrates the two cellular network scenarios; one is an infinite linear array of cells each equipped with a base station (BS) at the centre of each cell and the other is a finite array of cells arranged in circular fashion and equipped with a BS at the centre of each cell. A cell represents an area of coverage within which a number of users transmit information to a cell site receiver[2] also located within the cell. Assuming that all users use the entire available time and frequency resource, and then when a single user transmits information to its intended BS, it interferes with:

[2] In the context of terrestrial cellular communication network, a cell site receiver is also referred to as a base station (BS) and is interchangeably used throughout the thesis.

other users located within the same cells which are referred to as intra-cell interfering users; and users located in each of the adjacent cell which is referred to as inter-cell interfering users. In Figure 3-4, the sources of intra-cell and inter-cell interference at the BS of interest are indicated by solid and dashed arrows respectively.

Consider a circular version of Wyner cellular model (i.e. Wyner linear array of cells wrap to form a circle as shown in Figure 3-4b). This model was pioneered by Wyner in [29] under a very simplified channel gain assumption, where the path gain to the closest BS is 1, the path gain to adjacent BSs is Ω and it is zero elsewhere. Wyner considered optimal joint processing of all base stations. Later, Shamai and Wyner [27] and [28] considered a similar model with frequency flat fading and more conventional decoding schemes, ranging from the standard separated base station processing to some forms of limited cooperation. A very large literature followed and extended these works in various ways (for example see [31] and [32]).

We focus on the uplink of a conventional system, such that each BS decodes only the users in its own cell and treats inter-cell interference as noise. We extend the model in two directions: 1) we consider realistic propagation channel determined by a position-dependent path loss, and then 2) we derive the channel model for single user and multi-user Cellular MIMO Networks (CeMNets) for variable channel slow gain among the MTs and the BSs.

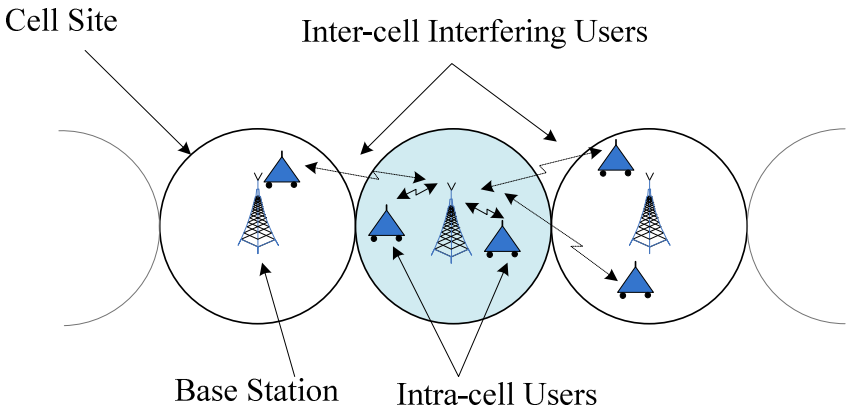

(a)

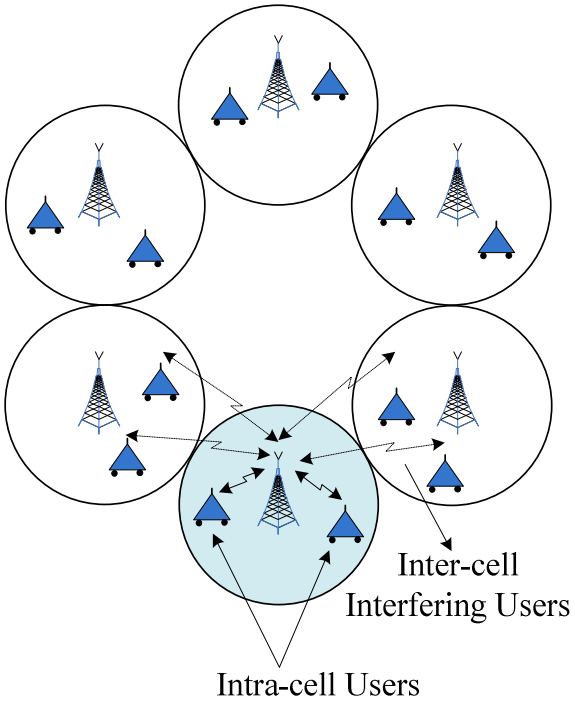

(b)

Figure 3-4: Graphical interpretation of intra-cell users (solid line) and inter-cell interfering users (dotted line): (a) linear arrangement of cells; (b) circular cellular arrangement formed by wrapping the linear cells into circle.

3.6.1 System Model

The existence of circular cellular setup found in Glasgow city centre is shown in Figure 3-5. The details of each BS are summarized in Table 3-1 [140]. The graphical interpretation of this setup with hexagonal cells (which is more realistic model of cell representation) is shown in Figure 3-6 with $N = 6$ cells and $N = 6$ BSs, arranged in a circular fashion. Assuming each cell contains K users such that the system contains $M = NK$ users. At given BS, the amplitude of the signals from the inter-cell users in two adjacent cells is scaled by channel slow gain $\Omega \in \left(0,1\right)$. It is assumed that the channel slow gain for every user located in adjacent cells of given BS are offering equal inter-cell interfering levels, see [31], [32], [33] and [133] and references there in. Interference from the users in cells located further than adjacent cells is considered negligible [93] and [94].

It is assumed that the channel slow gain for every user located in adjacent cells of given BS are offering equal inter-cell interfering levels, see [31], [32], [33] and [133] and references there in. Interference from the users in cells located further than adjacent cells is considered negligible.

Thus, assuming a perfect symbol and frame synchronization, at a given time instant the received signal at each of the BS is [3] [96] and [142]

$$y^j = \sum_{l=1}^{K} h^l_{B_j T_j} \, x^l_j + \sum_{i=\pm 1} \sum_{l=1}^{K} h^l_{B_j T_{j+i}} \, x^l_{j+i} + z_j \tag{3-3}$$

where $\{B_j\}_{j=1}^{N}$ are the BSs in each cell and $\{T_j\}_{j=1}^{N}$ are the MTs in each cell and x^l_j is the transmitted complex symbol from K^{th} transmitter in cell j^{th} and each z_j is an i.i.d. c.c.s. Gaussian noise random variable with zero mean and variance σ_z^2.

[3] $T_{j+1} \triangleq T_{j+1} \bmod N$.

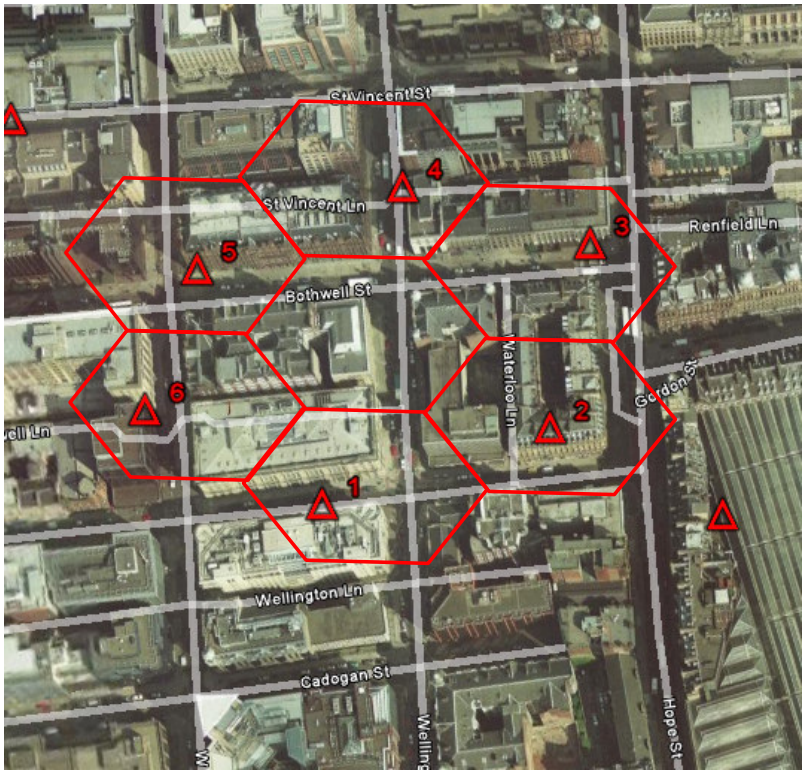

Figure 3-5: Snap shot of Glasgow city centre showing circular cellular setup. Each cell at least has one base station to cover the entire region. *Courtesy of Google Earth.*

Table 3-1: Details of BS arranged in circle in Glasgow City centre [140].

BS No.	h_b (m)	f_c (MHz)	Transmitter power (dBm)
1	7	1800	39
2	8	1800	40.8
3	8	1800	35.7
4	8	1800	46.1
5	7	1800	39
6	8	1800	36.8

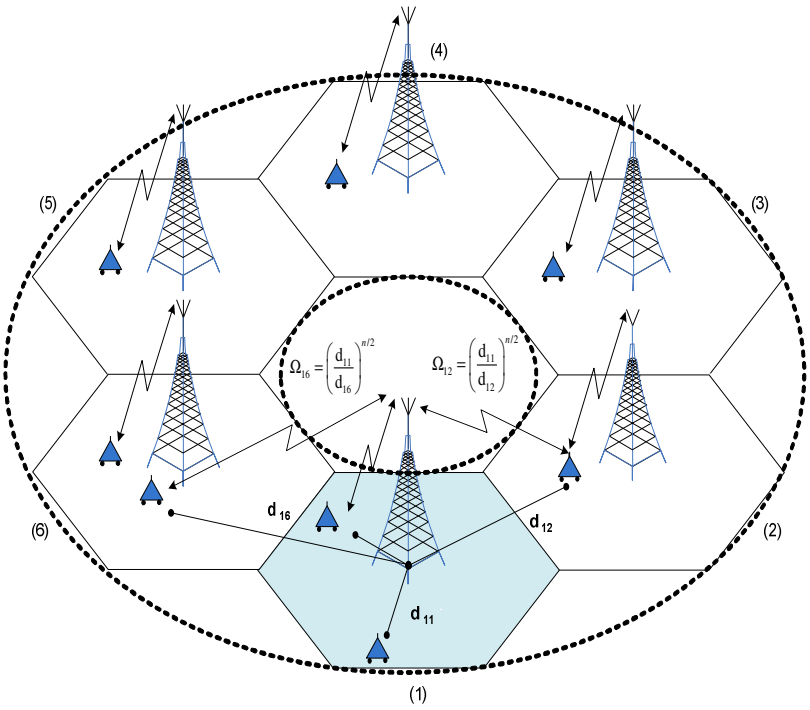

Figure 3-6: Graphical interpretation of circular cellular setup shown in Figure 3-5. Intra-cell users are representing by solid arrows and inter-cell interfering users are represents by dotted arrows. The calculation of channel slow gain between user in cell #2 and BS #1 and user is cell #6 and BS #1 is shown.

Each transmitted symbol is subject to the average power constraint $\mathbb{E}\left[x_j^l\, x_j^{l\,*}\right] \le P$ for all $(j,l) = (1 \cdots\cdots N) \times (1 \cdots\cdots K)$. The $h^l_{B_jT_j}$ is the channel gain between MTs T_j and BSs B_j.

We model the channel gain as a Hadamard product of two terms $h^l_{B_jT_j} = \left(g^l_{B_jT_j} \circ \Omega^l_{B_jT_j}(d)\right)$ where $\Omega^l_{B_jT_j}(d)$ denotes frequency flat path gain that depends on distance between the BS and MTs, $g^l_{B_jT_j}$ is the "small scale" fading term that depends on local scattering environment around the MTs and $(\circ)$ denotes

the Hadamard product of the channel fading gain $g^{l}_{B_jT_j}$ and the channel slow gain $\Omega^{l}_{B_jT_j}$.

These two components of the resultant channel are mutually independent as they are due to different propagation effects. We assume that the path losses change in time on a very slow scale, and can be considered as random, but constant, over the whole duration of transmission. In contrast, the small-scale fading changes relatively rapidly, even for moderately mobile users [1]. We assumed a flat fading channel mode which corresponds to when the signal bandwidth is much smaller than the coherence bandwidth and hence in discrete time the fading impulse response can be modelled as single tap [30]. In addition to the parameters and assumptions, let $g^{l}_{B_jT_j}[i]$ denote the fading coefficient of the signal from user l of the cell j received at the cell site receiver j at a given time instant i. These complex random processes model the time varying changes which are not provided to the transmitter due to the lack of adequately fast reliable feedback link [72] and [127], and are assumed to be independent, strictly stationary and ergodic. Furthermore, it is assumed that the fading processes each have unit power i.e., $\mathbb{E}\left[g^{l}_{B_jT_j}[i]\, g^{l}_{B_jT_j}[i]^{*}\right]=1$ (where the expectation is over the discrete time i). Therefore, omitting the time index i, the C-GCMAC model in (3.3) can be extended to account for fading as follows,

$$y^{j}=\sum_{l=1}^{K}\left(g^{l}_{B_jT_j}\circ\Omega^{l}_{B_jT_j}\right)x^{l}_{j}+\sum_{i=\pm1}\sum_{l=1}^{K}\left(g^{l}_{B_jT_{j+i}}\circ\Omega^{l}_{B_jT_{j+i}}\right)x^{l}_{j+i}+z_{j} \qquad (3\text{-}4)$$

The empirical calculation of $\Omega^{l}_{B_jT_j}$ is covered later in the Section 3.7. For notational convenience the entire signal model over C-GCMAC can be written in matrix form as (3.1), where $\boldsymbol{y}\in\mathbb{C}^{N\times1}$, $\boldsymbol{x}\in\mathbb{C}^{NK\times1}$, $\boldsymbol{z}\in\mathbb{C}^{N\times1}$ is c.c.s. Gaussian noise process with $\mathbb{E}[\boldsymbol{z}]=0$; $\mathbb{E}[\boldsymbol{z}\boldsymbol{z}^{H}]=\sigma_z^2\mathbf{I}_N$ and $\mathbf{H}\in\mathbb{C}^{N\times NK}$ which is defined as

$$\mathbf{H}\triangleq\left(\mathbf{G}\circ\boldsymbol{\Omega}\right) \qquad (3\text{-}5)$$

where $\mathbf{\Omega} \in \mathbb{R}^{N\times KN} \mid 0 < \Omega_{B_jT_j}^{l} \leq 1$ and $\mathbf{G} \in \mathbb{C}^{N\times NK} \mid g_{B_jT_j}^{l} \in \mathcal{CN}(0,1)$.

In component wise notation, the $N \times NK$ channel fading matrix $\mathbf{G}_{N,K}$ is block-circulant matrix and defined by[4]

$$\mathbf{G}_{N,K} = \begin{pmatrix} \boldsymbol{g}_{B_1T_1} & \boldsymbol{g}_{B_1T_2} & 0 & \cdots & \boldsymbol{g}_{B_1T_N} \\ \boldsymbol{g}_{B_2T_1} & \boldsymbol{g}_{B_2T_2} & \boldsymbol{g}_{B_2T_3} & & 0 \\ 0 & \ddots & \ddots & \ddots & \vdots \\ \vdots & & \boldsymbol{g}_{B_{N-1}T_{(N-1)-1}} & \boldsymbol{g}_{B_{N-1}T_{N-1}} & \boldsymbol{g}_{B_{N-1}T_{(N-1)+1}} \\ \boldsymbol{g}_{B_NT_{N+1}} & 0 & \cdots & \boldsymbol{g}_{B_NT_{N-1}} & \boldsymbol{g}_{B_NT_N} \end{pmatrix} \tag{3-6}$$

where $\boldsymbol{g}_{B_jT_j} \in \mathbb{C}^{1\times K}$ is row vector representing the fading between the j^{th} BS and K users in the j^{th} cell. For example, $\boldsymbol{g}_{B_1T_1} = \left(g_{B_1T_1}^{(1)}, g_{B_1T_1}^{(2)}, \cdots, g_{B_1T_1}^{(K)}\right)$ is the fading vector between the BS #1 and K intra-cell users in cell #1. Similarly, $\boldsymbol{g}_{B_1T_2} = \left(g_{B_1T_2}^{(1)}, g_{B_1T_2}^{(2)}, \cdots, g_{B_1T_2}^{(K)}\right)$ is the fading vector between the BS #1 and K inter-cell interfering users in adjacent cell #2.

Also, the channel fading matrix can be expressed in matrix notation as

$$\mathbf{\Omega}_{N,K} = \begin{pmatrix} \Omega_{B_1T_1} & \Omega_{B_1T_2} & 0 & \cdots & \Omega_{B_1T_N} \\ \Omega_{B_2T_1} & \Omega_{B_2T_2} & \Omega_{B_2T_3} & & 0 \\ 0 & \ddots & \ddots & \ddots & \vdots \\ \vdots & & \Omega_{B_{N-1}T_{(N-1)-1}} & \Omega_{B_{N-1}T_{N-1}} & \Omega_{B_{N-1}T_{(N-1)+1}} \\ \Omega_{B_NT_{N+1}} & 0 & \cdots & \Omega_{B_NT_{N-1}} & \Omega_{B_NT_N} \end{pmatrix} \tag{3-7}$$

[4] Note that the subscript $\mathbf{G}_{N,K}$ refers to the number of cells (N) and users per cell (K) of a C-GCMAC, not a number of rows and columns of a matrix as usually appears in matrix analysis texts. This nomenclature for circular channel matrix is used consistently throughout this thesis.

where $\Omega_{B_jT_j} \in \mathbb{R}^{1\times K}$ is row vector representing the channel average gain between the j^{th} BS and K users in the j^{th} cell. The Wyner model employed very crude approximation of channel slow gain with no path loss variability across the adjacent cells [27], [28] and [29]. Therefore, the inter-cell interfering users in each of the adjacent cell offering equal channel slow gain to the BS of interest. In reality, the users can be at the edge of the adjacent cell or near the BS of interest and hence offering variable levels of interferences to the BSs. By exploiting Wyner's assumption of equal slow gain among the MTs and BSs i.e., the slow gain of intra-cell MTs to the respective BS is 1 and the slow gain of every inter-cell MTs located in two adjacent cells to the BS in the middle cell is equal. Therefore, the channel slow gain matrix of (3.8) can be rewritten as

$$\mathbf{\Omega}_{N,K} = \begin{pmatrix} 1_K & \Omega 1_K & 0 & \cdots & \Omega 1_K \\ \Omega 1_K & 1_K & \Omega 1_K & & 0 \\ 0 & \ddots & \ddots & \ddots & \vdots \\ \vdots & & \Omega 1_K & 1_K & \Omega 1_K \\ \Omega 1_K & 0 & \cdots & \Omega 1_K & 1_K \end{pmatrix} \tag{3-8}$$

where $1_K = \left(1,\cdots,1\right)$ denotes $1\times K$ all ones vector such that the length of vector is the number of users per cell and $\Omega \in \left(0,1\right)$ is the slow gain among the MTs and BSs. The block circulant channel slow gain matrix of the form (3.8) can also be represented by

$$\mathbf{\Omega}_{N,K} = \mathbf{\Omega}_{N,1} \otimes 1_K \tag{3-9}$$

where $\otimes$ denotes the Kronecker product and $\mathbf{\Omega} \triangleq \mathbf{\Omega}_{N,1}$ is a $N \times N$ symmetric circulant matrix. Furthermore, using the properties of Kronecker products, it is

$$\mathbf{\Omega}_{N,K}\ \mathbf{\Omega}_{N,K}{}^{H} = K\,\mathbf{\Omega}^2 \tag{3-10}$$

The results in (3.9) and (3.10) are very useful to exploit the channel slow gain among the MTs and BS individually [142]. The topic is introduced and discussed next in the following Section.

3.7 Empirical Calculation of Channel Slow Gain

In this Section, we define the methodology of trials carried in Glasgow city centre. The process of finding the slow gain among the inter-cell and/or intra-cell MTs and the respective BSs involves the use of networking monitoring software. We used software referred to as the "Net-monitor". Net-monitor is a hidden mode on most Nokia cell phones used to measure network parameters. The mode can only be activated over a special FBUS, or MBUS cable; or in some cases over infrared [36]. We purchased the software with Field Test Display (FTD) Nokia 6230i from local vendor[5]. The FTD Nokia 6230i is a specially programmed Nokia handset to use for performing signal strength measurements in cellular networks. This tool provides us with the information about connected BSs including the channel number, cell ID and transmitting power etc. There are series of tests which provides information about the neighbouring BSs. There are several types of tests which are performed using Net-monitor. Later in this Section, we review the propagation models which are used to calculate the distance between the MT and the BS of interest. In the end of this Section, we define the normalized channel slow gain and summarize the trials scheme.

3.7.1 Experimental Trials and Methodology

The experiments have been carried out in conurbations such as Glasgow city centre. The existence of the circular cellular structure in Glasgow city centre is shown in Figure 3-5. The purpose of each of the tests we used during trials is presented in Table 3-2. The details of each of the tests utilized are enclosed in the Appendix D.

[5] Mobile Telecommunication International (MTI) UK, http://www.mti-ltd.com/UK.htm.

Table 3-2: Summary of Tests Utilized during the Trials [36]

S. No.	Test Name	Purpose of Test
1.	Test 01: *Serving Cell Information*	Shows the received signal power and the channel number of the serving cell.
2.	Test 03 - Test 05: *Selection characteristics of Serving cell and neighbour*	Shows information about the neighbouring cells including cell selection priority.
3.	Test 11: *Cell and Local Area Information*	Shows serving cell and serving network information, Mobile Country Code, Network Code, Cell ID and sector number.
4.	Test 12: *BTS Test*	Locks the mobile user to the base station of interest.

In the following sub Sections, we explain the methodology and schemes of the experiments carried out in Glasgow city centre.

- First using 'Net-monitor' software, one determines the Cell Identity (CI) code of each BS communicating with the MT. The software also displays the received signal strength (RxL) transmitted by each previously pointed out surrounding BS. More specifically, Test 01 in Net-monitor displays information related to the serving BS which includes, among others, carrier channel number (CH) used to communicate with the BS and cell ID of the serving cell. The CH is used to determine the carrier frequency (f_c) in MHz of the signal transmitted by the serving BS and received at the handset [16].

- The Test 03 in Net-monitor shows information related to the adjacent cells in terms of channel (CH) and received signal strength (RxL). The use of Test 12 allows us to force the handover by communicating directly with the adjacent

cells, or equivalently, adjacent BS, and therefore recording the associated CH and RxL.

- In order to determine the location of the BS, one uses the information available from the government [140], this updates the location of GSM and UMTS BS locations throughout the whole UK. The location of the BSs is also visible on the Google Earth. The antenna height and transmitter power of each BS involved in experiment is provided by Ofcom which are very useful for calculating the distance $d^{l}_{B_j T_j}$ between the MT and the BS. The available information for each BSs arranged in circle in Glasgow city centre is shown in Table 3-1 [140]. Using 'My Location'[6] feature provided by Google Maps, one can find out the location of MT. This feature is very helpful as it updates the MT location on Google Maps[7].

- The distance between the each BS and the MTs can be determined using one of the well known empirical propagation models. There is range of models which can be used. These models includes Hata-Okumura model, Cost 231 extended Hata's model, Walfish-Ikegami model and ECC model [1] and [8]. These models use the information about the received signal strengths as well extra information about each BS which is recorded using Net-monitor software. Some of these models also require additional information regarding the structure of the environment.

[6]The "My Location" feature is available for most web-enabled mobile phones, including Java, Blackberry, Windows Mobile, and Nokia/Symbian devices. This is beta version but Google is planning to launch it officially with effective coverage and accuracy.

[7] The "My Location" feature takes information broadcast from mobile towers near mobile phone to approximate the current location on the map - it's not GPS, but it comes pretty close.

- Once the BS-MT distance is obtained using one of the propagation models for the serving BS and each of the two adjacent BS, the normalized channel slow gain between the BS and the MTs can be determined.

- The trials have been carried out for one set of three cell i.e. one serving cell and the two adjacent cells. The similar patterns are assumed for each of the cells arranged in a circle. Due to lack of ability of device, the multi-user testing is not possible. However, we can still assume that each user in the multi-user case is offering gains to the BS of interest by different means.

3.7.2 Calculation of Channel Slow Gain

The average normalized channel slow gain between the MTs T_{j+i} in two adjacent cells and the BSs B_j, $\Omega^l_{B_jT_j}$ in (3.7) can be calculated by the path loss model given by [35]

$$\Omega^{l}_{B_jT_{j+i}} = \left(\frac{d_{B_jT_j}}{d^l_{B_jT_{j+i}}} \right)^{n/2} ; i = \pm 1 \tag{3-11}$$

where $d^l_{B_jT_j+i}$ is the distance between the K^{th} MT T_{j+i} and BS B_j as shown in Figure 3-5 and n is the path loss exponent. It is assumed that the path loss exponent for the urban cellular environment is 4 [8] and [16].

For detailed explanations of these models, the reader can consult reference [1]. Each model provides an expression of the path loss of the signal transmitted by BS transmitter (Tx) and received at the MT receiver (Rx) as a function of the distance between the two entities BS and MT.

The received signal power (RxL) and the frequency (f_c) of the signal will be measured by the handset using the network monitoring software 'Net-monitor'.

While the transmitted signal power (TxPwr) and the BS height can be retrieved from the BS data base [140]. Assume that the MT is at a distance d Km from the BS.

Let P_{Tx} denote the average power transmitted by the BS and P_{Rx} denote the average power received at the MT. Then, in a typical wireless channel, we have

$$PL\left(d\right) = P_{Tx} - P_{Rx} \tag{3-12}$$

where $PL\left(d\right)$ is the average path loss at distance d in Km.

The $d^{l}_{B_jT_j}$ in (3.11) can be determined by using one of the empirical propagation models[8]. Next, a propagation model is employed to accurately determine the distance. According to the "Sub-urban Macro" scenario which is based on the modified COST-231 Hata urban propagation model and defined in [16], distance dependant path loss can be expressed in a simplified form as

$$\begin{aligned} PL\left(d\right) = {} & \left(44.9 - 6.55\log_{10} h_b\right)\log_{10} d^{l}_{B_jT_j} + 45.5 + \\ & \left(35.46 - 1.1h_m\right)\log_{10}(f_c) - 13.82\log_{10}(h_b) + 0.7h_m + \mathfrak{C} \end{aligned} \tag{3-13}$$

$PL\left(d\right)$: path loss in dBs.

$d^{l}_{B_jT_j}$: MT-BS distance is in Km.

h_m: height of mobile phone in m.

f_c : carrier frequency in MHz.

h_b: height of BS in m.

$\mathfrak{C}$: constant factor define as

[8] First generation GSM systems operate at 900 MHz band. As the demand on the service increased, allocation of new channels to the service has been provided by assigning 1800 MHz band to the system. Hence, first system can use Hata Model for prediction since Hata Model covers frequency range of 100 to 1500 MHz. However, second system cannot. COST (COperation européenne dans le domaine de la recherche Scientifique et Technique) is a European Union Forum for cooperative scientific research which has developed COST231 model which covers frequency range of 1500 MHz to 2000 MHz [16].

$$\mathfrak{C} = \begin{cases} 0 \text{ dB} & \text{for medium city} \\ 3 \text{ dB} & \text{for metropolitian areas} \end{cases}$$

Setting these parameters to $h_b = 30$ m (effective BS height); $h_m = 1$ m; and $f_c = 1800$ MHz, the path-loss for medium city environments become, $PL\left(d\right) = 35.14 \log_{10} d^{l}_{B_j T_j} + 342.81$.

3.8 Results of Experimental Trials – Findings and Discussions

In [29], it is assumed that the path loss factor for every user in both adjacent cells is same i.e. all the users are located at equal distance from the BS of interest. For the first time, to the best of our knowledge; we extend the Wyner C-GCMAC model by assuming that all the users in both adjacent cells are experience fading with different means[9]. The channel slow gain is variable across the cell such that there are at least three classes of users in each cell. This has been tested during the trials carried out in Glasgow city centre using Net-monitor [142].

The Test 01 in Net-monitor shows that the received power at the MT is variable and is dependent on the distance between the BS of interest and MT. The signal received at the BS is the sum of the signals from intra-cell MTs and scaled version of the inter-cell MTs. The users located in the close vicinity of the BS of the interest offering higher level of interference. On the contrary, the users located at boundary of the adjacent cell are offering low or may be negligible level of interference. Using Test 12 in Net-monitor, the handset can be locked to the BS of interest such that there will be no handover to the adjacent BS even the received signal is disappeared. Exploiting this feature we able to find that when the power received level reaches -85 dBm the user is on the boundary of the cell of interest and the user is considered as an edge intra-cell MT. With the help of 'My Location' feature in Google Map it is possible to locate the current position of the MT.

[9] As would occur, for example, if the two users are at different distance from the BS.

When we moved further away from the BS of interest, the received power becomes more dissipated. It is found that when power is in the range -85 dBm and -90 dBm the user is just on the connecting edge of one of the adjacent cell. When the received power is between -90 dBm and -100 dBm, the user is almost located around the centre of the adjacent cell. Finally, when the received power is degraded more than -100 dBm the user is located at the maximum distance from the BS of interest and offers low level of interference. This exercise has been proved that the MTs in the adjacent cells do not offer equal interfering level to the BS of interest. The channel slow gain is variable across the cell as it strongly dependent on the distance between the MT and the BS of interest. Therefore, we split the cell into three zones depending on the distance between the MTs and the serving BS which are defined as follows[10]:

- **zone #1**: the near zone where interfering MT are located at minimum distance from BS of interest and offering high level of interference.
- **zone #2**: the near-far zone where inter-cell interfering MT offering moderate level of interference.
- **zone #3**: the far zone where the MTs are located at the maximum distance from the BS of interest and offering low level of interference.

The details of cell splitting into zones depending of level of interference are summarized in Table 3-3.

Table 3-3: Details of Cell Splitting

zone #	RxL (dBm)	Range of Slow Gain
1	-85 to -90	$1 > \Omega \geq 0.7$
2	-90 to -100	$0.6 \geq \Omega \geq 0.3$
3	< -100	$0.2 \geq \Omega \geq 0$

[10] Note that cell splitting throughout this thesis refers to formation of zones in each cell of Wyner C-CGMAC, not the cell splitting which is actually based on sectored antennas as in traditional cellular literature texts.

The modified circular representation of Figure 3-6 is shown as Figure 3-7. This tailored figure shows that each of the adjacent cells is split into three zones. The users close to the serving BS is considered as a maximum interfering MTs. This zone is referred to as zone #1. The users in zone #1 are at minimum distance from the serving BS and offering maximum level of interference. The users located far away from the BS of interest i.e. close to the opposite edge of the adjacent cell are considered as minimum interfering MTs. Therefore, when the users are offering minimum level of interference to the serving BS they are located at maximum distance from the BS of interest. This region of the cell located far away from BS of interest is referred to as zone #3. There are users, neither located in zone #1 nor in zone #3 i.e. the users neither located at maximum distance nor at the minimum distance from the BS of interest. The region where the users offering moderate level of interference to the BS of interest located at moderate distance is referred to as zone #2. Figure 3-7a represents a scenario when at BS #1 the signal is received from intra-cell MTs and inter-cell MTs in two adjacent cells numbered as (2) and (6).

Similarly, Figure 3-7b - Figure 3-7f shows that the signal received at next j^{th} BS in anti clock-wise direction from intra-cell MTs and inter-cell MTs in $\left(j-1\right)^{\text{th}}$ and $\left(j+1\right)^{\text{th}}$ adjacent cells. The each subsequent figure represents a $1\times NK$ row vector which constitutes a $N\times NK$ channel matrix at the end. An experimental trial reveals that the channel slow gain is variable across the cell which is contrary to the Wyner's original assumption [29]. The same has been shown in [142].

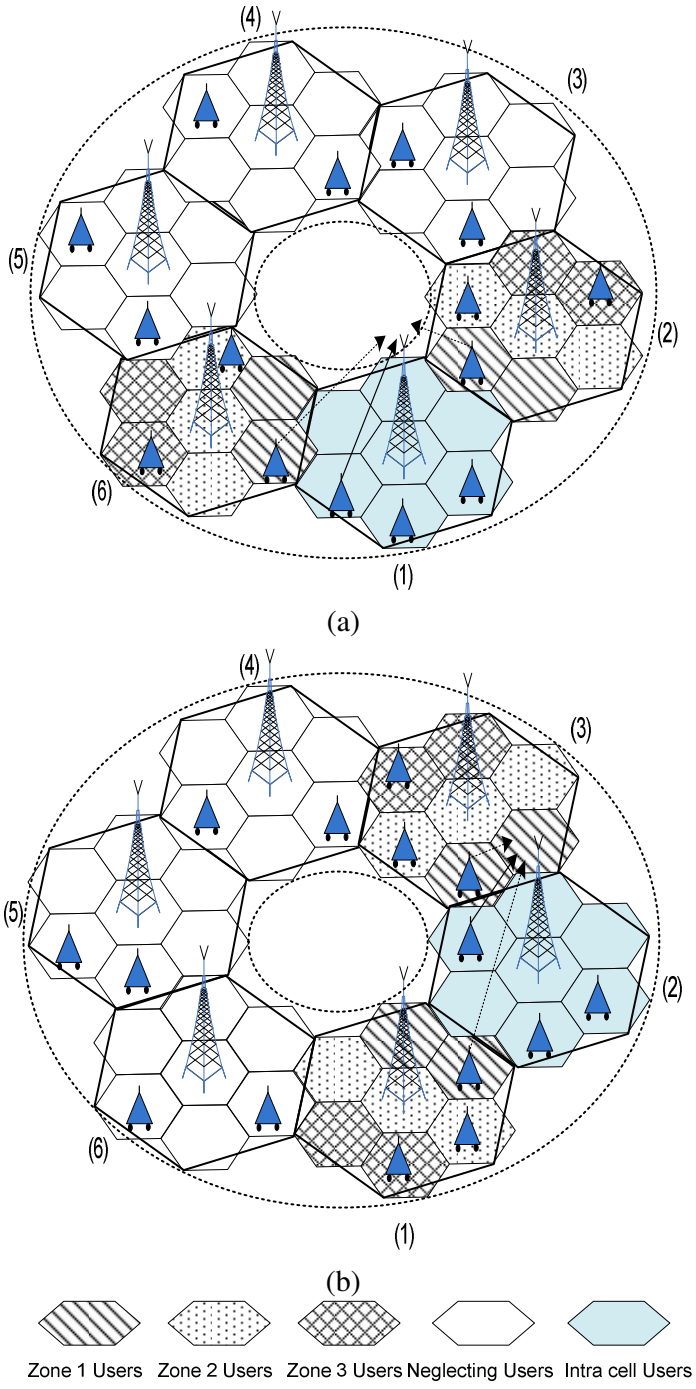

Figure 3-7: Graphical interpretation of circular cellular setup representing the division of each cell into three zones. (a) the signal is received at BS #1 from intra-cell MTs and inter-cell MTs in two adjacent cells (2) and (6); (b) the signal is received at BS #2 from intra-cell MTs and inter-cell MTs in two adjacent cells (1) and (3).

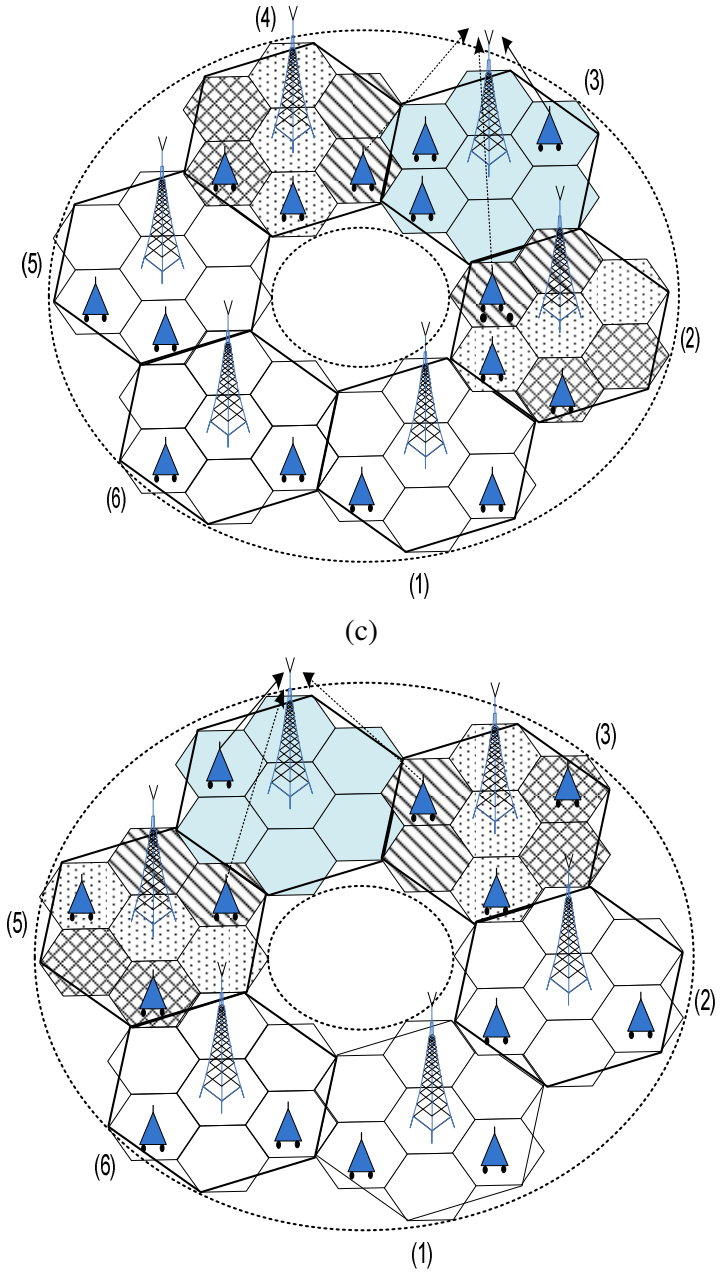

Figure 3-7: Graphical interpretation of circular cellular setup representing the division of each cell into three zones. (c) the signal is received at BS #3 from intra-cell MTs and inter-cell MTs in two adjacent cells (2) and (4); (d) the signal is received at BS #4 from intra-cell MTs and inter-cell MTs in two adjacent cells (3) and (5).

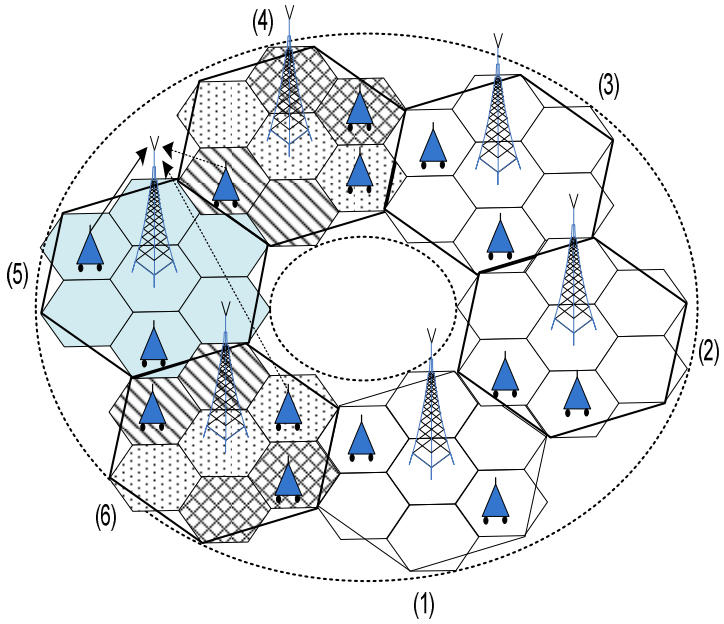

(e)

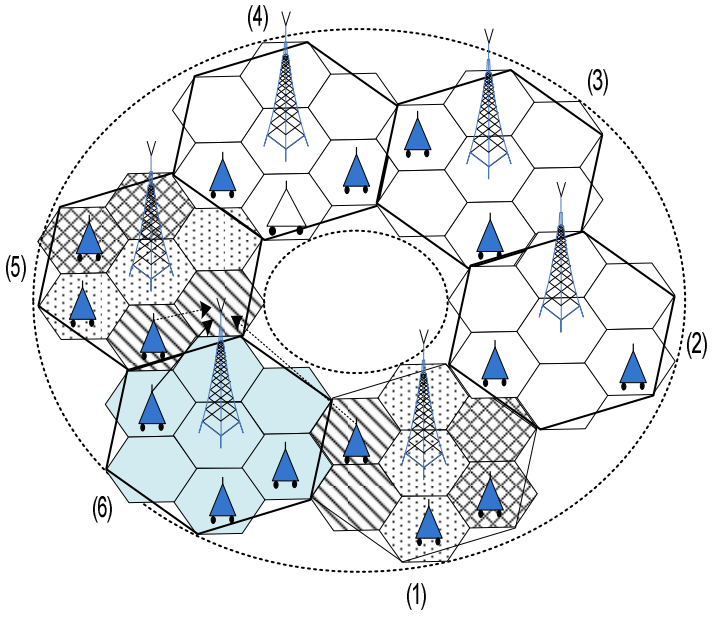

(f)

Figure 3-7: Graphical interpretation of circular cellular setup representing the division of each cell into three zones. (e) the signal is received at BS #5 from intra-cell MTs and inter-cell MTs in two adjacent cells (4) and (6); (f) the signal is received at BS #6 from intra-cell MTs and inter-cell MTs in two adjacent cells (5) and (1).

3.9 Modelling of Deterministic Channel with Variable Slow Gain

In this Section, we introduce the modelling of deterministic channel with variable slow gain among the MTs and respective BSs for a Single User Cellular MIMO Networks (SU-CeMNets) and the Multi-user Cellular MIMO Networks (MU-CeMNets) [144]. In each case, we present a set of examples to explain the variation of channel slow gain across the inter-cells and across the zones inside the cell. The same analogy will be used throughput the thesis in discussions and illustrations in later chapters. In order to understand the examples, we are presenting single user $K = 1$ and multi-user $K = 2$ and $K = 3$ scenarios separately in the following sub-Sections:

3.9.1 Single User Cellular MIMO Networks (SU-CeMNets) ($K = 1$; 2 Inter-Cell Interfering MTs)

There are two types of scenarios as explained below:

i. When MTs in each of the adjacent interfering cells offer interference within the same range i.e., both the MTs are located in the same zone.
ii. When MT in both adjacent cells are located in different zones. Therefore, they are offering different level of interference to the BS of interest.

Consider the later type of scenario, the Wyner C-GCMAC as shown in Figure 3-7, the total number of active MTs in adjacent two cells are given by $M = NK = 2K$, where $K = 1,2,\cdots$ is the active MTs in j^{th} cell. In order to derive the channel slow gain with respect to the location of MTs in the cells, we split each cell into three zones as explained in previous Section 3.8 and shown in Figure 3-7. The possible combinations of locations of MTs in adjacent cells across the three zones can be calculated generally as 3^M.

Table 3-4: Possible combination of location of users
K =1 (2 interfering users for each cell)

location of user #2 \ location of user #1			
	zone #1 zone #1	zone #1 zone #2	zone #1 zone #3
	zone #2 zone #1	zone #2 zone #2	zone #2 zone #3
	zone #3 zone #1	zone #3 zone #2	zone #3 zone #3

Consider a single user case where $K = 1$ and there are $3^2 = 9$ possible combination of location of users in both adjacent cells across the zones. The location of MTs is presented in the Table 3-4. The table clearly illustrated the location of users T_{j+1} and T_{j-1} in adjacent cells. The diagonal of the table represents the situation when both users are located in same zone i.e. (level of interference varies within specific range). Similarly, each row is representing a situation when user T_{j+1} is fixed in either of the zone and user T_{j-1} is changing its position across the cell from zone #1 to zone #3.

We introduce a more realistic model that the MTs in both adjacent cells can be located in same zone or different zone but covering a range of distances from the BS of interest or range of channel slow gain between the BS of interest and the MTs. Furthermore, for simplicity it is also assumed that the resultant channel slow gain matrix over N cells arranged in circular fashion as shown in Figure 3-6 and $M = KN$ users (with $K = 1$ under present scenario) is circulant.

Lemma 3.9.1: (Formation of Circulant matrix [39]) *Let* $\boldsymbol{\mathcal{S}}$ *be the circular permutation operator, viewed as* $N \times N$ *matrix relative to the standard basis for* $\mathbb{R}^6$. *For given circular cellular setup,* $K = 1, N = M = NK = 6$. Let $\left\{e_1, e_2, \cdots, e_6\right\}$ *be the standard row basis vectors for* $\mathbb{R}^6$ *such that* $e_i \, \boldsymbol{\mathcal{S}} = e_{i+1}$ for $i = 1,2,\cdots,N$. *Therefore, the shift operator matrix* $\boldsymbol{\mathcal{S}}$ *relative to the defined row basis vectors for* $\mathbb{R}^6$ *can be expressed as* [39]

$$\boldsymbol{\mathcal{S}} = \begin{pmatrix} 0 & 1 & 0 & 0 & 0 & 0 \\ 0 & 0 & 1 & 0 & 0 & 0 \\ 0 & 0 & 0 & 1 & 0 & 0 \\ 0 & 0 & 0 & 0 & 1 & 0 \\ 0 & 0 & 0 & 0 & 0 & 1 \\ 1 & 0 & 0 & 0 & 0 & 0 \end{pmatrix} \tag{3-14}$$

The matrix $\boldsymbol{\mathcal{S}}$ *is real and orthogonal, hence* $\boldsymbol{\mathcal{S}}^{-1} = \boldsymbol{\mathcal{S}}^{\mathrm{T}}$ *and also the basis vectors are orthonormal for* $\mathbb{R}^6$. *The path loss between the* MTs T_j *and the* BSs B_j *can be viewed as a row vector of the resultant* $N \times M$ *circular channel slow gain matrix* $\boldsymbol{\Omega}$ *and can be expressed as*[11] $\boldsymbol{\Omega}\left(1, :\right) = \left(\Omega_{B_j T_j}, \Omega_{B_j T_{j+1}}, 0, 0, 0, \Omega_{B_j T_{j-1}}\right)$ *where* $\Omega_{B_j T_j}$ *is the slow gain between the intra-cell MT and the respective BS and* $\Omega_{B_j T_{j+1}}$ *and* $\Omega_{B_j T_{j-1}}$ *are the slow gain between the MTs in the adjacent cell on the right side and right side of the BS of interest respectively. It is known that the shift invariant circular matrix* $\boldsymbol{\Omega}$ *can be expressed as a linear combination of powers of the shift operator* $\boldsymbol{\mathcal{S}}$ [39]. *Therefore, the resultant circular channel slow gain matrix in this scenario can be expressed as*

$$\boldsymbol{\Omega}_{N,1} = \mathbf{I}_N + \Omega_{B_j T_{j+1}} \boldsymbol{\mathcal{S}} + \Omega_{B_j T_{j-1}} \boldsymbol{\mathcal{S}}^T \tag{3-15}$$

[11] We used MATLAB format to express the row vector. For an example, $\boldsymbol{\Omega}\left(1, :\right)$ shows first row vector with all columns of $\boldsymbol{\Omega}$.

where $\mathbf{I}_N$ *is* $N \times N$ *identity matrix and* $\boldsymbol{\mathcal{S}}$ *is the shift operator. Let us define* $\Omega_{B_j T_{j+1}} = \Omega_R$ *as a channel slow gain of user on the right side of the given BS and* $\Omega_{B_j T_{j-1}} = \Omega_L$ *is a slow gain for user on the left side of the given BS. The resultant empirical form of* $\boldsymbol{\Omega}$ *becomes*

$$\boldsymbol{\Omega}_{N,1} = \begin{pmatrix} 1 & \Omega_R & 0 & 0 & 0 & \Omega_L \\ \Omega_L & 1 & \Omega_R & 0 & 0 & 0 \\ 0 & \Omega_L & 1 & \Omega_R & 0 & 0 \\ 0 & 0 & \Omega_L & 1 & \Omega_R & 0 \\ 0 & 0 & 0 & \Omega_L & 1 & \Omega_R \\ \Omega_R & 0 & 0 & 0 & \Omega_L & 1 \end{pmatrix} \tag{3-16}$$

Furthermore, for multi-user scenario with equal channel slow gain among the MTs in adjacent cell and BSs i.e., when $K > 1$*, the channel slow gain matrix model can be formulated as*

$$\boldsymbol{\Omega}_{N,K} = 1_K \otimes \mathbf{I}_N + \left\{\Omega^l_{B_j T_{j+1}}\right\}_{l=1}^{K} \otimes \boldsymbol{\mathcal{S}} + \left\{\Omega^l_{B_j T_{j-1}}\right\}_{l=1}^{K} \otimes \boldsymbol{\mathcal{S}}^T \tag{3-17}$$

3.9.2 Empirical Examples[12]

There can be several scenarios based on the location of MT in adjacent cell when K=1 (2 inter-cell interfering MTs). In the first empirical example, we assume that both MTs T_{j+1} and T_{j-1} are located in zone #1 and offering variable interference within the zone #1. The channel matrix of (3.16) can be expressed as

[12] The empirical examples are presented only to show that the slow gain among the users located in two adjacent cells to the BS of interest is variable. In simulations, we perform spatial averaging in order to remove the effect of fast fading and make sure that the possible random errors due to fast fading are smoothed out.

$$\mathbf{\Omega}=\begin{pmatrix} 1 & 0.9 & 0 & 0 & 0 & 0.7 \\ 0.7 & 1 & 0.9 & 0 & 0 & 0 \\ 0 & 0.7 & 1 & 0.9 & 0 & 0 \\ 0 & 0 & 0.7 & 1 & 0.9 & 0 \\ 0 & 0 & 0 & 0.7 & 1 & 0.9 \\ 0.9 & 0 & 0 & 0 & 0.7 & 1 \end{pmatrix}$$

This is the channel slow gain matrix where both interfering MT are located in zone #1 and offering high level of interference to the given BS. However, every T_{j+1} interfering MT is offering a slow gain 0.9 and every T_{j-1} interfering MT is offering a slow gain 0.7. Similarly, MT T_{j+1} is fixed in zone #1 and MT T_{j-1} is located in zone #2 such that the channel matrix becomes

$$\mathbf{\Omega}=\begin{pmatrix} 1 & 0.9 & 0 & 0 & 0 & 0.3 \\ 0.3 & 1 & 0.9 & 0 & 0 & 0 \\ 0 & 0.3 & 1 & 0.9 & 0 & 0 \\ 0 & 0 & 0.3 & 1 & 0.9 & 0 \\ 0 & 0 & 0 & 0.3 & 1 & 0.9 \\ 0.9 & 0 & 0 & 0 & 0.3 & 1 \end{pmatrix}$$

The overall interference level of the channel is reduced and the interfering MT is offering medium level of interference which may be advantageous with respect to information theory analysis (this feature is covered in next Chapter 4). Similarly, we assume MT T_{j+1} is still fixed in zone #1 and MT T_{j-1} is located in zone #3 (far zone) such that the channel matrix becomes

$$\mathbf{\Omega}=\begin{pmatrix} 1 & 0.9 & 0 & 0 & 0 & 0.1 \\ 0.1 & 1 & 0.9 & 0 & 0 & 0 \\ 0 & 0.1 & 1 & 0.9 & 0 & 0 \\ 0 & 0 & 0.1 & 1 & 0.9 & 0 \\ 0 & 0 & 0 & 0.1 & 1 & 0.9 \\ 0.9 & 0 & 0 & 0 & 0.1 & 1 \end{pmatrix}$$

This channel shows that among the 2 interfering MTs one is located in close vicinity of BS of interest and offering high level of interference to the BS while other

MT is located at the maximum distance from the BS of interest and offering low level of interference.

Similarly, several examples can be generated to show that every mobile terminal in each of the adjacent cells is offering variable level of inter-cell interference to the base station of interest i.e. channel slow gain is variable in each cells across the three zones. The range of each zone is given in Table 3-3. The empirical exmaples are presented to show the possible numerical values of slow gain among the MTs and the BSs. However, in the simulations the slow gain among the MTs and the BSs are the average of the gains with in the range of respective zone.

3.9.3 Multi-user Cellular MIMO Networks (MU-CeMNets) ($K > 1$; 2 K Inter-Cell Interfering MTs)

In the multi-user case, more than one MT is contributing to interfering level. It is assume that the inter-cell multiple interfering users can be located in either zone or can be distributed across the zones. The inter-cell interfering users in each of the adjacent cell offer variable channel slow gain across the cell to the BS of interest depending on the location of MTs and the channel slow gain matrix is derived as [144]

$$\boldsymbol{\Omega}_{N,K} = \left(\boldsymbol{\Omega}_{N,1}^{(1)} \quad \boldsymbol{\Omega}_{N,1}^{(2)} \quad \cdots \quad \boldsymbol{\Omega}_{N,1}^{(K)} \right) \breve{\boldsymbol{\mathcal{P}}}_{N,K} \tag{3-18}$$

where $\boldsymbol{\Omega}_{N,1}^{(K)} \in \mathbb{R}^{N \times N}$ is K^{th} user channel matrix as defined in (3.16) with variable slow gain and $\breve{\boldsymbol{\mathcal{P}}}_{N,K} \in \mathbb{P}^{NK \times NK}$ is permutation matrix which transforms the concatenated channel matrix in to $N \times NK$ multi-user resultant channel matrix. The transformation is shown in Figure 3-8.

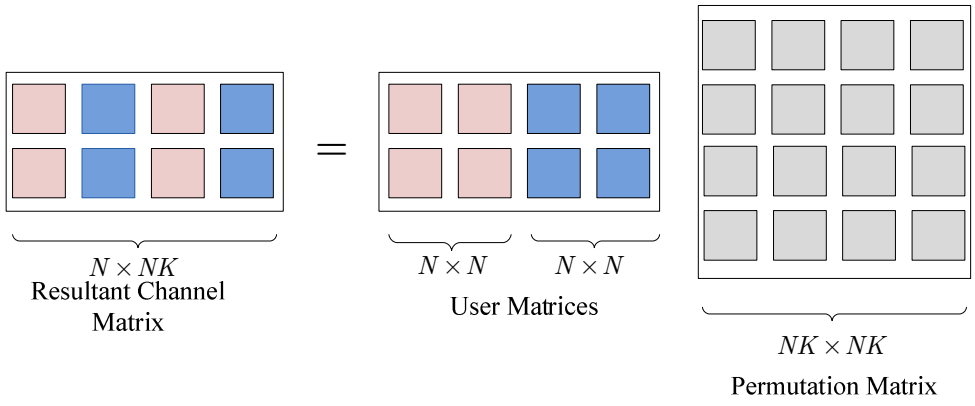

Figure 3-8: Transformation of individual user channel matrix into resultant channel matrix by exploiting Permutation matrix (3.18).

As an example, we consider two scenarios to present the modelling of the channel matrix for the multi-user case which incorporates the variable slow gain among the base stations and the mobile terminals. However, the details of formation of permutation matrix $\breve{\boldsymbol{\mathcal{P}}}_{N,K}$ are included in Appendix E.

Case I: When $K = 2$ and $N = 6$, the resultant channel matrix can be expressed as

$$\boldsymbol{\Omega}_{N=6,K=2} = \left(\boldsymbol{\Omega}_{N,1}^{(1)} \quad \boldsymbol{\Omega}_{N,1}^{(2)}\right) \breve{\boldsymbol{\mathcal{P}}}_{N=6,K=2} \tag{3-19}$$

The channel slow gain matrices $\boldsymbol{\Omega}_{N,1}^{(1)}$ and $\boldsymbol{\Omega}_{N,1}^{(2)}$ for user 1 and user 2 respectively can be modelled by using (3.16) and the permutation matrix $\breve{\boldsymbol{\mathcal{P}}}_{N=6,K=2} \in \mathbb{P}^{12\times 12}$ may be expressed as following

$$\breve{\boldsymbol{\mathcal{P}}}_{N=6,K=2} = \left(\begin{array}{cccccc|cccccc} 1&0&0&0&0&0&0&0&0&0&0&0\\ 0&0&1&0&0&0&0&0&0&0&0&0\\ 0&0&0&0&1&0&0&0&0&0&0&0\\ 0&0&0&0&0&0&1&0&0&0&0&0\\ 0&0&0&0&0&0&0&0&1&0&0&0\\ 0&0&0&0&0&0&0&0&0&0&1&0\\ \hline 0&1&0&0&0&0&0&0&0&0&0&0\\ 0&0&0&1&0&0&0&0&0&0&0&0\\ 0&0&0&0&0&1&0&0&0&0&0&0\\ 0&0&0&0&0&0&0&1&0&0&0&0\\ 0&0&0&0&0&0&0&0&0&1&0&0\\ 0&0&0&0&0&0&0&0&0&0&0&1 \end{array}\right) \tag{3-20}$$

Case II: When $K = 3$ and $N = 6$, the resultant channel matrix can be expressed as

$$\boldsymbol{\Omega}_{N=6,K=3} = \left(\boldsymbol{\Omega}_{N,1}^{(1)} \quad \boldsymbol{\Omega}_{N,1}^{(2)} \quad \boldsymbol{\Omega}_{N,1}^{(3)}\right)\breve{\boldsymbol{\mathcal{P}}}_{N=6,K=3} \tag{3-21}$$

The channel slow gain matrices $\boldsymbol{\Omega}_{N,1}^{(1)}$, $\boldsymbol{\Omega}_{N,1}^{(2)}$ and $\boldsymbol{\Omega}_{N,1}^{(3)}$ are for user 1, user 2 and user 3 respectively and can be modelled by using (3.16). The permutation matrix $\breve{\boldsymbol{\mathcal{P}}}_{N=6,K=3} \in \mathbb{P}^{18\times 18}$ may be expressed as

$$\breve{\boldsymbol{\mathcal{P}}}_{N=6,K=3} = \left(\begin{array}{cccccc|cccccc|cccccc}
0&1&0&0&0&0&0&0&0&0&0&0&0&0&0&0&0&0\\
0&0&0&0&1&0&0&0&0&0&0&0&0&0&0&0&0&0\\
0&0&0&0&0&0&0&1&0&0&0&0&0&0&0&0&0&0\\
0&0&0&0&0&0&0&0&0&0&1&0&0&0&0&0&0&0\\
0&0&0&0&0&0&0&0&0&0&0&0&0&1&0&0&0&0\\
0&0&0&0&0&0&0&0&0&0&0&0&0&0&0&0&1&0\\
\hline
0&1&0&0&0&0&0&0&0&0&0&0&0&0&0&0&0&0\\
0&0&0&0&1&0&0&0&0&0&0&0&0&0&0&0&0&0\\
0&0&0&0&0&0&0&1&0&0&0&0&0&0&0&0&0&0\\
0&0&0&0&0&0&0&0&0&0&1&0&0&0&0&0&0&0\\
0&0&0&0&0&0&0&0&0&0&0&0&0&1&0&0&0&0\\
0&0&0&0&0&0&0&0&0&0&0&0&0&0&0&0&1&0\\
\hline
0&0&1&0&0&0&0&0&0&0&0&0&0&0&0&0&0&0\\
0&0&0&0&0&1&0&0&0&0&0&0&0&0&0&0&0&0\\
0&0&0&0&0&0&0&0&1&0&0&0&0&0&0&0&0&0\\
0&0&0&0&0&0&0&0&0&0&0&1&0&0&0&0&0&0\\
0&0&0&0&0&0&0&0&0&0&0&0&0&0&1&0&0&0\\
0&0&0&0&0&0&0&0&0&0&0&0&0&0&0&0&0&1
\end{array}\right) \tag{3-22}$$

In a multi-user scenario, there are $2K$ inter-cell interfering in adjacent cells and offering variable level of interference. The variation in interference level is advantageous from information theory perspectives which is explained and analyzed in next chapter. By varying the interference level, various scenarios are created in order to highlight the difference when channel model based on variable in-cell interference is employed.

3.10 Conclusions

This chapter introduced Wyner's C-GCMAC which incorporated the fundamental aspects of a cellular network into the framework of well known Gaussian MAC. Wyner's analysis in [29], was one of the first papers to analyze cellular networks using information theoretic arguments for linear cellular setup. In this chapter, we extended the Wyner's GCMAC to C-GCMAC for variable inter-cell interference levels. The channel slow gain matrix between the BS and the MTs in adjacent cells is derived using experimental setup of circular cellular setup in Glasgow city centre. The experiments are carried out using network monitoring software referred to as Net-monitor. It is found that channel slow gain is variable across the cells; it is minimum when the users are located far away from the BS and it is maximum when uses are located near the BS of interest. Therefore, the entire cell is split into three zones depending on the distance between the interfering user and the BS. The interfering user offers a high level of interference when the users are located in close vicinity of the BS of interest. The interfering user offers medium level of interference when the users are located at medium distance from the BS of interest. Finally, the interfering user offers minimum level of interference when the users are located far away from the BS of interest. This chapter presents an empirical modelling of the channel slow gain by exploiting the variable inter-cell interference level strategy. Finally, the mathematical models for a single user and the multi-user scenarios are derived to incorporate the variable slow gain among the MTs and the BSs. This Chapter is an attempt to model the Wyner like cellular setup as close as possible to real scenario which forms the foundation of the discussions and investigations in the later Chapters.

Chapter 4

Information Theoretic Analysis

4.1 Introduction

The ever growing demand for wireless communication services has necessitated the development of systems with high bandwidth and power efficiency. In the last decade, recent developments in the Information Theory of wireless communication systems with multiple antenna and multiple users have provided additional newfound hope to satisfy this demand. Toward this end, numerous papers have been written to determine the information theoretical limitations of these systems. Thus, the main objective of this chapter is to analyze the information theoretic behaviour of the Wyner C-GCMAC when inter-cell interference levels are variable across the cell. The performance analysis includes analytical presentation of sum-rate expressions over multi-user and single user decoding strategies with and without intra-cell time division multiple access (TDMA). In § 4.2, an important information theoretic quantity – MMSE is introduced which is used throughout the chapter during the analytical discussions on Wyner C-GCMAC. In § 4.3 and § 4.4, capacity region of MAC and C-GCMAC are presented. In § 4.5, performance measures for C-GCMAC are presented. In this Section, the multi-user joint decoding, single user decoding, single user decoding with intra-cell TDMA and optimal joint decoding techniques are presented; the main contribution of this chapter is to highlight the advantage of variable inter-cell interference gain between the interfering users and the given BS. The capacity expressions are derived to include the effect of variable inter-cell interference level of each of the users in two adjacent cells. In § 4.6, we use recent results of large

random matrices to study the asymptotic behaviour of C-GCMAC and compare the performance with linear GCMAC. In § 4.7, numerical examples and discussions based on various simulation experiments are presented. This Section includes an eigenvalue distribution perspective as well to highlight the cause of improvement in optimum joint decoding capacity. Later in sub-Section 4.7.6, we summarize the discussions on simulation results. The impact of variable slow gain is summarized in Table 4-1 and Table 4-2 and presented in this Section. In § 4.9, a novel derivation of the upper bound on optimum joint decoding is presented using the Hadamard inequality, the application of the Hadamard inequality is justified with the support of several scenarios presented in this Section. Conclusions to this chapter are given in § 4.10.

4.2 Mean Square Error

An important quantity, which is used as a figure of merit in the information theoretical analysis of Gaussian linear vector memory less channels, is the MMSE. The MMSE determines the maximum achievable Signal to Interference and Noise Ratio (SINR). After filtering the channel output $\boldsymbol{y}$ using a linear filter. Recently in [40] and [41] it was shown that there is a close relationship between mutual information and MMSE. In this Section, these fundamental properties will be explored.

To find the MMSE, let $\boldsymbol{y}$ be the output symbols from a channel described by (3.1), with a deterministic channel matrix $\mathbf{H}$ and input covariance $\boldsymbol{\Phi}$. Let $\hat{\boldsymbol{x}} = \mathbf{A}\boldsymbol{y}$ define a linear filtering operation, i.e. the channel output $\boldsymbol{y}$ are linearly filtered using a $M \times N$ filter matrix $\mathbf{A}$. The linear MMSE filter is chosen to minimize the mean square error of the filter output [42], i.e.

$$\hat{\mathbf{A}} = \arg\min_{\mathbf{A}} \mathbb{E}\left[\left\|\boldsymbol{x} - \hat{\boldsymbol{x}}\right\|^2\right] \tag{4-1}$$

It is well known that the error sequence is orthogonal to the filter input [42], i.e. $\mathbb{E}\left[\left(\boldsymbol{x}-\hat{\boldsymbol{x}}\right)\boldsymbol{y}^H\right]$ and hence $\mathbb{E}\left[\boldsymbol{x}\,\boldsymbol{y}^H\right]=\mathbb{E}\left[\hat{\boldsymbol{x}}\,\boldsymbol{y}^H\right]$[42] and [43]-[45]. Use of this property results in

$$\hat{\mathbf{A}}\left(\sigma_z^2\mathbf{I}_N+\mathbf{H}\boldsymbol{\Phi}\mathbf{H}^H\right)=\boldsymbol{\Phi}\,\mathbf{H}^H \tag{4-2}$$

from which a solution for $\hat{\mathbf{A}}$ can be obtainable. Using this filter, MMSE can be determined as follows[1].

$$\mathbb{E}\left[\left(\boldsymbol{x}-\hat{\boldsymbol{x}}\right)\left(\boldsymbol{x}-\hat{\boldsymbol{x}}\right)^H\right]=\mathbb{E}\left[\boldsymbol{x}\,\boldsymbol{x}^H\right]-\mathbb{E}\left[\boldsymbol{x}\,\boldsymbol{y}^H\right]\hat{\mathbf{A}}^H+\hat{\mathbf{A}}\mathbb{E}\left[\boldsymbol{y}\,\boldsymbol{y}^H\right]\hat{\mathbf{A}}^H$$

$$\begin{aligned}&=\boldsymbol{\Phi}-\hat{\mathbf{A}}\mathbf{H}\boldsymbol{\Phi}-\boldsymbol{\Phi}\mathbf{H}^H\hat{\mathbf{A}}^H+\hat{\mathbf{A}}\left(\sigma_z^2\mathbf{I}_N+\mathbf{H}\boldsymbol{\Phi}\mathbf{H}^H\right)\hat{\mathbf{A}}^H\\&=\left(\mathbf{I}_M-\hat{\mathbf{A}}\mathbf{H}\right)\boldsymbol{\Phi}\end{aligned} \tag{4-3}$$

where the last line follows from the use of property (4.2). Using this property again, the MMSE of the k^{th} filtered output symbols is therefore,

$$\begin{aligned}\mathsf{mmse}_k\left(\mathbf{H};\boldsymbol{\Phi},\sigma_z^2\right)&\triangleq\left(\mathbb{E}\left[\left(\boldsymbol{x}-\hat{\boldsymbol{x}}\right)\left(\boldsymbol{x}-\hat{\boldsymbol{x}}\right)^H\right]\right)_{k,k}\\&=\left(\boldsymbol{\Phi}-\boldsymbol{\Phi}\mathbf{H}^H\left(\sigma_z^2\mathbf{I}_N+\mathbf{H}\boldsymbol{\Phi}\mathbf{H}^H\right)^{-1}\mathbf{H}\boldsymbol{\Phi}\right)_{k,k}\end{aligned} \tag{4-4}$$

The arithmetic mean over the M filtered output symbols is given by

$$\begin{aligned}\mathsf{mmse}_{\text{avg}}\left(\mathbf{H};\boldsymbol{\Phi},\sigma_z^2\right)&\triangleq\frac{1}{M}\sum_{k=1}^{M}\mathsf{mmse}_k\left(\mathbf{H};\boldsymbol{\Phi},\sigma_z^2\right)\\&=\frac{1}{M}\mathbb{E}\left[\left\|\boldsymbol{x}-\hat{\boldsymbol{x}}\right\|^2\right]\\&=\frac{1}{M}\,\mathrm{tr}\left(\boldsymbol{\Phi}-\boldsymbol{\Phi}\mathbf{H}^H\left(\sigma_z^2\mathbf{I}_N+\mathbf{H}\boldsymbol{\Phi}\mathbf{H}^H\right)^{-1}\mathbf{H}\boldsymbol{\Phi}\right)\end{aligned} \tag{4-5}$$

For the special case when $\boldsymbol{\Phi}=P\,\mathbf{I}_M$, (4.5) reduces to:

[1] Using the property that the expectation and trace commute [90].

$$\mathsf{mmse}_{\text{avg}}\left(\mathbf{H};\gamma\right) \triangleq \frac{P}{M}\,\mathrm{tr}\left(\mathbf{I}_{\boldsymbol{M}} - \gamma\,\mathbf{H}^{H}\left(\mathbf{I}_{N} + \gamma\,\mathbf{H}\mathbf{H}^{H}\right)^{-1}\mathbf{H}\right) \tag{4-6}$$

$$= P\left[\frac{1}{M}\,\mathrm{tr}\left(\left(\mathbf{I}_{N} + \gamma\,\mathbf{H}\mathbf{H}^{H}\right)^{-1}\right) + 1 - \frac{N}{M}\right] \tag{4-7}$$

$$= \frac{P}{M}\,\mathrm{tr}\left[\left(\mathbf{I}_{M} + \gamma\,\mathbf{H}^{H}\mathbf{H}\right)^{-1}\right] \tag{4-8}$$

There exist a fundamental relationship between this MMSE and mutual information [45], [40] and [41]. To see this relationship, differentiate (2.45) with respect to γ to yields

$$\frac{d}{d\gamma}\,\mathcal{I}\left(\boldsymbol{x};\boldsymbol{y} \mid \mathbf{H}\right) = \mathrm{tr}\left(\mathbf{H}^{H}\left(\mathbf{I}_{N} + \gamma\,\mathbf{H}\mathbf{H}^{H}\right)^{-1}\mathbf{H}\right) \tag{4-9}$$

Combining (4.6) and (4.9) it follows that

$$\mathsf{mmse}_{\text{avg}}\left(\mathbf{H};\gamma\right) = P\left[1 - \frac{N}{M}\,\gamma\,\frac{d}{d\gamma}\left(\frac{1}{N}\,\mathcal{I}(\boldsymbol{x};\boldsymbol{y} \mid \mathbf{H})\right)\right] \tag{4-10}$$

Other useful generalization and extensions to the fundamental relationship between mutual information and MMSE can be found in [47] and [48].

4.3 Capacity Regions of Multiple Access Channels (MAC)

Multiple access channels are characterized by a set of rate vectors known as the capacity region. To derive the capacity region of the Gaussian MAC given in Definition 3.5.1 the following lemma is employed[2].

Lemma 4.4.1 [137]**:** *Let* **A** *be an arbitrary* $L \times K$ *matrix, and define the diagonal matrix* $\mathbf{D} = diag\left(d_1^2,\cdots,d_K^2\right)$, *where* $d_{\boldsymbol{k}}$ *is real for all* $k = 1,\cdots,K$. *Then*

[2] Note that the Lemma 4.4.1 is a well known result in the literature of Gaussian MAC, see for example [137].

$\hat{\mathbf{D}} = diag\left(W_1^2, \cdots, W_K^2\right)$ *is a global solution to the constrained maximization problem*

$$\text{maximize: } \log\det\left(\mathbf{I}_L + \mathbf{ADA}^H\right) \tag{4-11}$$

$$\text{subject to: } d_k^2 \le W_k, \quad \forall k = 1, \cdots, K. \tag{4-12}$$

Proof (4.11): For maximization problem described by (4.11), construct the following Lagrangian

$$\mathcal{L}(\boldsymbol{q}, \boldsymbol{v}) = \log\det\left(\mathbf{I}_L + \frac{1}{\sigma_z^2}\mathbf{ADA}^H\right) - \sum_{k=1}^{K} v_k\left(d_k^2 - W_k\right) \tag{4-13}$$

where $\boldsymbol{v} = (v_1, \cdots, v_K)$ is a set of Lagrangian multipliers corresponding to the inequality constraints (4.12), and $\boldsymbol{d} = (d_1, \cdots, d_K)$. Note that for any **A**, since **D** is positive semi-definite, then $\mathbf{I}_L + \mathbf{ADA}^H$ is positive definite Hermitian. Furthermore, since log det **X** is a strictly concave function on the convex set of positive definite Hermitian matrices [24], and then any local solution to (4.12) is also a global solution [49].

Suppose $\hat{\mathbf{D}} = diag\left(\hat{d}_1^2, \cdots, \hat{d}_K^2\right) = diag\left(W_1^2, \cdots, W_K^2\right)$ is the solution to (4.11). For $\hat{\mathbf{D}}$ to be a local (and hence global) maximum of (4.11) the Kuhn-Tucker necessary conditions state [49] that a vector $\hat{\boldsymbol{v}} = (\hat{v}_1, \cdots, \hat{v}_K)$ must exist, satisfying

$$\hat{d}_k^2 - W_k \le 0 \tag{4-14}$$

$$\hat{v}_k\left(\hat{d}_k^2 - W_k\right) = 0 \tag{4-15}$$

$$\hat{v}_k \ge 0 \tag{4-16}$$

$$\frac{\partial}{\partial d_k}\mathcal{L}(\hat{\boldsymbol{d}}, \hat{\boldsymbol{v}}) = 0 \tag{4-17}$$

for all $k = 1,\cdots,K$. Since $\hat{d}_k^2 = W_k$ by supposition, it is obvious that conditions (4.14) and (4.15) are satisfied. It remains to show that the there exists positive scalars, i.e. (4.16), which also satisfies (4.17). Differentiating (4.13) with respect to d_k at $\mathbf{D} = \hat{\mathbf{D}}$ and equating to zero yields

$$\hat{v}_k = \text{tr}\left[\left(\mathbf{I}_K + \mathbf{A}\hat{\mathbf{D}}\mathbf{A}^H\right)^{-1} \boldsymbol{a}_k \boldsymbol{a}_k^\dagger\right] \tag{4-18}$$

where $\boldsymbol{a}_k$ denotes the k^{th} column vector of $\mathbf{A}$. Since $\mathbf{I}_K + \mathbf{A}\hat{\mathbf{D}}\mathbf{A}^H$ is positive definite, its inverse is also positive definite. The unit rank matrix $\boldsymbol{a}_k \boldsymbol{a}_k^\dagger$ is positive semi-definite Hermitian. Hence, by [24] the product inside the trace of (4.18) is also positive semi-definite. Therefore, $\hat{v}_k \geq 0$ for all $k = 1,\cdots,K$ and conditions (4.16) and (4.17) are satisfied, which implies $\hat{\mathbf{D}}$ is a global solution to the maximization problem (4.11). □

Theorem 4.4.1 [27]**:** (Gaussian MAC Capacity Region). *Let* $\boldsymbol{y} = \mathbf{H}\boldsymbol{x} + \boldsymbol{z}$ *models a Gaussian MAC as a given in Definition 3.5.1. Let* $\boldsymbol{P} = (P_1,\cdots,P_M)$ *denote a vector of average power constraints, i.e.* P_m *corresponds to* m^{th} *user's average power constraint* (3.2)*. Let* $R_1,\cdots,R_M$ *denote the rate in Bits/sec/Hz per channel usage assigned to user* $1,\cdots,M$ *respectively. Let* $\boldsymbol{R}(S)$ *denote a rate vector for a subset of users* $S \in \{1,\cdots,M\}$*, e.g. if* $S = \{2,5,7\}$ *then* $\boldsymbol{R}(S) = \{R_2, R_5, R_7\}$*. Similarly, let* $\boldsymbol{P}(S)$ *denote the vector of average power constraints corresponding to a subset of users S. Assuming* $\mathbf{H}$ *is deterministic, and then the capacity region is given by*

$$\mathcal{C}\left(\mathbf{H}, \boldsymbol{P}, \sigma_z^2\right) = \text{cl co}\left\{\boldsymbol{R}\ (S)\colon R_m \geq 0,\ \forall m \in S\right.$$

$$\sum_{m\in S} R_m \le \log\det\left(\mathbf{I}_N + \frac{1}{\sigma_z^2}\mathbf{H}(S)\mathbf{\Phi}(S)\mathbf{H}^H(S)\right), \forall\, S \subseteq \left\{1,\cdots,M\right\}\Bigg\} \quad (4\text{-}19)$$

where cl and co *denote the closure and convex hull operations respectively,* $\boldsymbol{x}(S)$ *is a subset of user symbols,* $\mathbf{H}(S)$ *is an* $N\times|S|$ *sub-matrix of* $\boldsymbol{H}$ *resulting from removing column vectors corresponding to* S^C *(where* S^C *denotes the compliment set of S), and* $\mathbf{\Phi}(S)=\text{diag}(\boldsymbol{P}(S))$ *is a* $|S|\times|S|$ *diagonal matrix.*

Proof (4.19): Using [22] and [27], i.e. for *M* – user MAC the capacity region is the closure of the convex hull of the rate vectors satisfying

$$\sum_{m\in S} R_m \le \mathcal{I}\left(\boldsymbol{x}(S);\boldsymbol{y}\mid \mathbf{H},\boldsymbol{x}(S^C)\right) \quad \forall S \subseteq \left\{1,\cdots,M\right\} \quad (4\text{-}20)$$

for some product distribution $p_1(x_1)p_2(x_2)\cdots p_M(x_M)$. Using Theorem 2.9.1 and Lemma 4.4.1 (satisfying the constraints (4.14) - (4.17)), it follows that for all subsets $S \subseteq \left\{1,\cdots,M\right\}$ the mutual information quantity in (4.20) is maximized when each user transmits zero mean c.c.s. Gaussian distributed symbols, at its maximum allowable average power, i.e. $\mathbf{\Phi} = \text{diag}(P_1,\cdots,P_M)$. Thus, it follows that

$$\mathcal{I}\left(\boldsymbol{x}(S);\boldsymbol{y}\mid \mathbf{H},\boldsymbol{x}(S^C)\right) \le \log\det\left(\mathbf{I}_N + \frac{1}{\sigma_z^2}\mathbf{H}(S)\mathbf{\Phi}(S)\mathbf{H}^H(S)\right) \quad \forall S \subseteq \left\{1,\cdots,M\right\}$$

this completes the proof. □

4.4 Capacity Region of C-GCMAC

In decoding the received symbols, it is assumed that a super receiver has delay-less access to the user's codebook and received symbols as well as full knowledge of the CSI. Thus in effect, the model can also be interpreted as single cell (decoding all users) using macroscopic antenna diversity, with receive antennas spaced in a wide area linear array [27] and [50]. Moreover, the C-GCMAC is

equivalent to the Gaussian MAC in Definition 3.5.1 as shown in Figure 3-3 with $M = NK$ users and the N receive antennas represents the N BS antennas.

The notion of a super receiver in a terrestrial setting may be unrealistic, since the cell site receivers (BS) are usually separated by vast distances. In [50], Grant *et. al*. showed that the same optimum joint decoding done by a super receiver can be achieved in a decentralized manner (whereby only local communication between BS is required) using well known forward-backward algorithm [52] (commonly associated with the decoding of Turbo codes [51]). Using this strategy, each cell site receiver performs only part of the required computation and passes its information on to adjacent cells. In [53], it was shown that linear MMSE filtering can also be performed in a distributed fashion. However, these distributed decoding techniques still require delay-less access between a cell site receiver and its adjacent cell site receiver.

The C-GCMAC falls under the framework of the Gaussian MAC discussed in Section 3.1. There are however, a few subtle differences relating to the nomenclature used in our definition of C-GCMAC in Section 3.6. These differences can be accounted for as follows. Let $R_{n,k}$ be the information rate of user k in cell n and define the rate vector $R(S) = (R_{n,k})$ for all $\left(n,k\right) \in S$, where $S \subseteq \mathbb{S}$ is a set of users, and $\mathbb{S} = \left\{1,\cdots,N\right\} \times \left\{1,\cdots,K\right\}$. Therefore, using Theorem 2.9.1, the capacity region of linear C-GCMAC is [127]

$$\mathcal{C}\left(\mathbf{H},\gamma\right) = \mathrm{cl}\,\mathrm{co}\left\{\boldsymbol{R}(S)\colon R_{n,k} \geq 0,\ \forall n \in S \right.$$

$$\left. \sum_{(n,k)\in S} R_{n,k} \leq \log\det\left(\mathbf{I}_N + \gamma\,\mathbf{H}(S)\mathbf{H}^H(S)\right),\ \forall\, S \subseteq \mathbb{S} \right\}. \qquad (4\text{-}21)$$

where $\gamma = P \,/\, \sigma_z^2$. cl and co are closure and convex hull operations respectively, $x\left(S\right) = \left\{x_{n,k}\right\}$ for all $\left(n,k\right) \in S$ and S^C denotes the compliment of the set S.

4.5 Performance Measure of Cellular Systems

In this Section two information theoretic performance measures commonly employed in analysis of Gaussian MACs are introduced; joint optimum decoding capacity $\left(\mathrm{C}_{\mathrm{opt}}\right)$ and the capacity offered by MMSE filtering followed by single user decoding $\left(\mathrm{C}_{\mathrm{mmse}}\right)$, which are both measured in Bits/sec/Hz per receive antenna[3] [27], [28], [29], [94], [95], [98] and [147]. For the C-GCMAC, there is only one receive antenna per cell and so this unit of measurement can be interpreted as the number of Bits/sec/Hz per cell. In this Section, additional information theoretic performance measures specific to a cellular setting are introduced, which are used consistently in this thesis henceforth. These measures include capacity offered by various single user and multi-user decoding strategy. These quantities are used to compare and contrast the capacity of the system when various transmission protocols and receiver decoding strategies are employed.

4.5.1 Multi-user Joint Decoding

The complexity of the joint decoding systems is exponential with the increase in number of users M of the system. The users can be jointly decoded by employing a super receiver, rendering the system impractical [27]. In order to reduce the complexity, one way is to relax the number of users to be jointly decoded. Consider a scenario when each BS optimally joint decodes only those users local to its own cell, treating users from adjacent cell as noise. This decoding strategy referred to as cell optimum joint decoding since decoding can be performed locally at the BS [27] and [28]. The total ergodic sum capacity per j^{th} cell using cell optimum joint decoding strategy[4] is denoted by $\mathrm{C}_{\mathrm{cell}}(\mathbf{H})$ and for C-GCMAC as defined in (3.1) is given by [98]

[3] In [27]-[29], all quantities were measured in nats per cell, throughout the thesis we measured all quantities in Bits/sec/Hz.
[4] Assuming all users transmit c.c.s. Gaussian symbols at the maximum average power constraint.

$$\mathbf{C}_{\text{cell}}(p(\mathbf{H});\gamma) = \mathbb{E}\left[\log_2\left(1+\frac{\gamma\sum_{l=1}^{K}\left|h^{l}_{B_jT_j}\right|^2}{1+\gamma\sum_{i=\pm1}\sum_{l=1}^{K}\left|h^{l}_{B_jT_{j+i}}\right|^2}\right)\right], \tag{4-22}$$

where γ is the signal to noise ratios (SNRs). Using the Hadamard decomposition of fading channel (3.5), the capacity over the fading channel can be expressed as[5]

$$\mathbf{C}_{\text{cell}}(p(\mathbf{H});\gamma) = \mathbb{E}\left[\log_2\left(1+\frac{\gamma\sum_{l=1}^{K}\left|g^{l}_{B_jT_j}\circ\Omega^{l}{}_{B_jT_j}\right|^2}{1+\gamma\sum_{i=\pm1}\sum_{l=1}^{K}\left|g^{l}_{B_jT_{j+i}}\circ\Omega^{l}{}_{B_jT_{j+i}}\right|^2}\right)\right], \tag{4-23}$$

In the absence of fading (non-fading case) between the MTs and BSs, the capacity expression over deterministic channel reduced to[6,7]

$$\mathrm{C}_{\text{cell}}(\mathbf{H};\gamma) = \log_2\left(1+\frac{\gamma K}{1+\gamma\sum_{i=\pm1}\sum_{l=1}^{K}\left|\Omega^{l}{}_{B_jT_{j+i}}\right|^2}\right), \tag{4-24}$$

From (4.24), it can be seen that using this decoding strategy the system is inter-cell interference limited since

$$\lim_{K,\gamma\to\infty}\mathrm{C}_{\text{cell}}(\mathbf{H};\gamma) = \log_2\left(1+\frac{1}{\sum_{i=\pm1}\left|\Omega_{B_jT_{j+i}}\right|^2}\right). \tag{4-25}$$

---

[5] The complex coefficients $g^{l}_{B_jT_j}$, $g^{l}_{B_jT_{j+1}}$, and $g^{l}_{B_jT_{j-1}} \in \mathbb{C}$ designate the flat fading processes experienced by the l^{th} user in j^{th}, $(j+1)^{\text{th}}$, and $(j-1)^{\text{th}}$ cell respectively. The channel slow gain $\Omega^{l}{}_{B_jT_j}$, $\Omega^{l}{}_{B_jT_{j+1}}$, and $\Omega^{l}{}_{B_jT_{j-1}} \in \mathbb{R}(0,1)$ represents the shadow fading by l^{th} user in j^{th}, $(j+1)^{\text{th}}$, and $(j-1)^{\text{th}}$ cell respectively.

[6] $\Omega^{l}{}_{B_jT_j} = 1$; Gain of intra-cell MTs.

[7] The non-fading case is treated as a special case where all the variances of the fading r.v.'s are set to zero.

4.5.2 Single User Decoding

Single user decoding refers to the strategy where only a single user is decoded and all other interfering users including the intra-cell users are treated as noise. This decoding strategy offers the lowest complexity among the decoding strategies used by most practical multi-access communication systems [1]. The total sum capacity per cell by exploiting single user decoding is denoted by $\mathrm{C}_{\mathrm{sud}}\left(p(\mathbf{H});\gamma\right)$ and for C-GCMAC is given by [98] and [142]

$$\mathbf{C}_{\mathrm{sud}}(p(\mathbf{H});\gamma)=\sum_{l=1}^{K}\mathbb{E}\left[\log_2\left(1+\frac{\gamma\left|h^{l}_{B_jT_j}\right|^2}{1+\gamma\left(\sum\limits_{i=\pm1}\sum\limits_{l=1}^{K}\left|h^{l}_{B_jT_{j+i}}\right|^2+\sum\limits_{l=1}^{K-1}\left|h^{l}_{B_jT_j}\right|^2\right)}\right)\right], \quad (4\text{-}26)$$

Applying the Hadamard decomposition as defined in (3.5), (4.26) becomes

$$\mathbf{C}_{\mathrm{sud}}(p(\mathbf{H});\gamma)=\sum_{l=1}^{K}\mathbb{E}\left[\log_2\left(1+\frac{\gamma\left|g^{l}_{B_jT_j}\circ\Omega^{l}_{B_jT_j}\right|^2}{1+\gamma\left(\sum\limits_{i=\pm1}\sum\limits_{l=1}^{K}\left|g^{l}_{B_jT_{j+i}}\circ\Omega^{l}_{B_jT_{j+i}}\right|^2+\sum\limits_{l=1}^{K-1}\left|g^{l}_{B_jT_j}\circ\Omega^{l}_{B_jT_j}\right|^2\right)}\right)\right] \quad (4\text{-}27)$$

In the absence of the fading between the MTs and BSs, the capacity for deterministic system $\mathrm{C}_{\mathrm{sud}}\left(\mathbf{H};\gamma\right)$ may be expressed as[7,8]

$$\mathbf{C}_{\mathrm{sud}}(\mathbf{H};\gamma)=K\log_2\left(1+\frac{\gamma}{1+\gamma\left(\sum\limits_{i=\pm1}\sum\limits_{l=1}^{K}\left|\Omega^{l}_{B_jT_{j+i}}\right|^2+\sum\limits_{l=1}^{K-1}\left|\Omega^{l}_{B_jT_j}\right|^2\right)}\right), \quad (4\text{-}28)$$

Furthermore, as the number of users per cell increases and $\gamma\rightarrow\infty$, the $\mathrm{C}_{\mathrm{sud}}\left(\mathbf{H};\gamma\right)$ is intra-cell interference limited and expressed as

$$\lim_{K,\gamma\to\infty} \mathbf{C}_{\text{sud}}(\mathbf{H};\gamma) = \frac{1}{1+\sum_{i\pm 1}\left|\Omega_{B_j T_{j+i}}\right|^2}. \tag{4-29}$$

4.5.3 Single User with TDMA

In most of the cellular setups, the intra-cell users are assigned orthogonal channels through either time or frequency division multiple access (TDMA/FDMA) to eliminate the intra-cell interferences [1]. This transmission protocol is referred to as intra-cell TDMA. By exploiting the intra-cell TDMA the entire transmission period is divided into K non-overlapping time slots. Each of the K users within a cell is assigned one of the time slots in which to transmit information. Only 1 out of the total K users within the same cell will be active simultaneously. Hence, we can reduce the number of simultaneously active users within the cell and alleviate the burden of multi-user detection at the receiver [1]. However, since the average power constraint $\mathbb{E}\left[x\,x^*\right] \le P$ is over the entire transmission period and each user only transmits for $1/K^{\text{th}}$ of this period. Hence, each user transmits at a power of KP within its time slot. The total capacity for j^{th} cell, $\mathbf{C}_{\text{sud}}^{\text{tdma}}(\mathbf{H})$ is given by [98] and [142]

$$\mathbf{C}_{\text{sud}}^{\text{tdma}}\left(p(\mathbf{H});\gamma\right) = \mathbb{E}\left[\log_2\left(1+\frac{\widehat{\gamma}\left|h_{B_j T_j}\right|^2}{1+\widehat{\gamma}\left(\sum_{i=\pm 1}\left|h_{B_j T_{j+i}}\right|^2\right)}\right)\right], \tag{4-30}$$

where $\widehat{\gamma} = K\,\gamma$ is the total signal to noise ratio of the system. The denominator of the argument reflects the fact that for each MT in j^{th} cell there are interferers located in the neighbouring cells. Using (3.5) the Hadamard representation of the capacity is given by

$$\mathbf{C}_{\text{sud}}^{\text{tdma}}(p(\mathbf{H});\gamma) = \mathbb{E}\left[\log_2\left(1+\frac{\widehat{\gamma}\left|g_{B_jT_j}\circ\Omega_{B_jT_j}\right|^2}{1+\widehat{\gamma}\left(\sum_{i=\pm1}\left|g_{B_jT_{j+i}}\circ\Omega_{B_jT_{j+i}}\right|^2\right)}\right)\right], \qquad (4\text{-}31)$$

For non-faded case (4.31) reduces to

$$\mathbf{C}_{\text{sud}}^{\text{tdma}}(\mathbf{H};\gamma) = \log_2\left(1+\frac{\widehat{\gamma}}{1+\widehat{\gamma}\left(\sum_{j=\pm i}\left|\Omega_{B_jT_{j+i}}\right|^2\right)}\right). \qquad (4\text{-}32)$$

4.5.4 Optimum Decoding Capacity

Theorem 4.4.1 states that for a Gaussian MAC described by Definition 3.5.1., the optimum transmit strategy is when each user transmits i.i.d. c.c.s. Gaussian symbols at its maximum average power constraint. The majority of the Gaussian MAC's analyzed in this thesis assume a uniform average power constraint across all users, i.e. $P_1 = P_2 = \cdots = P_M = P$, where $\gamma \triangleq P/\sigma_z^2$. Furthermore, the sum rate constraints in (4.21) is reduce to

$$\sum_{m\in S} R_m \le \log\det\left(\mathbf{I}_N + \gamma\mathbf{H}(S)\mathbf{H}^H(S)\right) \quad \forall S \subseteq \left\{1,\cdots,M\right\} \qquad (4\text{-}33)$$

Only those rate vectors $\boldsymbol{R} = \left(R_1,\cdots,R_M\right) \in \mathrm{C}\left(\mathbf{H};\gamma\right)$ are said to be achievable, i.e. each user can transmit at its allocated rate according to $\boldsymbol{R}$ reliably over the channel. A two user systems (4.33) defines three sum rate constraints and $\mathrm{C}\left(\mathbf{H};\gamma\right)$ is a two dimensional pentagon (bevelled box) [127]. For three users, (4.33) defines seven constraints and $\mathrm{C}\left(\mathbf{H};\gamma\right)$ is a three dimensional polytope [127]. In general, for an M user systems, there will be $2^M - 1$ sum rate constraints and interpretation of $\mathrm{C}\left(\mathbf{H};\gamma\right)$ becomes difficult. In the analysis of some channels (e.g. CDMA channels

with a large number of users), insights can only be gained by observing the asymptotic behaviour (large system analysis) of the channel, i.e. taking $N, M \to \infty$ with $\lim_{M,N\to\infty} \frac{M}{N} \triangleq \beta$ constant, in which case it is impossible to analyze the entire capacity region. The most commonly used figure of merit in the analysis of large systems is the normalized total sum rate constraint, which in this thesis is referred to as the optimum decoding capacity. For a Gaussian MAC with uniform average power constraints, this is defined as [1], [13] and [97]

$$\mathbf{C}_{\text{opt}}(\mathbf{H}, \gamma) = \frac{1}{N} \log_2 \det\left(\mathbf{I}_N + \gamma \mathbf{H}\mathbf{H}^H\right) \tag{4-34}$$

which has units of Bits/sec/Hz per receive antenna.

For random ergodic[8] channel matrices, the proof of Theorem 4.4.1 is easily extended to the ergodic case by performing the expectation of the log det term in (4.34) over $\mathbf{H}$. Thus, when $\mathbf{H}$ is random and ergodic, the optimum decoding capacity is [13] and [97]

$$\mathbf{C}_{\text{opt}}(p(\mathbf{H}), \gamma) = \frac{1}{N} \mathbb{E}\left[\log_2 \det\left(\mathbf{I}_N + \gamma \mathbf{H}\mathbf{H}^H\right)\right] \tag{4-35}$$

In the left hand side of (4.35), the dependence on $p(\mathbf{H})$ signifies that the channel matrix is ergodic with density $p(\mathbf{H})$. The BSs are herein assumed to be able to jointly decode the received signals in order to detect the transmitted vector $\boldsymbol{x}$. Applying the Hadamard decomposition to $\mathbf{H}$ as defined in (3.5), (4.35) becomes

$$\mathbf{C}_{\text{opt}}(p(\mathbf{G} \circ \boldsymbol{\Omega}), \gamma) = \frac{1}{N} \mathbb{E}\left[\log_2 \det\left(\mathbf{I}_N + \gamma (\mathbf{G} \circ \boldsymbol{\Omega})(\mathbf{G} \circ \boldsymbol{\Omega})^H\right)\right] \tag{4-36}$$

[8] In this thesis a random ergodic channel matrix is where $\mathbf{H}[i]$, at each time index, i is chosen independently at random form a given probability density function $p(\mathbf{H})$.

Optimum Decoding Capacity over the non-Fading Channel

For C-GCMAC over non-fading environment i.e. deterministic channel, when optimum joint decoding is performed, it is found that the same total capacity per cell can be achieved when intra-cell TDMA is employed, or when the system has only one user per cell, each transmitting at a power of KP, i.e.

$$\mathbf{C}_{\text{opt}}(\mathbf{H},\gamma) = \mathbf{C}_{\text{opt}}^{\text{tdma}}(\mathbf{H},\gamma) = \mathbf{C}_{\text{opt}}(\mathbf{H},K\gamma) \tag{4-37}$$

Proof of (4.37): From (4.34), for the non-fading case $\mathbf{C}_{\text{opt}}(\mathbf{H},\gamma)$ is expressed as[9]

$$\mathbf{C}_{\text{opt}}(\mathbf{H},\gamma) = \frac{1}{N}\log_2 \det\left(\mathbf{I}_N + \gamma \boldsymbol{\Omega}\boldsymbol{\Omega}^H\right)$$

Recall from (3.11), we have $\boldsymbol{\Omega}_{N,K}\ \boldsymbol{\Omega}_{N,K}{}^H = K\boldsymbol{\Omega}_{N,1}^2$

$$= \frac{1}{N}\log_2 \det\left(\mathbf{I}_N + \gamma K \boldsymbol{\Omega}_{N,1}^2\right)$$

$$= \mathbf{C}_{\text{opt}}^{\text{tdma}}(\mathbf{H},\gamma) = \mathbf{C}_{\text{opt}}(\mathbf{H},K\gamma) \qquad \square$$

This proves that when optimum decoding capacity is employed, any orthogonal intra-cell resource sharing scheme (time or frequency) with total power KP is capacity achieving. The simulation results are shown later in Section 4.7.

4.5.5 Equal Rate Capacity

Recall from previous Section 4.5.4 that $\mathbf{C}_{\text{opt}}$ is related to the total sum-rate bound of (4.33) as follows

$$\sum_{(n,k)\in\mathbb{S}} R_{n,k} \le \log_2 \det\left(\mathbf{I}_N + \gamma\mathbf{H}\mathbf{H}^H\right) = N\,\mathbf{C}_{\text{opt}}(\mathbf{H},\gamma) \tag{4-38}$$

[9] Proof is only valid when MTs in j^{th}, $j+1^{\text{th}}$, and $j-1^{\text{th}}$ cell are offering identical slow gain to the j^{th} BSs.

The total sum rate constraint (4.38) is merely a bound on the total sum of the individual user rates beyond which communication with arbitrarily low probability of error is impossible. It does not reveal any information about the rate vectors of (4.33) that can achieve this bound. More often than (particularly if the capacity region is asymmetric), these rate vectors will require individual users to transmit at different rates. In practical cellular networks the user application dictates the required rate and service providers guarantee a minimum/maximum rate that is equal for all users (in order to sustain a variety of service). Thus important information theoretic quantity in the analysis of cellular networks is the capacity of the system when the users are constrained to transmit simultaneously at the same rate. This is in fact Wyner's definition of capacity [29]. When optimum joint decoding is employed, this is the same as finding largest equal rate vector of (4.33), which can be determined by finding the 'biting constraint'[10], see below.

Lemma 4.5.1: (Biting Constraint) *The biting constraint is defined as average mutual information constraint of a Gaussian MAC that results in the smallest rate vector with equal rates. i.e.*[11]

$$\mathrm{C}_{\mathrm{eq}}(p(\mathbf{H}),\gamma) = \max_{S\subseteq\mathbb{S}} \min \frac{K}{|S|} \log\det\left(\mathbf{I}_N + \gamma \mathbf{H}(S)\mathbf{H}^H(S)\right) \quad (4\text{-}39)$$

The minimization in (4.39) *is over* $2^{NK}-1$ *possible constraints and* C_{eq} *is referred to as the equal rate capacity measured in Bits/sec/Hz per cell. If the biting constraint is the total sum rate constraint then* $\mathrm{C}_{\mathrm{opt}}$ *is achievable with equal rate users. Otherwise* C_{eq} *is penalized in that more capacity is possible by allowing users to transmit at different rates i.e.* $\mathrm{C}_{\mathrm{eq}} < \mathrm{C}_{\mathrm{opt}}$.

Furthermore, Wyner showed that asymptotically, the sum rate bound is the biting constraint, meaning that $\mathrm{C}_{\mathrm{opt}}$ is achievable with equal rate users and the minimization in (4.39) is unnecessary. i.e.

[10] In this thesis the biting constraint is defined as the mutual information constraint of a Gaussian MAC (for example (4.21)) that results in the smallest rate vector with equal rates.
[11] Wyner's results are measured in terms of nats per user, which is the same as dividing (4.39) by K.

$$\lim_{N\to\infty} \mathbf{C}_{\text{eq}}(\mathbf{H},\gamma) = \lim_{N\to\infty} \mathbf{C}_{\text{opt}}(\mathbf{H},\gamma) \tag{4-40}$$

4.5.6 Linear MMSE Filtering Capacity

Optimum multi-user detection is achieved when the received sequence is optimally joint detected, i.e. the optimal multi-user receiver must make joint decisions, rather than treating interfering users as noise. In general, the multi-user detection problem is NP-Hard [54]. To make the problem even more difficult, to achieve optimum decoding capacity, information theory indicates that multi-user coding techniques are required (e.g. joint-typical set decoding [22]). This problem has lead to intensive effort by researchers to find practical methods that optimize the trade-off between performance and complexity. In recent years, a vast number of sub-optimal multi-user joint decoding algorithms have emerged based on the turbo principle (discovered by Berrou *et. al.* for the iterative decoding of Turbo codes) whereby the users signals are iteratively decoded (see [59], [60], [61], [62] and [64] for initial contributions on this topic). However, the complexity of such algorithms is still exponential with the number of users M. From a practical point of view, decoders, or estimators with linear or (at worst) polynomial complexity are preferred. One technique that has received much attention in the literature is the combination of linear filtering and interference cancellation [55]. Of particular importance is the linear MMSE filter, which has polynomial complexity and obtains the maximum achievable SINR by a linear filter [46]. For this reason, the MMSE is particularly important figure of merit in the information theoretic analysis of wireless communication systems.

The simplest sub-optimal multi-user decoding technique that involves linear MMSE filtering is to perform single user decoding directly from the filter outputs. Suppose (3.1) models a Gaussian MAC as given in Definition 3.5.1 with uniform average power constraint $P_1 = P_2 = \cdots = P_M = P$. Furthermore, suppose the users transmit symbols with $\mathbf{\Phi} = P\,\mathbf{I}_M$ (although this may not be the optimum transmit

strategy when MMSE filtering is employed). For this special case the MMSE for user k (4.4) reduces to

$$\mathsf{mmse}_k\left(\mathbf{H};\gamma\right) = P\left[\left(\mathbf{I}_M + \gamma\mathbf{H}^{\dagger}\mathbf{H}\right)^{-1}\right]_{k,k}. \tag{4-41}$$

Assuming the above MMSE is Gaussian distributed then the capacity of the Gaussian MAC (in Bits/sec/Hz per receive antenna) when linear MMSE filtering followed by single user decoding is employed is given by

$$\mathrm{C}_{\mathrm{mmse}}(p(\mathbf{H});\gamma) = \frac{1}{N}\sum_{k=1}^{M}\log_2\frac{P}{\mathrm{mmse}_k(\mathbf{H};\gamma)} \tag{4-42}$$

$$= \frac{1}{N}\sum_{k=1}^{M}\log_2\left[\left(\mathbf{I}_M + \gamma\mathbf{H}^{H}\mathbf{H}\right)^{-1}\right]_{k,k}. \tag{4-43}$$

4.6 The Limiting Eigenvalue Distribution

In the last few years, Random Matrix Theory (RMT) has been applied to solve several problems in Information theory. In particular a large amount of literature has emerged on the study of multi-user and multi-antenna wireless communication systems that employ concepts from RMT. The objective of this section is to introduce only those concepts from RMT that are useful in understanding of Information theoretic aspects of C-GCMAC. In this Section, we derive the optimum coding capacity and MMSE capacity for asymptotic case. Now, we consider following definitions to support the analysis of random matrices [67], [21], [23] and [128].

Definition 4.6.1 [21]**:** (Empirical Eigenvalue Distribution). *Let* $\mathbf{A}$ *be a* $N \times N$ *Hermitian matrix. The empirical eigenvalue distribution of* $\mathbf{A}$ *is defined as*

$$F_{\mathbf{A}}^{N}(x) \triangleq \frac{1}{N}\sum_{i=1}^{N} 1\left\{\lambda_i(\mathbf{A}) \le x\right\} \tag{4-44}$$

where $1\left\{\cdot\right\}$ *is the indicator function.*

In Definition 4.6.1, if $\mathbf{A}$ *is a random matrix, then the empirical eigenvalue distribution of a random probability measure on* $\mathbb{R}$ *and in probability theory, such a measure is often referred to as distribution on the space of probability measure*.

Definition 4.6.2 [21]**:** (Limiting Eigenvalue Distribution). *Let* $\mathbf{A}$ *be a random* $N \times N$ *Hermitian matrix, normalized such that* $\mathbb{E}\left[\left\|\mathbf{A}\right\|\right] = 1$. *In the limit as* $N \to \infty$ *with* $\mathbb{E}\left[\left\|\mathbf{A}\right\|\right] = 1$, *suppose the empirical eigenvalue distribution of* $\mathbf{A}$, a *random probability measure on* $\mathbb{R}$, *converges almost surely (a.s.) to a non-random probability measure, i.e.*

$$\lim_{N\to\infty} F_{\mathbf{A}}^{N}(x) \xrightarrow[a.s.]{} F_{\mathbf{A}}(x) \tag{4-45}$$

then the function $F_{\mathbf{A}}(x)$ *is defined as the limiting eigenvalue distribution.*

In addition to Definition 4.6.2, if (4.45) is differentiable with respect to x, then $p_{\mathbf{A}}(x)$ denotes the limiting eigenvalue density of the random matrix $\mathbf{A}$.

Asymptotic Capacity interms of Eigenvalues of Channel

In this sub-Section we derived asymptotic optimum joint decoding capacity and MMSE capacity using the Definition 4.6.1 and Definition 4.6.2. Using the property $\det(\mathbf{A}) = \prod_{i=1}^{N} \lambda_i(\mathbf{A})$ for an arbitrary $N \times N$ matrix $\mathbf{A}$, from (4.35) it follows that

$$\mathrm{C}_{\mathrm{opt}}(p(\mathbf{H});\gamma) = \mathbb{E}\left[\frac{1}{N}\sum_{i=1}^{N}\log_2\left(1+\gamma\,\lambda_i(\mathbf{H}\,\mathbf{H}^H)\right)\right] \tag{4-46}$$

Since $\mathbf{H}$ is a random matrix and the $N \times N$ Hermitian matrix $\mathbf{H}\mathbf{H}^H$ and has a limiting eigenvalue distribution $F_{HH^H}(x)$. Taking $N,M \to \infty$ with $\lim_{N,M\to\infty} N / M \triangleq \beta$, (4.46) becomes

$$\lim_{N,M\to\infty} \mathrm{C}_{\mathrm{opt}}(p(\mathbf{H});\gamma) = \lim_{N,M\to\infty} \mathbb{E}\left[\frac{1}{N}\sum_{i=1}^{N}\log_2\left(1+\gamma\,\lambda_i(\mathbf{H}\mathbf{H}^H)\right)\right] \quad (4\text{-}47)$$

Finally, the asymptotic value of (4.47) becomes

$$= \int_0^\infty \log(1+\gamma\, x)\, dF_{\mathbf{H}\mathbf{H}^H}(x) \quad (4\text{-}48)$$

For the same channel model assumptions and the property $\mathrm{tr}\,\mathbf{A} = \sum_{i=1}^{N}\lambda_i(\mathbf{A})$ for an arbitrary $N \times N$ matrix $\mathbf{A}$, from (4.7) it is straight forward to show that

$$\mathrm{mmse}_{\mathrm{avg}}(p(\mathbf{H});\gamma) = P\left[\frac{1}{M}\sum_{i=1}^{N}\frac{1}{1+\gamma\,\lambda_i(\mathbf{H}\mathbf{H}^H)} + 1 - \frac{N}{M}\right] \quad (4\text{-}49)$$

where $\mathrm{mmse}_{\mathrm{avg}}(p(\mathbf{H});\gamma)$ is the average MMSE over random matrix $\mathbf{H}$ with density $p(\mathbf{H})$. The capacity offered by MMSE filtering followed by single user decoding over the fading channel $\mathbf{H}$ is given by

$$\mathrm{C}_{\mathrm{mmse}}(p(\mathbf{H});\gamma) = \frac{1}{N}\sum_{i=1}^{N}\mathbb{E}\left[\log_2\frac{P}{\mathrm{mmse}(\mathbf{H};\gamma)}\right] \quad (4\text{-}50)$$

substituting (4.49) into (4.50), we have MMSE capacity

$$= -\frac{1}{N}\sum_{i=1}^{M}\mathbb{E}\left[\log_2\frac{1}{M}\sum_{i=1}^{N}\frac{1}{1+\gamma\,\lambda_i(\mathbf{H}\mathbf{H}^H)} + 1 - \frac{N}{M}\right] \quad (4\text{-}51)$$

when intra-cell TDMA is employed (4.51) becomes

$$\mathrm{C}_{\mathrm{mmse}}^{\mathrm{tdma}}(p(\mathbf{H});\gamma) = -\mathbb{E}\left[\log_2 \frac{1}{N}\sum_{i=1}^{N}\frac{1}{1+\gamma\,\lambda_i(\mathbf{H}\,\mathbf{H}^H)}\right] \tag{4-52}$$

Now, we find the asymptotic MMSE capacity by assuming that $N,M \to \infty$ with $\lim_{N,M\to\infty} N / M \triangleq \beta$, then (4.52) becomes

$$\lim_{N,M\to\infty} \mathrm{C}_{\mathrm{mmse}}(p(\mathbf{H});\gamma) = -\beta\log\left(\frac{1}{\beta}\int_0^{\infty}\frac{1}{1+\gamma\,x}\,dF_{\mathbf{H}\mathbf{H}^H}(x)+1-\frac{1}{\beta}\right) \tag{4-53}$$

MMSE Capacity over non-Fading Channel

In this Section, we derive MMSE capacity for the non-fading channel and use the results in the next section to calculate the asymptotic capacity. The capacity offered by MMSE filtering followed by single user decoding schemes for the non-fading scenario can be derived from (4.53) as

$$\mathrm{C}_{\mathrm{mmse}}(\mathbf{H};\gamma) = -\frac{M}{N}\left[\log_2 \frac{1}{M}\sum_{i=1}^{N}\frac{1}{1+\gamma\,\lambda_i(\mathbf{\Omega}\,\mathbf{\Omega}^H)}+1-\frac{N}{M}\right] \tag{4-54}$$

Since $M = NK$, (4.54) may be expressed as

$$= -K\left[\log_2 \frac{1}{NK}\sum_{i=1}^{N}\frac{1}{1+\gamma\,\lambda_i(\mathbf{\Omega}\,\mathbf{\Omega}^H)}+1-\frac{1}{K}\right] \tag{4-55}$$

Also, when intra-cell TDMA is employed i.e. substituting $K = 1$ in (4.55), we have

$$\mathrm{C}_{\mathrm{mmse}}^{\mathrm{tdma}}(\mathbf{H};\gamma) = -\left[\log_2 \frac{1}{N}\sum_{i=1}^{N}\frac{1}{1+\gamma\,\lambda_i(\mathbf{\Omega}\,\mathbf{\Omega}^H)}\right] \tag{4-56}$$

Asymptotic Capacity for Non-Fading Scenario

In this Section, we derive the asymptotic optimum joint decoding capacity and MMSE capacity over non-fading scenario by exploiting the circular cellular

setup of the base stations. It is to note that in this case the deterministic channel $\mathbf{\Omega}$ is a circulant as shown in (3.16). It is well known that the eigenvalues of a circulant matrix are obtainable by evaluating the Discrete Fourier Transform (DFT) of its first row [58], [38] and [65]. Hence, the eigenvalues of $\mathbf{\Omega}$ in (4.54) – (4.56) can be expressed as

$$\lambda_i(\Omega) = 1 + \Omega_R \cos(2\pi i / N) + \Omega_L \cos(2\pi i / N)\; i = 1, \cdots, N \quad \text{(4-57)}$$

Also, if $\theta_i = \dfrac{i}{N}$, we may expressed (4.57) as

$$\lambda_i(\Omega, \theta_i) = 1 + \Omega_R \cos(2\pi \theta_i) + \Omega_L \cos(2\pi \theta_i)$$

Thus, in the limit as $N \to \infty$, $\lim_{N\to\infty} \theta_i = \theta$ and (4.57) becomes

$$\lambda(\Omega, \theta) = 1 + \Omega_R \cos(2\pi\theta) + \Omega_L \cos(2\pi\theta) \quad \text{(4-58)}$$

and (4.54), (4.55) , (4.56) respectively becomes

$$\lim_{N\to\infty} \mathrm{C}_{\mathrm{opt}}\left(\mathbf{H};\gamma\right) = \int_0^1 \log\left(1 + K\gamma\lambda\left(\Omega,\theta\right)^2\right) d\theta \quad \text{(4-59)}$$

$$\lim_{N\to\infty} \mathrm{C}_{\mathrm{mmse}}\left(\mathbf{H};\gamma\right) = -K\log\left(\frac{1}{K}\int_0^1 \log\left(1 + K\gamma\lambda\left(\Omega,\theta\right)^2\right)^{-1} d\theta + 1 - \frac{1}{K}\right) \quad \text{(4-60)}$$

$$\lim_{N\to\infty} \mathrm{C}_{\mathrm{mmse}}^{\mathrm{tdma}}\left(\mathbf{H};\gamma\right) = -\log\left(\frac{1}{K}\int_0^1 \log\left(1 + K\gamma\lambda\left(\Omega,\theta\right)^2\right)^{-1} d\theta\right) \quad \text{(4-61)}$$

Capacity for Linear Cellular Scenario

It is known that for linear cellular setup as shown in Figure 3-4a, the channel gain matrix is a tri-diagonal channel matrix [96], [97] and [98]. It is observed that apart from the bottom left and top right corner entries, it is almost circulant, i.e.[12]

$$\mathbf{\Omega}_{N,1} = \begin{pmatrix} 1 & \Omega_R & 0 & 0 & 0 & \Omega_L \\ \Omega_L & 1 & \Omega_R & 0 & 0 & 0 \\ 0 & \Omega_L & 1 & \Omega_R & 0 & 0 \\ 0 & 0 & \Omega_L & 1 & \Omega_R & 0 \\ 0 & 0 & 0 & \Omega_L & 1 & \Omega_R \\ \Omega_R & 0 & 0 & 0 & \Omega_L & 1 \end{pmatrix} \simeq \begin{pmatrix} 1 & \Omega_R & 0 & 0 & 0 & 0 \\ \Omega_L & 1 & \Omega_R & 0 & 0 & 0 \\ 0 & \Omega_L & 1 & \Omega_R & 0 & 0 \\ 0 & 0 & \Omega_L & 1 & \Omega_R & 0 \\ 0 & 0 & 0 & \Omega_L & 1 & \Omega_R \\ 0 & 0 & 0 & 0 & \Omega_L & 1 \end{pmatrix} = \breve{\mathbf{\Omega}}_{N,1} \tag{4-62}$$

Therefore, $\mathbf{\Omega}$ and $\breve{\mathbf{\Omega}}$ are in fact asymptotically equivalent [29], i.e.

Definition 4.6.3 (Asymptotic Equivalent Matrices) [38] and [58]. *Let* $\mathbf{A}$ *and* $\mathbf{B}$ *be two* $N \times N$ *bounded matrices such that* $\max_k \lambda_k\left(\mathbf{A}^H\mathbf{A}\right) \le M \le \infty$ *and* $\max_k \lambda_k\left(\mathbf{B}^H\mathbf{B}\right) \le M \le \infty$. *Then* $\mathbf{A}$ *and* $\mathbf{B}$ *are said to be asymptotically*[13] *equivalent denoted by* $\mathbf{A} \simeq \mathbf{B}$ *if* $\lim_{N\to\infty} \frac{1}{\sqrt{N}} \left\|\mathbf{A} - \mathbf{B}\right\| = 0$.

In [58] and [38], it is shown that any finite order Toeplitz matrix is asymptotically equivalent to a circulant matrix constructed by filling in the bottom left and top right corner entries of the original Toeplitz matrix with appropriate entries. This is shown to imply that their eigenvalue behave similarly. Recall from (4.59) and (4.69) that $\mathrm{C}_{\mathrm{opt}}$ and $\mathrm{C}_{\mathrm{mmse}}$ are dependent on the eigenvalues of the channel matrix. Therefore, the capacity derived in (4.59), (4.60) and (4.61) can also

[12] Note that $\breve{\mathbf{\Omega}}_{N,1}$ is a $N \times N$ tri-diagonal matrix for the linear GCMAC. The setup is shown in Figure 3-2a. Also note that $\breve{\mathbf{\Omega}}_{N,1}$ is a non-symmetric tri-diagonal matrix where users are offering variable slow gain to the BSs, not like [27]-[29] where users are offering equal slow gain to the BS of interest and the slow gain channel matrix is symmetric tri-diagonal.

[13] In the limit as $N \to \infty$.

be used to evaluate the capacity for linear cellular setup. Next Section presents the simulations to show this fact (See Figure 4-10).

4.7 Simulations and Discussions

In this Section, we present numerical examples and discussions on capacity offered by C-GCMAC with decoding strategies.

4.7.1 Capacity Variation over Range of SNR and Ω

In order to analyze the dependency of the capacity on inter-cell interfering gain between the given BS and MTs of the adjacent cells, we present the 3D view[14] of $\mathrm{C}_{\mathrm{cell}}\left(\mathbf{H};\gamma\right)$, $\mathrm{C}_{\mathrm{opt}}\left(\mathbf{H};\gamma\right)$, $\mathrm{C}_{\mathrm{sud}}\left(\mathbf{H};\gamma\right)$ and $\mathrm{C}_{\mathrm{mmse}}^{\mathrm{tdma}}\left(\mathbf{H};\gamma\right)$ (Bits/sec/Hz) in Figure 4-1, Figure 4-2, Figure 4-3 and Figure 4-4 respectively. In each case, it is assumed that the inter-cell interfering MTs are at the same distance from the given BS. In Figure 4-1a, we present the first case, where only $K = 1$ intra-cell MTs are jointly decoded at the local BS over deterministic channel. The figure shows that the cell optimum decoding strategy offers higher capacity for low level of inter-cell interference. The increase in capacity at higher SNRs for low level of inter-cell interference is also evident from the Figure 4-1. For example, at γ = 40 dB and Ω = 0.2, $\mathrm{C}_{\mathrm{cell}}$ = 3.5 Bits/sec/Hz. In Figure 4-1b, we present the case, where only $K = 5$ intra-cell MTs are jointly decoded at the local BS. From the figure it is observed that with the increase in number of intra-cell MTs to be jointly decoded, the increase in capacity is evident. For example, at γ = 40 dB and Ω = 0.2, $\mathrm{C}_{\mathrm{cell}}$ = 4 Bits/sec/Hz. However, it is important to note that the cell optimum capacity is advantageous only when the inter-cell interfering users are farthest away from the given BS.

In Figure 4-2a and Figure 4-2b, we present capacity using optimum decoding strategy over deterministic channel with $K = 1$ and $K = 5$ respectively. In Figure

[14] MATLAB command surf and surfc are used to view 3D behaviour of mathematical functions over a rectangular region. Particularly, capacity (Bits/sec/Hz), slow gain (Ω) and SNR (dBs) are on z-axis, y-axis and x-axis respectively.

4-2, we present the case when KN users are jointly decoded at the super central receiver. The figure shows that the optimum decoding strategy is advantageous over cell optimum decoding strategy specifically at high levels of inter-cell interference. The cell optimum decoding strategy is interference limited therefore it offers lowest capacity of multi-user decoding strategies. The optimum decoding scheme is the best strategy in terms of capacity, however the exponential complexity with N, renders it impractical for any realistic cellular system.

In Figure 4-3a and Figure 4-3b, we present the capacity variation over range of SNR and inter-cell interference using single user decoding strategy over deterministic channel with $K = 1$ and $K = 5$ respectively. In Figure 4-3a, it is shown that capacity offered by single user decoding strategy is equal to the capacity offered by cell optimum decoding strategy for $K = 1$. In Figure 4-3b, we present the case when $K = 5$ MTs are active in each cell and employing single user decoding strategy i.e. single MT is decoded and all other inter-cell and intra-cell MTs are treated as noise. This figure shows that the single user decoding scheme offers minimum capacity for $K > 1$ in comparison with multi-user decoding schemes. The figure also shows that the system employing single user decoding scheme for K >1 is intra-cell interference limited. Similarly, Figure 4-4a and Figure 4-4b shows the capacity when linear MMSE filtering followed by single user decoding is employed over non-fading channel when $K = 1$ and $K = 5$ respectively. It can be seen from Figure 4-4a, that capacity increases with $\Omega \to 0$. However, the increase in capacity is significant at higher levels of SNR. The abrupt fall in capacity curves are due to ill conditioned non-fading channel matrix. It is reported in Chapter 5 that as $\Omega \to 0.5$, rank of the channel matrix reduces and subsequently the MMSE is effected. The phenomenon is discussed in Section 5.6.6. Similarly, with the increase in number of users the average capacity increases and the behaviour of the capacity curves is same as we observed for single user case.

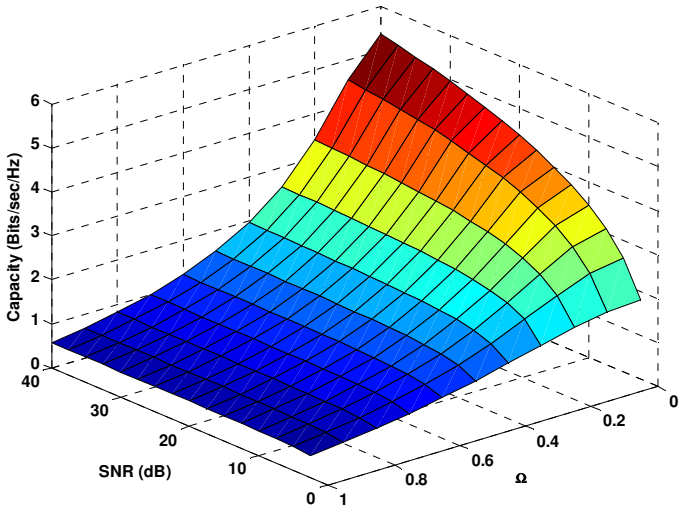

(a) $K = 1$

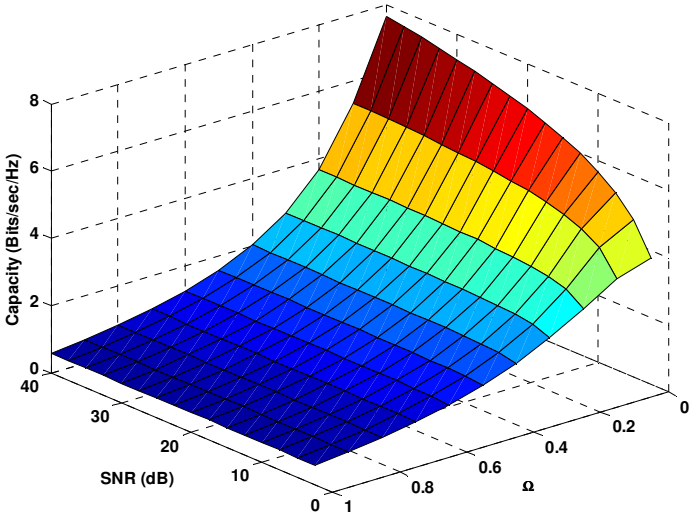

(b) $K = 5$

Figure 4-1: Variation of capacity using cell optimum decoding strategy over range of SNRs and inter-cell interference levels; (a) $K = 1$ (2 inter-cell interference seen by each BS); (b) $K = 5$ (10 inter-cell interference seen by each BS).

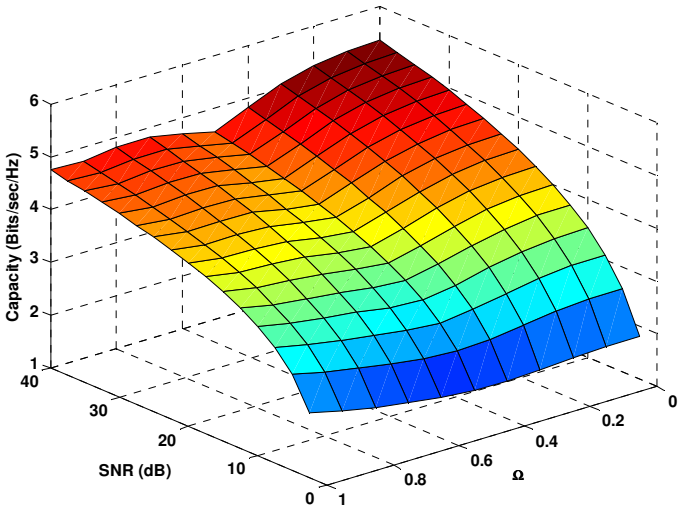

(a) $K = 1$

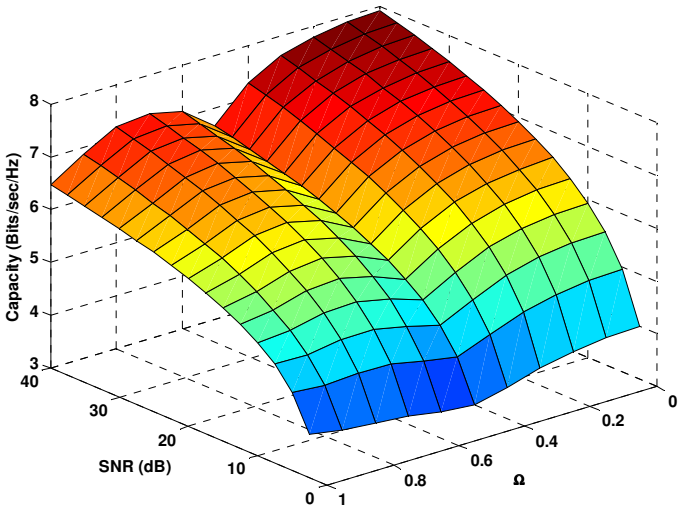

(b) $K = 5$

Figure 4-2: Variation of capacity using optimum decoding strategy over range of SNRs and inter-cell interference levels; (a) $K = 1$ (2 inter-cell interference seen by each BS); (b) $K = 5$ (10 inter-cell interference seen by each BS).

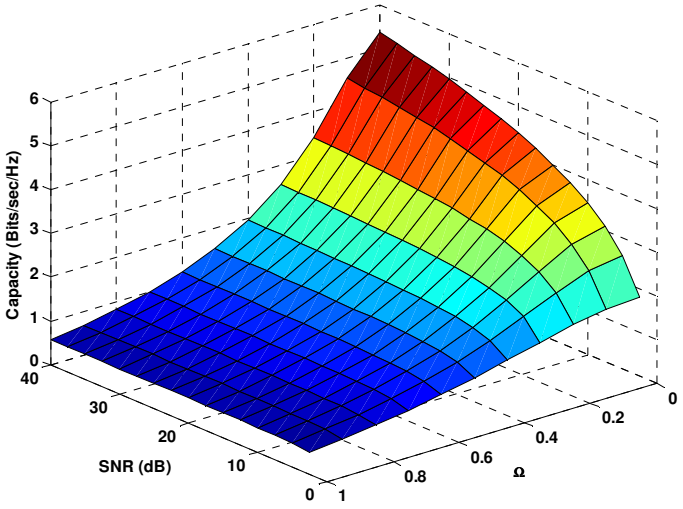

(a) $K = 1$

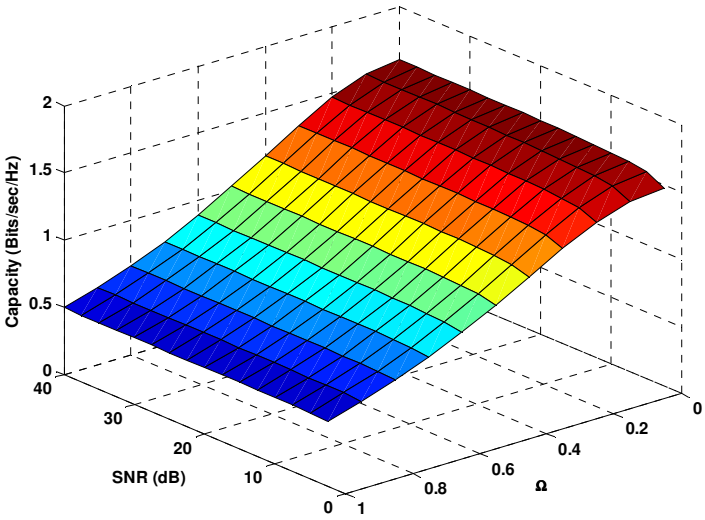

(b) $K = 5$

Figure 4-3: Variation of capacity using single user decoding strategy over range of SNRs and inter-cell interference levels; (a) $K = 1$ (2 inter-cell interference seen by each BS); (b) $K = 5$ (10 inter-cell interference seen by each BS).

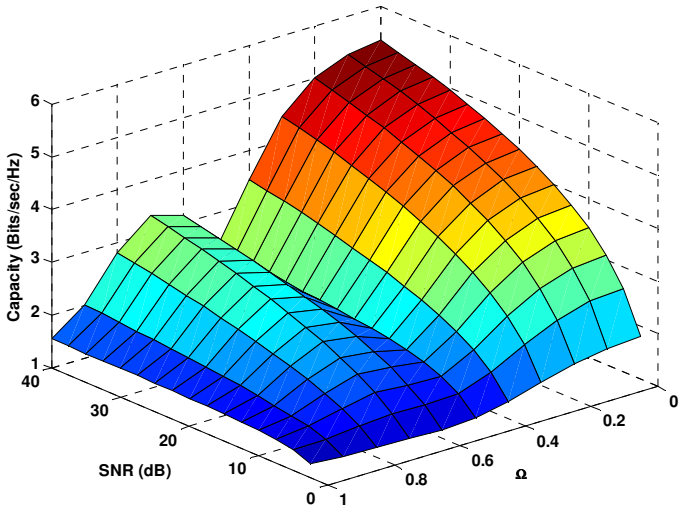

(a) $K = 1$

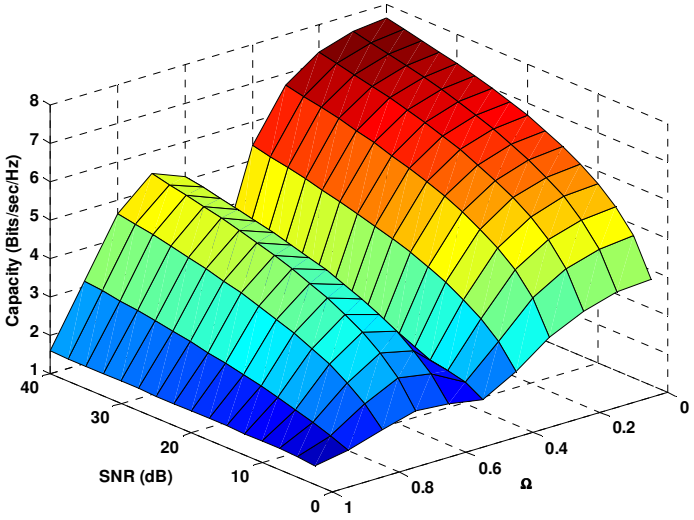

(b) $K = 5$

Figure 4-4: Variation of capacity using MMSE filtering followed by single user decoding with intra-cell TDMA strategy over range of SNRs and inter-cell interference levels; (a) $K = 1$ (2 inter-cell interference seen by each BS); (b) $K = 5$ (10 inter-cell interference seen by each BS).

4.7.2 Optimal Capacity for Single and Multi-user Scenario

In this section, we present comparison of decoding strategies over non-fading and fading channel. The analysis is supported by numerical examples to illustrate the effect of slow gain on C-GCMAC capacity. Figure 4-5 shows $\mathbf{C}_{\text{cell}}$, $\mathbf{C}_{\text{opt}}$, $\mathbf{C}_{\text{sud}}$ and $\mathbf{C}_{\text{sud}}^{\text{tdma}}$ over the deterministic C-GCMAC with $K=1$ and $K=2$ for $\gamma=0$ dB. This figure shows that when only a single user is active in each cell, it is observed that $\mathbf{C}_{\text{cell}}(\mathbf{H})=\mathbf{C}_{\text{sud}}(\mathbf{H})=\mathbf{C}_{\text{cell}}^{\text{tdma}}(\mathbf{H})=\mathbf{C}_{\text{sud}}^{\text{tdma}}(\mathbf{H})$ for the C-GCMAC. In the multi-user case, when $K=2$, it is observed that the per cell capacity offered by system exploiting cell optimum decoding, in combination with intra-cell TDMA and single user decoding in combination with intra-cell TDMA are equal for any number of MTs over C-GCMAC, i.e. $\mathbf{C}_{\text{cell}}(\mathbf{H})=\mathbf{C}_{\text{cell}}^{\text{tdma}}(\mathbf{H})=\mathbf{C}_{\text{sud}}^{\text{tdma}}(\mathbf{H})$. In this case, $\mathbf{C}_{\text{sud}}(\mathbf{H})$ offers the lowest per cell capacity due to intra-cell interfering limited behaviour of the system. It is shown that when $\Omega \to 0$, the $\mathbf{C}_{\text{opt}}$ decreases with Ω. On the contrary, $\mathbf{C}_{\text{cell}}$ and $\mathbf{C}_{\text{sud}}$ increase with Ω.

Figure 4-6 shows $\mathbf{C}_{\text{cell}}$, $\mathbf{C}_{\text{opt}}$, $\mathbf{C}_{\text{sud}}$ and $\mathbf{C}_{\text{sud}}^{\text{tdma}}$ for a deterministic C-GCMAC with *K*=1 and *K*=2 for γ= 5 dB. This figure also shows that when only one user is active in each cell, $\mathbf{C}_{\text{cell}}(\mathbf{H})=\mathbf{C}_{\text{sud}}(\mathbf{H})=\mathbf{C}_{\text{cell}}^{\text{tdma}}(\mathbf{H})=\mathbf{C}_{\text{sud}}^{\text{tdma}}(\mathbf{H})$ for the non-fading C-GCMAC. However, the increase in capacity in each case is observable due to the increase in SNR. In multi-user scenario, when *K* = 2 in each cell, it is observed that as $\Omega \to 0$ the cell optimum decoding strategy offers substantial gains over single user decoding, single user decoding with TDMA and cell optimum decoding with TDMA. The increase in $\mathbf{C}_{\text{cell}}$ is obvious with the increase in users to be jointly decoded. It is observed that as $\gamma \to 0$ $\mathbf{C}_{\text{cell}}$, $\mathbf{C}_{\text{sud}}$ and $\mathbf{C}_{\text{sud}}^{\text{tdma}}$ follows $\mathbf{C}_{\text{opt}}$ for $\Omega < 0.1$ when $K=1$ (see Figure 4-5a). On the other hand only $\mathbf{C}_{\text{cell}}$ and $\mathbf{C}_{\text{sud}}^{\text{tdma}}$ follows $\mathbf{C}_{\text{opt}}$ for $\Omega < 0.1$ when number of active users increases to $K=2$ per cell

(see Figure 4-5b). Therefore, in multi-user scenarios, for $\Omega \ll 0.2$ the single user decoding strategy with intra-cell TDMA is optimal. It has been shown that the single user decoding scheme shows intra-cell interference limited behaviour in multi-user scenario. Figure 4-6a and Figure 4-6b shows that with the increase in SNR i.e. $\gamma = 5$ dB the threshold for which C_{cell}, C_{sud} and C_{sud}^{tdma} follows C_{opt} is deceased to $\Omega \ll 0.1$. On the other hand $C_{cell} = C_{sud}^{tdma} = C_{opt}$ as $\Omega \rightarrow 0$ when number of active users per cell increases at higher SNR (see Figure 4-6b).

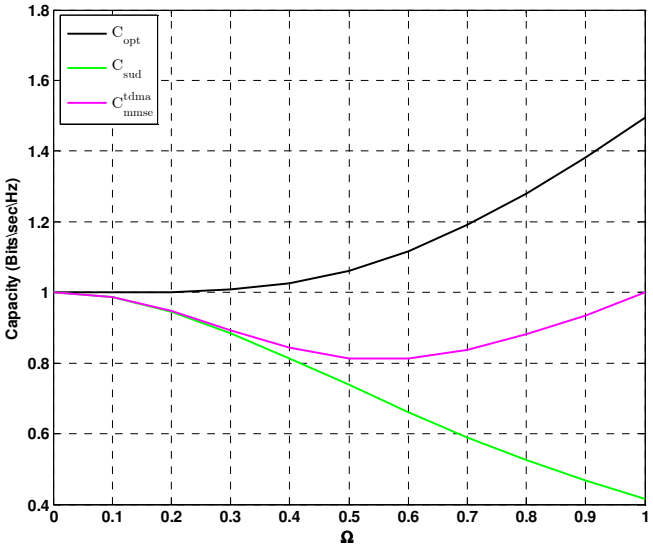

(a) $K = 1$

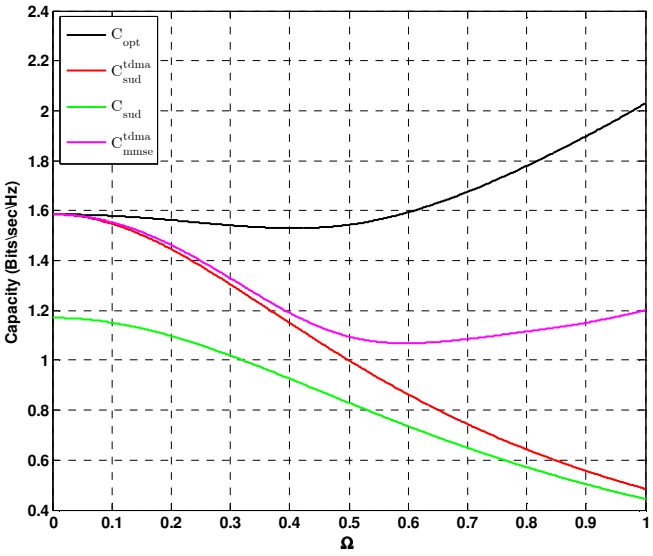

(b) $K = 2$

Figure 4-5: Summary of C-GCMAC decoding strategies, $N = 6$, $\gamma = 1$dB: optimum decoding capacity; intra-cell TDMA with linear MMSE filtering capacity; cell optimum decoding capacity; single user decoding capacity.

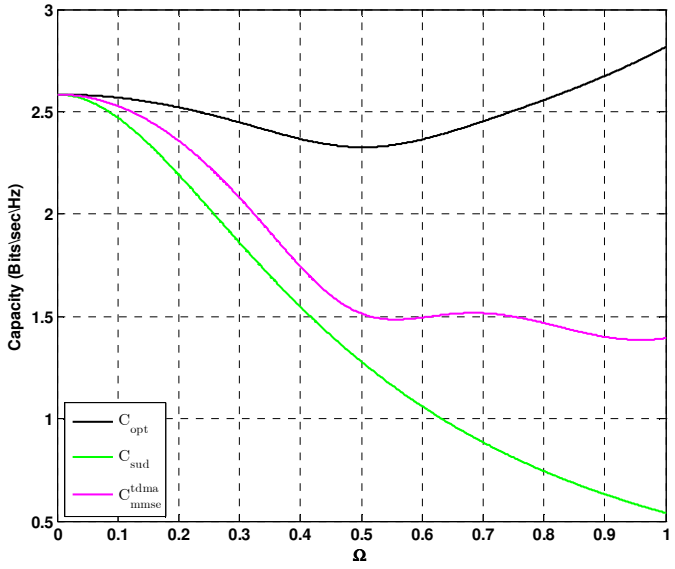

(a) $K = 1$

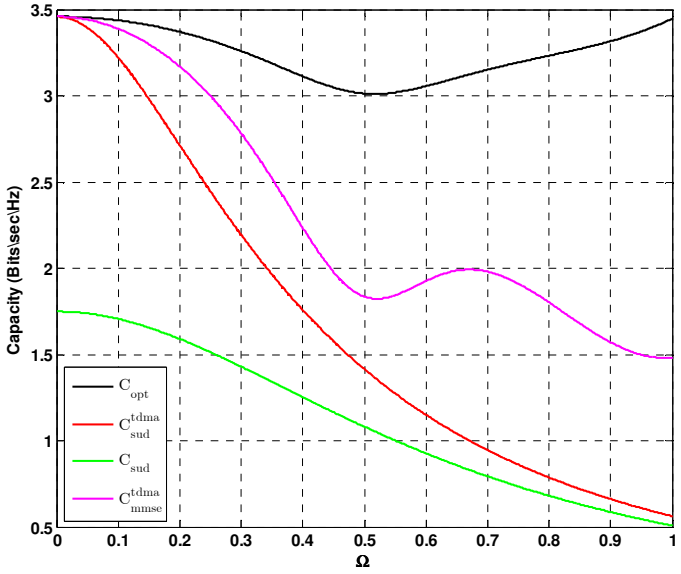

(b) $K = 2$

Figure 4-6: Summary of C-GCMAC decoding strategies, $N = 6$, $\gamma = 5$ dB: optimum decoding capacity; intra-cell TDMA with linear MMSE filtering capacity; cell optimum decoding capacity; single user decoding capacity.

Let us take a closer look at the impact of fading on the optimum decoding strategy over C-GCMAC over various SNR scenarios. In this sub-section we analyze the effect of inter-cell interference when wideband (multi-user decoding) decoding and intra-cell TDMA decoding strategies are employed. Figure 4-7 and Figure 4-8 shows $\mathrm{C}_{\mathrm{opt}}$ over fading, non-fading and fading with intra-cell TDMA strategies for $K = 2$ and $K = 5$ per cell respectively. From both figures it can be seen that at both low and high SNR, when intra-cell TDMA is employed the capacity of the fading channel exceeds that of the non-fading channel for moderate levels of inter-cell interference i.e. $\Omega = 0.4$. It can be also be seen when wideband transmission is employed this threshold level of Ω decreases with the increase in number of users to be jointly decoded. For an example, from Figure 4-7 when $K = 2$ per cell, fading does not improve the optimum decoding capacity beyond the non-fading channel until $\Omega \approx 0.3$ at both low and high SNR. Similarly, from Figure 4-8 when $K = 5$ per cell, where the threshold reduces to $\Omega \approx 0.2$.

4.7.3 Special Case: Large Number of Users per Cell with No Intra-cell TDMA

In [63], Somekh and Shamai also analyzed the scenarios when no intra-cell TDMA is employed and system contains a large number of users per cell. They showed that intra-cell TDMA is suboptimal when fading is present, i.e.

$$\mathrm{C}_{\mathrm{opt}}\left(p(\mathbf{H});\gamma\right) \geq \mathrm{C}_{\mathrm{opt}}^{\mathrm{tdma}}\left(p(\mathbf{H});\gamma\right) \tag{4-63}$$

this is in contrast to the non-fading channel, where wideband and intra-cell TDMA transmission schemes achieve the same optimum decoding capacity [29]. Furthermore, in [63], Somekh and Shamai used the strong law of large number to show that $\mathbf{H}\mathbf{H}^{H}$ converges to the diagonal matrix $K\left(1+\Omega_R^2+\Omega_L^2\right)\mathbf{I}_N$ as K increases, and hence

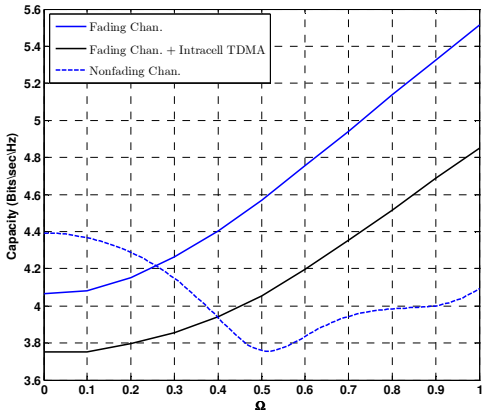

(a) $\gamma = 10$ dB

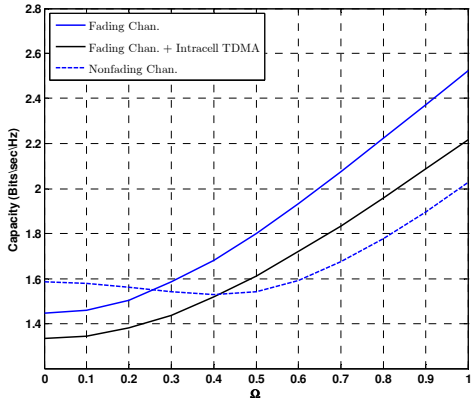

(b) $\gamma = 0$ dB

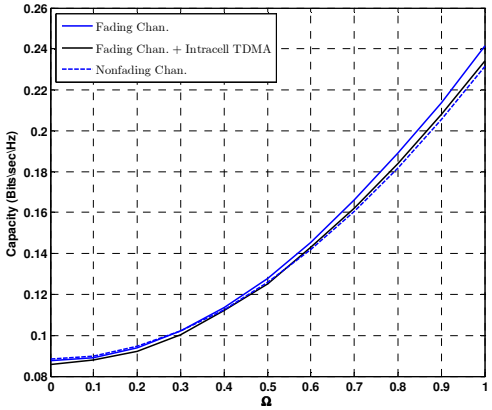

(c) $\gamma = -15$ dB

Figure 4-7: Summary of optimum decoding strategy over C-GCMAC, $N = 6$, $K = 2$.

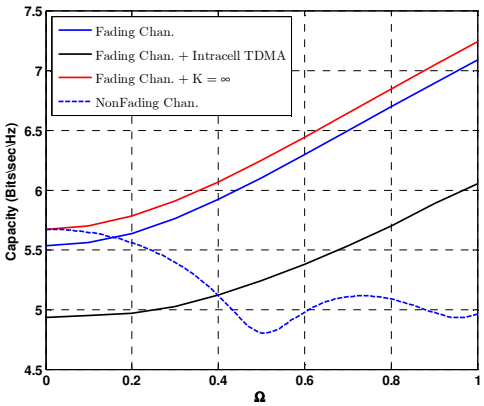

(a) $\gamma = 10$ dB

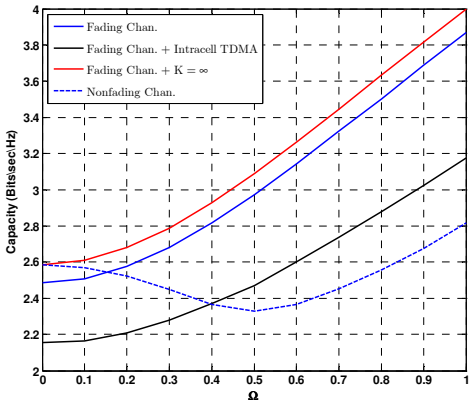

(b) $\gamma = 0$ dB

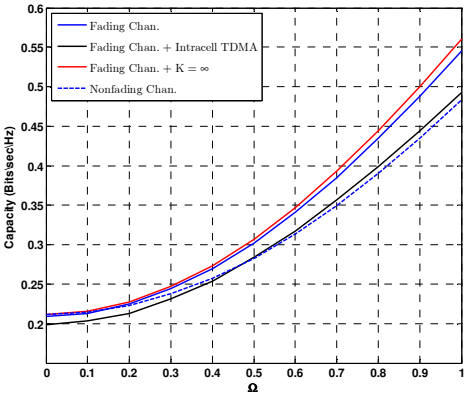

(c) $\gamma = -15$ dB

Figure 4-8: Summary of optimum decoding strategy over C-GCMAC, $N = 6$, $K = 5$.

$$\lim_{K\to\infty} \mathrm{C}_{\mathrm{opt}}\Big(p(\mathbf{H});\gamma\Big) = \log\Big(1+K\gamma\Big(1+\Omega_R^2+\Omega_L^2\Big)\Big) \qquad (4\text{-}64)$$

Figure 4-9a and Figure 4-9b shows capacity over fading and non-fading channels using MMSE filtering followed by single user decoding with $K\gamma = 1$ and $K\gamma = 10$ respectively. From the figure it can be seen that for intra-cell TDMA (which corresponds to the $K = 1$curves), like the optimum decoding scenario in Figure 4-7 and Figure 4-8, fading does not improve capacity beyond the non-fading channel until $\Omega \approx 0.4$. Similarly, for the wideband scenario (which corresponds to $K = 5$ curves), where the threshold reduces to $\Omega \approx 0.2$. Another interesting observation is that for low levels of SNR when fading is present, there is not an overly large advantage in terms of capacity (as in the case of non-fading channel capacity) as compared with the case when intra-cell TDMA is employed (compare solid red curve with sold blue curve in Figure 4-9a). Of course, from a decoding complexity point of view, intra-cell TDMA is still preferable. At high SNR, capacity using intra-cell TDMA ($K = 1$) outperforms the capacity of wideband transmission ($K = 5$) (see Figure 4-9b).

4.7.4 Special Case: Capacity Performance of Asymptotic Channel Matrices

The comparison of $\mathrm{C}_{\mathrm{opt}}\big(\mathbf{H};\gamma\big)$ and $\mathrm{C}_{\mathrm{mmse}}^{\mathrm{tdma}}\big(\mathbf{H};\gamma\big)$ over the deterministic Circular-GCMAC and Linear-GCMAC is shown in Figure 4-10. This figure presents a special case when $N \to \infty$. The capacity offered by such asymptotic channel matrices is compared with capacity offered by finite order channel matrices i.e. when $K = 1$ and $N = NK = 6$. The Capacity using the optimum joint decoding strategy and MMSE filtering followed by single user decoding with intra-cell TDMA over circulant-GMAC is equal to the capacity offered by these techniques over linear-GMAC. Thus in the limit as $N \to \infty$, circulant matrix and tri-diagonal matrix are asymptotically equivalent (compare the solid black curve with the red dots and the solid blue curve with the brown dots in Figure 4-10a and Figure 4-10b).

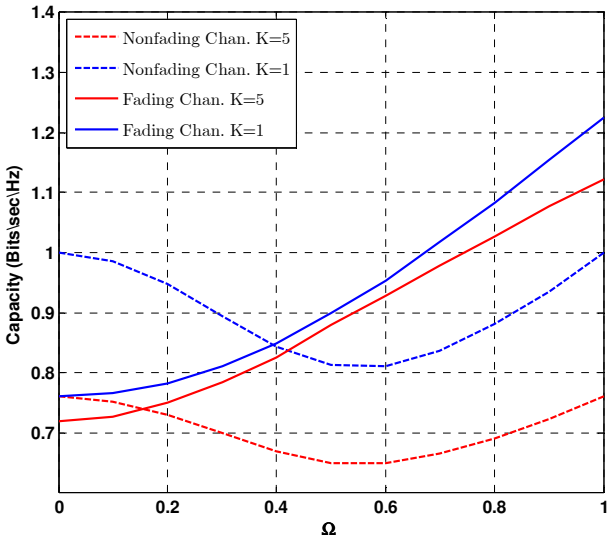

(a) $K\gamma = 1$

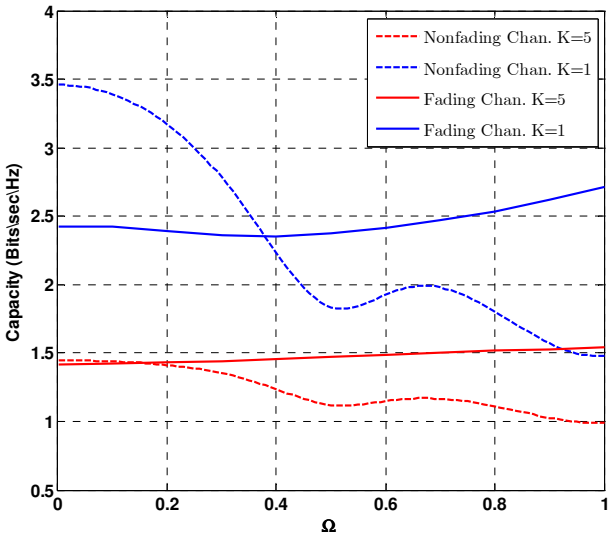

(b) $K\gamma = 10$

Figure 4-9: Capacity of circular cellular channel with Rayleigh fading when linear MMSE filtering followed by single user decoding is employed: solid lines fading channel capacity with 1000 trials per simulation point; dashed lines, non-fading channel capacity.

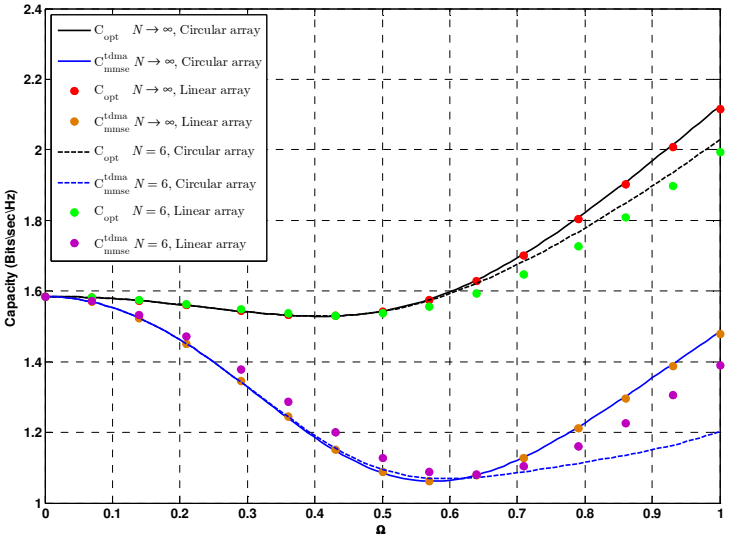

(a) $\gamma = 0$ dB

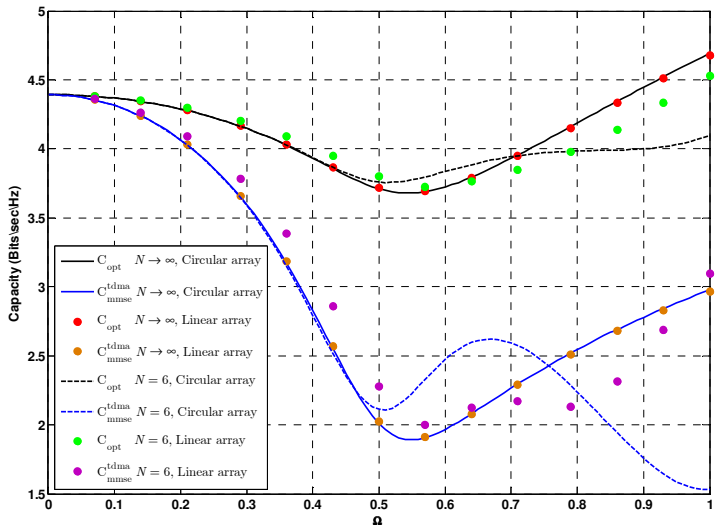

(b) $\gamma = 10$ dB

Figure 4-10: Summary of capacity over deterministic C-GCMAC and linear-GCMAC for $K = 2$; (a) $\gamma = 0$ dB (b) $\gamma = 10$ dB.

At low range of SNR, capacity offered by finite order channel matrix e.g. $N = 6$ follows capacity offered by channel matrix where $N \to \infty$ till medium range of interference $\Omega \approx 0.6$ (see Figure 4-10a) where as at high SNR this threshold increases to $\Omega \approx 0.7$. Thus, at low level of interference the information theoretic performance of linear-GCMAC and circular-GCMAC are approximately same.

4.7.5 Contribution of Variable Inter-cell Interfering Gain

In this Section, we present the performance analysis of capacity using cell optimum decoding, optimum joint decoding, single user and single user with intra-cell TDMA decoding strategies over the variable inter-cell interference gain between the MTs and the given BS [142].

4.7.5.1 Effect of Variable Inter-Cell Interference over Non-Fading Channel

Let us first consider the case when the fading between the MTs and the given BS is not present. Figure 4-11, Figure 4-12 and Figure 4-13 presents capacity variation when $K = 1$ user per cell is active which corresponds to two interfering users for each BS. The figures present the scenario when inter-cell interference of one of the inter-cell interfering user is fixed and the interference level of other user varies at full range of interference i.e. $\Omega \in (0,1)$. Each of the three figures has sub-figures to show the effect of variable inter-cell interference. It can be seen from Figure 4-11 that cell optimum decoding capacity increases drastically when interference level of one of the inter-cell interfering user is fixed and interference level of the other user varies. It is interesting to note that capacity increases when $\Omega \to 0$. In each figure, the black curve with circle marker shows the capacity offered by decoding strategy when both users are offering equal inter-cell interfering gain. For example, from Figure 4-11a, where interference level of one user is $\Omega = 0.9$ i.e. one user is offering high level of interference and the interference level of other user is varies from 0 to 1. Cell optimum capacity increases from 0.6 Bits/sec/Hz to 1.3 Bits/sec/Hz as $\Omega \to 0$.

Similarly, when the interference level of one of the user is fixed at $\Omega = 0.2$ i.e. low level interference and interference level of the other user is $\Omega < 0.2$, the capacity improvement is up to 1 Bit/sec/Hz in contrast with the case when both of the users are offering interference level of $\Omega = 0.2$ (see Figure 4-11e).

Figure 4-12 shows optimum decoding capacity over non-faded channel by varying the inter-cell interference of only one user among the two interfering users while the interference level of other user is fixed. It is interesting to note that optimum decoding capacity increases with the decrease in inter-cell interference level $\Omega > 0.5$ of one user when interference level of other user is fixed at $\Omega \geq 0.5$. For an example, when the inter-cell interference level is fixed at $\Omega = 0.6$, the variation in inter-cell interference level of other user doesn't increase the capacity till $\Omega = 0.5$. It can be seen from the Figure 4-12a, Figure 4-12e and Figure 4-12f that when interference level of one of the user is fixed at high or low level, the advantage of varying the interference of the other user is not as great as when interference is fixed at a medium level of interference.

Figure 4-13 shows the capacity when linear MMSE filtering followed by single user decoding is employed over non-fading channel. It can be seen from Figure 4-13a, that when interference offered by one of the user is fixed at high level, the capacity increases till the interference level of the other user reaches $\Omega = 0.5$. It is observed that when the interference level of one user is fixed to moderate level, the variability of interference of other user doesn't increase the capacity till 0.5. When interference level of one of the user is fixed at moderate level such that $\Omega \geq 0.5$, the capacity increases for $\Omega < 0.5$ (see Figure 4-13b and Figure 4-13c). On the other side, when interference of one of the user is fixed at $\Omega < 0.5$, the capacity increases only when the interference level of the other user is greater than the fixed interference level (see Figure 4-13d and Figure 4-13e). For an example, when $\Omega = 0.4$ the higher capacity can only be guaranteed when the interference of the other user is $\Omega < 0.4$ (see Figure 4-13d)

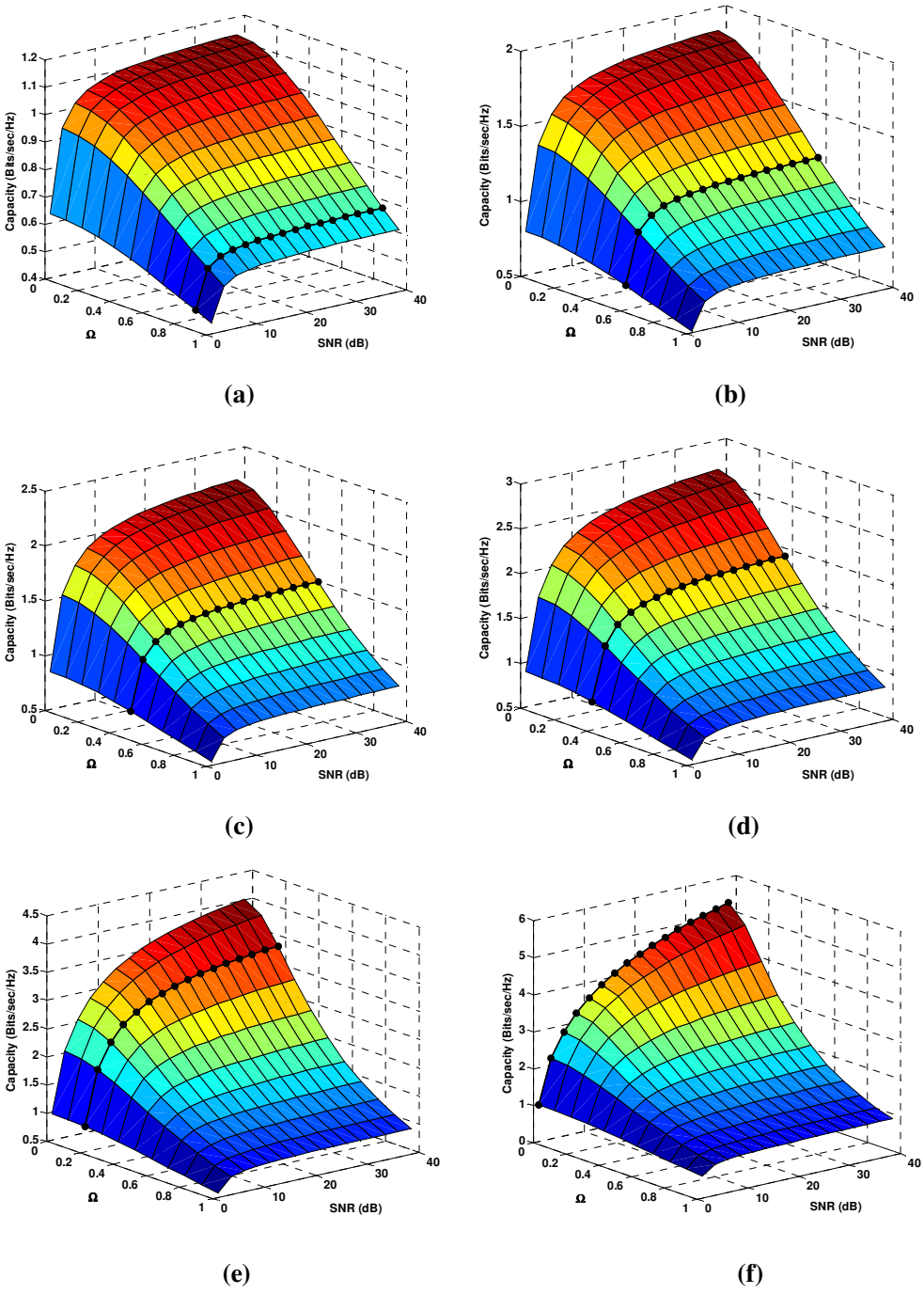

Figure 4-11: Summary of capacity using cell optimum decoding strategy with $K = 1$ (2 inter-cell interference) over non-faded circular channel by varying the inter-cell interference of users T_{j-1} and fixing the interference level of users T_{j+1} at (a) $\Omega_R = 0.9$; (b) $\Omega_R = 0.6$; (c) $\Omega_R = 0.5$; (d) $\Omega_R = 0.4$; (e) $\Omega_R = 0.2$; (f) $\Omega_R = 0$; Curve with black circle marker is the capacity when users in both adjacent cells offers equal level of inter-cell interference.

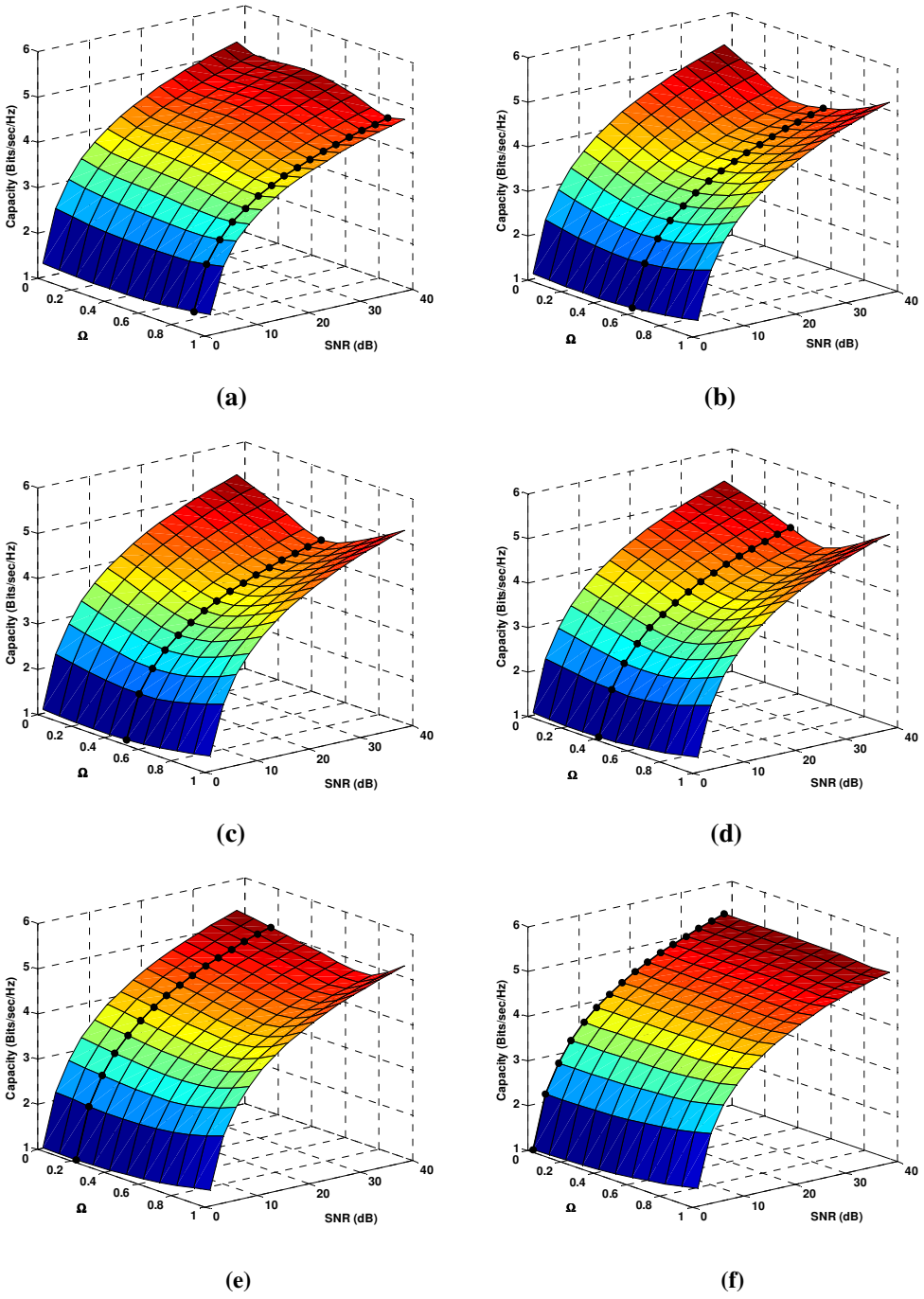

Figure 4-12: Summary of capacity using optimum decoding strategy with $K = 1$ (2 inter-cell interference) over non-faded circular channel by varying the inter-cell interference of users T_{j-1} and fixing the interference level of users T_{j+1} at (a) $\Omega_R = 0.9$; (b) $\Omega_R = 0.6$; (c) $\Omega_R = 0.5$; (d) $\Omega_R = 0.4$; (e) $\Omega_R = 0.2$; (f) $\Omega_R = 0$; Curve with black circle marker is the capacity when users in both adjacent cells offers equal level of inter-cell interference.

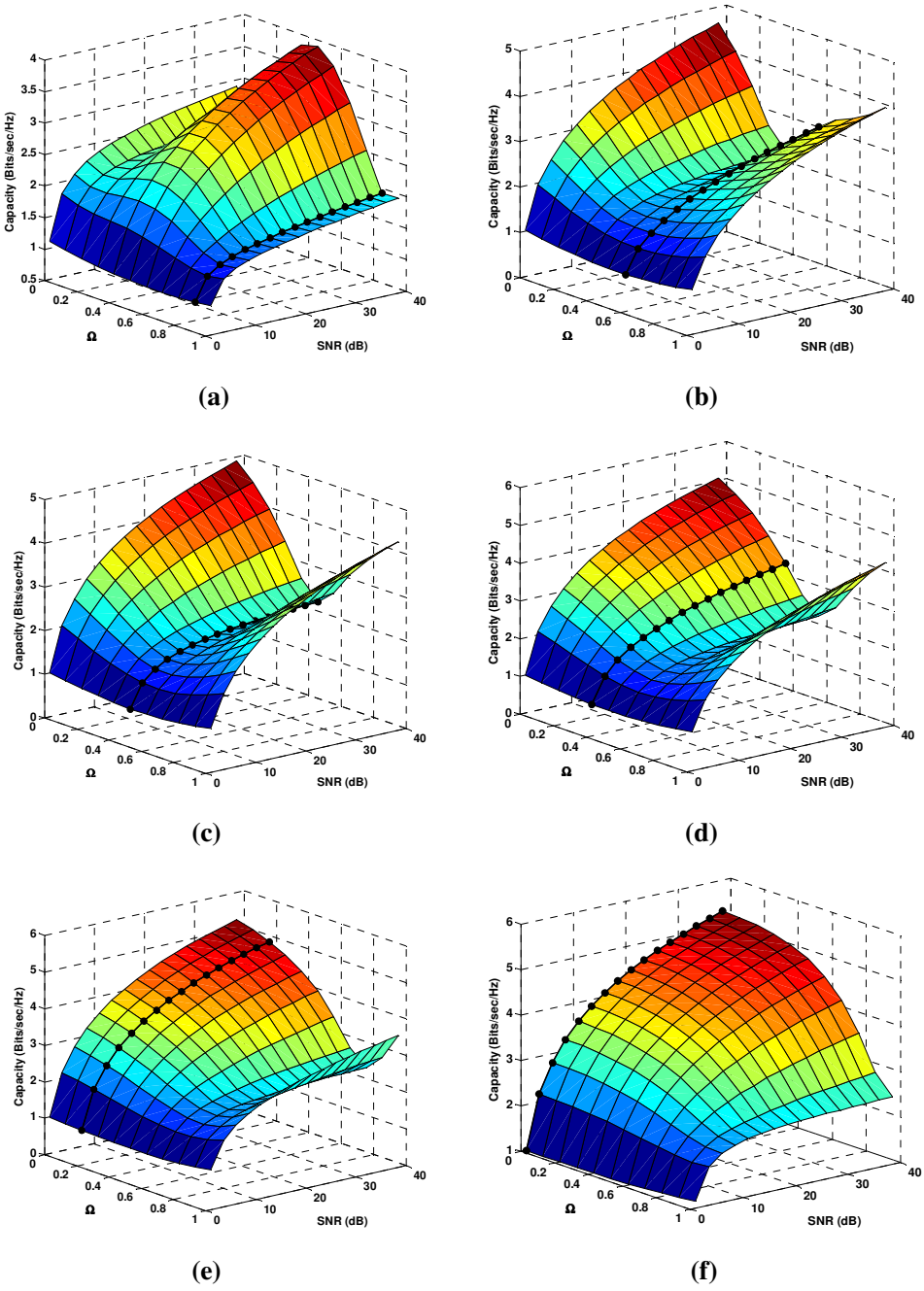

Figure 4-13: Summary of capacity using MMSE filtering with intra-cell TDMA strategy with $K = 1$ (2 inter-cell interference) over non-faded circular channel by varying the inter-cell interference of users T_{j-1} and fixing the interference level of users T_{j+1} at (a) $\Omega_R = 0.9$; (b) $\Omega_R = 0.6$; (c) $\Omega_R = 0.5$; (d) $\Omega_R = 0.4$; (e) $\Omega_R = 0.2$; (f) $\Omega_R = 0$; Curve with black circle marker is the capacity when users in both adjacent cells offers equal level of inter-cell interference.

4.7.5.2 Effect of Variable Inter-Cell Interference over Fading Channel

In this sub Section, we present the effect of variable inter-cell interference on decoding strategies over the fading channel. The analysis is supported by complementary cumulative distribution function (CCDF)[15] curves obtained using cell optimum decoding strategies, optimum decoding, single user with TDMA and single user decoding strategies. In all simulation experiment, we assumed that the link between the given BS and MTs is Rayleigh flat faded. The CCDF curves are obtained after averaging 5000 Monte Carlo trials of resultant channel matrix $\mathbf{H}$. The CCDF curves are used to analyze how often the capacity is above the threshold. For clarity of understanding, we denote $\Omega_R \in \mathbb{R}^{1\times K}$ as an interfering gain vector for the inter-cell MTs located on right side of the given BS i.e. between the MTs T_{j+1} and BS. Likewise $\Omega_L \in \mathbb{R}^{1\times K}$ is for the inter-cell MTs located on left side of the given BS i.e. between the MTs T_{j-1} and BS. The capacity $\mathbf{C}_{\text{cell}}(p(\mathbf{H}),\gamma)$, $\mathbf{C}_{\text{opt}}(p(\mathbf{H}),\gamma)$, $\mathbf{C}_{\text{sud}}(p(\mathbf{H}),\gamma)$ and $\mathbf{C}_{\text{sud}}^{\text{tdma}}(p(\mathbf{H}),\gamma)$ are obtained at $\gamma = 20$ dB for $K = 1$ (two inter-cell interfering users) and K = 2(four inter-cell interfering users). A reasonable performance indicator is the capacity that can be supported with 10% outage.

Figure 4-14, Figure 4-15 and Figure 4-16 presents the scenario for K = 1 (2 interfering users) when interference level of only one of the user among the two interfering users is variable. Figure 4-14 shows when user T_{j-1} is located in zone #1 i.e. user offering high level of interference and located in close vicinity of given BS.

[15] For every real number x, the CDF of a real-valued random variable X is given by $\mathrm{x} \mapsto \mathrm{F}_{\mathrm{X}}(\mathrm{x}) = p(\mathrm{X} \le \mathrm{x})$ where the right side represents the probability that the random variable takes on a value less than or equal to x. Sometimes, it is useful to study the opposite question and ask how often the random variable is above a particular threshold. This is called the complementary CDF (CCDF), define as $\mathrm{F}_{\mathrm{c}}(\mathrm{x}) = p(\mathrm{X} > \mathrm{x}) = 1 - \mathrm{F}(\mathrm{x})$ where $\mathrm{F}_{\mathrm{c}}(\mathrm{x})$ is commonly referred to as reliability function in engineering literature [90].

The interference level of other user T_{j+1} varies as it moves from zone #1 to zone #3 (see Figure 4-14a - Figure 4-14c). The CCDF curves of capacity with circle marker are for the scenario when both interfering users are offering equal level of interference. Similarly, the CCDF curves of capacity with square marker are for the scenario when interference level of one user is variable. Figure 4-14a show when both interfering users are located in zone #1 which corresponds to interference level $0.7 \leq \Omega \leq 1$. The capacity offered is compared with when both user offers equal interference level. It can be seen that the capacity offered with variable inter-cell interference with in zone #1 is equal to the capacity offered when inter-cell interference level of users is $\Omega = 0.8$. It is also found that capacity with variable interference is greater than the capacity when both users are offering high level of interference i.e. $\Omega = 0.9$.

Figure 4-14b shows the CCDF curves when one user T_{j-1} is in zone #1 and another user T_{j+1} is moved to zone #2 which corresponds to range of interference $0.3 \leq \Omega \leq 0.7$. The capacity with variable slow gain outperforms the capacity when interference level of both users is equal i.e. both are offering high level of interference while located in zone #1.

Figure 4-14c shows the CCDF curves when user T_{j-1} is in zone #1 and another user T_{j+1} is moved to zone #3 which corresponds to range of interference $0 \leq \Omega \leq 0.2$. The capacity with variable interference outperforms the capacity when interference level of both users is equal i.e. both are offering high level of interference while located in zone #1.

Figure 4-15 shows the CCDF curves when one user T_{j-1} is located in zone #2 and other user T_{j+1} is located in zone #1 (see Figure 4-15a), in zone #2 (see Figure 4-15b) and in zone #3 (see Figure 4-15c). The capacity offered with variable interference is compared with the capacity offered when both users are offering equal

level of interference (medium level interference) while staying in zone #2 i.e. when both users are offering equal interference of the range $0.3 \leq \Omega \leq 0.7$.

Figure 4-16 shows the CCDF curves when one user T_{j-1} is located in zone #3 and other user T_{j+1} is located in zone #1 (see Figure 4-16a), in zone #2 (see Figure 4-16b) and in zone #3 (see Figure 4-16c). The capacity using cell optimum, single user with TDMA and single user decoding strategies outperforms the capacity when interference level of both users is equal (both users are offering high level of interference of range $0.7 \leq \Omega \leq 1$ (see Figure 4-16a) and when both users are offering medium level of interference of range $0.3 \leq \Omega \leq 0.7$ (see Figure 4-16b). Figure 4-16c shows the scenario when both users are located in zone #3 with variable interference level. The capacity with variable interference level outperforms the capacity when interference level of both users is $\Omega = 0.1$. It is interesting to note that variable interference level strategy is advantageous when at least one of the users is offering low level of interference. For example, the fractional gain yielded by 10% outage capacity[16] using cell optimum decoding strategy denoted by $\mathbf{C}_{\text{cell}}(p(\mathbf{H}), \gamma)^{0.1}$ with variable interference level (user T_{j-1} located in zone #3 and user T_{j+1} located in zone #1) is 54% over capacity offered by decoding strategy when both users are offering interference $\Omega = 0.7$ (see Figure 4-16a). Similarly, fractional gain yielded by $\mathbf{C}_{\text{cell}}(p(\mathbf{H}), \gamma)^{0.1}$ when user T_{j-1} located in zone #3 and user T_{j+1} located in zone #2 over the capacity when both user are offering equal interference level $\Omega = 0.3$ is 8% and is increases to 36 % when $\Omega = 0.4$ (Figure 4-16b). Similarly, the fractional gain yielded by $\mathbf{C}_{\text{cell}}(p(\mathbf{H}), \gamma)^{0.1}$ when both users are located in zone #3 over the capacity when both users are offering equal interference level $\Omega = 0.1$ is 25%. This is to note that this fractional gain in capacity using variable interference over equal interference level increases with the increase in

[16] The outage capacity is the capacity that is attained with some given probability (when it is not satisfied, an outage event is declared). Throughout the thesis the outage probability is 0.1.

interference level of both users (see Figure 4-16a and Figure 4-16b and compare curves with square marker with the curves with circle marker). It can be seen from the Figure 4-14, Figure 4-15 and Figure 4-16 that variable interference strategy is not advantageous for optimum decoding capacity since we compare the capacity obtained with variable interference with the capacity obtained using equal interference for both users when they are located in higher zone. Since optimum decoding capacity increases with the increase in interference level therefore when we compare the optimum decoding capacity with variable interference with capacity by users located in low zone (this comparison is discuss in detail in the next subsection). In Figure 4-17, Figure 4-18 and Figure 4-19 we present the scenario for K = 2 (4 interfering users for each BS) when interferene level of users is variable[17]. Figure 4-17 shows CCDF curves of capacity offered by optimum decoding strategy when maximum 4 and minimum 3 users are located in zone #1 (high level interference) with variable interference level in the range $0.7 < \Omega < 1$. It can be seen from Figure 4-17a when 4 users are located in zone #1 with variable interference (CCDF curves with square marker) and when 4 users are offering equal level of interferene $\Omega = 0.9$ (CCDF curves with the circle marker). Improvement in $\mathbf{C}_{\text{cell}}(p(\mathbf{H}), \gamma)$, $\mathbf{C}_{\text{sud}}(p(\mathbf{H}), \gamma)$ and $\mathbf{C}_{\text{sud}}^{\text{tdma}}(p(\mathbf{H}), \gamma)$ is observed with variable level of interference when compare with capacity offered by equal level of interference. It is interesting to note that $\mathbf{C}_{\text{cell}}(p(\mathbf{H}), \gamma)$, $\mathbf{C}_{\text{sud}}(p(\mathbf{H}), \gamma)$ and $\mathbf{C}_{\text{sud}}^{\text{tdma}}(p(\mathbf{H}), \gamma)$ increases when at least one of the interfering user offer low level of interference (see Figure 4-17b and Figure 4-17c).

[17] In the multi-user scenario for example $K = 2$, where channel slow gain is variable in each of the adjacent cells across the zones, the location and number of users are expressed as zone #1(2 user) i.e. both users are located in zone 1. Similarly, when one user is located in zone 1 and other user is located in zone 2; the location and number of users are expressed as zone #1(1 user), zone #2(1 user).

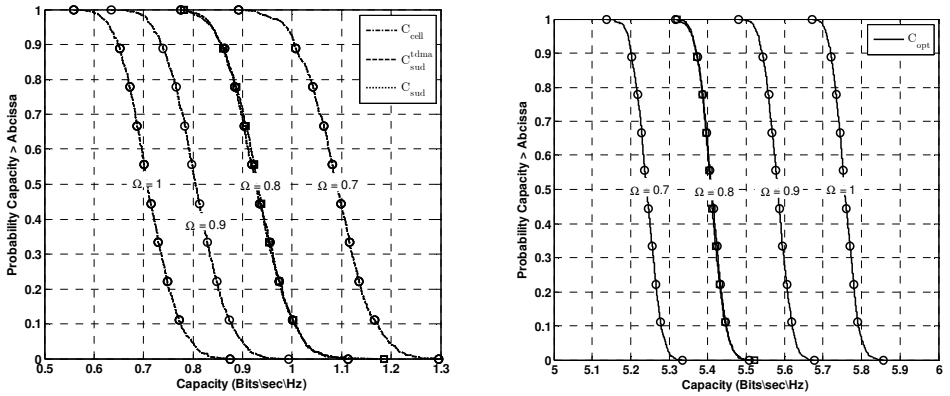

(a)

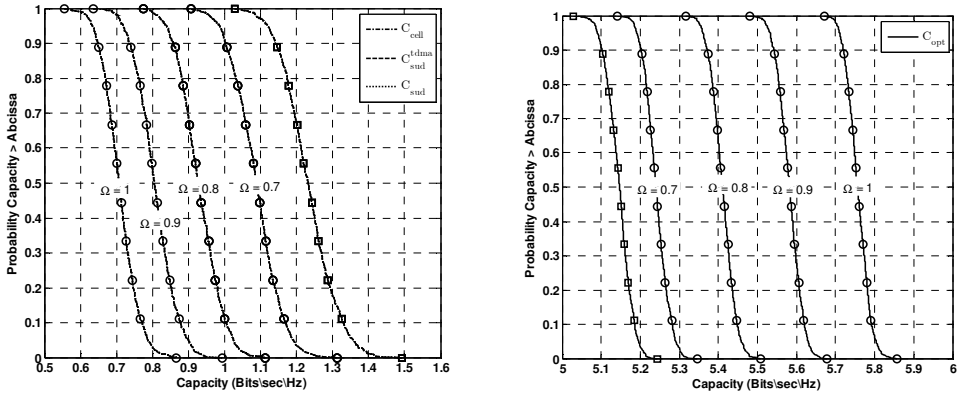

(b)

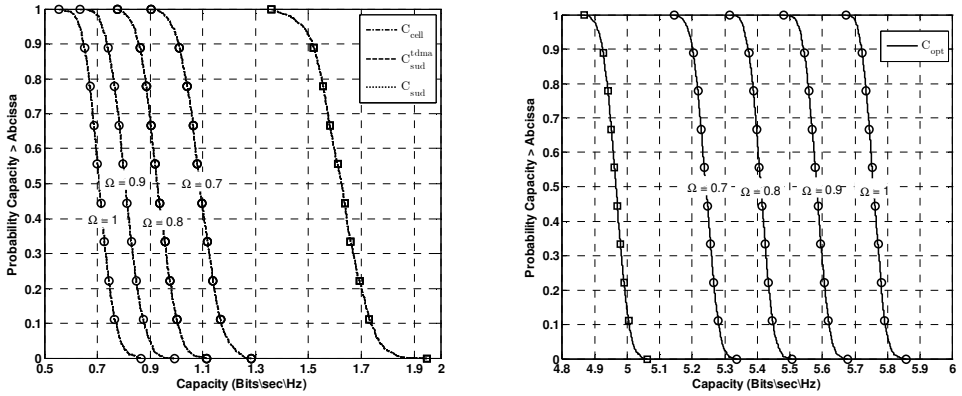

(c)

Figure 4-14: Summary of comparison of capacity over faded C-GCMAC offered by variable inter-cell interfering users (square marker) and with equal inter-cell interfering users (circle marker): (a) both users are located in zone #1 (b) one user is located in zone #1 and other is in zone #2 (c) one user is located in zone #1 and one is in zone #3.

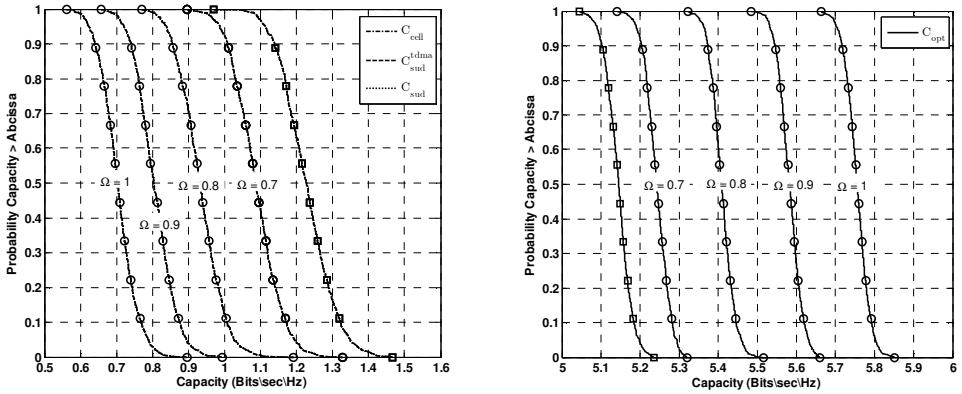

(a)

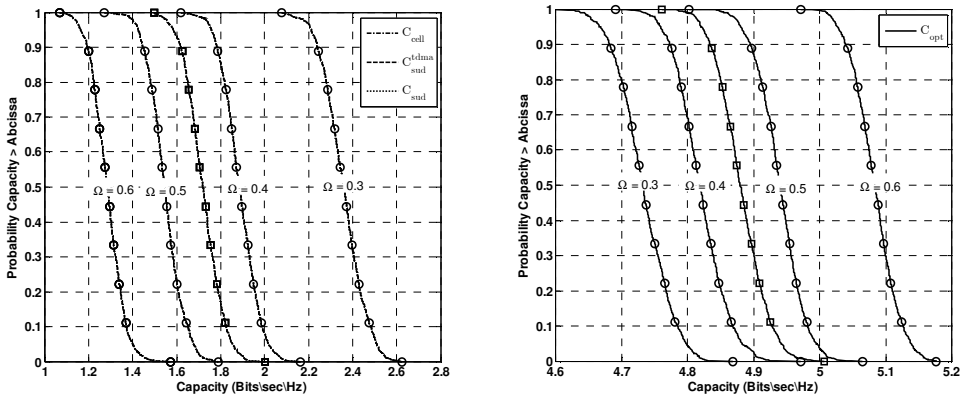

(b)

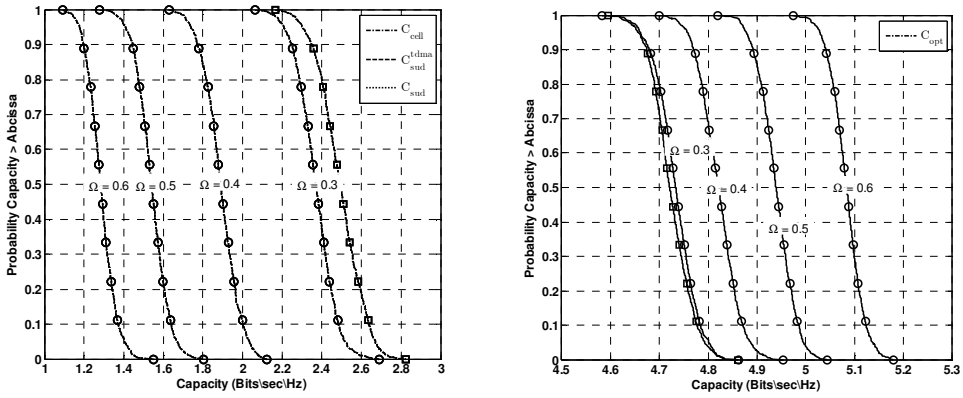

(c)

Figure 4-15: Summary of comparison of capacity over faded C-GCMAC offered by variable inter-cell interfering users (square marker) and with equal inter-cell interfering users (circle marker): (a) one user is located in zone #2 and other is in zone #1 (b) both users are located in zone #2 (c) one user is located in zone #2 and other is in zone #3.

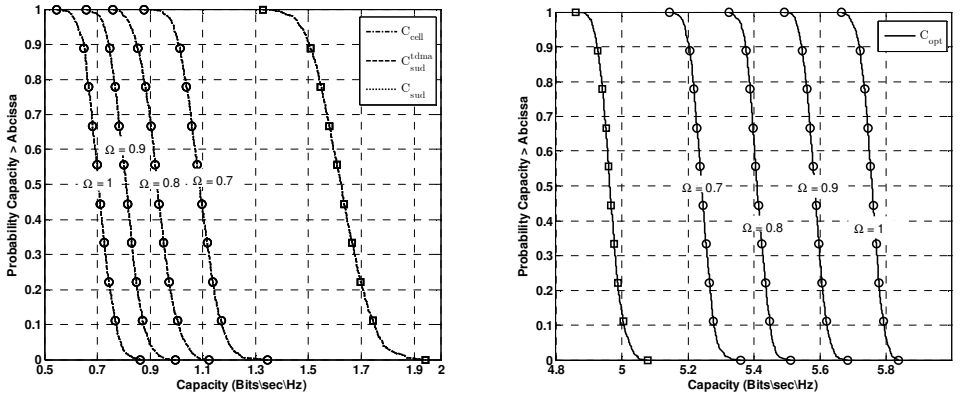

(a)

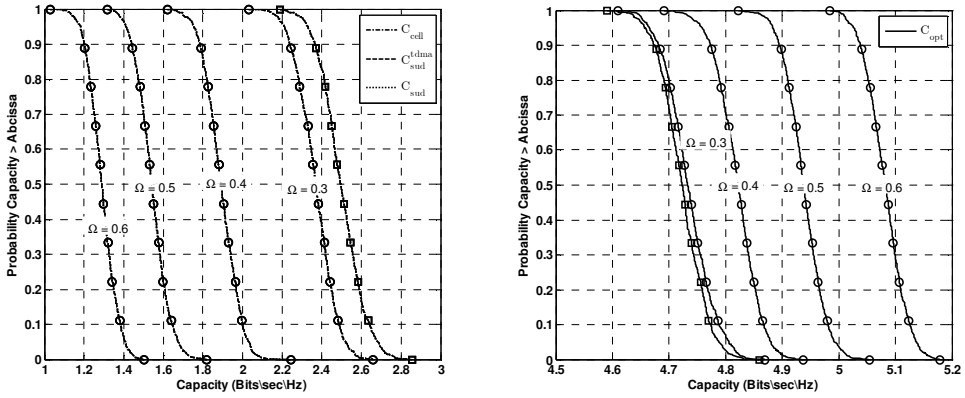

(b)

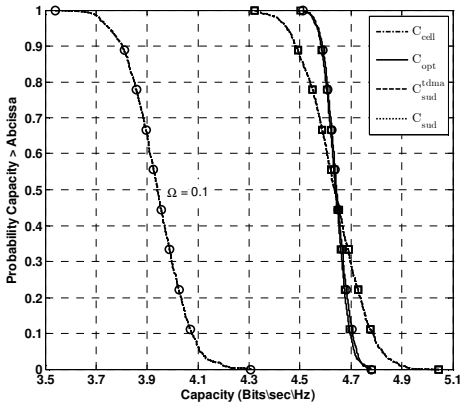

(c)

Figure 4-16: Summary of comparison of capacity over faded C-GCMAC offered by variable inter-cell interfering users (square marker) and with equal inter-cell interfering users (circle marker): (a) one user is located in zone #3 and other is in zone #1 (b) one user is located in zone #3 and other is in zone #2 (c) both users are located in zone #3.

In Figure 4-18, we present the scenario when most of users are offering a medium level of interference of range $0.3 < \Omega < 0.7$. For example Figure 4-18a shows the scenario when 3 users are offering medium level of interference (zone #2) and 1 user is offering high level of interference (zone #1). The improvement in capacity can be seen by comparing capacity with variable interference level over capacity with equal interference when $\Omega = 0.9$. Similarly, in Figure 4-18b all 4 users are located in zone #2 i.e., they are offering medium level of interference. The capacity with variable interference (curves with square marker) outperforms the capacity with equal interference level $\Omega = 0.6$. In Figure 4-18c, 3 users are located in zone #2 and 1 user is located in zone #3 (low level of interference). Further improvement in capacity is due to the fact that with the decrease in interference level the capacity increases.

In Figure 4-19, we present the CCDF curves when most of the users offer low level of interference (zone #3). For an example, Figure 4-19a shows the scenario when 3 users are offering low of interference (zone #3) and 1 user offering high level of interference (zone #1). The CCDF curves with variable interference outperform the capacity curves when users are offering equal interference level $\Omega = 0.9$. It can be seen that variable interference is extremely advantageous for cell optimum, single user with intra-cell TDMA and single user decoding strategies when more than 2 users are offering low levels of interference as compared to the scenario when interfering users offering equal interference level.

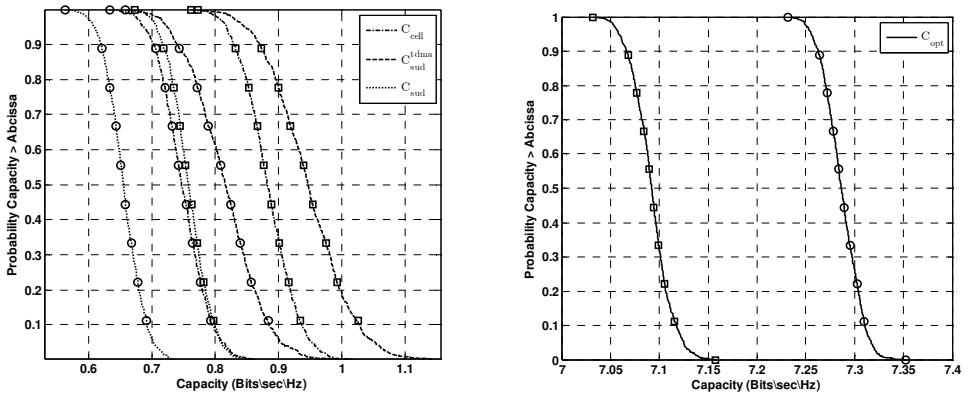

(a)

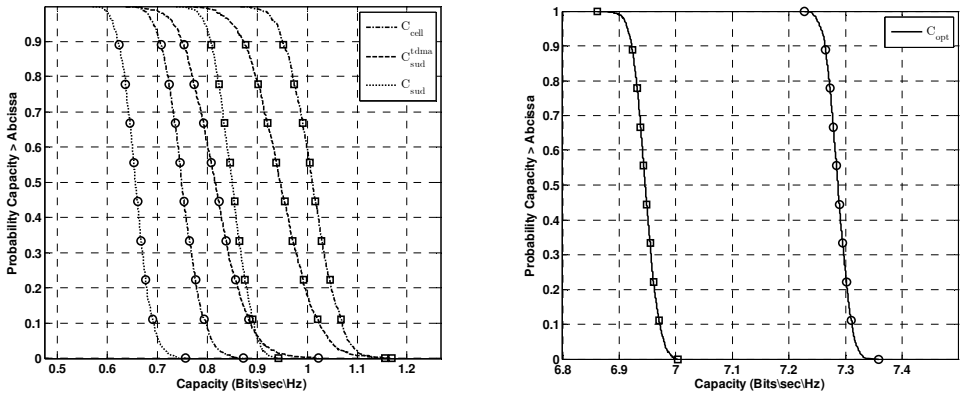

(b)

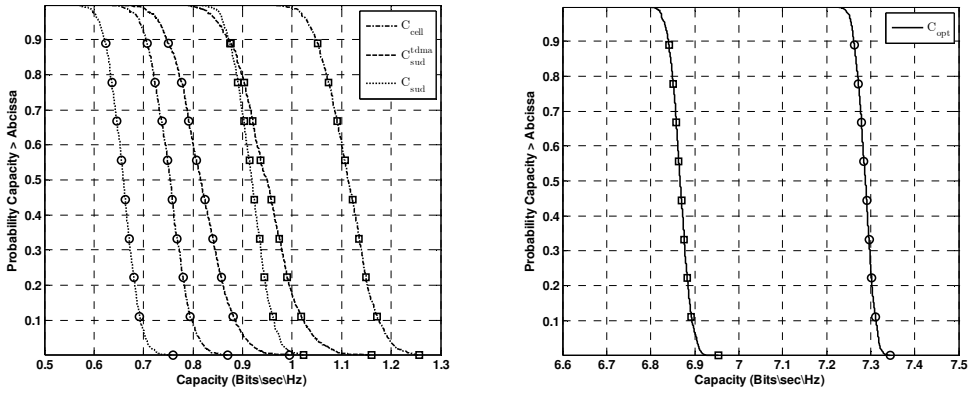

(c)

Figure 4-17: Summary of comparison of capacity over faded C-GCMAC offered by variable inter-cell interfering users (square marker) and with equal inter-cell interfering users (circle marker) with $K = 2$ and $\gamma = 20$ dB : (a) zone #1(4 users); (b) zone #1(3 user), zone #2(1 user); (c) zone #1(3 user), zone #3(1 user).

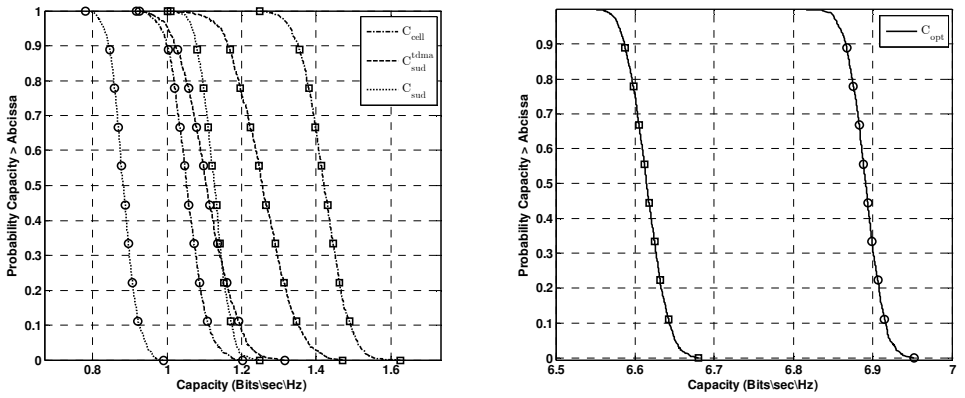

(a)

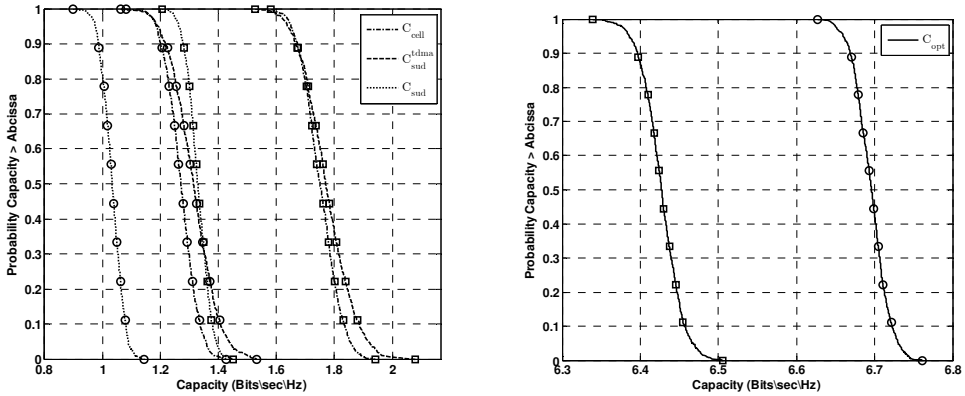

(b)

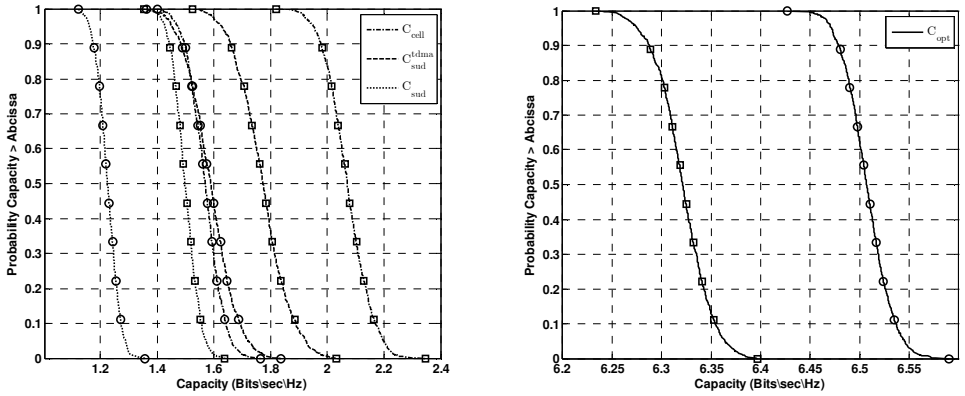

(c)

Figure 4-18: Summary of comparison of capacity over faded C-GCMAC offered by variable inter-cell interfering users (square marker) and with equal inter-cell interfering users (circle marker) with $K = 2$ and $\gamma = 20$ dB : (a) zone #2(3 users), zone #1(1 user); (b) zone #2(4 user); (c) zone #2(3 user), zone #3(1 user).

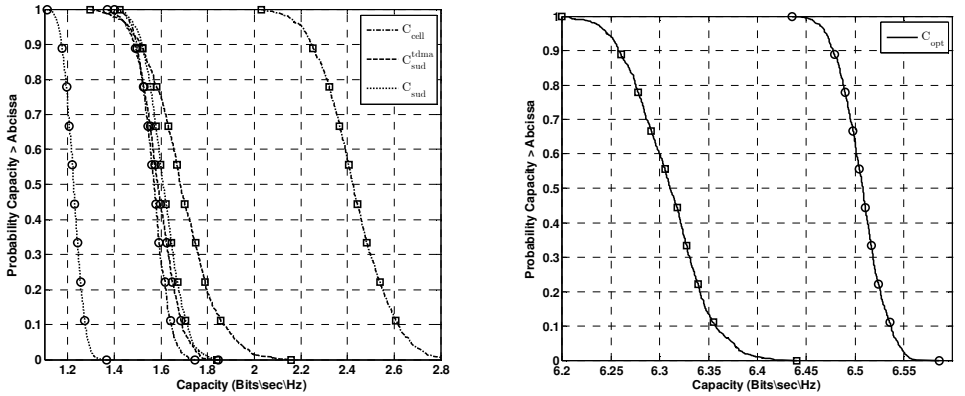

(a)

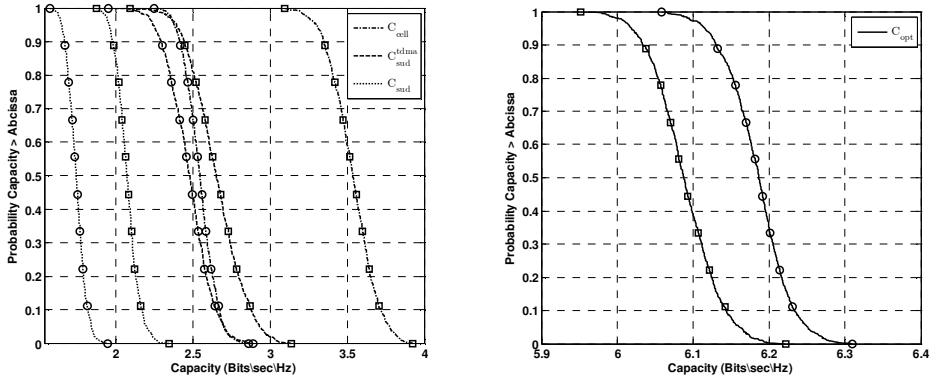

(b)

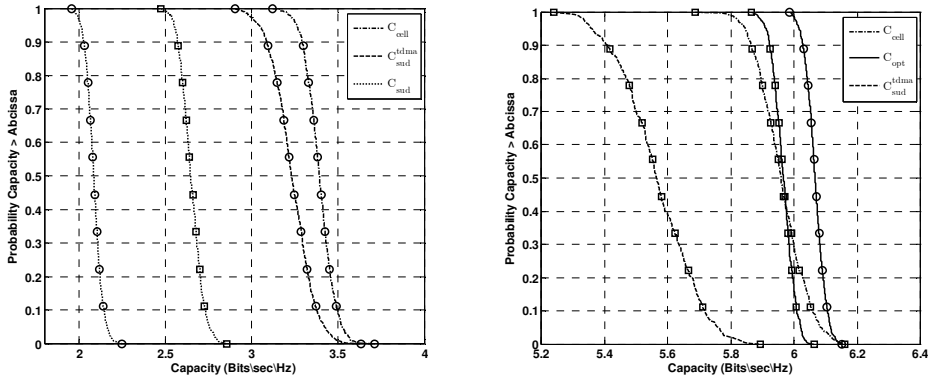

(c)

Figure 4-19: Summary of comparison of capacity over faded C-GCMAC offered by variable inter-cell interfering users (square marker) and with equal inter-cell interfering users (circle marker) with $K = 2$ and $\gamma = 20$ dB : (a) zone #3(3 users), zone #1(1 user); (b) zone #3(3 user), zone #1(1 user); (c) zone #3(4 user).

4.7.5.3 Eigenvalue Distribution Perspective

In this sub-Section, we present the optimum joint decoding capacity with variable inter-cell interference for K = 1 and γ = 20 dB. The analysis is supported by CCDF curves obtained over 5000 Monte Carlo simulation trials of channel matrix $\mathbf{H}$. The gain in optimum capacity is compared with the capacity offered by optimim decoding strategy when users are offering equal level of interfrence while located in low interference zone. For example, Figure 4-20 shows gain yielded by optimum decoding capacity when interference level of user T_{j-1} is increases while user T_{j+1} is located in zone #3. In Figure 4-20, the Solid line (capacity when both users are offering equal level of interference) is compared with the dashed line (when one user T_{j-1} is moved to medium level of interference zone #2) and the dashed dot line (when user T_{j-1} is moved to high level of interference zone #1). The frational gain yielded by $\mathbf{C}_{\text{cell}}(p(\mathbf{H}),\gamma)^{0.1}$ when user T_{j+1} is offering a low level of interference (zone #3) and T_{j-1} is offering a high level of interference (zone #1) over $\mathbf{C}_{\text{opt}}(p(\mathbf{H}),\gamma)^{0.1}$ when both users are offering low level of interfernce is 10%. It is interesting to note that variable interference level strategy is advantageous for optimum decoding strategy when at least one of the users is offering high level of interference.

The improvement in capacity over the fading channel when variable inter-cell interference strategy is employed is analyzed using power distribution analysis of eigenvalues of $\mathbf{H}\,\mathbf{H}^{H}$ in each scenario. Figure 4-21 shows the power distribution of eigenvalues of $\mathbf{H}\,\mathbf{H}^{H}$ in descending order. It can be seen from the figure that last four eigenvalues are the main contributing eigenvalues to improve the capacity. The mean power of the eigenvalues increases with the increase in inter-cell interference level of one of the user, compare Figure 4-21b with Figure 4-21a and Figure 4-21c

with Figure 4-21a. The mean gains of each eigenvalue are also shown in each figure. For example, the mean gain of largest eigenvalue when both users are offering low level of interference is 6.7 dB. Similarly, when one of the users is offering medium level of interference (located in zone #2) the mean gain is improved to 8.2 dB and when this user offer high level of interference (located in zone #1) the mean gain increases to 9.6 dB which corresponds to increase in optimum decoding capacity by varying the interference level. The similar kind of investigation can be established from Figure 4-24. The increase in optimum capacity is obvious when one of the mobile users moved to lower zone.

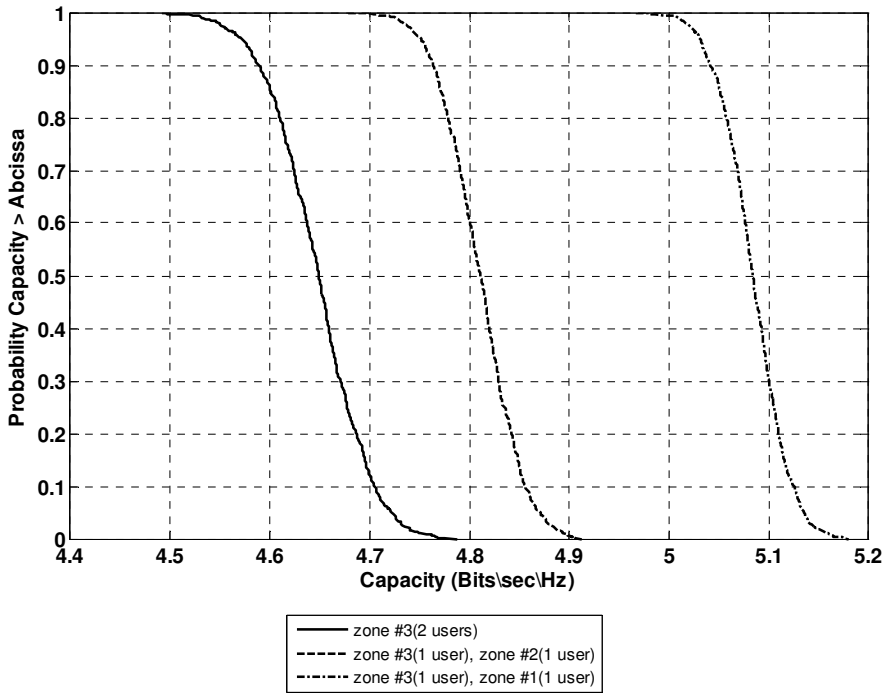

Figure 4-20: Improvement in optimum decoding capacity over faded C-GCMAC by exploiting variable inter-cell interference gain between the user and given BS; $K = 1$ and $\gamma = 20$ dB.

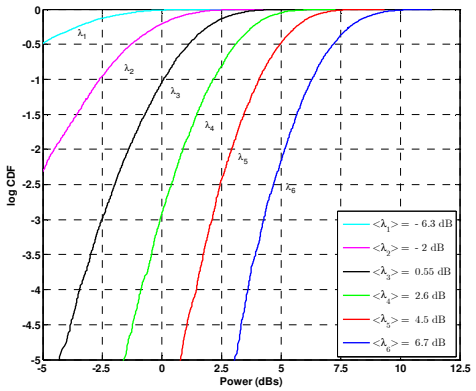

(a)

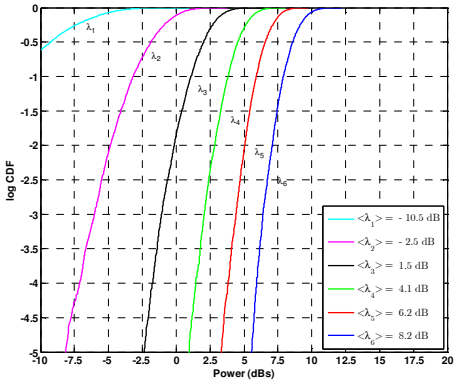

(b)

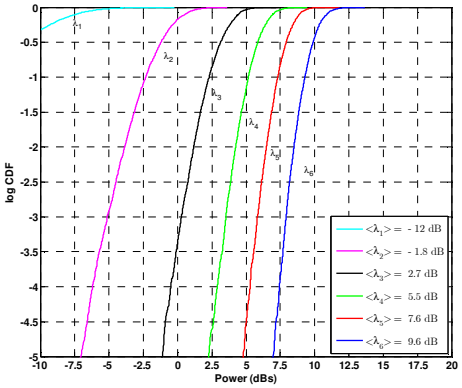

(c)

Figure 4-21: Summary of power distribution of the eigenvalues of $\mathbf{H}\mathbf{H}^H$ for $K = 1$ (2 inter-cell interference for each BS): (a) zone #3(2 users); (b) zone #3(1 user), zone #2(1 user); (c) zone #3(1 user), zone #1(1 user).

In Figure 4-22, we present the optimum joint decoding capacity with variable inter-cell interference for K = 2 (4 inter-cell interference for each BS) and γ = 20 dB over Rayleigh flat fading channel. The Solid black line shows CCDF of capacity offered by optimum decoding strategy when all 4 users are located in zone #3 with an equal level of interference $\Omega = 0.1$; the dashed black CCDF curves is for capacity when 3 users are located in zone #3 i.e. offeirng low level of interference and 1 user is moved to zone 2 (medium level interference). The fractional gain in capacity over the scenario when 4 usres are offering low level of interference is 3 %. Similarly, the capacity increases with the increase in number of users offering high level of interference. Finally, the fractional gain in capacity when 2 users are located in zone #1 (high level of interference) and 2 users are located in zone #3 (low level of interference) over the scenario when 4 users offeirng low level of interference is 15 %. The gain in capacity due to variable level of interference is due to improvement in mean power of eigenvalues of $\mathbf{H}\,\mathbf{H}^{H}$. The power distribution of eigenvalues of the channel matrix is shown in Figure 4-23. It can be seen from the figure that the last four eigenvalues are more contributing to the capacity. For example, the mean power of largest eigenvalue when all 4 users are offering low level of interference is $\langle \lambda_6 \rangle = 9\,\text{dB}$ (see Figure 4-23a). This gain increases to $\langle \lambda_6 \rangle = 11.7\,\text{dB}$ when 2 users are offering low level of interference and two are offering high level of interference (see Figure 4-23f). The mean gain of each eigenvalue for various scenarios is mentioned in Figure 4-23a - Figure 4-23f.

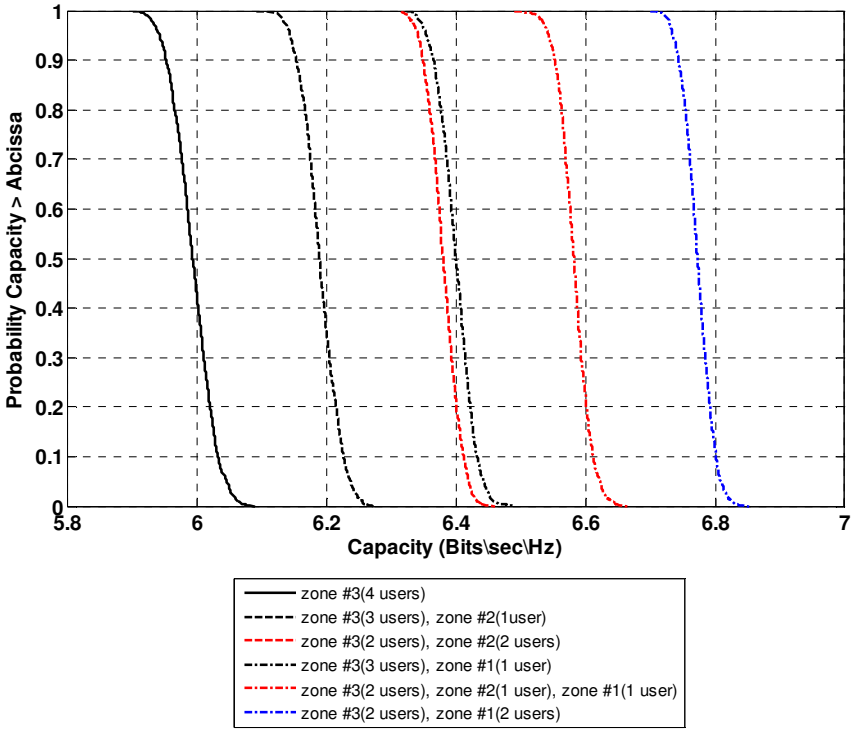

Figure 4-22: Improvement in optimum decoding capacity over faded C-GCMAC by exploiting variable inter-cell interference gain between the user and given BS; $K = 2$ and $\gamma = 20$ dB .

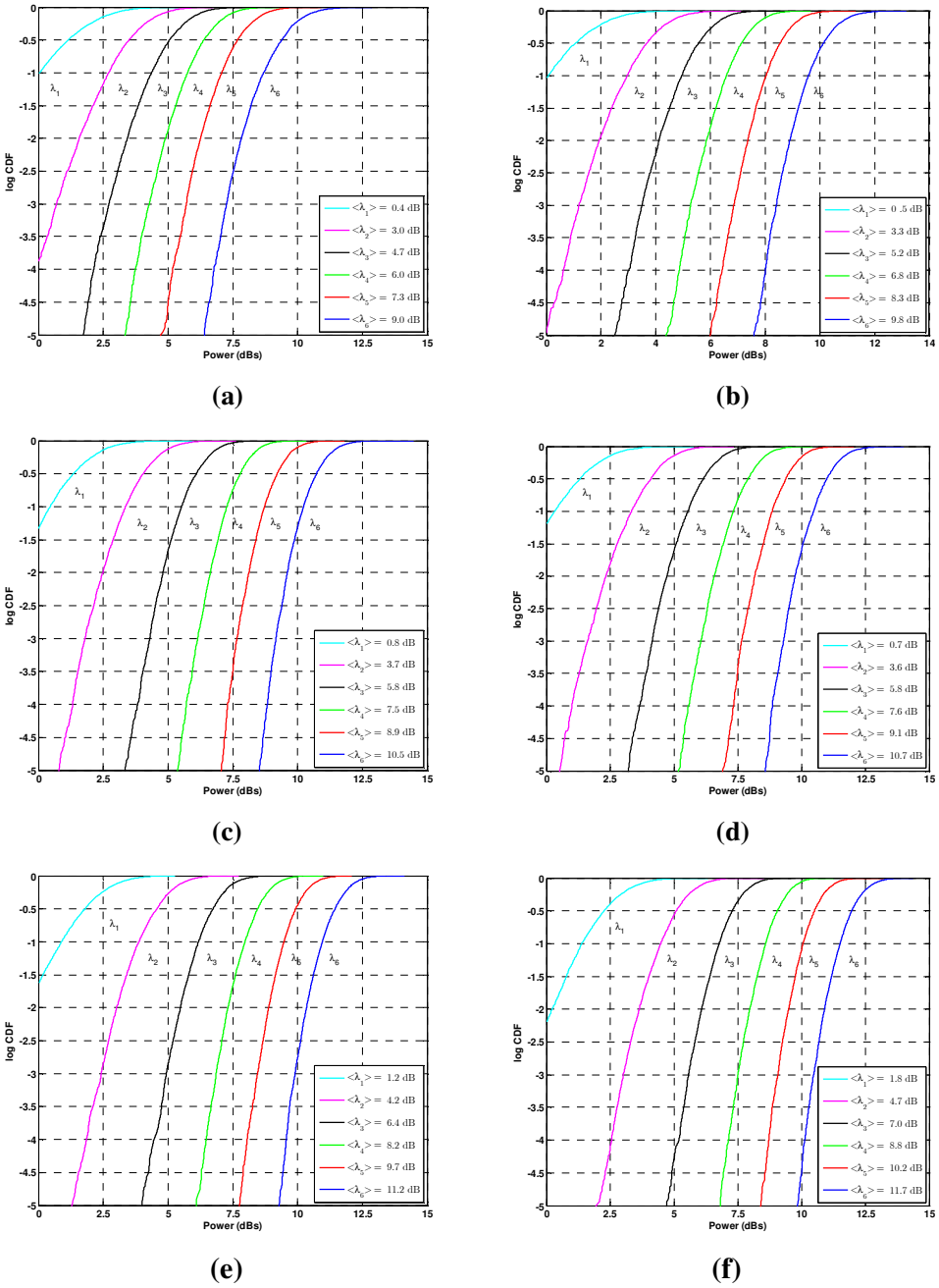

Figure 4-23: Summary of power distribution of eigenvalues of $\mathbf{H}\mathbf{H}^H$ for K =2 (4 inter-cell interference for each BS): (a) zone #3(4 users); (b) zone #3(3 user), zone #2(1 user); (c) zone #3(2 user), zone #2(2 user); (d) zone #3(3 user), zone #(1 user); (e) zone #3(2), zone #1(1 user), zone #2(1 user); (f) zone #3(2 user), zone #1(2 users).

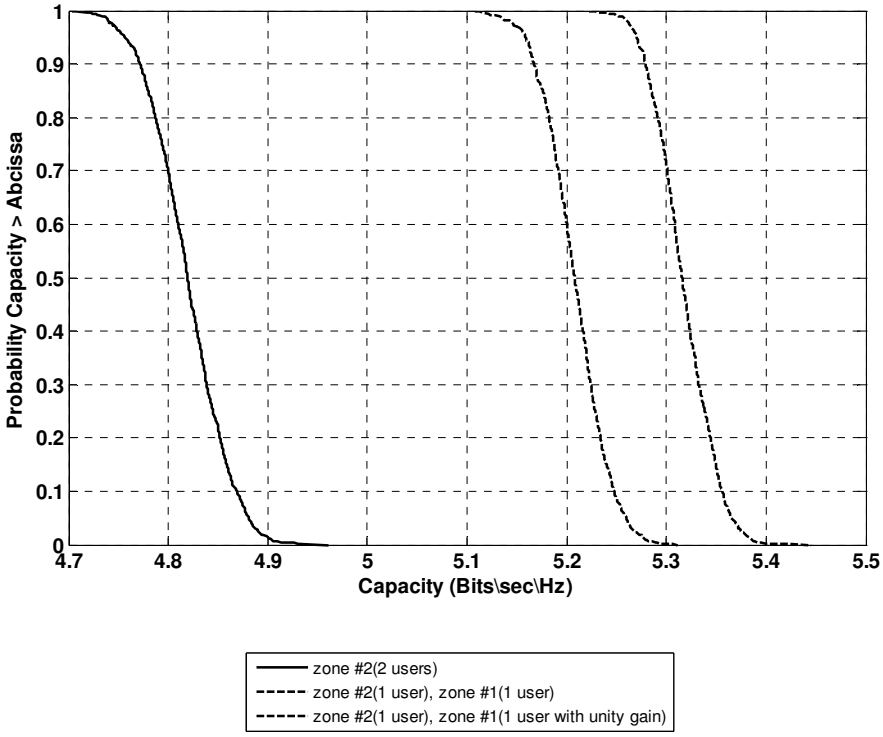

Figure 4-24: Improvement in optimum decoding capacity over faded C-GCMAC by exploiting variable inter-cell interference gain between the user and given BS; $K = 1$ and $\gamma = 20$ dB.

4.7.6 Remarks on Simulation Scenarios

Several remarks on simulation scenarios are now in order:

- Summary of simulation results for a single user case $K=1$ and for the multi-user case $K=2$ are presented in Table 4-1 and Table 4-2 respectively.
- It is recognized that the spectral efficiency of the cell optimum decoding capacity, single user decoding capacity and single user decoding with intra-cell TDMA is improved by varying the channel slow gain among the mobile terminals and the BSs.
- It is found that for a single user scenario i.e. $K=1$ $\mathrm{C}_{\mathrm{cell}}\left(p(\mathbf{H});\gamma\right)=\mathrm{C}_{\mathrm{sud}}\left(p(\mathbf{H});\gamma\right)=\mathrm{C}_{\mathrm{sud}}^{\mathrm{tdma}}\left(p(\mathbf{H});\gamma\right)$. The same has been shown in Table 4-1, it can be seen that cell optimum decoding capacity increases when at least one of the interfering mobile terminals in two adjacent cells is offering low level of inter-cell interference. On the contrary, optimum decoding capacity increases when at least one of the mobile terminals offers high level of inter-cell interference.
- By exploiting the variable channel slow gain among the mobile terminals and the BSs cell optimum decoding strategy is the optimal solution to achieve the capacity in the single user case.
- For the multi-user case $K=2$, there are 4 inter-cell interfering mobile terminals which are located in two adjacent cells. It can be seen from Table 4-2 that the capacity offered by the cell optimum decoding, single user decoding and single user decoding with TDMA increases when at least one the mobile terminals out of 4 interfering terminals is located in higher zone i.e. offering low level of inter-cell interference.
- By comparing the gains in cell optimum decoding capacity, we can see that the benefits of cell optimum decoding capacity over a single user decoding capacity for low levels of inter-cell interference. It is found that when $\Omega\rightarrow 0$, (4.25) is unbounded, where as (4.29) approaches unity (compare the cell optimum capacity and optimum joint decoding capacity in scenario 9 in Table 4-2).

- It is found that for low levels of inter-cell interference $\mathrm{C}_{\mathrm{cell}}\left(p(\mathbf{H});\gamma\right) \approx \mathrm{C}_{\mathrm{opt}}\left(p(\mathbf{H});\gamma\right)$ by exploiting the channel slow gain independently for each of the mobile terminals in both the adjacent cells across the three zones. (See Figure 4-16c for a single user case and Figure 4-19c for multi-user case).

Table 4-1: Summary of Impact of variable channel slow gain on the Capacity for $K=1$.

Scenario No.	T_{j-1}	T_{j+1}	$\mathrm{C}_{\mathrm{cell}}\left(p(\mathbf{H});\gamma\right)^{0.1} = \mathrm{C}_{\mathrm{sud}}\left(p(\mathbf{H});\gamma\right)^{0.1} = \mathrm{C}_{\mathrm{sud}}^{\mathrm{tdma}}\left(p(\mathbf{H});\gamma\right)^{0.1}$	$\mathrm{C}_{\mathrm{opt}}\left(p(\mathbf{H});\gamma\right)^{0.1}$
	User 1	User 2	Bits/sec/Hz	
1.	zone#1	zone#1	1.0	5.4
2.	zone#1	zone#2	1.32	5.2
3.	zone#1	zone#3	1.75	5.0
4.	zone#2	zone#1	1.31	5.19
5.	zone#2	zone#2	1.82	4.92
6.	zone#2	zone#3	2.62	4.79
7.	zone#3	zone#1	1.74	5.0
8.	zone#3	zone#2	2.62	4.72
9.	zone#3	zone#3	4.8	4.7

Table 4-2: Summary of Impact of variable channel slow gain on the Capacity for $K = 2$.

Scenario No.	T_{j-1}		T_{j+1}		$C_{cell}\left(p(\mathbf{H});\gamma\right)^{0.1}$	$C_{sud}^{tdma}\left(p(\mathbf{H});\gamma\right)^{0.1}$	$C_{sud}\left(p(\mathbf{H});\gamma\right)^{0.1}$	$C_{opt}\left(p(\mathbf{H});\gamma\right)^{0.1}$
	User 1	User 2	User 1	User 2	Bits/sec/Hz			
1.	zone #1	zone #1	zone #1	zone #1	0.9	1.0	0.8	7.1
2.	zone #1	zone #1	zone #1	zone #2	1.0	1.0	0.9	7.0
3.	zone #1	zone #1	zone #1	zone #3	1.2	1.0	0.9	6.9
4.	zone #2	zone #2	zone #2	zone #1	1.5	1.4	1.2	6.65
5.	zone #2	zone #2	zone #2	zone #2	1.9	1.8	1.4	6.46
6.	zone #2	zone #2	zone #2	zone #3	2.2	1.9	1.5	6.35
7.	zone #3	zone #3	zone #3	zone #1	2.6	1.9	1.7	6.35
8.	zone #3	zone #3	zone #3	zone #2	3.7	2.8	2.2	6.15
9.	zone #3	zone #3	zone #3	zone #3	6.1	5.6	2.7	6.0

4.8 Upper Bound on Optimum Decoding Capacity

In this Section, a novel expression for a new upper bound on optimum joint decoding capacity over the Wyner C-GCMAC is derived by exploiting the Hadamard inequality [69]. The upper bound can be considered as the maximum capacity that can be achieved by exploiting the Hadamard inequality over Wyner C-GCMAC. However, a lower bound solution to the capacity when optimum joint decoding is employed is still unknown.

We consider an architecture where BSs can cooperate to jointly decode all users' data (macro-diversity). Thus, we dispense with the cellular structure altogether and consider the entire network of BSs and users as a MAC. Each user has a link to each BS and BSs cooperate to jointly decode all users' data. Since BSs are typically not mobile, BSs can share information using high speed reliable connections over wireline links or wireless links [31]. Assume firstly that the receiver has perfect CSI

while the transmitter knows neither the statistics nor the instantaneous CSI. In this case, a sensible choice for the transmitter is to split the total amount of power equally among all data streams and, consequently, an equal-power transmission scheme takes place. The justification for adopting this scheme, though not optimal, originates from the so-called maxmin property [127] which demonstrated the robustness of the above mentioned technique for maximizing the capacity of the worst fading matrix. For the Wyner C-GCMAC with a uniform average power constraint, the sum-capacity of the system when optimum joint decoding is performed is expressed (4.35) [13] and [97].

The Base Stations (BSs) are herein assumed to be able to jointly decode the received signals in order to detect the transmitted vector $\boldsymbol{x}$. It has been shown that the multi-user decoding strategies are distinctly advantageous over single user decoding strategies [27] and [28]. The Hadamard representation of the optimum joint decoding capacity is also expressed as (4.36) by substituting (3.5) into (4.35). The Hadamard product and Kronecker product of the two matrices $\mathbf{G}$ and $\boldsymbol{\Omega}$ are related by following Theorem 4.8.1.

Theorem 4.8.1: (Hadamard product and Kronecker product) [69]

Let $\mathbf{G}$ and $\boldsymbol{\Omega}$ be arbitrary $N \times M$ matrices. Then [24], [68] and [69]

$$\mathbf{G} \circ \boldsymbol{\Omega} = \boldsymbol{\mathcal{P}}_N^T \left(\mathbf{G} \otimes \boldsymbol{\Omega} \right) \boldsymbol{\mathcal{P}}_M \tag{4-65}$$

where $\boldsymbol{\mathcal{P}}_N$ and $\boldsymbol{\mathcal{P}}_M$ are $n^2 \times n$ and $m^2 \times m$ partial permutation matrices respectively. The j^{th} column of $\boldsymbol{\mathcal{P}}_N$ and $\boldsymbol{\mathcal{P}}_M$ has 1 in its $\left((j-1)n+j\right)^{\text{th}}$ and $\left((j-1)m+j\right)^{\text{th}}$ position respectively and zero elsewhere. The proof of (4.65) is as follows:

Proof of (4.65): Compute

$$\boldsymbol{\mathcal{P}}_N^T \left(\mathbf{G} \otimes \boldsymbol{\Omega} \right) \boldsymbol{\mathcal{P}}_M = \left[E_{11}^{(N)} \cdots\cdots E_{NN}^{(N)} \right] \begin{pmatrix} g_{11}\boldsymbol{\Omega} & \cdots & g_{1M}\boldsymbol{\Omega} \\ \vdots & & \vdots \\ g_{N1}\boldsymbol{\Omega} & \cdots & g_{NM}\boldsymbol{\Omega} \end{pmatrix} \begin{pmatrix} E_{11}^{(M)} \\ \vdots \\ E_{MM}^{(M)} \end{pmatrix}$$

$$= \sum_{k=1}^{M} diag\left(g_{1k}, g_{2k}, \cdots, g_{Nk} \right) \boldsymbol{\Omega} E_{kk}^{M}$$

$$= \sum_{k=1}^{M} g_{ik}\Omega_{ij}\delta_{jk}$$

$$= g_{ij}\Omega_{ij} = \mathbf{G} \circ \mathbf{\Omega} \qquad \square$$

The following corollary lists several useful properties of the partial permutation matrices $\mathcal{P}_N$ and $\mathcal{P}_M$.

Corollary 4.8.2[18]:

For brevity, the partial permutation matrices $\mathcal{P}_N$ and $\mathcal{P}_M$ will be denoted by $\mathcal{P}$ unless it is necessary to emphasize its order. In the same way, the matrices $\mathcal{Q}_N$ and $\mathcal{Q}_M$, defined below, is denoted by $\mathcal{Q}$.

i. $\mathcal{P}_N$ and $\mathcal{P}_M$ are the only matrices of zeros and ones that satisfy (4.65) for all $\mathbf{G}$ and $\mathbf{\Omega}$.

ii. $\mathcal{P}^T\mathcal{P} = \mathbf{I}$ and $\mathcal{P}\mathcal{P}^T$ is the diagonal matrix of zeros and ones, so $0 \le \mathcal{P}\mathcal{P}^T \le 1$.

iii. There exists a $n^2 \times \left(n^2 - n\right)$ matrix $\mathcal{Q}_N$ and $m^2 \times \left(m^2 - m\right)$ matrix $\mathcal{Q}_M$ of zeros and ones such that $\boldsymbol{\pi} \triangleq \left(\mathcal{P}\mathcal{Q}\right)$ is the permutation matrix. The matrix $\mathcal{Q}$ is not unique but for any choice of $\mathcal{Q}$, following holds;

$$\mathcal{P}^T\mathcal{Q} = 0;\ \mathcal{Q}^T\mathcal{Q} = \mathbf{I} \text{ and } \mathcal{Q}\mathcal{Q}^T = \mathbf{I} - \mathcal{P}\mathcal{P}^T$$

iv. Using the properties of a permutation matrix together with the definition of $\boldsymbol{\pi}$ in (iii); we have

$$\boldsymbol{\pi}\boldsymbol{\pi}^T = \left(\mathcal{P}\mathcal{Q}\right)\begin{pmatrix}\mathcal{P}^T \\ \mathcal{Q}^T\end{pmatrix} = \mathcal{P}\mathcal{P}^T + \mathcal{Q}\mathcal{Q}^T = \mathbf{I}$$

[18] As an example, for $N = 6$ and $K = 1$ the permutation matrices $\mathcal{P} \in \mathbb{P}^{36\times 6}$ and $\mathcal{Q} \in \mathbb{P}^{36\times 30}$ are presented in Appendix F.

Theorem 4.8.3: (Hadamard Inequality) [68]

Let $\mathbf{G}$ and $\mathbf{\Omega}$ be arbitrary $N \times M$ matrices. Then

$$\mathbf{G}\mathbf{G}^H \circ \mathbf{\Omega}\mathbf{\Omega}^H = \left(\mathbf{G} \circ \mathbf{\Omega}\right)\left(\mathbf{G} \circ \mathbf{\Omega}\right)^H + \Gamma_{(\boldsymbol{\mathcal{P}},\boldsymbol{\mathcal{Q}})} \tag{4-66}$$

where $\Gamma_{(\boldsymbol{\mathcal{P}},\boldsymbol{\mathcal{Q}})} = \boldsymbol{\mathcal{P}}_N^T \left(\mathbf{G} \otimes \mathbf{\Omega}\right)\boldsymbol{\mathcal{Q}}_M \boldsymbol{\mathcal{Q}}_M^T \left(\mathbf{G} \otimes \mathbf{\Omega}\right)^H \boldsymbol{\mathcal{P}}_N$ and we called it the Gamma Function.

From (4.66), we can deduce [69]

$$\mathbf{G}\mathbf{G}^H \circ \mathbf{\Omega}\mathbf{\Omega}^H \geq \left(\mathbf{G} \circ \mathbf{\Omega}\right)\left(\mathbf{G} \circ \mathbf{\Omega}\right)^H \tag{4-67}$$

This inequality is referred to as the Hadamard inequality which will be employed to find the upper bound on the capacity (4.36). Also, (4.67) ensures that

$$\mathbf{G}\mathbf{G}^H \circ \mathbf{\Omega}\mathbf{\Omega}^H = \left(\mathbf{G} \circ \mathbf{\Omega}\right)\left(\mathbf{G} \circ \mathbf{\Omega}\right)^H \text{ for } \Gamma_{(\boldsymbol{\mathcal{P}},\boldsymbol{\mathcal{Q}})} = 0 \tag{4-68}$$

Proof of (4.66):

Using the well known property of the Kronecker product $\mathbf{A}\mathbf{C} \otimes \mathbf{B}\mathbf{D} = (\mathbf{A} \otimes \mathbf{B})(\mathbf{C} \otimes \mathbf{D})$ [68], we have

$$\mathbf{G}\mathbf{G}^H \otimes \mathbf{\Omega}\mathbf{\Omega}^H = \left(\mathbf{G} \otimes \mathbf{\Omega}\right)\left(\mathbf{G} \otimes \mathbf{\Omega}\right)^H$$

Corollary 4.8.2(iii) ensures that $\boldsymbol{\mathcal{P}}_M \boldsymbol{\mathcal{P}}_M^T + \boldsymbol{\mathcal{Q}}_M \boldsymbol{\mathcal{Q}}_M^T = \mathbf{I}$, subsequently we have

$$= \left(\mathbf{G} \otimes \mathbf{\Omega}\right)\left(\boldsymbol{\mathcal{P}}_M \boldsymbol{\mathcal{P}}_M^T + \boldsymbol{\mathcal{Q}}_M \boldsymbol{\mathcal{Q}}_M^T\right)\left(\mathbf{G} \otimes \mathbf{\Omega}\right)^H$$

$$= \left(\mathbf{G} \otimes \mathbf{\Omega}\right)\boldsymbol{\mathcal{P}}_M \boldsymbol{\mathcal{P}}_M^T \left(\mathbf{G} \otimes \mathbf{\Omega}\right)^H + \left(\mathbf{G} \otimes \mathbf{\Omega}\right)\boldsymbol{\mathcal{Q}}_M \boldsymbol{\mathcal{Q}}_M^T \left(\mathbf{G} \otimes \mathbf{\Omega}\right)^H$$

Multiply each term by partial permutation matrix $\boldsymbol{\mathcal{P}}$ of appropriate order to ensure Theorem 4.8.1.

$$\boldsymbol{\mathcal{P}}_N^T \left(\mathbf{G}\mathbf{G}^H \otimes \mathbf{\Omega}\mathbf{\Omega}^H\right)\boldsymbol{\mathcal{P}}_M = \boldsymbol{\mathcal{P}}_N^T \left(\mathbf{G} \otimes \mathbf{\Omega}\right)\boldsymbol{\mathcal{P}}_M \boldsymbol{\mathcal{P}}_M^T \left(\mathbf{G} \otimes \mathbf{\Omega}\right)^H \boldsymbol{\mathcal{P}}_N + \boldsymbol{\mathcal{P}}_N^T \left(\mathbf{G} \otimes \mathbf{\Omega}\right)\boldsymbol{\mathcal{Q}}_M \boldsymbol{\mathcal{Q}}_M^T \left(\mathbf{G} \otimes \mathbf{\Omega}\right)^H \boldsymbol{\mathcal{P}}_M$$

Recall from Theorem 4.8.1, i.e. $\boldsymbol{\mathcal{P}}^T \left(\mathbf{G} \otimes \mathbf{\Omega}\right)\boldsymbol{\mathcal{P}} = \left(\mathbf{G} \circ \mathbf{\Omega}\right)$, we have

$$\mathbf{G}\mathbf{G}^H \circ \mathbf{\Omega}\mathbf{\Omega}^H = \left(\mathbf{G} \circ \mathbf{\Omega}\right)\left(\mathbf{G} \circ \mathbf{\Omega}\right)^H + \boldsymbol{\mathcal{P}}_N^T \left(\mathbf{G} \otimes \mathbf{\Omega}\right)\boldsymbol{\mathcal{Q}}_M \boldsymbol{\mathcal{Q}}_M^T \left(\mathbf{G} \otimes \mathbf{\Omega}\right)^H \boldsymbol{\mathcal{P}}_M$$

This proves (4.66). □

4.8.1 Upper Bound on Optimum Capacity

In this Section, we first introduce the upper bound on optimum capacity using Jensen's Inequality and then we derive the upper bound using the Hadamard Inequality as defined in (4.66).

Theorem 4.8.4: (Jensen's Inequality)

For any concave function [22]

$$\mathbb{E}\left[f\left(X\right)\right] \leq f\,\mathbb{E}\left[X\right] \tag{4-69}$$

Using concavity of $\log\left(.\right)$ and Jensen's inequality, we have $\mathbb{E}\left[\log\left(X\right)\right] \leq \log \mathbb{E}\left[X\right]$. The upper bound on optimum capacity is given by

$$\begin{aligned} \mathbf{C}_{\text{opt}}(p(\mathbf{H});\gamma) &\leq \tilde{\mathbf{C}}_{\text{opt}}(p(\mathbf{H});\gamma) \\ &= \frac{1}{N}\left[\log_2 \det\left(\mathbf{I}_N + \gamma\,\mathbb{E}\left[\mathbf{H}\mathbf{H}^H\right]\right)\right] \end{aligned} \tag{4-70}$$

The Hadamard representation of upper bound using Jensen's inequality is expressed as

$$\tilde{\mathbf{C}}_{\text{opt}}(p(\mathbf{G}\circ\boldsymbol{\Omega}),\gamma) = \frac{1}{N}\left[\log_2 \det\left(\mathbf{I}_N + \gamma\,\mathbb{E}\left[\left(\mathbf{G}\circ\boldsymbol{\Omega}\right)\left(\mathbf{G}\circ\boldsymbol{\Omega}\right)^H\right]\right)\right] \tag{4-71}$$

The upper bound on optimum capacity using the Hadamard inequality (4.66) is given by

$$\begin{aligned} \mathbf{C}_{\text{opt}}(p(\mathbf{G}\circ\boldsymbol{\Omega}),\gamma) &\leq \overline{\mathbf{C}}_{\text{opt}}(p(\mathbf{G}\circ\boldsymbol{\Omega}),\gamma) \\ &= \frac{1}{N}\,\mathbb{E}\left[\log_2 \det\left(\mathbf{I}_N + \gamma\left(\mathbf{G}\mathbf{G}^H\right)\circ\left(\boldsymbol{\Omega}\boldsymbol{\Omega}^H\right)\right)\right] \end{aligned} \tag{4-72}$$

This is to note that (4.72) is the unique application of (4.66). However, an analytical closed form expression for (4.36) can be derived using (4.72). The work is part of on-going research [144].

4.8.2 Tightness of Hadamard Upper Bound

In this Section, we show that the new Hadamard upper bound on $\mathrm{C}_{\mathrm{opt}}$ converges to the conventional capacity at low SNRs whereas at high SNRs, the offset from the conventional capacity is constant which is advantageous. In general, the absolute gain Δ inserted by Hadamard upper bound is given as [144]

$$\Delta = \overline{\mathrm{C}}_{\mathrm{opt}}\left(p(\mathbf{G}\circ\boldsymbol{\Omega});\gamma\right) - \mathrm{C}_{\mathrm{opt}}\left(p(\mathbf{G}\circ\boldsymbol{\Omega});\gamma\right) \tag{4-73}$$

which asymptotically tends to zero as $\gamma \longrightarrow 0$, given as

$$\lim_{\gamma\to 0}\Delta = \frac{1}{N}\mathbb{E}\left(\log_2\left(1+\gamma\,\mathrm{tr}\left(\Gamma_{\mathcal{P},\mathcal{Q}}\right)\right)\right) \tag{4-74}$$

Proof of (4.74): Using (4.73), we have

$$\begin{aligned}\Delta &= \left[\frac{1}{N}\mathbb{E}\left[\log_2\det\left(\mathbf{I}_N+\gamma\,\mathbf{G}\mathbf{G}^H\circ\boldsymbol{\Omega}\boldsymbol{\Omega}^H\right)\right]\right]\\ &\quad-\left[\frac{1}{N}\mathbb{E}\left[\log_2\det\left(\mathbf{I}_N+\gamma(\mathbf{G}\circ\boldsymbol{\Omega})(\mathbf{G}\circ\boldsymbol{\Omega})^H\right)\right]\right]\\ &= \frac{1}{N}\mathbb{E}\left(\log_2\left(\frac{\det\left(\mathbf{I}_N+\gamma\,\mathbf{G}\mathbf{G}^H\circ\boldsymbol{\Omega}\boldsymbol{\Omega}^H\right)}{\det\left(\mathbf{I}_N+\gamma(\mathbf{G}\circ\boldsymbol{\Omega})(\mathbf{G}\circ\boldsymbol{\Omega})^H\right)}\right)\right)\\ &= \frac{1}{N}\mathbb{E}\left(\log_2\left(\frac{1+\gamma\,\mathrm{tr}\left(\mathbf{G}\mathbf{G}^H\circ\boldsymbol{\Omega}\boldsymbol{\Omega}^H\right)}{1+\gamma\,\mathrm{tr}\left((\mathbf{G}\circ\boldsymbol{\Omega})(\mathbf{G}\circ\boldsymbol{\Omega})^H\right)}\right)\right)\end{aligned}$$

where we have made use of property[19] $\det(\mathbf{I}+\varepsilon\mathbf{A}) = 1+\varepsilon\mathrm{tr}(\mathbf{A})+\mathcal{O}(\varepsilon^2)$ [90]. We can now show that using Hadamard inequality (4.67), we have

$$= \frac{1}{N}\mathbb{E}\left(\log_2\left(\frac{1+\gamma\,\mathrm{tr}\left((\mathbf{G}\circ\boldsymbol{\Omega})(\mathbf{G}\circ\boldsymbol{\Omega})^H\right)+\gamma\,\mathrm{tr}\left(\Gamma_{\mathcal{P},\mathcal{Q}}\right)}{1+\gamma\,\mathrm{tr}\left((\mathbf{G}\circ\boldsymbol{\Omega})(\mathbf{G}\circ\boldsymbol{\Omega})^H\right)}\right)\right)$$

[19] Terms with higher power of ε can be ignored $\Leftrightarrow \varepsilon^x \approx 0\ \forall\ ; x = 2,3,\cdots$ [89].

$$= \frac{1}{N}\mathbb{E}\left\{\log_2\left(1+\frac{\gamma\,\mathrm{tr}\left(\Gamma_{\mathcal{P},\mathcal{Q}}\right)}{1+\gamma\,\mathrm{tr}\left((\mathbf{G}\circ\boldsymbol{\Omega})(\mathbf{G}\circ\boldsymbol{\Omega})^H\right)}\right)\right\}$$

as $\gamma \to 0$, we may have

$\lim_{\gamma\to 0}\Delta = \frac{1}{N}\mathbb{E}\left(\log_2\left(1+\gamma\,\mathrm{tr}\left(\Gamma_{\mathcal{P},\mathcal{Q}}\right)\right)\right)$; which proves (4.74).

4.8.3 Simulation Results and Comparisons

The upper bound on optimum joint decoding capacity over flat faded C-GCMAC for $K = 1$ is shown in Figure 4-25. The curves are obtained over 5000 Monte Carlo simulation trials of $\mathbf{H}$. It is shown that the capacity upper bound using Hadamard inequality (4.72) is improved as compared to capacity upper bound using Jensen's inequality (4.71) (compare blue curve with red and black curves). The improvement in Bits/sec/Hz is shown in Figure 4-26 with respect to range of SNRs and inter-cell interference levels. The difference between the two upper bounds is constant over medium to higher range of SNRs. The improvement in upper bound is constant for $\Omega > 0.4$. As the SNR approaches zero, both upper bounds gets closer to each other.

The improvement in capacity using the Hadamard inequality over a non-fading channel is shown in Figure 4-27a and over a fading channel is shown in Figure 4-27b. It is observed that the improvement in capacity over a non-fading channel using the Hadamard inequality increases with the increase in SNRs and with the increase in inter-cell interference. The effect is significant at higher SNRs. For example, at γ = 40 dB and Ω = 0.9, the gain is Δ = 3.1 Bits/sec/Hz. On the other hand, γ = 40 dB and Ω = 0.1, and gain is Δ = 1.5 Bits/sec/Hz. From the Figure 4-27b, it is shown that gain in capacity over fading channel using Hadamard inequality is almost constant with respect to level of inter-cell interference (except the case when there is no inter-cell interference). It is also demonstrated that as $\gamma \to 0$, the gain $\Delta \approx 0$ and both capacities are getting closer to each other i.e. $\bar{\mathrm{C}}_{\mathrm{opt}}\left(p(\mathbf{H});\gamma\right) \approx \mathrm{C}_{\mathrm{opt}}\left(p(\mathbf{H});\gamma\right)$.

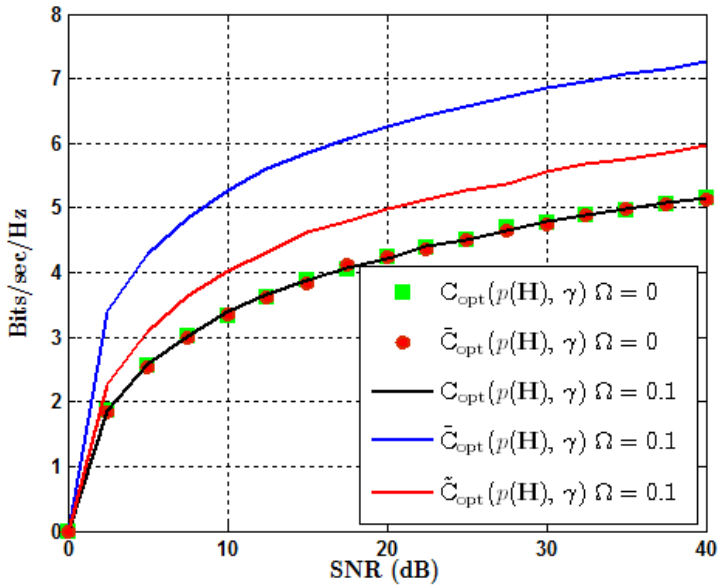

Figure 4-25: Summary of capacity comparison: capacity using (4.72) Hadamard inequality with low level of interference (blue curve); capacity using (4.71) Jensen's inequality (red curve); capacity using (4.72) Hadamard inequality with no intra-cell interference (red dots); capacity using (4.36) with no intra-cell interference (green square); capacity using (4.36) with low level of interference (black curve).

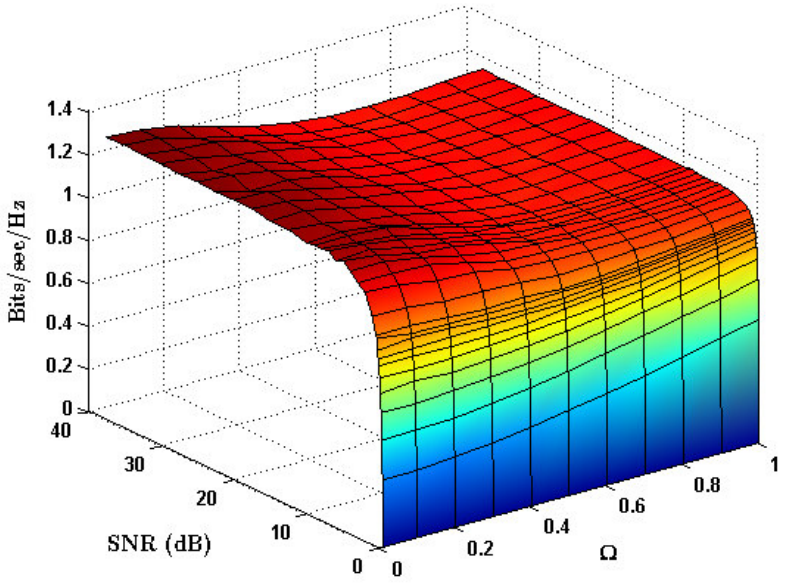

Figure 4-26: Difference between the capacity using Hadamard inequality and using Jensen's inequality with respect to inter-cell interference and SNRs with $K = 1$.

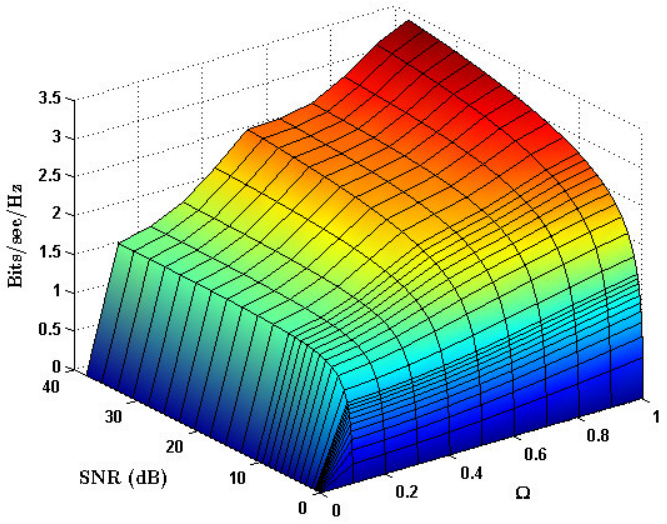

(a)

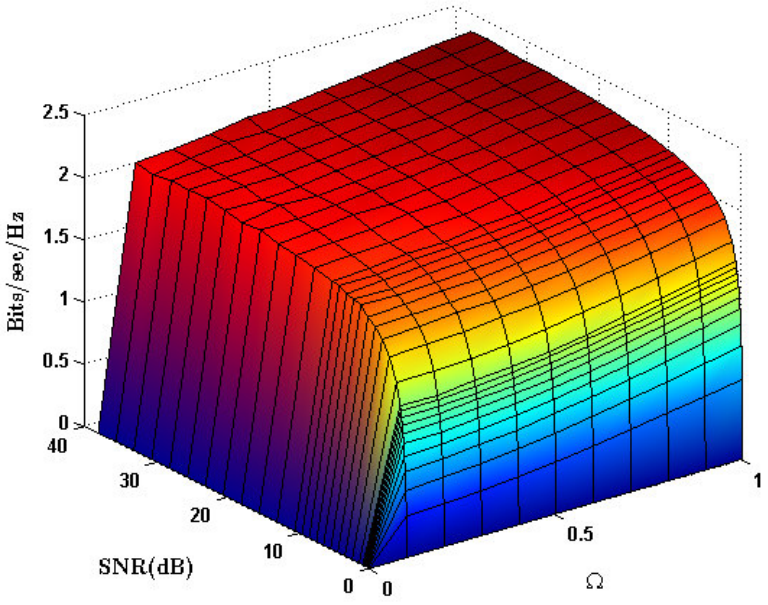

(b)

Figure 4-27: Difference between capacity using Hadamard inequality (4.72) and capacity using (4.36) with $K = 1$: (a) over non-faded circular cellular channel; (b) over faded C-GCMAC.

4.8.4 Special Case: No Inter-cell Interference (Employing Inter-cell TDMA)

In this Section, we discuss the applications of (4.67) and (4.68) in the Wyner C-GCMAC to justify the use of the Hadamard inequality. Now, we present following scenarios when inter-cell TDMA is employed or users from the adjacent cells are ignored [141].

a. Single User Case $K=1$:

Note that (4.68) holds if and only if $\Gamma_{(\boldsymbol{\mathcal{P}},\boldsymbol{\mathcal{Q}})}=0$, which is equivalent to $\boldsymbol{\mathcal{P}}_N^T\left(\mathbf{G}\otimes\boldsymbol{\Omega}\right)\boldsymbol{\mathcal{P}}_M=0$. It is found that $\Gamma_{(\boldsymbol{\mathcal{P}},\boldsymbol{\mathcal{Q}})}=0$ only when $\mathbf{G}_{N,1}$ and $\boldsymbol{\Omega}_{N,1}$ are diagonal matrices[20]. Let us define $\mathbf{G}\in\mathbb{C}^{N\times N}$ such that $g_{ij}\in\mathbb{C}\mathcal{N}(0,1)$ if $i=j$ and $g_{ij}=0$ if $i\neq j$. Similarly, $\boldsymbol{\Omega}\in\mathbb{R}^{N\times N}$ such that $\Omega_{ij}=1$ if $i=j$ and $\Omega_{ij}=0$ if $i\neq j$ i.e. $\boldsymbol{\Omega}_{N,1}=\mathbf{I}_N$.

This is considered as a special case in C-GCMAC modelling when each base station only decodes only a local user[21] and there is no inter-cell interference. The resultant channel matrix is a diagonal matrix such that[22] $\boldsymbol{\mathcal{P}}_N^T\left(\mathbf{G}\otimes\boldsymbol{\Omega}\right)\boldsymbol{\mathcal{Q}}_M=0$ and subsequently (4.68) holds.

Proof of (4.68)[23] :

To arrive at (4.68), we first notice from (4.66) that $\boldsymbol{\mathcal{P}}_N^T\left(\mathbf{G}\otimes\boldsymbol{\Omega}\right)\boldsymbol{\mathcal{Q}}_M\boldsymbol{\mathcal{Q}}_M^T=0$ and using the fact from Corollary 4.8.2(iii) that $\boldsymbol{\mathcal{Q}}_M\boldsymbol{\mathcal{Q}}_M^T=\mathbf{I}-\boldsymbol{\mathcal{P}}_M\boldsymbol{\mathcal{P}}_M^T$, subsequently we have

$$\boldsymbol{\mathcal{P}}_N^T\left(\mathbf{G}\otimes\boldsymbol{\Omega}\right)\left(\mathbf{I}-\boldsymbol{\mathcal{P}}_M\boldsymbol{\mathcal{P}}_M^T\right)=0$$

$$\boldsymbol{\mathcal{P}}_N^T\left(\mathbf{G}\otimes\boldsymbol{\Omega}\right)=\boldsymbol{\mathcal{P}}_N^T\left(\mathbf{G}\otimes\boldsymbol{\Omega}\right)\boldsymbol{\mathcal{P}}_M\boldsymbol{\mathcal{P}}_M^T$$

[20] In single user scenario, the channel matrix $\mathbf{H}$ is diagonal only when inter-cell TDMA is employed.
[21] Intra-cell users.
[22] It is to note that $\boldsymbol{\mathcal{P}}_N^T\left(\mathbf{G}\otimes\boldsymbol{\Omega}\right)\boldsymbol{\mathcal{Q}}_M=0$ iff $K=1$ and $\mathbf{G}$ and $\boldsymbol{\Omega}$ are diagonal matrices. However, in multi-user scenario the result of (4.68) is still valid if intra-cell TDMA is employed.
[23] For the sake of simplicity all the indices have been omitted.

Multiply both sides by $\left(\mathbf{G}\otimes\boldsymbol{\Omega}\right)^H \boldsymbol{\mathcal{P}}_N$

$$\boldsymbol{\mathcal{P}}_N^T\left(\mathbf{G}\otimes\boldsymbol{\Omega}\right)\left(\mathbf{G}\otimes\boldsymbol{\Omega}\right)^H \boldsymbol{\mathcal{P}}_N = \boldsymbol{\mathcal{P}}_N^T\left(\mathbf{G}\otimes\boldsymbol{\Omega}\right)\boldsymbol{\mathcal{P}}_M\ \boldsymbol{\mathcal{P}}_M^T\left(\mathbf{G}\otimes\boldsymbol{\Omega}\right)^H \boldsymbol{\mathcal{P}}_N$$

$$\boldsymbol{\mathcal{P}}_N^T\left(\mathbf{G}\mathbf{G}^H\otimes\boldsymbol{\Omega}\boldsymbol{\Omega}^H\right)\boldsymbol{\mathcal{P}}_N = \boldsymbol{\mathcal{P}}_N^T\left(\mathbf{G}\otimes\boldsymbol{\Omega}\right)\boldsymbol{\mathcal{P}}_M\ \boldsymbol{\mathcal{P}}_M^T\left(\mathbf{G}\otimes\boldsymbol{\Omega}\right)^H \boldsymbol{\mathcal{P}}_N$$

Recall from Theorem 4.8.1 i.e. $\boldsymbol{\mathcal{P}}^T\left(\mathbf{G}\otimes\boldsymbol{\Omega}\right)\boldsymbol{\mathcal{P}} = \mathbf{G}\circ\boldsymbol{\Omega}$, finally we arrive at

$$\mathbf{G}\mathbf{G}^H\circ\boldsymbol{\Omega}\boldsymbol{\Omega}^H = \left(\mathbf{G}\circ\boldsymbol{\Omega}\right)\left(\mathbf{G}\circ\boldsymbol{\Omega}\right)^H$$

when $\Gamma_{(\boldsymbol{\mathcal{P}},\boldsymbol{\mathcal{Q}})} = 0$. □

The scenario is simulated and shown in Figure 4-25. This is the case when $\Gamma_{\boldsymbol{\mathcal{P}},\boldsymbol{\mathcal{Q}}} = 0$, subsequently $\mathrm{C}_{\mathrm{opt}}\left(p\left(\mathbf{G}\circ\boldsymbol{\Omega}\right);\gamma\right) = \overline{\mathrm{C}}_{\mathrm{opt}}\left(p\left(\mathbf{G}\circ\boldsymbol{\Omega}\right);\gamma\right)$ i.e. the capacity using (4.36) is equal to the upper bound on optimum joint decoding capacity using (4.72) and subsequently (4.68) holds true; compare the green square markers and the red circle makers. It is also demonstrated that $\mathbf{C}_{\mathrm{opt}}\left(p(\mathbf{G}\circ\boldsymbol{\Omega}),\gamma\right)_{\Omega=0} \approx \lim_{\Omega\to 0}\overline{\mathrm{C}}_{\mathrm{opt}}\left(p(\mathbf{G}\circ\boldsymbol{\Omega}),\gamma\right)$; observe the black curve when inter-cell interference between the users and the given BS is low i.e. $\Omega \to 0$.

b. Multi-user Case $K > 1$ with Intra-Cell TDMA:

In the multi-user case when K users are active in each of the adjacent cell, the channel matrix is no longer diagonal and hence (4.68) is not valid and subsequently $\Gamma_{(\boldsymbol{\mathcal{P}},\boldsymbol{\mathcal{Q}})} \neq 0$. However, the result of (4.68) is still valid when intra-cell TDMA (i.e. only 1 user is active in each cell) is employed.

For an example, when $K = 2$ the channel slow gain matrix can be modelled as[24] (3.19)

[24] Recall form Chapter 3 that $\boldsymbol{\Omega}_{N,K}$ is a $N \times NK$ channel slow gain matrix as defined in (3.8)

$$\mathbf{\Omega}_{N,K} = \left(\mathbf{\Omega}_{N,1}^{(1)}\ \mathbf{\Omega}_{N,1}^{(2)}\right)\breve{\boldsymbol{\mathcal{P}}}_{N,K} \tag{4-75}$$

where $\mathbf{\Omega}_{N,1}^{(1)} = \mathbf{\Omega}_{N,1}^{(2)} = \mathbf{I}_N$ and $\breve{\boldsymbol{\mathcal{P}}}_{N,K}$ is $NK \times NK$ permutation matrix as defined in (3.20). Similarly,

$$\mathbf{G}_{N,K} = \left(\mathbf{G}_{N,1}^{(1)}\ \mathbf{G}_{N,1}^{(2)}\right)\breve{\boldsymbol{\mathcal{P}}}_{N,K} \tag{4-76}$$

where $g_{ij} \in \mathbb{C}\mathcal{N}\left(0,1\right)$; $\forall\, i = j$ and $g_{ij} = 0$;$\forall\, i \neq j$. The resultant channel matrix $\mathbf{H}$ can be expressed as

$$\mathbf{H}_{N,K} = \left(\mathbf{G}_{N,K} \circ \mathbf{\Omega}_{N,K}\right) \tag{4-77}$$

In matrix notation, (4.77) can be expressed as (4.81)

Let us assume that intra-cell TDMA is employed i.e. only 1 user is active in each cell. Given that Ξ_{tdma}^{l} is a intra-cell TDMA user coder[25] for l^{th} intra-cell user such that

$$\mathbf{H}_{N,1}^{l} = \mathbf{H}_{N,K}\Xi_{\text{tdma}}^{l} \tag{4-78}$$

where Ξ_{tdma}^{l} can be designed as follows:

TDMA User Coder:

For $N \times NK$ channel matrix $\mathbf{H}_{N,K}$, Ξ_{tdma}^{l} is a $NK \times N$ matrix which transforms the resultant multi-user channel into single user per cell channel. The j^{th} column of Ξ_{tdma}^{l} has 1 in its $\left(l+\left(j-1\right)K\right)^{\text{th}}$ position and zero elsewhere, where $l = 1,2,\ldots,K$. As an example, for user one, $l = 1$[26]

[25] This is to note that TDMA user coder is not a coding technique. The coder is used in simulations to employ intra-cell TDMA. This is the implementation technique.

[26] For $l = 2$; The j^{th} column of $\Xi_{\text{tdma}}^{l=2}$ has 1 in its $\left(2+\left(j-1\right)K\right)^{\text{th}}$ position and zero elsewhere, i.e. for $j = 1,2,\cdots,6$ $\Xi_{\text{tdma}}^{l=2}$ has 1 at 2, 4,6,8,10 and 12 positions.

$$\left[\Xi\right]_{\text{tdma}}^{l=1} = \begin{pmatrix} 1 & 0 & 0 & 0 & 0 & 0 \\ 0 & 0 & 0 & 0 & 0 & 0 \\ 0 & 1 & 0 & 0 & 0 & 0 \\ 0 & 0 & 0 & 0 & 0 & 0 \\ 0 & 0 & 1 & 0 & 0 & 0 \\ 0 & 0 & 0 & 0 & 0 & 0 \\ 0 & 0 & 0 & 1 & 0 & 0 \\ 0 & 0 & 0 & 0 & 0 & 0 \\ 0 & 0 & 0 & 0 & 1 & 0 \\ 0 & 0 & 0 & 0 & 0 & 0 \\ 0 & 0 & 0 & 0 & 0 & 1 \\ 0 & 0 & 0 & 0 & 0 & 0 \end{pmatrix} \tag{4-79}$$

In matrix notation, (4.78) can be expressed as (4.82).

Subsequently, the channel after employing intra-cell TDMA becomes

$$\mathbf{H}_{N,1}^{l=1} = \left(\mathbf{G}_{N,1}^{l=1} \circ \mathbf{\Omega}_{N,1}^{l=1}\right) \tag{4-80}$$

where $\mathbf{G}_{N,1}^{l}$ and $\mathbf{\Omega}_{N,1}^{l}$ are exactly diagonal matrices as discussed in previous single user case. Hence (4.67) holds equality and (4.68) is valid.

$$\mathbf{H} = \begin{pmatrix} \left(g^1_{B_1T_1} \circ \Omega^1_{B_1T_1}\right) & \left(g^2_{B_1T_1} \circ \Omega^2_{B_1T_1}\right) & 0 & 0 & 0 & 0 & 0 & 0 & 0 & 0 & 0 & 0 \\ 0 & 0 & \left(g^1_{B_2T_2} \circ \Omega^1_{B_2T_2}\right) & \left(g^2_{B_2T_2} \circ \Omega^2_{B_2T_2}\right) & 0 & 0 & 0 & 0 & 0 & 0 & 0 & 0 \\ 0 & 0 & 0 & 0 & \left(g^1_{B_3T_3} \circ \Omega^1_{B_3T_3}\right) & \left(g^2_{B_3T_3} \circ \Omega^2_{B_3T_3}\right) & 0 & 0 & 0 & 0 & 0 & 0 \\ 0 & 0 & 0 & 0 & 0 & 0 & \left(g^1_{B_4T_4} \circ \Omega^1_{B_4T_4}\right) & \left(g^2_{B_4T_4} \circ \Omega^2_{B_4T_4}\right) & 0 & 0 & 0 & 0 \\ 0 & 0 & 0 & 0 & 0 & 0 & 0 & 0 & \left(g^1_{B_5T_5} \circ \Omega^1_{B_5T_5}\right) & \left(g^2_{B_5T_5} \circ \Omega^2_{B_5T_5}\right) & 0 & 0 \\ 0 & 0 & 0 & 0 & 0 & 0 & 0 & 0 & 0 & 0 & \left(g^1_{B_6T_6} \circ \Omega^1_{B_6T_6}\right) & \left(g^2_{B_6T_6} \circ \Omega^2_{B_6T_6}\right) \end{pmatrix} \tag{4-81}$$

$$\mathbf{H}_{N,1} = \begin{pmatrix} \left(g^1_{B_1T_1} \circ \Omega^1_{B_1T_1}\right) & 0 & 0 & 0 & 0 & 0 \\ 0 & \left(g^1_{B_2T_2} \circ \Omega^1_{B_2T_2}\right) & 0 & 0 & 0 & 0 \\ 0 & 0 & \left(g^1_{B_3T_3} \circ \Omega^1_{B_3T_3}\right) & 0 & 0 & 0 \\ 0 & 0 & 0 & \left(g^1_{B_4T_4} \circ \Omega^1_{B_4T_4}\right) & 0 & 0 \\ 0 & 0 & 0 & 0 & \left(g^1_{B_5T_5} \circ \Omega^1_{B_5T_5}\right) & 0 \\ 0 & 0 & 0 & 0 & 0 & \left(g^1_{B_6T_6} \circ \Omega^1_{B_6T_6}\right) \end{pmatrix} \tag{4-82}$$

c. Multi-user Case $K > 1$ without Intra-Cell TDMA:

It is well known that the increase in number of users to be decoded jointly increases the channel capacity [27] and [28]. From (4.81), it can be seen that with inter-cell TDMA and without intra-cell TDMA the local users are located along the main diagonal of a rectangular matrix.

The optimum joint decoding capacity obtained using (4.36) is shown in Figure 4-28. The upper bound on the capacity using the Hadamard inequality is also shown in this figure. It can be seen that improvement in capacity is significant. The gain is depending on the number of intra-cell users to be jointly decoded (see Figure 4-29). Thus, using inequality (4.67), the multi-user Cellular MIMO Networks (MU-CeMNets) offers $\log_2\left(K\right)$ times higher capacity as compared to the conventional capacity definition when inter-cell TDMA is employed i.e. using (4.36), $\Delta = \log_2\left(K\right)$ (see Figure 4-29). As a by-product of employing the Hadamard inequality in this scenario, we also observed that

$$\begin{aligned} \mathbf{G}\mathbf{G}^H \circ \boldsymbol{\Omega}\boldsymbol{\Omega}^H &= \left(\mathbf{G}\circ\boldsymbol{\Omega}\right)\left(\mathbf{G}\circ\boldsymbol{\Omega}\right)^H + \left(K-1\right)\left(\mathbf{G}\circ\boldsymbol{\Omega}\right)\left(\mathbf{G}\circ\boldsymbol{\Omega}\right)^H \\ &= K\left(\mathbf{G}\circ\boldsymbol{\Omega}\right)\left(\mathbf{G}\circ\boldsymbol{\Omega}\right)^H \end{aligned} \qquad (4\text{-}83)$$

Thus, using an inequality (4.67), the multi-user Cellular MIMO Networks (MU-CeMNets) offers $\log_2\left(K\right)$ times higher capacity and it has been demonstrated that the gain is dependent on the number of intra-cell users to be jointly decoded. This is to note that the result (4.83) is only valid when inter-cell TDMA is employed in the multi-user scenario.

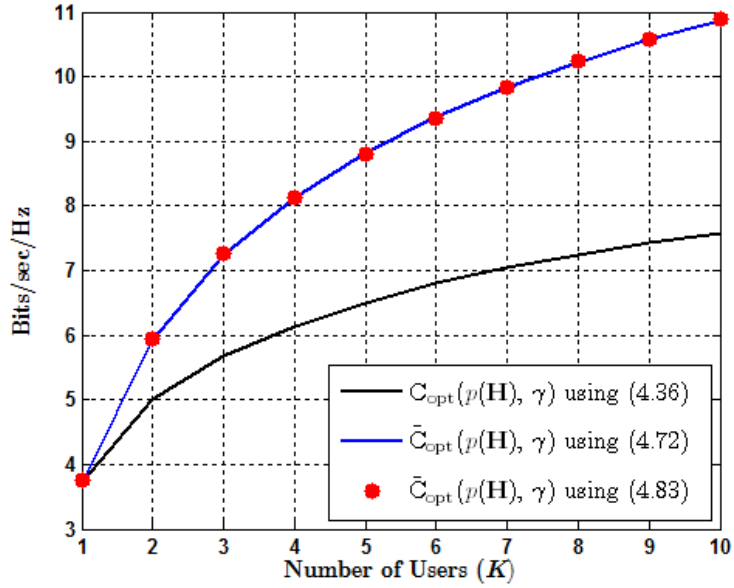

Figure 4-28: Variation of capacities with respect to number of intra-cell users K employing inter-cell TDMA and exploiting the Hadamard inequality (4.67) for $\gamma = 10\,\text{dB}$.

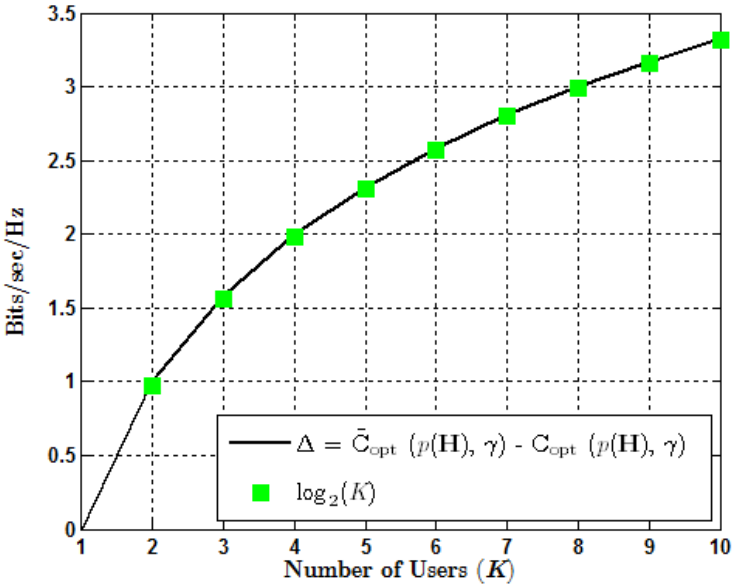

Figure 4-29: Gain in capacity using Hadamard inequality (4.67) without intra-cell TDMA for $\gamma = 10\,\text{dB}$.

4.8.5 Hadamard Inequality for Rank-one channel matrix[27]:

In the case that $\mathbf{A}$ and $\mathbf{B}$ are rank-one matrices, we can also derive an alternate version of (4.66) that also proves (4.67) for such matrices. Let us define $\mathbf{A} = u v^H$ and $\mathbf{B} = w z^H$, where u, v, w, z are $N \times 1$ column vectors which corresponds to a vector channel between the user in any of N cells and every N BS. Then,

$$\mathbf{A} \circ \mathbf{B} = (u \circ w)(v \circ z)^H \tag{4-84}$$

also is of rank at most one, and we calculate that

$$(\mathbf{A} \circ \mathbf{B})(\mathbf{A} \circ \mathbf{B})^H = (u \circ w)(v \circ z)^H (v \circ z)(u \circ w)^H \tag{4-85}$$

$$= \| v \circ z \|^2 (u \circ w)(u \circ w)^H \tag{4-86}$$

On the other hand, we have

$$\mathbf{A}\mathbf{A}^H = (u v^H)(v u^H) = \| v \|^2 (u u^H) \tag{4-87}$$

$$\mathbf{B}\mathbf{B}^H = (u v^H)(v u^H) = \| v \|^2 (u u^H) \tag{4-88}$$

This gives the formula,

$$(\mathbf{A}\mathbf{A}^H) \circ (\mathbf{B}\mathbf{B}^H) = \| v \|^2 \| z \|^2 (u u^H) \circ (w w^H) \tag{4-89}$$

$$= \| v \|^2 \| z \|^2 (u w) \circ (u^H w^H) \tag{4-90}$$

Comparing these formulas, we obtain the identity

$$(\mathbf{A}\mathbf{A}^H) \circ (\mathbf{B}\mathbf{B}^H) = \frac{\| v \|^2 \| z \|^2}{\| v \circ z \|^2} (\mathbf{A} \circ \mathbf{B})(\mathbf{A} \circ \mathbf{B})^H \tag{4-91}$$

In particular, since the norm is sub-multiplicative relative to the Hadamard product:

$$\| v \circ z \| \le \| v \| \| z \|, \tag{4-92}$$

[27]The proof can be extended for channel matrix of any rank $L > 1$ since if a matrix $\mathbf{A}$ is diagonalizable matrix of size N and rank L. Then there are L square matrices $\mathbf{A}_1 + \mathbf{A}_2 +, \cdots, +\mathbf{A}_L$, each of size N and rank 1 such that $\mathbf{A} = \mathbf{A}_1 + \mathbf{A}_2 +, \cdots, +\mathbf{A}_L$ [90]. Using Eq. (4.94) for each of the rank 1 matrix, desired result can be obtained. The result can be applied to the correlated scenario where the rank of matrix may reduce to 1.

Equation (4.91) gives another proof of (4.66) in this special case.

4.9 Conclusions

This chapter discussed the fundamental principals from information theory and random matrix theory for C-GCMAC. Inter-cell interfering users used to be considered at the same level of interference in both adjacent cells [27], [28] and [29]. We exploit the slow gain of inter-cell interfering users in both adjacent cells separately in order to increase the cell optimum capacity and reduce the fractional gain in C_{opt} over C_{cell} at moderate SNR. We derive the capacity when two or more MTs experience fading with different means. For example, if two MTs are located at different distances from the BS of interest. It has been shown that the cell optimum decoding strategy is optimal at low levels of inter-cell interference. The cell optimum decoding scheme suffers from interference limited behaviour and offers the lowest capacity of multi-user decoding schemes at high level of interferences. Multi-user decoding strategy is advantageous over single user decoding at all level of interferences since the single user decoding is intra-cell interference limited. It has been shown that optimal performance is attainable using intra-cell TDMA; and, that inter-cell TDMA is distinctly sub-optimal.

Finally in Section 4.8, a new upper bound referred to as the Hadamard upper bound is derived for optimum joint decoding capacity for Wyner C-GCMAC. New results have been shown to compare the upper bound to the well known Jensen's upper bound. The gain in optimum capacity is referred to as Gamma capacity which is the maximum capacity achieved by employing optimum joint decoding. However, the modified form of an inequality is introduced in Section 4.8.4c (without intra-cell TDMA). It has been shown that for the multi-user scenario, the optimum joint decoding is optimal choice in terms of the capacity when inter-cell TDMA is employed. The increase in capacity is $\log_2\left(K\right)$ times more as compared to the situation when intra-cell TDMA is employed (see sub-Sections 4.8.4a and 4.8.4c). Furthermore, the improvement in optimum joint decoding capacity is the original application of the Hadamard inequality.

Chapter 5
Transmission Design for Wyner C-GCMAC

5.1 Introduction

The radio spectrum is one of the most precious resources in the wireless network environment. Multiple-input multiple-output (MIMO) wireless networks, which employ multiple transmitting and receiving antennas at both sides of the communication link, are an extremely promising way to cope with the challenges of future generation networks. This chapter deals with the performance analysis based on simulation of two types of transmission strategies namely: V-BLAST MMSE and Zero Forcing – Dirty Paper Coding (ZF-DPC); design by employing recent decomposition techniques referred to as Geometrical Mean Decomposition (GMD) over Wyner uncorrelated and correlated C-GCMACs as introduced in Chapter 2 [143], Section 2.7. The impact of inter-cell interference on information theory has been investigated in the previous Chapter 4. The reliance of Bit Error Rate (BER) on the inter-cell interference over both uncorrelated and correlated scenarios is the key contribution of this chapter. The analysis is established in the light of eigenvalue analysis and power distribution of the eigenvalues of the channel matrix. Furthermore, a new model for a correlated Wyner circular cellular setup is derived. This fading model is based on rearranging the entries of random channel fading matrix $\mathbf{G}$, such that the channel appears as an unsystematic correlated structure. The channel is referred to as the Permuted channel throughout the chapter. The Chapter is organized as follows: § 5.2, presents an introduction to the cellular structure and transmission techniques; § 5.3, presents an overview of correlated Wyner structures, this Section also includes understanding of correlated and uncorrelated channels by analyzing the eigenvalue distributions; and §

5.4, presents our proposed correlated structure derived by rearranging the entries of a random matrix; § 5.5, presents an insights into the transmission design over the Wyner channels by exploiting GMD; § 5.6, presents simulation results and discussions. A typical behaviour of correlated channel due to rank reduction is investigated and reported in sub-Section 5.6.6 and regularization of such channel matrix is discussed as follows; conclusions to the Chapter are in given in § 5.7.

5.2 Transmission Strategies

Consider the modified Wyner's circular cellular setup as shown in Figure 5-1, with simple scheduling under the assumption of N identical cells and K identical users i.e. they have same the propagation loss (constant for non-fading channel and i.i.d for flat fading channels) towards the cell sites; employing the same communication protocols and are subjected to an equal power constraint. The identical cells in such setup are defined in the same spirit. In most of the cellular setup, the intra-cell users are assigned orthogonal channels through either time or frequency division multiple access (TDMA/FDMA). The intra-cell TDMA is optimal in terms of per cell sum rate when the out-of-cell interference in non negligible [70]. The rate expression in this case depends only on the total cell power. Hence it is enough to consider one user per cell using the total cell power constraint [70] and [71]. By exploiting the intra-cell TDMA only 1 out of the total of K users within the same cell will be active simultaneously. Hence, we can reduce the number of simultaneously active users within the cell and alleviate the burden of multi-user detection at the receiver [70].

In this Chapter, we focus on the Wyner like CeMNets with base station (BSs) cooperation (MCP) and mobile terminal cooperation (mobile conferencing) [108], [127] and [97] as reviewed in Chapter 3, Section 3.4. Therefore, for the uplink where receiver (BSs) performs multi-cell processing while transmitter (MTs) is allowed to cooperate over finite capacity link[1] (see Figure 5-2); all the MTs are able to exchange the local messages with all the other active MTs in the network.

[1] Finite capacity links that are available to enable cooperation are considered as additional spectral resources orthogonal to the main uplink or downlink channel.

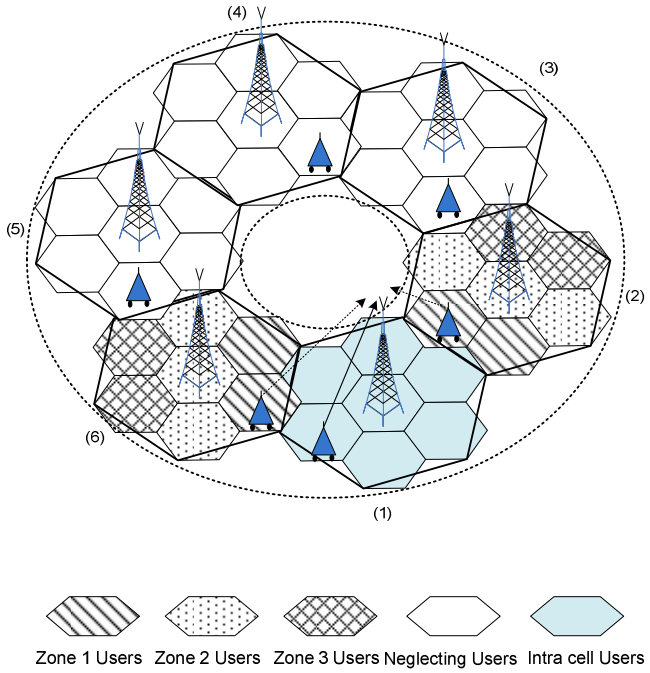

Figure 5-1: Graphical interpretation of circular cellular setup representing the division of each cell into three zones: zone #1 near zone; zone #2 near-far zone; zone #3 far zone.

The system at hand is thus equivalent to virtual MIMO system for which standard waterfilling algorithm is known to be optimal in terms of sum-rate [100] and [94]. For more information on the BS and MT cooperation readers may referred to [107], [127], [135], [136] and the references there in. However, a sum-rate analysis of such networks is out of scope of this thesis.

The main focus of the Chapter is on the simulation of transmission schemes over correlated and uncorrelated Wyner Circular cellular setup by exploiting recently introduced decomposition technique GMD as we discussed in Chapter 2 [2] and [143]. The transmission design over such scenarios may have two implementation forms. One is the combination of GMD with linear precoder and a Minimum Mean Squared Error Vertical Bell Labs Space Time (V-BLAST - MMSE) detector, which is referred to as GMD V-BLAST with MMSE, and the other comprises of a Dirty Paper Coding Zero Forcing (ZF-DPC) precoder and a linear equalizer followed by a DP precoder, this is referred to as GMD ZF-DPC.

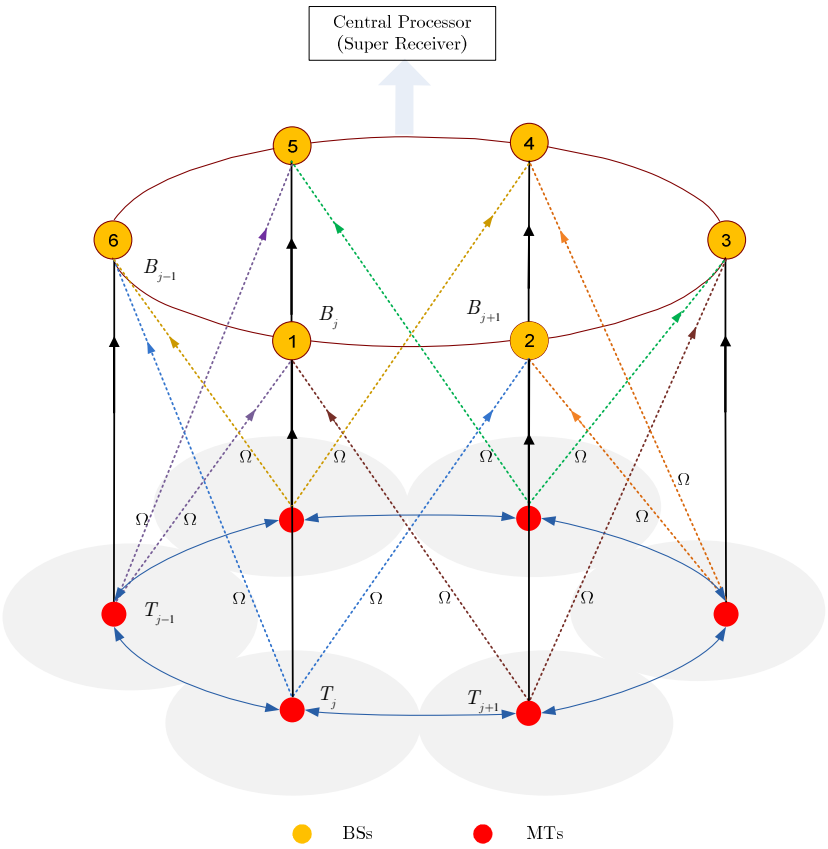

Figure 5-2: Node diagram of Uplink of cooperative Wyner C-GCMAC. For the sake of graphical simplicity we show only one MT active in each cell. At the given BS, the received signal is the sum of the signal from intra-cell MTs (the solid arrows) and from inter-cell MTs located in two adjacent cells only (the dotted arrows). The amplitude of the signals from the inter-cell users in two adjacent cells is scaled by channel slow gain $\Omega \in (0,1)$. Users located farther away than the adjacent cells are ignored for the sake of simplicity in channel modelling.

Hence, by exploiting either the sequential signal cancellation or the ZF-DPC, we can regard the MIMO channel as identical, parallel and independent pipes for data transmission (as shown in Figure 2-5).

5.3 Correlated Wyner C-GCMAC

In general, the Wyner channel transmission links (matrix entries), may have uncorrelated, semi-correlated and fully correlated fading statistics. There will also be difference in the BER performance and spectral efficiency for the different types of channels. In this chapter we investigate the performance of transmission schemes over correlated and uncorrelated channel types. The correlated channel can be modeled by well established Kronecker MIMO correlated channel models [1], [127] and [8]. Also, in [134], a model based on actual measurements for in-door setup is introduced. There are many other recently introduced MIMO correlated channel models [12].

We consider a simple correlated model in order to observe the impact of inter-cell interference on such a correlated structure [75]. Consider a scenario, where a cluster of scatterers are situated far from the transmitters and receivers and they are assumed to be scattered in space such that within each clusters there is a multitude of scatterers and the scatterers are assumed to have complex Gaussian scattering coefficients. The cluster looks like a point source and almost all the incident waves form the scatterers of the cluster has approximately the same angle of incidence form the transmitter (see Figure 5-3). Obviously, this scenario creates a correlated channel matrix with individual entries (each transmission link) be Rayleigh fading.[2,3] .

Consider a Wyner cellular setup as shown in Figure 5-3 with N transmitters and $M = NK$ receivers with ν clusters far from the transmitter and receiver [75]. Within each cluster, there are about κ scatterers. Let $\mathbf{G}_N$ is the MIMO transmission matrix connecting the N transmitters and ν clusters and having a dimension of $N \times \nu\kappa$. Similarly, $\mathbf{G}_M$ is the MIMO transmission matrix connecting the M receivers and ν clusters and having a dimension of $M \times \nu\kappa$, then the resultant

[2] For simplicity, our model assumes a random scattering coefficient for each scatterer. In real case, the scattering coefficients depend on array geometry, material properties of the scatterers, polarization of incident waves and so on.

[3] The cluster is far from the transmitter and receiver such that it looks like a point source for the transmitter and/or receiver. In this case the propagation path lengths traversed by each individual scattered wave (the path scattered from scatterers) are almost identical as seen from each transmitter and/or receiver [75].

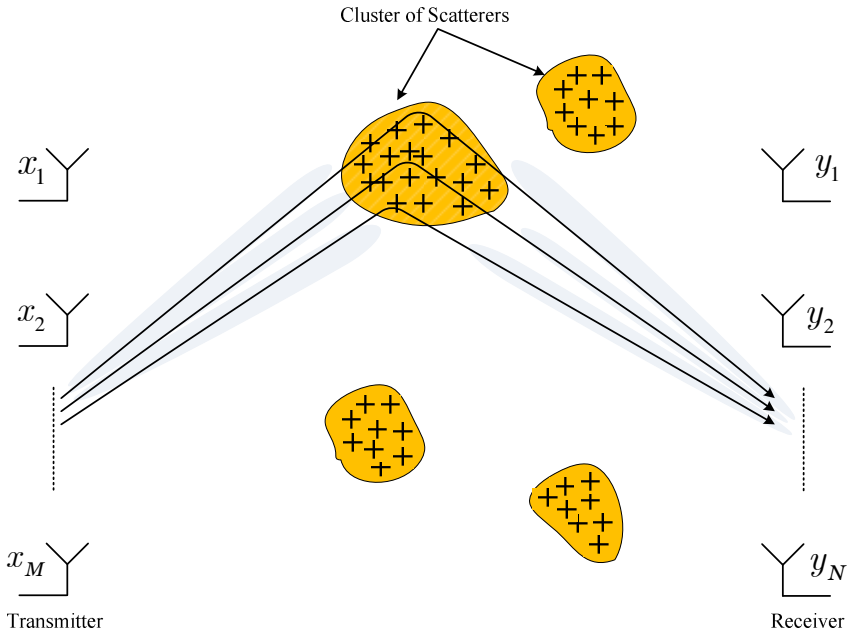

Figure 5-3: Transmitter and Receiver in a clustered scattering wireless environment: Clusters are assumed far from the transmitter and receiver (illustration of simple correlated Rayleigh fading scenario)

correlated fading channel matrix may be expressed as [75]

$$\mathbf{G} = \mathbf{G}_N \, \mathbf{G}_M^H \tag{5-1}$$

The above MIMO correlated fading channel is computed by taking into consideration the scattering coefficients. For Wyner C-GCMAC setup, the resultant channel $\mathbf{H}$ is the Hadamard product of the channel fading matrix $\mathbf{G}$ and the channel slow gain matrix $\mathbf{\Omega}$ when $K = 1$, and can be expressed as[4] [75] and [127]

$$\begin{aligned} \mathbf{H} &= \mathbf{G}_N \, \mathbf{G}_M^H \circ \mathbf{\Omega}_{N,1} \\ &= \mathbf{G}_{N,1} \circ \mathbf{\Omega}_{N,1} \end{aligned} \tag{5-2}$$

This simple model will be used to model the correlated Wyner cellular setup throughout this Chapter.

[4] $N = M$.

5.3.1 Eigenvalue Distribution of Correlated Structure

In this sub-Section, we investigate the power distribution of the eigenvalues of the correlated Wyner structures and compare these with the power distribution of eigenvalues of uncorrelated Wyner structure. Consider the correlated scenario where $N = M = 6$; the number of clusters is $\nu = 1$ and number of scatterers is $\kappa = 25$. The eigenvalue distribution of resultant correlated channel $\mathbf{H}$ (as demonstrated before for uncorrelated channel in Section 4.7.5.3) is shown in Figure 5-4a and Figure 5-4b for low level of interference i.e. $\Omega = 0.3$ and high level of interference i.e. $\Omega = 0.9$ respectively. It can be seen from Figure 5-4a that the first two Eigen channels with the smallest mean gain are so weak that pouring power may be wasteful. The mean gain of the third Eigen channel is $2.0\,\text{dB}$ less than the conventional systems with one antenna on both side of the transmission link (see black dotted curve). Consider the last three Eigen channels with the corresponding mean gain $\langle \lambda_4 \rangle = 4\,\text{dB}$, $\langle \lambda_5 \rangle = 7\,\text{dB}$ and $\langle \lambda_6 \rangle = 9.8\,\text{dB}$ which share the total transmitter-receiver mean gain[5]. The increment in gain is significant as compared to conventional system with one antenna on both side of transmission link. Similarly, Figure 5-4b shows the eigenvalue distribution of correlated channel when the level of interference increases to $\Omega = 0.9$. It is observed that with the increase in inter-cell interference the channel becomes highly correlated and the first three Eigen channels are so weak such that the mean power of all Eigen channels reduced to $\left\langle \lambda_{i=1}^{6} \right\rangle = -1\,\text{dB}$ for $\Omega = 0.9$ from $\left\langle \lambda_{i=1}^{6} \right\rangle = 1.5\,\text{dB}$ for $\Omega = 0.3$.

In order to compare the eigenvalue distribution of the correlated structure, we present the eigenvalue distribution of the uncorrelated structure in Figure 5-5a and Figure 5-5b for low level of inter-cell interference and high level of inter-cell interference respectively. It can be seen from the Figure 5-5a that the first two Eigen channels with the smallest gain are so weak that pouring power may be wasteful. The mean gain of the third Eigen channel is $0.8\,\text{dB}$ less than the conventional systems

[5] Mean gains (average eigenvalues) are obtained after averaging 5000 Monte Carlo trials of resultant channel matrix $\mathbf{H}$.

with (see black dotted curve) which is $2.0\,\mathrm{dB}$ less than the conventional system in case of correlated channel. The mean gains of the last three Eigen channels are $\langle\lambda_4\rangle = 4.1\mathrm{dB}$, $\langle\lambda_5\rangle = 6.3\mathrm{dB}$ and $\langle\lambda_6\rangle = 8.5\mathrm{dB}$ which are more than the mean gain of the conventional $(1,1)$ systems (see the black dotted curve). It is observed that the behaviour of the uncorrelated channel is identical to the correlated channel for low level of inter-cell interference. Investigations on this statement are provided later in this chapter in Section 5.6.4. Figure 5-5b shows that scenario, when the inter-cell interference between the MTs and BS is increase to $\Omega = 0.9$ in the presence of uncorrelated fading channel $\mathbf{G}$. It can be seen from the figure that with the increase in inter-cell interference levels the number of effective distinct paths increases. From Figure 5-5a, the behaviour of Eigen channels of correlated channel is close to the behaviour of uncorrelated channel. The correlation between the transmission link decreases with the increase in inter-cell interference and hence this indicates that we are getting closer and closer to the fully uncorrelated Rayleigh fading scenario with uncorrelated transmission links (i.i.d channel matrix entries). In this case the performance of transmission schemes will get better as there will be a higher possibility of recovering the transmitted sub-streams independently. Correspondingly, the diversity order of the eigenmodes will be enhanced and besides that the number of available transmission pipes (eigenmodes) will increase effectively and enhancing the total spectral efficiency. Also, the mean power of all eigenvalues increases to $\left\langle\lambda_{i=1}^{6}\right\rangle = 4.6\mathrm{dB}$ for $\Omega = 0.9$ from $\left\langle\lambda_{i=1}^{6}\right\rangle = 1.7$ dB for $\Omega = 0.3$. At low level of inter-cell interference, the mean power of eigenmodes is almost identical.

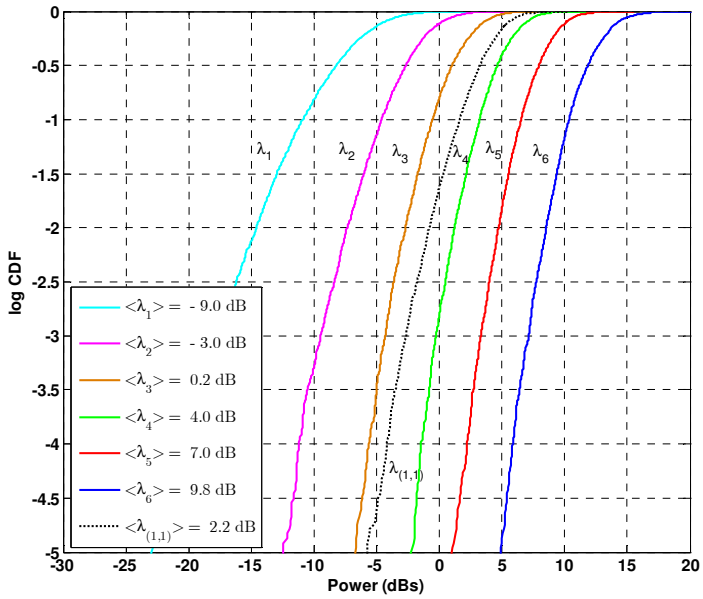

(a) $\Omega = 0.3$

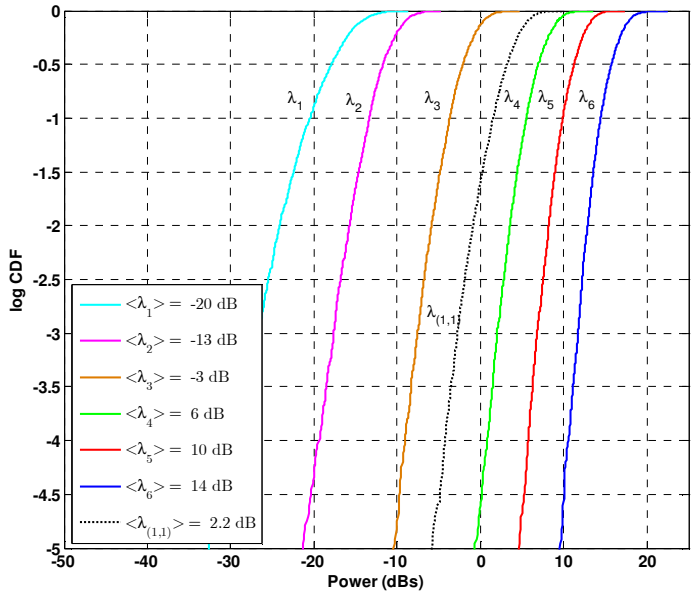

(b) $\Omega = 0.9$

Figure 5-4: The distribution of eigenvalues of the $\mathbf{H}(N, M) = (6, 6)$ Wyner correlated cellular setup with only one cluster of scatterers: (a) when MTs are offering low level of inter-cell interference; (b) when MTs are offering high level of interference. The dotted black line shows the theoretical Rayleigh, the power distribution of the $\mathbf{H}(1,1)$ case. The SISO scenario is given for reference purpose.

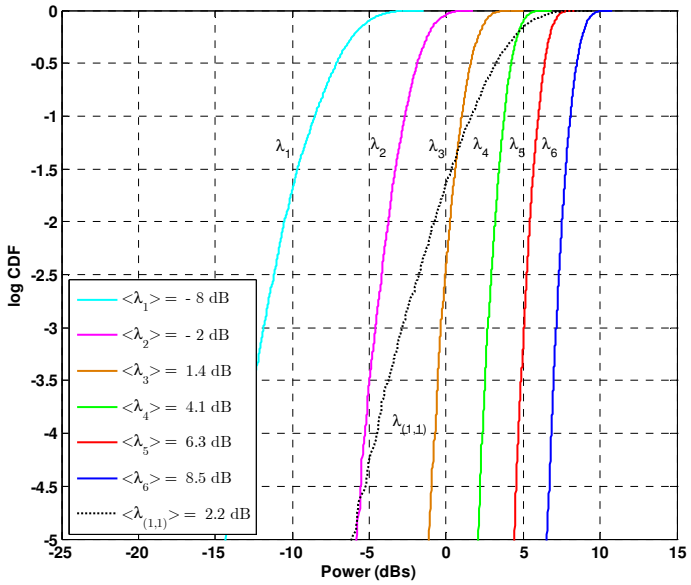

(a) $\Omega = 0.3$

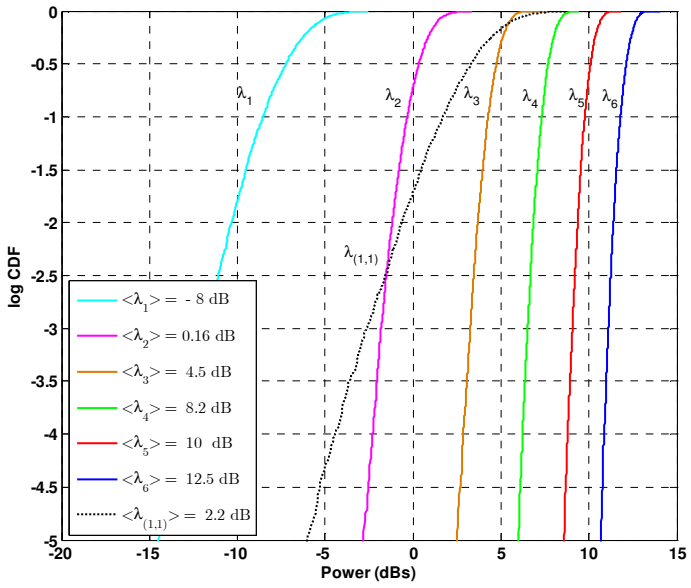

(b) $\Omega = 0.9$

Figure 5-5: The distribution of eigenvalues of the $\mathbf{H}(N,M) = (6,6)$ Wyner Uncorrelated cellular setup with only one cluster of scatterers: (a) when MTs are offering low level of inter-cell interference; (b) when MTs are offering high level of interference. The dotted black line shows the theoretical Rayleigh, the power distribution of the $\mathbf{H}(1,1)$ case. The SISO scenario is given for reference purpose.

5.3.2 Rank of Hadamard Product

When the fading statistics are correlated, the rank of the channel fading matrix $\mathbf{G}$ in (3.5) is reduced subsequently affecting the statistics of the overall resultant Hadamard channel. The rank reduction is the inherent property of the Hadamard operation between the channel gain matrix and channel slow gain matrix[6]. In this Section, we introduce important theorems to produce more accurate analysis of system performance when the channel is correlated and the rank is reduced.

Theorem 5.3.1 [24]**:** If $\mathbf{A}$ and $\mathbf{B}$ are complex $N \times M$ matrices with arbitrary ranks r_A and r_B respectively. Then the rank of $\left(\mathbf{A} \circ \mathbf{B}\right)$ denoted by $r_{A\circ B}$, can be expressed as

$$\text{Rank}\left(\mathbf{A} \circ \mathbf{B}\right) \geq \max\left\{\text{Rank}\left(\mathbf{A}\right), \text{Rank}\left(\mathbf{B}\right)\right\} \tag{5-3}$$

$$\text{or equivalently, } r_{A\circ B} \geq \max\left\{r_A, r_B\right\}$$

Theorem 5.3.2: If $\mathbf{A}$ is a $N \times M$ positive definite matrix, then $\text{Rank}\left(\mathbf{A} \circ \mathbf{B}\right) \geq \text{Rank}\left(\mathbf{B}\right)$ or equivalently, $r_{A\circ B} \geq r_B$. If $r_A = 1$, then $\text{Rank}\left(\mathbf{A} \circ \mathbf{B}\right) = r_{A\circ B}$ is given by

$$\text{Rank}\left(\mathbf{A} \circ \mathbf{B}\right) = \text{Rank}\left(\mathbf{B}\right)$$

$$\text{or equivalently, } r_{A\circ B} = r_B \tag{5-4}$$

Our proof of (5.4) is included in Appendix G.

[6] The rank reduction in Wyner C-GCMAC is due the fact that more than one eigenvalues of channel slow gain matrix are approaching zero at more than one instances. The details are covered later in sub-Section 5.6.6.

5.4 Hadamard Permuted Channel (HPC)

There are different types of correlated structures [1]. In fact, although in mathematics and statistics the definition of correlation is unique; in the Cellular MIMO Networks (CeMNets) context where random matrices exist there could be different definitions for correlation. In the widest sense, by a correlated MIMO structure, we mean a structure in which there is some kind of dependency between the signals. Two different classes of correlated MIMO structures can be distinguished: systematic and unsystematic [127]. A systematic correlated structure is a structure in which the correlation between the signals is embedded in the channel matrix i.e. the correlation arises from some random variables being repeated, alone or in linear combinations, in the channel matrix; even if the individual variables values are independent. So, the correlation is distinguishable by just observing the channel matrix configuration without needing to investigate the elements themselves. In this case the correlation is in some way fixed or predictable. On the contrary, an unsystematic structure introduces a random correlation between the signals and doesn't obey a fixed or pre-defined configuration. So, for this class of correlated structure it is not possible to determine the correlation just by investigating the channel matrix and we need to know the elements.[75]

5.4.1 Modelling of HPC

The fading channel statistics depends on the number of clusters between the transmission links. When there is only one or very few clusters (a cluster consisting of multitude of scatterers) in the radio channel there will not be enough distinct paths between the transmission link to recover the data streams independently. Therefore, there will be a strong correlation between the transmission links (channel matrix entries) [75]. The proposed unsystematic correlated fading channel matrix is modelled by rearranging the entries of i.i.d completely random channel matrix $\mathbf{G}$ and by exploiting the circular arrangement of the base stations in Wyner like cellular setup. The proposed correlated channel model is referred to as the Hadamard Permuted Channel (HPC) ssince the new correlated channel fading matrix is the permuted version of the i.i.d completely random matrix. It is important to note that

no random variables are repeated in such unsystematic correlated fading channel matrix. However, propagation conditions may cause the random variables to become correlated.

Consider a circulant systematic structure $\mathbf{G}^c$ such that every row is the cyclic shift of the row above it, in the resultant matrix. The circular matrix can be constructed by exploiting the circular permutation operator $\boldsymbol{\mathcal{S}}$, viewed as $N \times N$ matrix relative to the standard basis for $\mathbb{R}^N$ as shown in Chapter 3, lemma 3.9.1 [39].

If the first row of the circulant structure $\mathbf{G}^c$ is expressed as $\boldsymbol{g}_1^c = \left(g_0^c, g_1^c, g_2^c, \cdots, g_{N-1}^c\right)$ such that $g_{i,j}^c \in \mathbb{C}\,\mathcal{N}(0,1)$. Using lemma 3.9.1, it is known that the shift invariant circular matrix $\mathbf{G}^c$ can be expressed as a linear combination of powers of the shift operator $\boldsymbol{\mathcal{S}}$.

$$\mathbf{G}^c = \sum_{j=0}^{N-1} g_j^c\, \mathbf{S}^j \quad \text{for } j = 0,1,2,\cdots,N-1 \tag{5-5}$$

$$= g_0^c\, \mathbf{I} + g_1^c\, \mathbf{S} + g_2^c\, \mathbf{S}^2 + g_3^c\, \mathbf{S}^3 + g_4^c\, \mathbf{S}^4 + g_5^c\, \mathbf{S}^5$$

where $\mathbf{I}$ is the identity matrix and $\boldsymbol{\mathcal{S}}$ is the shift operator. In matrix notation, the circulant structure can be expressed as

$$\mathbf{G}^c = \begin{pmatrix} g_0^c & g_1^c & \cdots & g_{N-1}^c \\ g_{N-1}^c & g_0^c & \cdots & g_{N-2}^c \\ \vdots & \vdots & \ddots & \vdots \\ g_1^c & \cdots & \cdots & g_0^c \end{pmatrix} \tag{5-6}$$

The modelling of the proposed HPC by exploiting the permutation distance is based on the following corollary.

Corollary 5.4.1: To find the i^{th} row of the permuted channel matrix $\breve{\mathbf{G}}$, we compare the possible permutations of entries in the i^{th} row of the i.i.d channel

matrix $\mathbf{G}$ with the i^{th} row of circulant channel matrix $\mathbf{G}^c$. The metric we defined to compare the possible permutations of i^{th} row, is the permutation distance Γ_i^p, and is given by

$$\Gamma_i^p = \sum_{j=1}^{N} \left(\left| g_{i,j}^p \right| - \left| g_{i,j}^c \right| \right)^2 \tag{5-7}$$

where i and j are the number of rows and columns respectively given by $i = 1,2,\cdots N$ and $j = 1,2,\cdots N$ respectively; $g_{i,j}^p$ is the $\left(i^{\text{th}}, j^{\text{th}}\right)$ entry of the p^{th} *permuted* row vector $\boldsymbol{g}_i^p$ of $\mathbf{G}$, and $g_{i,j}^c$ is the $\left(i^{\text{th}}, j^{\text{th}}\right)$ entry of the row vector $\boldsymbol{g}_i^c$ of $\mathbf{G}^c$.

The permutation which gives the smallest permutation distance Γ_i^p will be set as a i^{th} row of the new rearranged channel matrix $\breve{\mathbf{G}}$ referred to as *Permuted channel*. If $\boldsymbol{g}_i^p$ is the p^{th} permutation of the i^{th} row vector of the random matrix $\mathbf{G}$ which gives smallest permutation distance with the i^{th} row of $\mathbf{G}^c$, then $\boldsymbol{g}_i^p$ will be set as the i^{th} row of the Permuted channel matrix $\breve{\mathbf{G}}$.

5.4.2 Example of Formation of Permuted Channel

As an example, let us define a matrix $\mathbf{G}^{3\times 3} \in \mathbb{R}\mathcal{N}\left(0,1\right)$, in order to illustrate the formation of Permutated matrix.

$$\mathbf{G} = \begin{pmatrix} \boldsymbol{g}_1 \\ \boldsymbol{g}_2 \\ \boldsymbol{g}_3 \end{pmatrix} = \begin{pmatrix} 0.3509 & 1.1082 & 0.7508 \\ 0.8921 & 0.0259 & 0.5002 \\ 1.5783 & 1.1106 & 0.5173 \end{pmatrix}$$

where $\boldsymbol{g}_i$ is the i^{th} row of $\mathbf{G}$ such that each row has $p = 3! = 6$ possible permuted versions define as $\left\{\boldsymbol{g}_i^p\right\}_{p=1}^{p=3!}$. Similarly, $\left\{\boldsymbol{g}_i^c\right\}_{i=1}^{i=3}$ are the i rows of the reference circulant matrix. The permutation distances between the p^{th} permuted version of i^{th} row of $\mathbf{G}$ and i^{th} row of $\mathbf{G}^c$ is calculated from (5.7) and numerical values are shown in Table 5-1.

Table 5-1: Numerical values of Permutation distances among the p^{th} permutation of i^{th} row of $\mathbf{G}$ and i^{th} row of reference channel matrix from (5.7)

p	Γ_1^p	Γ_2^p	Γ_3^p
1	0.1999	0.3496	0.7164
2	0.0767	0.5338	1.1515
3	0.4040	0.9847	0.5173
4	0.6319	0.8327	1.5783
5	0.2310	0.8212	1.1106
6	0.4931	0.4848	1.5783

From the Table 5-1, it is clear that the permutation distances $\Gamma_1^{p=2}$, $\Gamma_2^{p=1}$ and $\Gamma_3^{p=3}$ are the smallest distances and hence according to Corollary 5.4.1., the corresponding permuted row of the i^{th} row of $\mathbf{G}$ will be set as the i^{th} row of the Hadamard Permuted channel matrix $\breve{\mathbf{G}}$, as shown below:

$$\breve{\mathbf{G}} = \begin{pmatrix} \boldsymbol{g}_1^{p=2} \\ \boldsymbol{g}_2^{p=1} \\ \boldsymbol{g}_3^{p=3} \end{pmatrix} = \begin{pmatrix} 0.3509 & 0.7508 & 1.1082 \\ 0.8921 & 0.0259 & 0.5002 \\ 1.1106 & 1.5783 & 0.5173 \end{pmatrix}$$

The resultant matrix is referred to as a non-systematic type of correlated structure.

5.5 Transmission Design over Parallel, Independent and Identical Pipes[7,8]

In this Section, we present the transmission design over Wyner C-GCMAC. We first review the linear Minimum Mean Square Error (MMSE) detector and then present V-BLAST MMSE detector based on QR decomposition and GMD. Later, in this Section, we review Zero Forcing Dirty Paper Coding (ZF-DPC) scheme for Wyner C-GCMAC in order to provide comparative analysis for the transmission designs. At the end of this Section, we show the formation of identical, parallel and independent transmission pipes over Wyner cellular MIMO channel by exploiting GMD as we introduced in Chapter 2, Section 2.7.2.

Recall from Chapter 2, for wireless communication systems with M transmitters and N receivers, then the overall input output transmission equation becomes $\boldsymbol{y} = \mathbf{H}\boldsymbol{x} + \boldsymbol{z}$, where $\boldsymbol{x} \in \mathbb{C}^{M\times 1}$ is the transmit signal vector, $\boldsymbol{y} \in \mathbb{C}^{N\times 1}$ is the received signal vector, $\mathbf{H} \in \mathbb{C}^{N\times M}$ is the channel matrix with the $h_{n,m}$ element denoting the fading coefficient between the n^{th} transmitting and m^{th} receiving antennas. As in (2.1), we again assume $\mathbb{E}\left[\boldsymbol{x}\,\boldsymbol{x}^H\right] = \sigma_x^2\mathbf{I}_M$ and $\boldsymbol{z} \sim \mathcal{CN}\left(0, \sigma_z^2\mathbf{I}_N\right)$ is zero mean complex circularly symmetric Gaussian noise, $\mathbf{I}_N$ is the identity matrix with dimension N. We also define the SNR as [6]

$$\gamma = \frac{\mathbb{E}\left[\boldsymbol{x}^H\,\boldsymbol{x}\right]}{\sigma_z^2} = \frac{\sigma_x^2}{\sigma_z^2} \triangleq \frac{1}{\alpha}$$

where α is the noise to signal ratio define as $\alpha = \dfrac{\sigma_z^2}{\sigma_x^2}$.

[7] Precoding over the uplink clearly requires every node to be aware of the messages to be sent by the other terminals (at least of the neighbours, as in [138] not only the CSI i.e. either inter-cell or intra-cell conferencing at the user terminals plus CSI at the Tx to design precoder.
[8] For more details, the reader is referred to [135] and [136].

In the following sub-Section, we first review the linear MMSE and then present the GMD version of the V-BLAST scheme followed by QR version of V-BLAST.

5.5.1 Linear MMSE

The linear detector is a suboptimal detection scheme for estimating the transmitted signals. The block diagram of linear detection is shown in Figure 5-6. The receive vector $\boldsymbol{y}$ is multiplied with a filter matrix $\boldsymbol{w}$ followed by a parallel decision on all layers.

It is well understood that in case of zero forcing (ZF) detection small eigenvalues of $\mathbf{H}^H \mathbf{H}$ will lead to large errors due to noise amplification [73]. The problem of noise enhancement has already been addressed [1] and [74].

In order to improve the performance of the linear detector the noise term can be included in the design of filter matrix $\boldsymbol{w}$. This is done in the MMSE detector, where the filter $\boldsymbol{w}$ represents a tradeoff between the noise amplification and interference suppression [1]. Minimizing the mean square error (MSE) between the actually transmitted symbols and the output of the linear detector leads to a filter matrix $\boldsymbol{w}$, given by [1] and [8],

$$\boldsymbol{w} = \left(\mathbf{H}^H \mathbf{H} + \alpha \mathbf{I}_M\right)^{-1} \mathbf{H}^H \tag{5-8}$$

Subsequently the nulling vector for i^{th} layer is given by

$$w_i = \left(\sum_{j=1}^{i} h_j^H h_j + \alpha \mathbf{I} \right)^{-1} h_i^H \tag{5-9}$$

The resulting filter output is given by

$$\tilde{\boldsymbol{x}} = \boldsymbol{w}\,\boldsymbol{y} \tag{5-10}$$

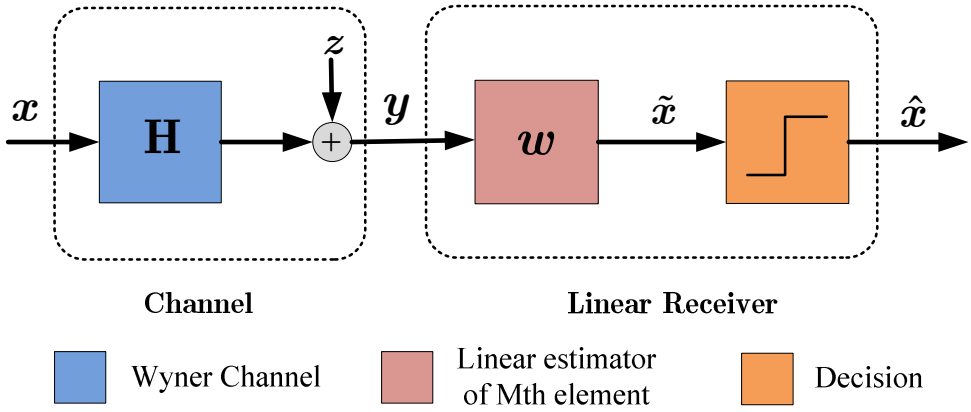

Figure 5-6: Block diagram of a transceiver design with linear detector.

where $\tilde{\boldsymbol{x}}$ is the filter output vector and $\boldsymbol{y}$ is the received vector. The derivation of nonlinear version of MMSE detection algorithm is presented in Section 5.5.3 and Section 5.5.4, we define an $\left(N+M\right)\times N$ augmented channel matrix and $\left(N+M\right)\times 1$ augmented received vector as follows [127]

$$\underline{\mathbf{H}} = \begin{bmatrix} \mathbf{H} \\ \sqrt{\alpha}\,\mathbf{I}_N \end{bmatrix}; \quad \underline{\boldsymbol{y}} = \begin{bmatrix} \boldsymbol{y} \\ \mathbf{0}_{N\,x1} \end{bmatrix} \tag{5-11}$$

With these definitions we can rewrite the nulling matrix (5.8) as

$$\underline{\boldsymbol{w}} = \left(\left[\mathbf{H}^H \sqrt{\alpha}\,\mathbf{I}_M \right] \begin{bmatrix} \mathbf{H} \\ \sqrt{\alpha}\,\mathbf{I}_M \end{bmatrix} \right)^{-1} \left[\mathbf{H}^H \sqrt{\alpha}\,\mathbf{I}_M \right] \tag{5-12}$$

where α is the noise to signal ratio.

The subsequent filter output of the MMSE filter can be expressed as

$$\tilde{\boldsymbol{x}} = \underline{\boldsymbol{w}}\,\underline{\boldsymbol{y}} \tag{5-13}$$

Substituting the nulling vector (5.12), the filter output (5.13) becomes

$$\tilde{\boldsymbol{x}} = \left(\left[\mathbf{H}^H \sqrt{\alpha}\, \mathbf{I}_M \right] \begin{bmatrix} \mathbf{H} \\ \sqrt{\alpha}\, \mathbf{I}_M \end{bmatrix} \right)^{-1} \left[\mathbf{H}^H \sqrt{\alpha}\, \mathbf{I}_N \right] \begin{bmatrix} \boldsymbol{y} \\ \mathbf{0}_{M \times 1} \end{bmatrix},$$

$$\tilde{\boldsymbol{x}} = \left(\underline{\mathbf{H}}^H \underline{\mathbf{H}} \right)^{-1} \underline{\mathbf{H}}^H \underline{\boldsymbol{y}},$$

$$\tilde{\boldsymbol{x}} = \underline{\mathbf{H}}^{+} \underline{\boldsymbol{y}} \tag{5-14}$$

Thus, the MMSE detector can be interpreted as ZF detector with respect to the extended system mode [1]. This simple observation will be important for incorporating the MMSE criterion into the nonlinear detection algorithm in the following sub-Sections.

5.5.2 V-BLAST MMSE Systems

In this Section, we review the V-BLAST system proposed in [6] for cellular networks. The V-BLAST is a simple sub-optimal receiver interface which is used in the MIMO system that initially assumes only CSIR is available. Figure 5-7 shows the V-BLAST unprecoded scheme, where $\boldsymbol{y} \in \mathbb{C}^{N \times 1}$, $\boldsymbol{x} \in \mathbb{C}^{NK \times 1}$, $\boldsymbol{z} \in \mathbb{C}^{N \times 1}$ is c.c.s. Gaussian noise process with $\mathbb{E}\left[\boldsymbol{z}\right] = 0$; $\mathbb{E}\left[\boldsymbol{z}\boldsymbol{z}^H\right] = \sigma^2 \mathbf{I}_N$ and $\mathbf{H} \in \mathbb{C}^{N \times NK}$ which is defined as (3.5).

For a cellular circular setup as shown in Figure 5-1 with $K = 1$, $N = M = NK = 6$ and, the transmitter (MTs) allocates independent bit streams across the N transmitting antennas without precoding. To decode the transmitted information symbol, V-BLAST first estimates the signal with the spatial structure h_M, where h_i denotes the i^{th} column of $\mathbf{H}$, and then cancels it out from the received signal vector. Next, it estimates the signal with spatial structure h_{M-1} and so on. The signal cancellation can be done by employing MMSE estimator. This decoding scheme involves sequential nulling and cancellation which is proved to be equivalent to the Generalized Decision Feedback Equalizer (GDFE) [5].

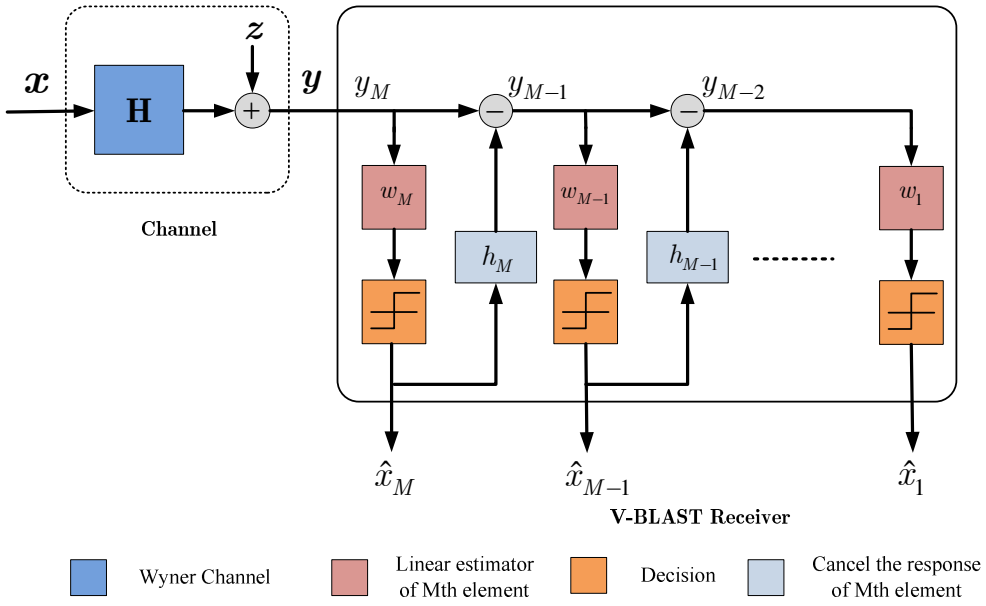

Figure 5-7: Schematic diagram of V-BLAST scheme.

This process repeats until all of the symbols are decoded. The decoding order can be further optimized. Some proper reordering of the columns of $\mathbf{H}$ is helpful to improve the BER performance [12], [5], and [8]. For convenience, we assume the decoding order is $(M, M-1, \cdots, 1)$ as shown in Figure 5-7. This sequence can be easily modified by inserting a permutation matrix in between the channel matrix $\mathbf{H}$ and the V-BLAST decoder [146].

The main drawback of the V-BLAST detection algorithm lies in the computational complexity as we explained in a review in Chapter 2. To this end, we restate the MMSE detection using QR decomposition of the channel matrix, yielding the perfect detection sequence and thereby the performance of V-BLAST scheme. The main advantage of this combined scheme comes with the complexity reduction, as it requires only a fraction of the complexity effort of the original V-BLAST algorithm [73].

In Figure 5-7 $\boldsymbol{w}_i$ is a $1\times N$ vector such that $\boldsymbol{w}_i\boldsymbol{y}_i$ is the MMSE estimator of the i^{th} element of $\boldsymbol{x}$ (denoted as $x(i)$) based on the input $\boldsymbol{y}_i$ where $\boldsymbol{y}\in\mathbb{C}^{N\times 1}$ and

$i = 1, 2, \cdots, M-1, M$. It can be found from the following optimization problem:[73] and [74]

$$\min_{w_i} \mathbb{E}\left| w_i y_i - x(i) \right|^2 \tag{5-15}$$

After this estimation, $\boldsymbol{w}_i \boldsymbol{y}_i$ is sent to the slicer and feedback to cancel the interference caused by $x(i)$. That is

$$\boldsymbol{y}_{(i-1)} = \boldsymbol{y}_i - \boldsymbol{h}_i \, \hat{x}(i) \tag{5-16}$$

where $\hat{x}(i) = \mathcal{C}\left[\boldsymbol{w}_i \boldsymbol{y}_i\right]$ and $\mathcal{C}[\cdot]$ denote the slicer. We also assume that there is no error propagation [1], [7], [8], [12] and [14]. We discussed this assumption in Chapter 2, Section 2.7.2. That is, when considering the i^{th} input $\boldsymbol{y}_i$, we assume $\hat{x}(k) = x(k)$ $k = M, M-1, \cdots, i+1$. Therefore,

$$\boldsymbol{y}_i = \boldsymbol{y} - \sum_{k=i+1}^{M} \boldsymbol{h}_k \, x(k) \tag{5-17}$$

$$= \mathbf{H}\boldsymbol{x} + \boldsymbol{z} - \sum_{k=i+1}^{M} \boldsymbol{h}_k \, x(k)$$

$$= \mathbf{H}_i \, \boldsymbol{x}_i + \boldsymbol{z} \tag{5-18}$$

where $\mathbf{H}_i$ is denote the sub-matrix containing the first i^{th} columns of $\mathbf{H}$ and $\boldsymbol{x}_i$ denote the column vector containing only first i^{th} entries. From (5.15) - (5.18), we can derive $\boldsymbol{w}_i$ and the corresponding MSE by the orthogonally principle and obtain

$$\boldsymbol{w}_i = \left(\mathbf{H}_i{}^H \mathbf{H}_i + \alpha \mathbf{I}_i \right)^{-1} \mathbf{H}_i{}^H \tag{5-19}$$

$$\mathbb{E}\left| x(i) - \boldsymbol{w}_i \boldsymbol{y}_i \right|^2 = \left(\mathbf{H}_i{}^H \mathbf{H}_i + \alpha \mathbf{I}_i \right)^{-1}_{i,i} \tag{5-20}$$

In this expression, a matrix inversion has to be computed for each $\boldsymbol{w}_i$. Therefore, this direct computation is very complex. A fast and efficient way to compute these is by using the QR algorithm [73] and [74] described in the following Section below.

5.5.3 V-BLAST MMSE with QR Decomposition

In order to extend the QR based MMSE V-BLAST detection, we can exploit the similarity of linear ZF and MMSE detection. For this purpose, we introduce QR decomposition of the extended channel matrix $\underline{\mathbf{H}}$, given by [73]

$$\begin{aligned}\underline{\mathbf{H}} &= \underbrace{\begin{bmatrix}\mathbf{H}\\ \sqrt{\alpha}\mathbf{I}_M\end{bmatrix}}_{(N+M)\times M}\\ &= \mathbf{Q}_{\underline{H}}\,\mathbf{R}_{\underline{H}}\end{aligned} \tag{5-21}$$

$$= \underbrace{\begin{pmatrix} q_{\underline{H},11} & q_{\underline{H},12} & \cdots & q_{\underline{H},1M}\\ q_{\underline{H},21} & q_{\underline{H},22} & \cdots & q_{\underline{H},2M}\\ \vdots & \vdots & \vdots & \vdots\\ q_{\underline{H},N1} & q_{\underline{H},N2} & \cdots & q_{\underline{H},NM}\\ \vdots & \vdots & \vdots & \vdots\\ q_{\underline{H},(N+M),1} & q_{\underline{H},(N+M),2} & \cdots & q_{\underline{H},(N+M),M}\end{pmatrix}}_{(N+M)\times M} \underbrace{\begin{pmatrix} r_{\underline{H},11} & r_{\underline{H},12} & \cdots & r_{\underline{H},1M}\\ 0 & r_{\underline{H},22} & \cdots & r_{\underline{H},2M}\\ \vdots & \ddots & \ddots & \vdots\\ 0 & \cdots & 0 & r_{\underline{H},MM}\end{pmatrix}}_{M\times M} \tag{5-22}$$

where $\mathbf{R}_{\underline{H}} \in \mathbb{C}^{N\times N}$ is an upper triangular matrix with positive diagonal elements and $\mathbf{Q}_{\underline{H}} \in \mathbb{C}^{(N+M)\times N}$ is the unitary matrix. Observing the first i columns of the $\underline{\mathbf{H}}$, let us define a sub-matrix $\underline{\mathbf{H}}_i$ as follows

$$\underline{\mathbf{H}}_i = \begin{pmatrix} \mathbf{H}_i \\ \sqrt{\alpha}\,\mathbf{I}_i \\ \mathbf{0}_{(M-i)\times i} \end{pmatrix} \tag{5-23}$$

$$= \mathbf{Q}_{\underline{H}} \begin{pmatrix} \mathbf{R}_{\underline{H}} \\ \mathbf{0}_{(M-i)\times i} \end{pmatrix} \tag{5-24}$$

The nulling vector can be readily obtained by using following lemma: exploiting $\mathbf{Q}_{\underline{H}}^{u}$ and $\mathbf{R}_{\underline{H}}$ as shown in the following lemma.

Lemma 5.5.1: The unitary matrix $\mathbf{Q}_{\underline{H}} \in \mathbb{C}^{(N+M)\times M}$ is partitioned into the $\mathbf{Q}_{\underline{H}}^{u} \in \mathbb{C}^{N\times M}$ and $\mathbf{Q}_{\underline{H}}^{l} \in \mathbb{C}^{M\times M}$. Note that $\mathbf{H} = \mathbf{Q}_{\underline{H}}^{u}\,\mathbf{R}_{\underline{H}}$ is not the QR decomposition of channel matrix $\mathbf{H}$ since $\mathbf{Q}_{\underline{H}}^{u}$ is not a unitary matrix.

Let $\left\{\boldsymbol{q}_{\underline{H},i}\right\}_{i=1}^{M}$ denote the columns of $\mathbf{Q}_{\underline{H}}^{u}$ and $\left\{r_{\underline{H},ii}\right\}_{i=1}^{M}$ is the diagonal elements of $\mathbf{R}_{\underline{H}}$, where $\mathbf{Q}_{\underline{H}}^{u}$ and $\mathbf{R}_{\underline{H}}$ are given by (5.21). The nulling vectors of (5.20) satisfy [72]

$$\boldsymbol{w}_i = r_{\underline{H},ii}^{-1}\,\mathbf{q}_{\underline{H},i}^{u} \quad i = 1,2,\cdots,M. \tag{5-25}$$

Proof of (5.25):

The solution of $\boldsymbol{w}_i$ can be rewritten as

$$\boldsymbol{w}_i = \left(\left(\underline{\mathbf{H}}_i^{H}\,\underline{\mathbf{H}}_i\right)^{-1}\underline{\mathbf{H}}_i^{H}\right)$$

Substituting the QR decomposition of $\underline{\mathbf{H}}_i$, we obtain

$$\boldsymbol{w}_i = \left(\left(\begin{pmatrix} \mathbf{R}_{\underline{H}} \\ \mathbf{0}_{(M-i)\times i} \end{pmatrix}^{H} \mathbf{Q}_{\underline{H}}^{H}\,\mathbf{Q}_{\underline{H}} \begin{pmatrix} \mathbf{R}_{\underline{H}} \\ \mathbf{0}_{(M-i)\times i} \end{pmatrix}\right)^{-1} \begin{pmatrix} \mathbf{R}_{\underline{H}} \\ \mathbf{0}_{(M-i)\times i} \end{pmatrix}^{H} \mathbf{Q}_{\underline{H}}^{H}\right)$$

The unitary matrix $\mathbf{Q}_{\underline{H}} \in \mathbb{C}^{(N+M)\times M}$ is partitioned into the $\mathbf{Q}_{\underline{H}}^{u} \in \mathbb{C}^{N\times M}$ and $\mathbf{Q}_{\underline{H}}^{l} \in \mathbb{C}^{M\times M}$. Substituting this into above, we have

$$= \left(\left(\begin{pmatrix} \mathbf{R}_{\underline{H}} & \mathbf{0}_{(M-i)\times i} \end{pmatrix} \begin{pmatrix} \mathbf{R}_{\underline{H}} \\ \mathbf{0}_{(M-i)\times i} \end{pmatrix} \right)^{-1} \begin{pmatrix} \mathbf{R}_{\underline{H}} & \mathbf{0}_{(M-i)\times i} \end{pmatrix} \begin{pmatrix} \mathbf{Q}_{\underline{H}}^{u\,H} \\ \mathbf{Q}_{\underline{H}}^{l\,H} \end{pmatrix} \right)$$

$$= \left(\mathbf{R}_{\underline{H}}^{-1} \mathbf{Q}_{\underline{H}}^{u\,H} \right)$$

$$= \begin{pmatrix} r_{\underline{H},11} & r_{\underline{H},12} & \cdots & r_{\underline{H},1M} \\ 0 & r_{\underline{H},22} & \cdots & r_{\underline{H},2M} \\ \vdots & \ddots & \ddots & \vdots \\ 0 & \cdots & 0 & r_{\underline{H},MM} \end{pmatrix}^{-1} \begin{pmatrix} q_{\underline{H},11}^{u} & q_{\underline{H},12}^{u} & \cdots & q_{\underline{H},1i}^{u} \\ q_{\underline{H},21}^{u} & q_{\underline{H},22}^{u} & \cdots & q_{\underline{H},2i}^{u} \\ \vdots & \vdots & \vdots & \vdots \\ q_{\underline{H},N1}^{u} & q_{\underline{H},N2}^{u} & \cdots & q_{\underline{H},Ni}^{u} \end{pmatrix}$$

The i^{th} row vector can be expressed as

$$\boldsymbol{w}_i = r_{\underline{H},ii}^{-1} \begin{pmatrix} q_{1i}^{u} \\ q_{2i}^{u} \\ \vdots \\ q_{Ni}^{u} \end{pmatrix}^{H}$$

The last equality comes from the fact that $\mathbf{R}_{\underline{H}}$ is an upper triangular matrix. The above equation can also be expressed as

$$\boldsymbol{w}_i = r_{\underline{H},ii}^{-1} \mathbf{q}_{\underline{H},i}^{u} \qquad \square$$

Now, the MSE in (5.20) can be rewritten as

$$\mathbb{E}\left| s(i) - \boldsymbol{w}_i \boldsymbol{y}_i \right|^2 = \left(\underline{\mathbf{H}}_i^{H} \, \underline{\mathbf{H}}_i^{H} \right)_{ii}^{-1} \tag{5-26}$$

Substituting the QR decomposition of $\underline{\mathbf{H}}_i$, we obtain

$$= \left(\begin{pmatrix} \mathbf{R}_{\underline{H}} \\ \mathbf{0}_{(M-i)\times i} \end{pmatrix}^H \mathbf{Q}_{\underline{H}}^H \mathbf{Q}_{\underline{H}} \begin{pmatrix} \mathbf{R}_{\underline{H}} \\ \mathbf{0}_{(M-i)\times i} \end{pmatrix} \right)^{-1}$$

$$= \left(\begin{pmatrix} \mathbf{R}_{\underline{H}} & \mathbf{0}_{(M-i)\times i} \end{pmatrix} \begin{pmatrix} \mathbf{R}_{\underline{H}} \\ \mathbf{0}_{(M-i)\times i} \end{pmatrix} \right)^{-1}$$

$$= r_{\underline{H},ii}^{-2} \tag{5-27}$$

Thus, by exploiting the QR decomposition of $\underline{\mathbf{H}}_i$ in (5.21), all of the MMSE estimator coefficients can be obtained by (5.25) and the MSE can be obtained by (5.27). This is more efficient than the direct computation in (5.19) and (5.20).

5.5.4 V-BLAST MMSE with GMD

In this Section, we first review the GMD scheme as introduced in [2]. It can be viewed as a V-BLAST scheme which consists of an optimal precoder derived from channel information and MMSE V-BLAST detector [11]. Figure 5-8 shows V-BLAST precoded system schematically. The optimal precoder is the linear precoder $\mathbf{P}$ as shown in the figure. The main purpose of this precoder is to force each symbol stream to have an identical MSE at the receiver. It can be viewed as alternative to the bit loading strategy. We call this precoder "Identical MSE (IMSE) precoder" throughout this chapter. From (5.27) it has been shown that the MSE is related to the diagonal elements of the matrix $\mathbf{R}$, obtained using QR decomposition in (5.21). Therefore, the IMSE precoder $\mathbf{P}$ can be designed such that the precoded channel $\mathbf{HP}$ has a corresponding upper triangular matrix with identical diagonal elements. The schematic diagram of the precoded V-BLAST MMSE systems is shown in Figure 5-8. The upper triangular matrix $\mathbf{R}$ with identical diagonal entries is employed to form identical eigenmodes over Wyner C-GCMAC for data transmission. This can be obtained by exploiting GMD.

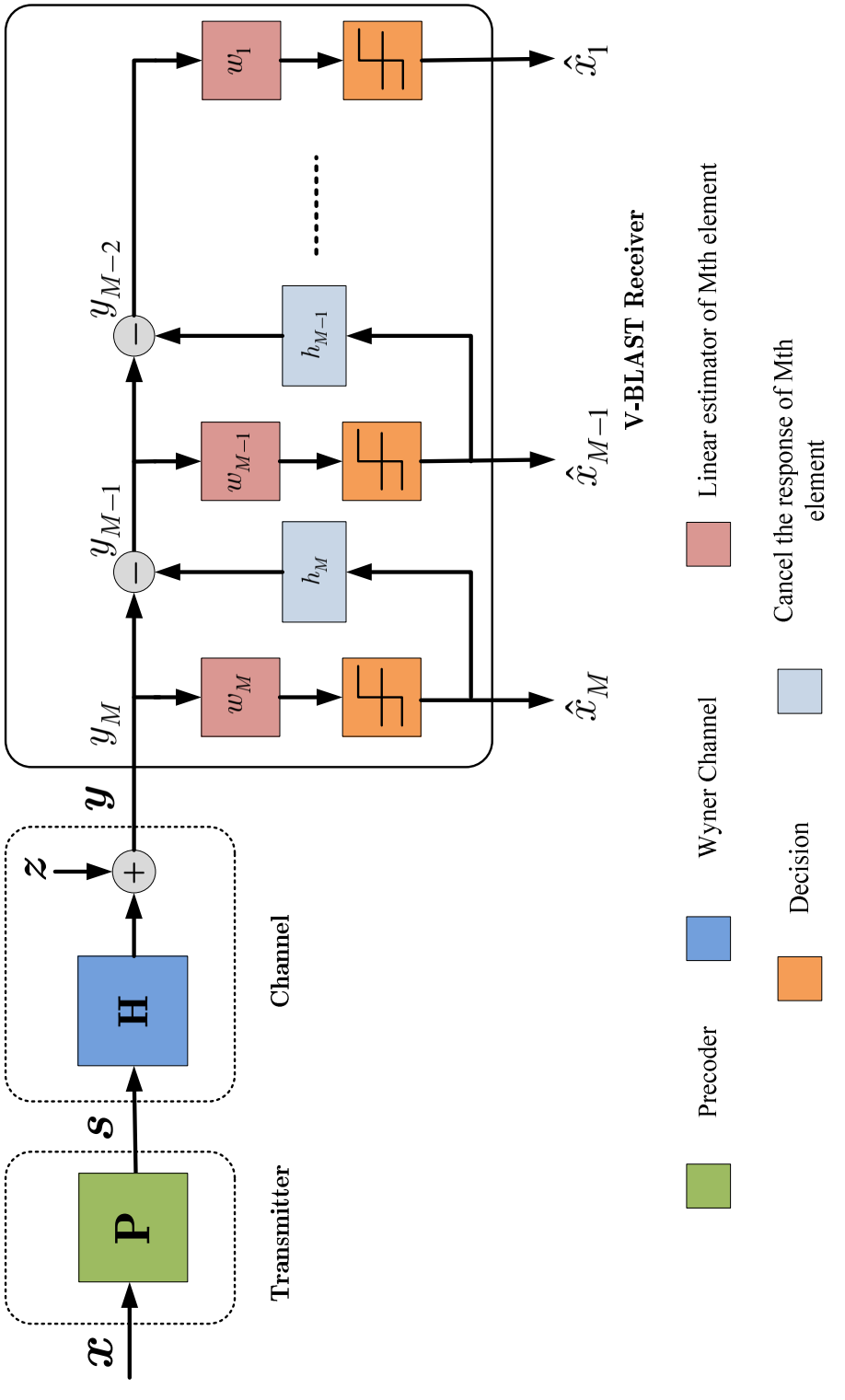

Figure 5-8 Schematic diagram of precoded GMD based V-BLAST systems.

The GMD algorithm is based on lemma 2.6.1, which states that any complex or real matrix $\mathbf{H} \in \mathbb{C}^{N \times M}$ can be decomposed as (2.11) as shown in Figure 2-5 [143]. The gains of each of the scalar sub-channels are given by (2.12) (geometric mean of the non-zero singular values of the channel matrix $\mathbf{H}$).

5.5.5 Precoded V-BLAST MMSE

We extend the GMD based detection with respect to the MMSE criterion for precoded channel. Let $\mathbf{P}$ be the precoder such that the precoded channel has a corresponding upper triangular matrix with identical diagonal elements. The equivalent eigenmode channel can be obtained as [2]

$$\tilde{\mathbf{Q}}_{\underline{H}}^{H} \mathbf{H}_{\underline{H}} \mathbf{P} = \tilde{\mathbf{R}}_{\underline{H}} \tag{5-28}$$

In order to find the QR decomposition of the precoded channel, we obtained the GMD of the augmented channel matrix as[9] [3]

$$\underline{\mathbf{H}}_{i} = \tilde{\mathbf{Q}}_{\underline{H}} \tilde{\mathbf{R}}_{\underline{H}} \mathbf{P}^{H} \tag{5-29}$$

where $\tilde{\mathbf{Q}}_{\underline{H}}$ and $\mathbf{P}^{H}$ are unitary matrices and $\tilde{\mathbf{R}}_{\underline{H}}$ is $M \times M$ upper triangular matrix with identical diagonal elements given by (2.12). We abuse the notation slightly for the sake of notational simplicity. The matrices $\tilde{\mathbf{Q}}$ and $\tilde{\mathbf{R}}$ given in (5.28) are not related to those given in (5.21). In matrix notation, the GMD of extended channel matrix $\underline{\mathbf{H}}$ may be expressed as [2]

[9] $\underline{\mathbf{H}}_{i}$ is the matrix with the first i columns of $\underline{\mathbf{H}}$.

$$\underbrace{\begin{pmatrix}\mathbf{H}\\ \sqrt{\alpha}\mathbf{I}_M\end{pmatrix}}_{(N+M)\times M} = \underbrace{\begin{pmatrix} \tilde{q}_{\underline{H},11} & \tilde{q}_{\underline{H},12} & \cdots & \tilde{q}_{\underline{H},NM} \\ \tilde{q}_{\underline{H},21} & \tilde{q}_{\underline{H},22} & \cdots & \tilde{q}_{\underline{H},NM} \\ \vdots & \vdots & \vdots & \vdots \\ \tilde{q}_{\underline{H},N1} & \tilde{q}_{\underline{H},N2} & \cdots & \tilde{q}_{\underline{H},NM} \\ \vdots & \vdots & \vdots & \vdots \\ \tilde{q}_{\underline{H},(N+M),1} & \tilde{q}_{\underline{H},(N+M),2} & \cdots & \tilde{q}_{\underline{H},(N+M),M} \end{pmatrix}}_{(N+M)\times M} \times \underbrace{\begin{pmatrix} \tilde{r}_{\underline{H},11} & \tilde{r}_{\underline{H},12} & \cdots & \tilde{r}_{\underline{H},1M} \\ 0 & \tilde{r}_{\underline{H},22} & \cdots & \tilde{r}_{\underline{H},2M} \\ \vdots & \ddots & \ddots & \vdots \\ 0 & \cdots & 0 & \tilde{r}_{\underline{H},MM} \end{pmatrix}}_{M\times M} \underbrace{\mathbf{P}^H}_{M\times M} \tag{5-30}$$

Let $\underline{\mathbf{H}}_P$ be the precoded channel matrix given as

$$\underline{\mathbf{H}}_P = \begin{pmatrix}\mathbf{HP}\\ \sqrt{\alpha}\,\mathbf{I}_M\end{pmatrix} \tag{5-31}$$

$$= \begin{pmatrix}\mathbf{I}_N & \mathbf{0}_{N\times M}\\ \mathbf{0}_{M\times N} & \mathbf{P}^H\end{pmatrix}\begin{pmatrix}\mathbf{H}\\ \sqrt{\alpha}\,\mathbf{I}_M\end{pmatrix}\mathbf{P} \tag{5-32}$$

Substituting the GMD of the extended channel matrix $\underline{\mathbf{H}}$, we have

$$= \begin{pmatrix}\mathbf{I}_N & \mathbf{0}_{N\times M}\\ \mathbf{0}_{M\times N} & \mathbf{P}^H\end{pmatrix}\tilde{\mathbf{Q}}_{\underline{H}}\,\tilde{\mathbf{R}}_{\underline{H}}\underbrace{\mathbf{P}^H\mathbf{P}}_{\mathbf{I}_M} \tag{5-33}$$

$$= \begin{pmatrix} \mathbf{I}_N & \mathbf{0}_{N\times M} \\ \mathbf{0}_{M\times N} & \mathbf{P}^H \end{pmatrix} \times$$

$$\underbrace{\begin{pmatrix} \tilde{q}_{\underline{H},11} & \tilde{q}_{\underline{H},12} & \cdots & \tilde{q}_{\underline{H},NM} \\ \tilde{q}_{\underline{H},21} & \tilde{q}_{\underline{H},22} & \cdots & \tilde{q}_{\underline{H},NM} \\ \vdots & \vdots & \vdots & \vdots \\ \tilde{q}_{\underline{H},N1} & \tilde{q}_{\underline{H},N2} & \cdots & \tilde{q}_{\underline{H},NM} \\ \vdots & \vdots & \vdots & \vdots \\ \tilde{q}_{\underline{H},(N+M),1} & \tilde{q}_{\underline{H},(N+M),2} & \cdots & \tilde{q}_{\underline{H},(N+M),M} \end{pmatrix}}_{(N+M)\times M} \underbrace{\begin{pmatrix} \tilde{r}_{\underline{H},11} & \tilde{r}_{\underline{H},12} & \cdots & \tilde{r}_{\underline{H},1M} \\ 0 & \tilde{r}_{\underline{H},22} & \cdots & \tilde{r}_{\underline{H},2M} \\ \vdots & \ddots & \ddots & \vdots \\ 0 & \cdots & 0 & \tilde{r}_{\underline{H},MM} \end{pmatrix}}_{M\times M}$$

(5-34)

Let us define unitary matrix

$$\underbrace{\mathbf{Q}_{\underline{H}_P} = \begin{pmatrix} \mathbf{I}_N & \mathbf{0}_{N\times M} \\ \mathbf{0}_{M\times N} & \mathbf{P}^H \end{pmatrix}}_{(N+M)\times(N+M)} \underbrace{\begin{pmatrix} \tilde{q}_{\underline{H},11} & \tilde{q}_{\underline{H},12} & \cdots & \tilde{q}_{\underline{H},NM} \\ \tilde{q}_{\underline{H},21} & \tilde{q}_{\underline{H},22} & \cdots & \tilde{q}_{\underline{H},NM} \\ \vdots & \vdots & \vdots & \vdots \\ \tilde{q}_{\underline{H},N1} & \tilde{q}_{\underline{H},N2} & \cdots & \tilde{q}_{\underline{H},NM} \\ \vdots & \vdots & \vdots & \vdots \\ \tilde{q}_{\underline{H},(N+M),1} & \tilde{q}_{\underline{H},(N+M),2} & \cdots & \tilde{q}_{\underline{H},(N+M),M} \end{pmatrix}}_{(N+M)\times M} \tag{5-35}$$

Thus, the QR representation of GMD of the $\underline{\mathbf{H}}_P$ can be expressed as

$$\underline{\mathbf{H}}_P = \tilde{\mathbf{Q}}_{\underline{H}_P} \tilde{\mathbf{R}}_{\underline{H}} \tag{5-36}$$

$$\underline{\mathbf{H}}_P = \underbrace{\begin{pmatrix} \tilde{q}_{\underline{H}_P,11} & \tilde{q}_{\underline{H}_P,12} & \cdots & \tilde{q}_{\underline{H}_P,NM} \\ \tilde{q}_{\underline{H}_P,21} & \tilde{q}_{\underline{H}_P,22} & \cdots & \tilde{q}_{\underline{H}_P,NM} \\ \vdots & \vdots & \vdots & \vdots \\ \tilde{q}_{\underline{H}_P,N1} & \tilde{q}_{\underline{H}_P,N2} & \cdots & \tilde{q}_{\underline{H}_P,NM} \\ \vdots & \vdots & \vdots & \vdots \\ \tilde{q}_{\underline{H}_P,(N+M),1} & \tilde{q}_{\underline{H}_P,(N+M),2} & \cdots & \tilde{q}_{\underline{H}_P,(N+M),M} \end{pmatrix}}_{(N+M)\times M} \underbrace{\begin{pmatrix} \tilde{r}_{\underline{H},11} & \tilde{r}_{\underline{H},12} & \cdots & \tilde{r}_{\underline{H},1M} \\ 0 & \tilde{r}_{\underline{H},22} & \cdots & \tilde{r}_{\underline{H},2M} \\ \vdots & \ddots & \ddots & \vdots \\ 0 & \cdots & 0 & \tilde{r}_{\underline{H},MM} \end{pmatrix}}_{M\times M} \tag{5-37}$$

Thus, the extended precoded channel matrix can be decomposed into QR matrices $\tilde{\mathbf{Q}}_{\underline{H}_P} \in \mathbb{C}^{(N+M)\times M}$ and $\tilde{\mathbf{R}}_{\underline{H}} \in \mathbb{C}^{M\times M}$. Again, if the unitary matrix $\tilde{\mathbf{Q}}_{\underline{H}_P}$ is partitioned into the $\tilde{\mathbf{Q}}^u_{\underline{H}_P} \in \mathbb{C}^{N\times M}$ and $\mathbf{Q}^l_{\underline{H}_P} \in \mathbb{C}^{M\times M}$ i.e. $\tilde{\mathbf{Q}}^u_{\underline{H}_P}$ denotes the first M columns of the unitary matrix $\tilde{\mathbf{Q}}_{\underline{H}_P}$. According to the Lemma 5.5.1, the nulling vector for i^{th} element can be expressed as [2]

$$\boldsymbol{w}_i = \tilde{r}^{-1}_{\underline{H},ii}\, \tilde{\mathbf{q}}^{u\ H}_{\underline{H}_P,i} \quad i = 1,2,\cdots,M. \tag{5-38}$$

where $\tilde{r}_{\underline{H},ii}$ is the i^{th} diagonal element of upper triangular matrix $\tilde{\mathbf{R}}_{\underline{H}}$ and $\tilde{\mathbf{q}}^u_{\underline{H}_P,i}$ is the i^{th} column of $\tilde{\mathbf{Q}}^u_{\underline{H}_P}$.

5.5.6 Identical MSE (IMSE)

The GMD ensures identical MSE (IMSE) for all i. Thus, by (5.25), with the above precoder, the MSE corresponding to the i^{th} element is given by [3]

$$\mathbb{E}\left|x(i) - \boldsymbol{w}_i \boldsymbol{y}_i\right|^2 = \tilde{r}^{-2}_{\underline{H},ii}$$

$$= \det\left(\mathbf{H}^H \mathbf{H} + \alpha \mathbf{I}_M\right)^{-(1/M)} \tag{5-39}$$

It is found that the IMSE is equal to the geometric mean of the MSEs of the original V-BLAST system.

Proof of (5.39):

The identical diagonal value of matrix $\tilde{\mathbf{R}}_{\underline{H}}$ can be expressed as

$$\tilde{r}_{\underline{H},ii} = \overline{\lambda} = \left(\prod_{i=1}^{M} \lambda_i\right)^{1/2M}$$

$$= \det\left(\mathbf{H}^H \mathbf{H} + \alpha \mathbf{I}_M\right)^{(1/2M)}$$

From (2.11), $r_{\underline{H},ii}$ is the diagonal value of matrix $\mathbf{R}_{\underline{H}}$. Therefore, $\tilde{r}_{\underline{H},ii}$ can also be expressed as

$$\tilde{r}_{\underline{H},ii} = \left(\prod_{i=1}^{M} r_{\underline{H},ii}\right)^{1/M}$$

the MSE corresponding to the i^{th} element is

$$\mathbb{E}\left|x(i) - \boldsymbol{w}_i \boldsymbol{y}_i\right|^2 = \left(\prod_{i=1}^{M} r_{\underline{H},ii}\right)^{(-2/M)}$$

subsequently, we can also show

$$= \det\left(\mathbf{H}^H \mathbf{H} + \alpha \mathbf{I}_M\right)^{-(1/M)}$$

this proved (5.39). □

5.5.7 Zero Forcing – Dirty Paper Coding (ZF-DPC) with GMD

With full base station cooperation, the downlink in CeMNets becomes effectively a MIMO broadcast channel. In a recent result [86], it is shown that the capacity region of broadcast channel can be obtained through dirty paper coding (DPC). Nevertheless, it is computationally intensive to determine the optimal DPC region and many suboptimal but more practical schemes have been explored [87] and [88]. The capacity of MIMO broadcast channels, however, is an open problem due to lack of a general theory on non-degraded broadcast channels. In a pioneering work by Shamai [127], a set of achievable rates (the achievable region) for MIMO broadcast channel was obtained by applying dirty paper results [80] at the transmitters or alternatively, coding for non-causal known interference. In [88], it was established that the dirty paper region of MIMO broadcast channel with power constraint P is exactly equal to the capacity region of MIMO MAC with sum power constraint P.

In the following Section, we consider MIMO broadcast channel where the role of transmitter and receiver is exchanged with N transmitting and M receiving antennas such that $M \geq N$. By exploiting intra-cell TDMA, only one MT is active in each cell i.e. $K = 1$ and therefore $N = M = L$. The channel is again modeled as (3.5). We also assume that the transmitter has perfect knowledge of channel matrix.

It is well known that the uplink-downlink duality is vital in converting the uplink solution to the downlink scenario. The uplink-downlink duality results [87], [88] will now be used to construct a DPC scheme that consumes the same power and achieves the same rate as a given MMSE-DFE scheme.

As a dual form of GMD V-BLAST, the GMD scheme can be implemented by exploiting DPC, which we refer to as GMD ZF-DPC. Therefore, we exploit the uplink-downlink duality to obtain ZF-DPC [87] and [88]. In the following, we outline the Zero Forcing – Dirty Paper Coding (ZF-DPC) scheme. The schematic diagram of ZF-DPC is shown in Figure 5-9. The ZF scheme is attractive because of its relative simplicity. The ZF-DPC scheme, although sub-optimal in general [78], [86] has been demonstrated to capture most of the benefit of BS cooperation and is

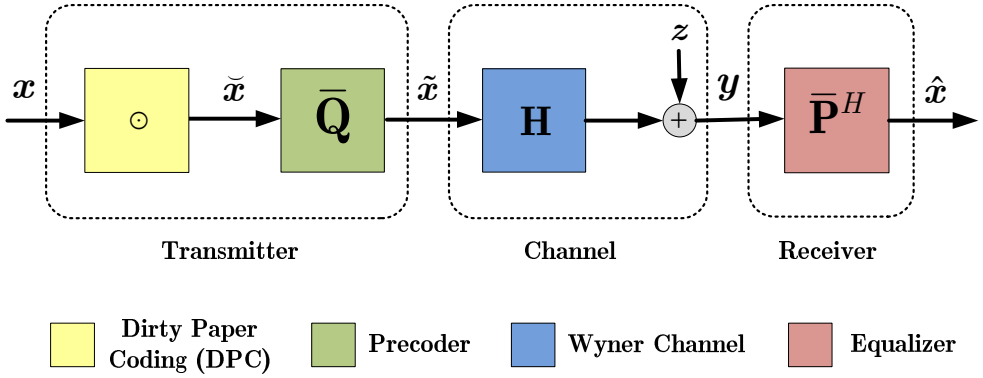

Figure 5-9: Block diagram of ZF-DPC transmission scheme.

close to optimal. We refer readers to [78], [86] for more details and references therein. We convert the ZF-DPC problem into V-BLAST problem in the reverse channel where the role of the transmitter and receiver are exchanged. The system may be model as [87]

$$\boldsymbol{y} = \mathbf{H}^H \tilde{\boldsymbol{x}} + \boldsymbol{z} \tag{5-40}$$

The GMD V-BLAST scheme can be applied to the above channel, which yields the precoding matrix $\bar{\mathbf{P}}$ and the equalizer matrix $\bar{\mathbf{Q}}$ respectively. Let $\boldsymbol{x}$ denote the data symbols which is passed into the dirty paper coder.

The GMD of $\mathbf{H}^H \in \mathbb{C}^{M\times N}$ which is expressed as [2]

$$\mathbf{H}^H = \bar{\mathbf{Q}}\bar{\mathbf{R}}\bar{\mathbf{P}}^H \tag{5-41}$$

where $\bar{\mathbf{Q}} \in \mathbb{C}^{M\times M}$ and $\bar{\mathbf{P}} \in \mathbb{C}^{N\times N}$ are unitary matrices and are regarded as the linear equalizer and linear precoder respectively in the reverse channel so that $\bar{\mathbf{R}} \in \mathbb{C}^{M\times N}$ is a triangular matrix with identical diagonal entries given by (2.12). According to the uplink-downlink duality, the linear precoder in the reverse channel can be employed as the linear equalizer in ZF-DPC scheme [87] and [88]. After the linear equalization at the receiver, the equivalent MIMO channel model over Wyner cellular setup can be expressed as

$$\hat{\boldsymbol{x}} = \bar{\mathbf{P}}^H \boldsymbol{y} \tag{5-42}$$

Substituting the received signal (5.40) in (5.42), we have

$$= \bar{\mathbf{P}}^H \mathbf{H}\, \tilde{\boldsymbol{x}} + \bar{\mathbf{P}}^H \boldsymbol{z} \tag{5-43}$$

Next, we encoded DP coder output $\breve{\boldsymbol{x}}$ via linear precoding matrix $\bar{\mathbf{Q}}$ and then transmitted through N transmitting antennas such that the transmitted vector $\tilde{\boldsymbol{x}} \in \mathbb{C}^{M\times 1}$ is given by

$$\tilde{\boldsymbol{x}} = \bar{\mathbf{Q}}\, \breve{\boldsymbol{x}} \tag{5-44}$$

$$\hat{\boldsymbol{x}} = \bar{\mathbf{P}}^H \bar{\mathbf{P}} \bar{\mathbf{R}}^H \bar{\mathbf{Q}}^H\ \bar{\mathbf{Q}}\, \breve{\boldsymbol{x}} + \bar{\mathbf{P}}^H \boldsymbol{z},$$

knowing $\bar{\mathbf{Q}}\bar{\mathbf{Q}}^H = \mathbf{I} \,\&\, \bar{\mathbf{P}}\bar{\mathbf{P}}^H = \mathbf{I}$, the estimated signal vector becomes

$$\hat{\boldsymbol{x}} = \bar{\mathbf{R}}^H \breve{\boldsymbol{x}} + \tilde{\boldsymbol{z}} \tag{5-45}$$

where $\tilde{\boldsymbol{z}}$ is the modified noise vector and $\bar{\mathbf{R}}^H$ is the lower triangular matrix. Also in component wise notation, (5.45) becomes [72]

$$\begin{pmatrix} \hat{x}_1 \\ \hat{x}_2 \\ \vdots \\ \hat{x}_N \end{pmatrix} = \begin{pmatrix} \bar{r}_{1,1} & \cdots & \cdots & \mathbf{0} \\ \bar{r}_{2,1} & \bar{r}_{2,2} & & \vdots \\ \vdots & \ddots & \ddots & \vdots \\ \bar{r}_{N,1} & \cdots & \cdots & \bar{r}_{N,N} \end{pmatrix} \begin{pmatrix} \breve{x}_1 \\ \breve{x}_2 \\ \vdots \\ \breve{x}_N \end{pmatrix} + \begin{pmatrix} \tilde{z}_1 \\ \tilde{z}_2 \\ \vdots \\ \tilde{z}_N \end{pmatrix} \tag{5-46}$$

Due to lower triangular structure of $\bar{\mathbf{R}}^H$, the i^{th} element of $\hat{\boldsymbol{x}}$ is given by

$$\hat{x}_i = \bar{r}_{i,i}\, \breve{x}_i + \sum_{j=1}^{i-1} r_{i,j}\, \breve{x}_j + \tilde{z}_i \tag{5-47}$$

For GMD, we know that $r_{ii} = \bar{\lambda}$ for $i = 1,2,\cdots,n,\cdots,N$. The precoder and equalizer are selected by exploiting GMD such that the equivalent channel matrix becomes a lower triangular matrix.

It is shown that the precoding matrix $\bar{\mathbf{Q}}$ and linear receiver $\bar{\mathbf{P}}$ matrix are designed such that the interference caused by the users $n > m$ is forced to zero. In addition, for each user m, there is a known non-causal interference given by $\sum_{j=1}^{i-1} \bar{r}_{i,j}\, \breve{x}_j$. By exploiting the successive DP coding approach, the transmitter can

mitigate the known interference in order to make its capacity the same as in the case where the interference is not present and the noise is at the same level [87], [88] and [127].

In order to find the solution to (5.46) let us define $\overline{\mathbf{R}}_{diag} \in \mathbb{R}^{N\times N}$ is a diagonal matrix with elements equal to the diagonal elements of $\overline{\mathbf{R}}$. Denote $\boldsymbol{x} \in \mathbb{C}^{N\times 1}$ as the data vector that contains the N symbols to be transmitted (zero mean, normalized and uncorrelated, that is, $\mathbb{E}[\boldsymbol{x}\boldsymbol{x}^H] = \mathbf{I}$ drawn from a set of constellations) for the N receivers (users). We wish to have $\breve{\boldsymbol{x}}$, satisfying [72]

$$\begin{pmatrix} r_{1,1}\, x_1 \\ r_{2,2}\, x_2 \\ \vdots \\ r_{N,N}\, x_N \end{pmatrix} = \begin{pmatrix} \overline{r}_{1,1} & \cdots & \cdots & \mathbf{0} \\ \overline{r}_{2,1} & \overline{r}_{2,2} & & \vdots \\ \vdots & \ddots & \ddots & \vdots \\ \overline{r}_{N,1} & \cdots & \cdots & \overline{r}_{N,N} \end{pmatrix} \begin{pmatrix} \breve{x}_1 \\ \breve{x}_2 \\ \vdots \\ \breve{x}_N \end{pmatrix} \tag{5-48}$$

.

The solution to (5.48) implies that

$$\breve{\boldsymbol{x}} = \overline{\mathbf{R}}^{-H}\, \overline{\mathbf{R}}_{diag}\, \boldsymbol{x} \tag{5-49}$$

However, the matrix inversion can significantly increase the norm of $\breve{\boldsymbol{x}}$ which can lead to additional power consumption at the transmitter. By exploiting the finite alphabet property of the communication signals, the Tomlinson Harashima Precoder (THP) can be applied to bound the value of transmitted signal [72].

5.5.8 Remarks to Transmission Design

Several remarks are now in order:

a) Using either the sequential detected signal cancellation or DPC, we can cancel the interference due to the off diagonal entries of $\mathbf{R}$ and obtain $N = M = L$ identical scalar sub-channels, given by

$$\hat{x}_i = \overline{\lambda}_{ii}\, x_i + \tilde{z}_i \qquad i = 1, 2, \cdots, L \tag{5-50}$$

b) V-BLAST is shown to be able to achieve only about 72% of the capacity [76]. That is because imposing the same rate of transmission on all the transmitters limits the channel capacity to the worst of the L scalar sub-channels.

c) ZF-DPC can achieve broadcast channel capacity for high SNR [78], but the sub-channels have different fading levels. Hence the transmitter, as the aforementioned linear transceiver, has to consider the tradeoffs between the BER performance and the capacity throughput.

d) As the practical implementation of the DPC, the Tomlinson-Harashima Precoder (THP) [81] and [82] can be used to achieve known interference cancellation at the transmitter. This leads to input power increase of $M/(M-1)$ for *M*-QAM symbols. Nevertheless, for a system with high dimensionality and/or using large constellation, the ZF-DPC is a better choice than the V-BLAST since it is free of propagation error. The same is investigated in the simulation Section 5.6.1.

e) Both ZF-DPC and V-BLAST transmission schemes involve non-linear operations.

5.6 Simulation Results and Discussions

Consider a circular variant of the infinite linear Wyner model depicted in Figure 5-1, in which N cells with K users in each cell are arranged on a circle. Assuming a synchronous intra-cell TDMA scheme, according to which only one user is selected for transmission per-cell. The channel is modelled as described in Section 3.6 (3.5) where $\mathbf{\Omega} \in \mathbb{R}^{N \times M}$ such that $0 < \Omega_{ij} \leq 1$ are the inter-cell interference factor, representing the geometrical path losses. In addition, $\mathbf{G} \in \mathbb{C}^{N \times M}$ such that $g_{ij} \in \mathbb{C}\,\mathcal{N}(0,1)$ are the independent flat fading coefficients of the signals transmitted by the transmitter $(j-1)^{\text{th}}$, j^{th} and $(j+1)^{\text{th}}$, and received by the j^{th} receiver. However, the structure of $\mathbf{G}$ may be uncorrelated, correlated and semi-correlated. In all simulation scenarios, ergodic block fading processes are assumed where the fade values remain constant during the TDMA slot duration. Each of the $M = NK$ users, perfectly measures its own fade coefficients, which are fed back to the multi-cell transmitter via an ideal delay less feedback channel.

In order to discuss the performance of Hadamard Wyner channel, the BER curves are obtained over uncorrelated fading channel. In this Section, we present the numerical analysis of uncorrelated channel based on BER curves obtained after various simulation scenarios. In each case the curves are obtained after averaging 10,000 Monte Carlo trials of the resultant Hadamard channel $\mathbf{H}$. We simulate the transmission over Rayleigh fading Hadamard channel based on GMD V-BLAST and GMD ZF-DPC with $N = M = 6$ transmitting and receiving antennas. We simulate the transmission for *M* independent symbols, modulated as 16 - quadrature amplitude modulation (16-QAM) and as 64 - quadrature amplitude modulation (64-QAM).

5.6.1 BER Comparison over Uncorrelated Scenario

In this Section, the analysis is based on Wyner's channel model when users are offering equal inter-cell interference. The BER curves for both transmission designs with different constellations are shown in Figure 5-10a and Figure 5-11a. Figure 5-10a shows the BER curves obtained when $\Omega = 0.1$ for 16-QAM and 64-QAM. The red curves shows the BER over V-BLAST MMSE and green curves shows ZF-DPC. In each of the transmission designs, GMD is employed to form parallel identical and independent pipes for data transmission. The BER performance of GMD ZF-DPC outperforms the GMD V-BLAST MMSE decoder significantly at higher SNRs. Moreover, the BER curves of ZF-DPC scheme falls off much faster as compared with the V-BLAST MMSE decoder, which means that the diversity gain offered by DPC scheme is much better than conventional V-BLAST technique. To present a benchmark, we also compare the BER curves with GMD genie which is an imaginary scenario, where at each layer; a genie would eliminate the influence of erroneous detection from the previous layers when using GMD V-BLAST MMSE.

Figure 5-10a clearly shows that the V-BLAST MMSE may suffer from small degradation in BER due to error propagation as compared with imaginary scenario GMD genie. The GMD ZF-DPC, on the contrary, is free of error propagation and hence, has an improved BER performance as compared with V-BLAST MMSE and also very close to the benchmark performance, GMD genie. The small degradation of ZF-DPC as compared with GMD genie is mainly due to the inherent power amplification effect of the Tomlinson Harashima precoder [81], [82].

It is clearly shown that the BER performance of V-BLAST MMSE is also degraded as compared with ZF-DPC with 64-QAM. It is also noted that the performance degradation is more as in comparison with degradation in 16-QAM due to the fact that the error propagation effect is pronounced with higher constellation sizes. It is also observed that performance degrades with the increase in constellation sizes. It is due to the fact that the smaller constellations offers better diversity as compare with higher constellation seizes. The same has been shown in Figure 5-10a. In order to analyze the BER degradation in V-BLAST MMSE as compared with ZF-

DPC, we define a measure, referred to as BER Relative Reduction Ratio (R^3) $\left(\zeta\right)$ as follows: If p_e denotes the BER, then the BER R^3 between the two transmission schemes V-BLAST and ZF-DPC may be expressed as $\zeta = \left(p_{e_{VBLAST}} - p_{e_{ZF-DPC}}\right) / p_{e_{VBLAST}}$. The relative measured curves for both constellations are shown in Figure 5-10b. It is shown that at lower SNRs V-BLAST MMSE outperforms the ZF-DPC scheme due to the fact that at lower SNR the effect of noise is pronounced which leads to a slight rise in BER curve at lower SNR. It is observed that the BER performance of ZF-DPC outperforms after $\gamma \approx 15\,\text{dB}$, as compared with V-BLAST MMSE. The degradation in BER when V-BLAST MMSE is employed is due to error propagation effect in the transmission. The BER R^3 at 25 dB is 18% and at 40 dB it has reached the value of 82 %. It is observed that the BER performance of ZF-DPC with 64-QM starts improving after 20 dB. The BER R^3 at 25 dB is 33.5% and at 40 dB it has reached the value of 95.5 %. Hence, the relative improvement in ZF-DPC is significant in case of 64-QAM.

Figure 5-11a shows the BER curves obtained when $\Omega = 0.5$ (medium level of inter-cell interference) with 16-QAM and 64-QAM. The red curves shows the BER over V-BLAST MMSE and green curves shows ZF-DPC. It is observed that with the increase in inter-cell interference, the BER performance of the transmission schemes is improved. The inter-cell interference is an important factor in Wyner channel model. The effect of inter-cell interference on the BER of these transmission schemes is analyzed in the next sub-Section. Figure 5-11b shows BER R^3 when $\Omega = 0.5$. At low range of SNRs, the V-BLAST MMSE outperforms ZF-DPC and on the contrary, ZF-DPC has superior performance at higher range of SNRs. The impact of inter-cell interference is dominant at higher range of SNRs. The BER R^3 of ZF-DPC with reference to V-BLAST is summarized in Table 5-2. The performance of transmission schemes is improved with the increase in inter-cell interference over uncorrelated channel. It can be seen that the performance of V-BLAST outperforms the performance of ZF-DPC at low levels of SNR, however, the performance of ZF-DPC improves as compared to V-BLAST at high levels of SNR.

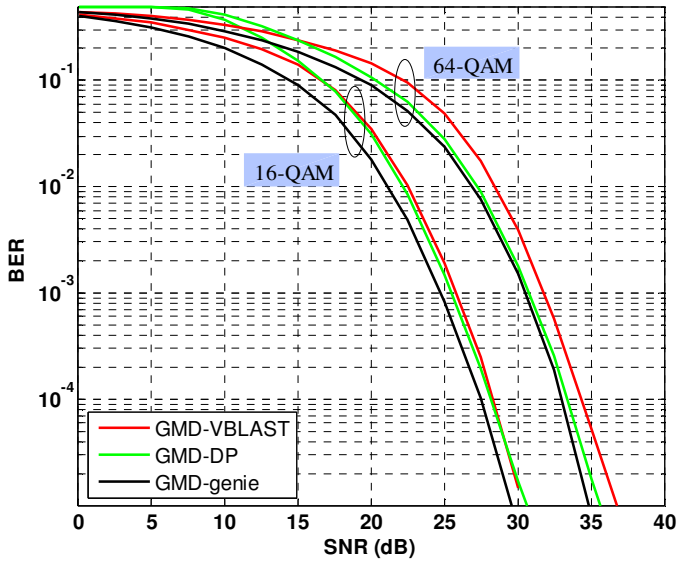

(a)

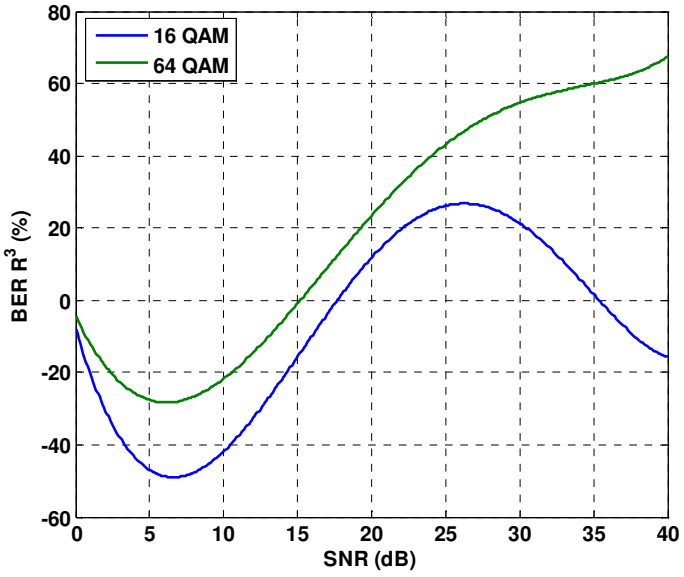

(b)

Figure 5-10: Summary of BER analysis using V-BLAST-GMD and ZF-DPC-GMD over Uncorrelated Wyner C-GCMAC; $\Omega_{j+1} = \Omega_{j-1} = 0.1$ and $K = 1$: (a) BER curves with 16-QAM and 64-QAM; (b) Improvement in BER as a measure of BER Relative Reduction Ratio (R^3).

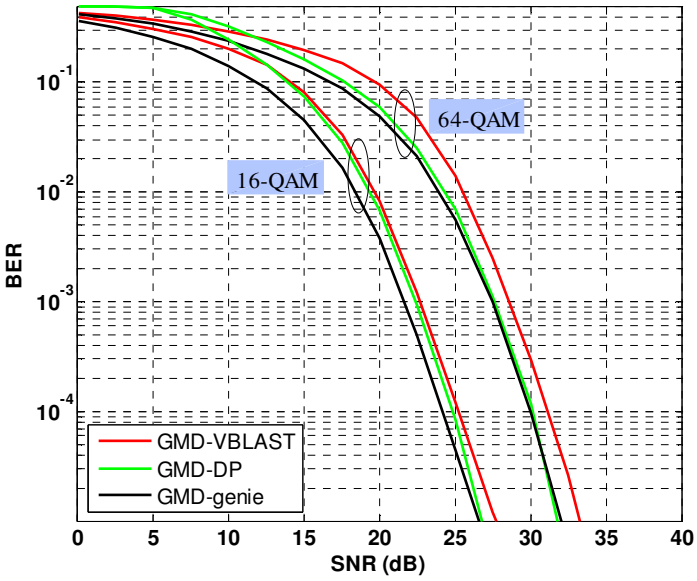

(a)

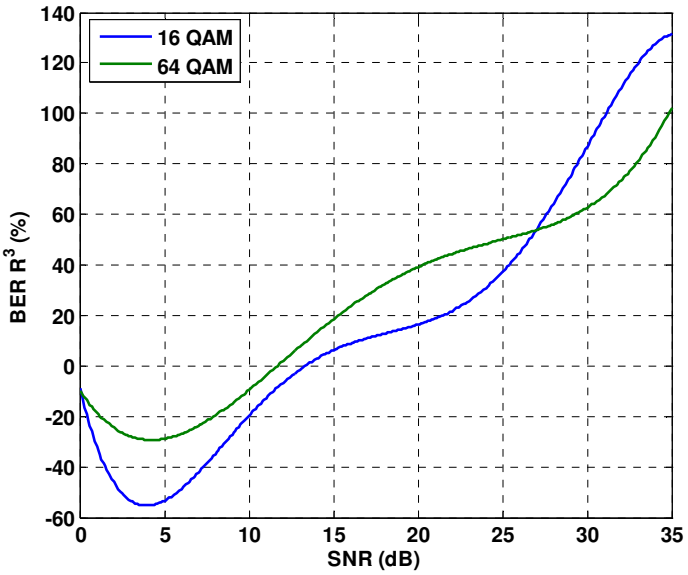

(b)

Figure 5-11: Summary of BER analysis using V-BLAST-GMD and ZF-DPC-GMD over Uncorrelated Wyner C-GCMAC; $\Omega_{j+1} = \Omega_{j-1} = 0.5$ and $K = 1$: (a) BER curves with 16-QAM and 64-QAM; (b) Improvement in BER as a measure of BER Relative Reduction Ratio (R^3).

Table 5-2: Summary of performance of ZF-DPC and V-BLAST interms of BER R[3]

S. No.	γ (dB)	(ζ) at $\Omega = 0.1$ (%)		(ζ) at $\Omega = 0.5$ (%)	
		16-QAM	64-QAM	16-QAM	64-QAM
1.	5	-50	-28	-55	-28
2.	20	10	41	20	50
3.	35	0	60	130	100

5.6.2 Impact of Inter-Cell Interference on BER Performance of Uncorrelated Channel[10]

In this sub-Section, we present the impact of inter-cell interference on the BER performance of transmission schemes. In order to incorporate the realistic empirical channel mode into Wyner channel model, it is very important to find BER performance over the range of inter-cell interference $\Omega \in (0,1)$. Figure 5-12 and Figure 5-13 shows the BER confidence on inter-cell interference for 16-QAM and 64-QAM respectively. The BER solid lines show V-BLAST MMSE and BER dotted lines show ZF-DPC scheme. It has been shown that the BER performance of V-BLAST MMSE and ZF-DPC schemes is improved with the increase in channel slow gain at both 16-QAM and 64-QAM. However, the superior BER performance offered by ZF-DPC as compared to V-BLAST MMSE is due to no propagation in former transmission scheme at higher SNRs. It is observed that the BER performance of the ZF-DPC doesn't improve beyond the performance offered by V-BLAST MMSE until $\Omega \approx 0.7$ for 16-QAM. Similarly, this threshold reduces to $\Omega \approx 0.5$ when 64-QAM is employed for data transmission. The same effect is shown in Figure 5-12b and Figure 5-13b for the uncorrelated Wyner cellular model.

[10] Independently and identically distributed (i.i.d) complex Gaussian channel entries (with variance of each entry one) are assumed in the case of uncorrelated Rayleigh fading channel.

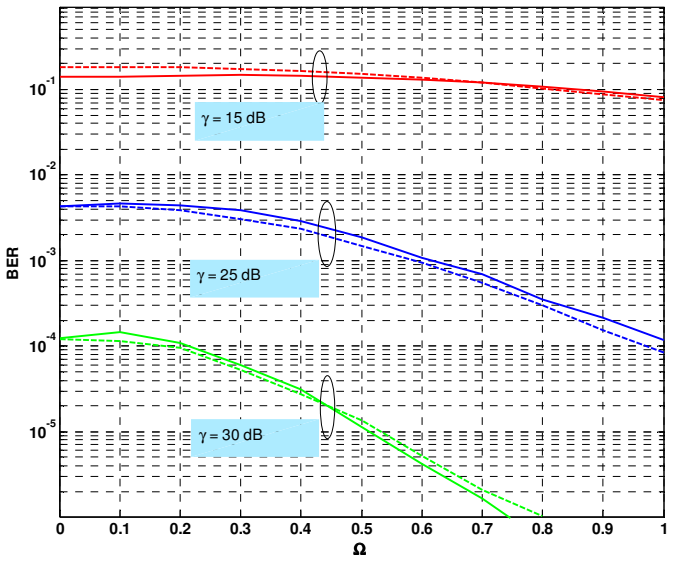

(a)

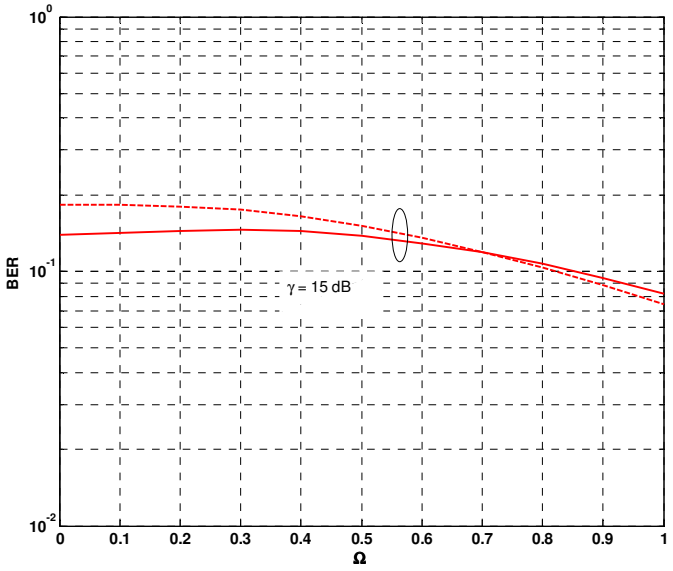

(b)

Figure 5-12: Summary Comparison of BER variation over C-GCMAC with $N = 6$, $K = 1$ and 16-QAM: Solid lines shows V-BLAST MMSE and dotted lines shows DPZF transmission schemes. (a) variation over range of SNRs; (b) a close-up of BER variation over low SNR, showing the threshold interference level $\Omega \simeq 0.7$ after which BER offered by ZF-DPC starts improving.

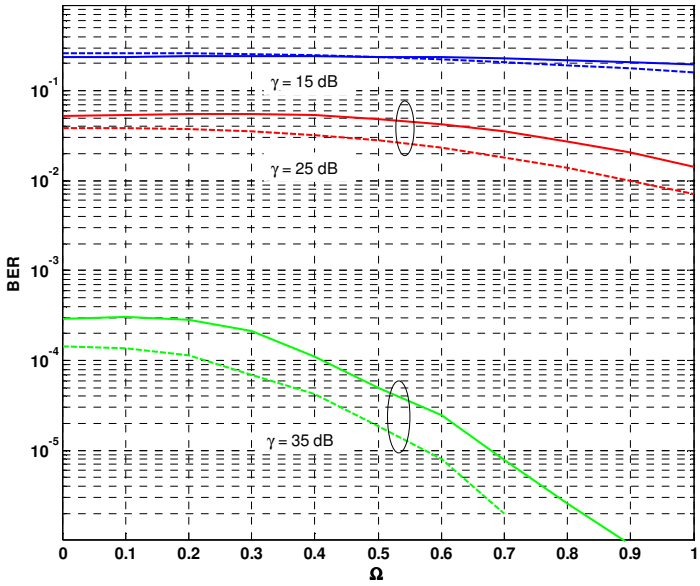

(a)

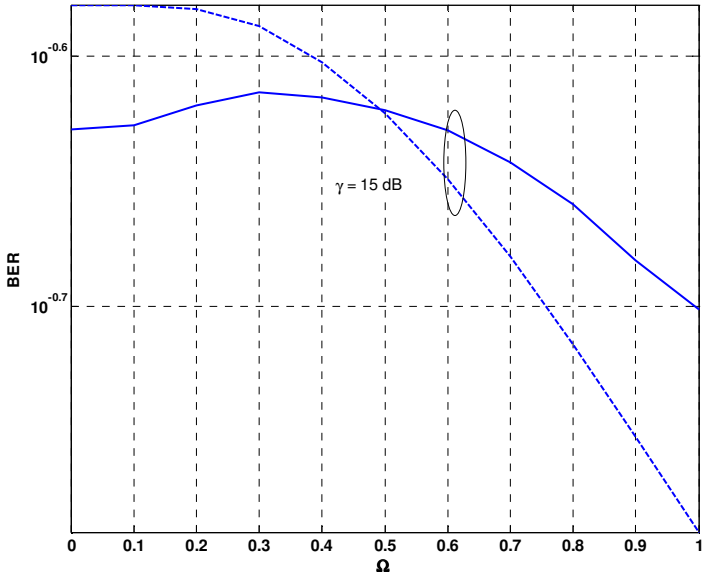

(b)

Figure 5-13: Summary Comparison of BER variation over C-GCMAC with $N = 6$, $K = 1$ and 64-QAM: Solid lines shows V-BLAST MMSE and dotted lines shows DPZF transmission schemes. (a) variation over range of SNRs; (b) close-up of BER variation over low SNR, showing the threshold interference level $\Omega \simeq 0.5$ after which BER offered by ZF-DPC starts improving.

5.6.3 Contribution of Variable Inter-Cell interference on BER Performance

In this Section, we investigate the impact of varying the inter-cell interference on the BER performance of V-BLAST MMSE and ZF-DPC. Figure 5-14a and Figure 5-14b shows the BER curves obtained for V-BLAST MMSE and ZF-DPC respectively over Wyner uncorrelated channel, when both interfering MTs are located in zone #1. The solid line shows BER, when both interfering MTs are offering equal level of interference i.e. $\Omega = 0.7$; and dashed line shows BER, when MTs are still located in zone #1 and offering variable level of interference. As an example, consider a scenario, when MT T_{j+1} (MTs on the right side of every BS) offering interference level $\Omega = 0.7$ and MT T_{j-1} (MTs on the left side of every BS) offering interference level $\Omega = 0.9$ i.e. the MTs are located in close vicinity of the BSs. It is observed that the BER starts improving, when inter-cell interference is variable intra-zone as compared with BER when MTs offering equal level of interference. However, the significant improvement is expected when the level of interference varies inter-zones.

Figure 5-15a and Figure 5-15b shows the BER curves obtained for V-BLAST MMSE and ZF-DPC Wyner uncorrelated channel, when at least one of the inter-cell interfering MTs is offering medium level of interference i.e. they are located in zone #2. It observed that the BER performance over both transmission schemes with variable inter-cell interference outperforms the BER performance when MTs are offering equal level of interference. However, the improvement is significant when the variation in inter-cell interference level is inter-zones. As an example, consider the scenarios as shown in Figure 5-15, when inter-cell interference level of MT T_{j+1} is fixed at $\Omega = 0.3$ and of MT T_{j-1} varies inter-zones and intra-zone. The BER performance when MT T_{j-1} is offering high level interference $\Omega = 0.9$ i.e. MT is located in zone #1 is significantly improved as compare to the BER performance when T_{j-1} is offering intra-zone variable interference level, (compare

dashed lines – T_{j-1} in zone #1; T_{j+1} in zone #2 with dotted lines - T_{j-1} in zone #2 with high level of interference as compare with other MT; T_{j+1} in zone #2 and solid lines - T_{j-1}; T_{j+1} in zone #2).

Figure 5-16a and Figure 5-16b shows the BER curves obtained for V-BLAST MMSE and ZF-DPC, when at least one of the inter-cell interfering MT is offering low level of interference and located in zone #3. As shown in figure, when inter-cell interfering level of MT T_{j-1} is increased from low to medium and from low to high, the BER of the transmission schemes is improved. However, the BER performance is compromising in comparison with BER curves in Figure 5-14 and Figure 5-15 as BER degrades with the decrease in inter-cell interference level (channel slow gain).

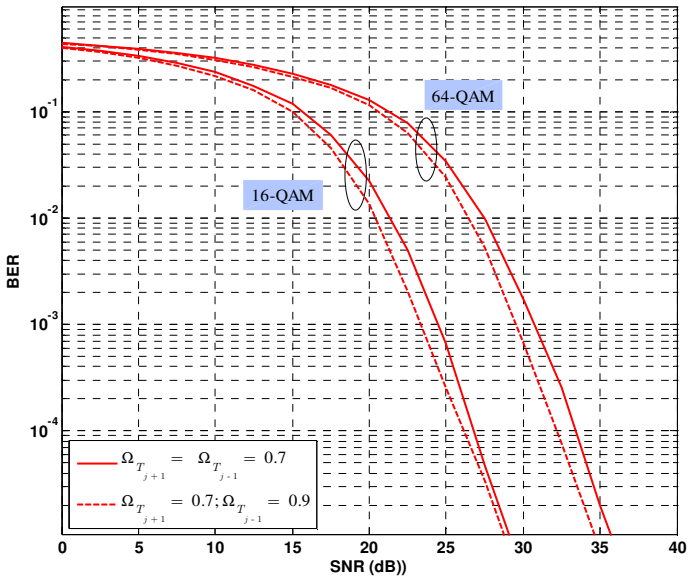

(a) V-BLAST MMSE

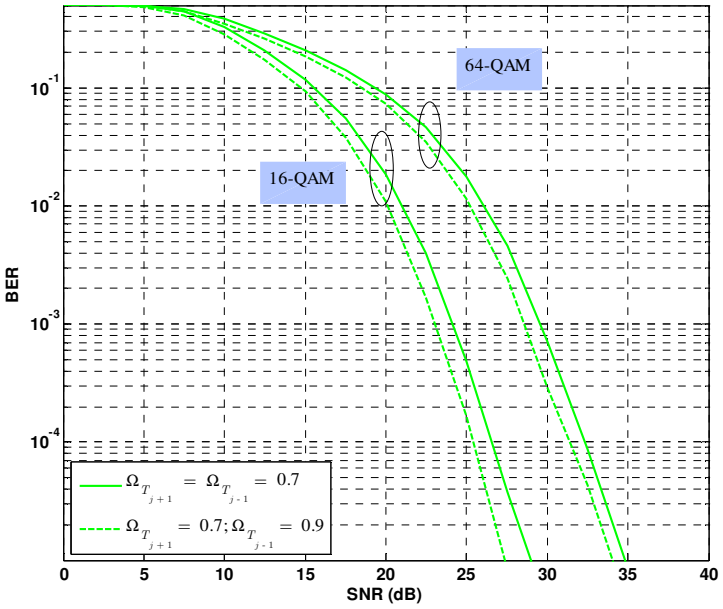

(b) ZF-DPC

Figure 5-14: Improvement in BER by exploiting the inter-cell interference in each of the adjacent cells separately with $K = 1$ (two interfering MTs), $N = 6$: Solid lines shows when MTs T_{j+1} and T_{j-1} are located in zone #1 and offering equal level of interference; dashed lines shows when MTs are still located zone #1 and offering variable level of interference to the BS of interest.

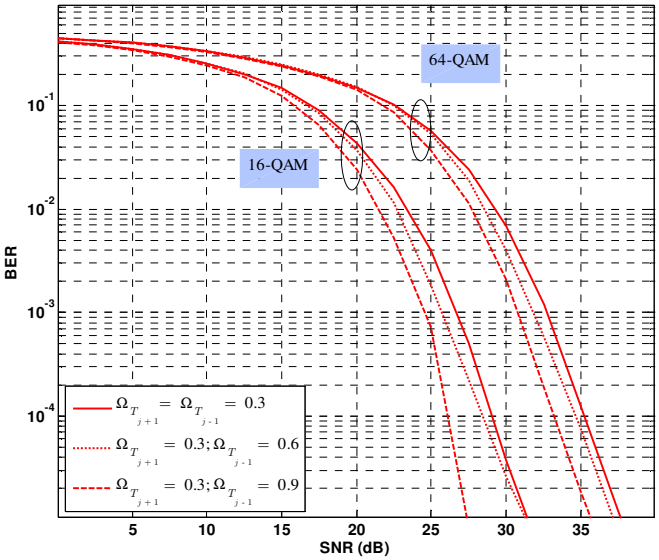

(a) V-BLAST MMSE

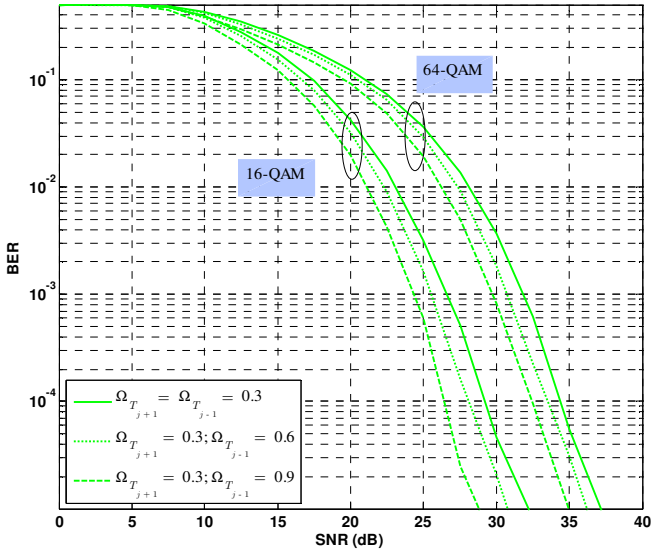

(b) ZF-DPC

Figure 5-15: Improvement in BER by exploiting the inter-cell interference in each of the adjacent cells separately with $K = 1$ (two interfering MTs), $N = 6$: Solid lines shows when MTs T_{j+1} and T_{j-1} are located in zone #2 and offering equal level of interference; dotted lines shows when MTs are still located zone #2 and offering variable level of interference to the BS of interest; dashed lines shows when MT T_{j+1} are located in zone #2 and MTs T_{j-1} are located in zone #1.

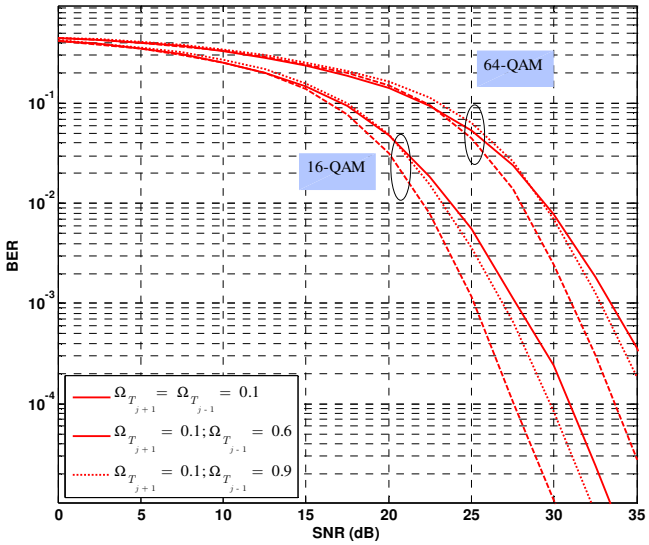

(a) V-BLAST MMSE

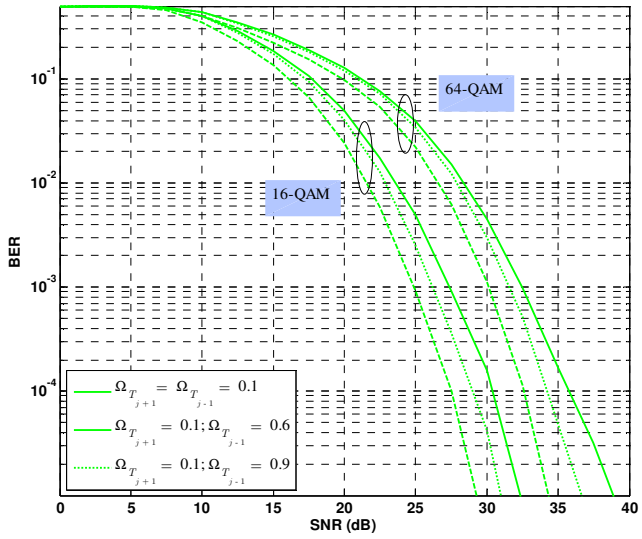

(b) ZF-DPC

Figure 5-16: Improvement in BER by exploiting the inter-cell interference in each of the adjacent cells separately with $K = 1$ (two interfering MTs), $N = 6$: Solid lines shows when MTs T_{j+1} and T_{j-1} are located in zone #3 and offering equal level of interference; dotted lines shows when MTs T_{j+1} are located zone #3 and T_{j-1} are located in zone #2; dashed lines shows when MT T_{j+1} are located in zone #3 and MTs T_{j-1} are located in zone #1.

5.6.4 BER Comparison over Correlated Scenario

In this Section, we compare the performance of V-BLAST MMSE and ZF-DPC over the correlated Wyner Hadamard channel based on BER curves obtained after various simulation scenarios. Figure 5-17, Figure 5-18 and Figure 5-19 presents the scenarios when the inter-cell interference between the transmitter and the receiver is of low level, medium level and high level respectively. In each scenario, the curves are obtained after averaging 10,000 Monte Carlo trials of the resultant correlated Wyner Hadamard channel $\mathbf{H}$. The transmission is designed by exploiting GMD with V-BLAST MMSE and ZF-DPC. The BER curves obtained over correlated scenario are compared with BER curves obtained over uncorrelated fading channel. Figure 5-17 shows the scenario when both inter-cell interfering transmitters are offering low level of interference i.e. they are located in zone #3 $\left(\Omega = 0.2\right)$; Figure 5-18 shows the scenario when both inter-cell interfering transmitters are offering medium level of interference i.e. they are located in zone #2 $\left(\Omega = 0.4\right)$; and Figure 5-19 shows the scenario when both inter-cell interfering transmitters are offering high level of interference i.e. they are located in zone #1 $\left(\Omega = 0.9\right)$. At this point in this Section, we exploit the interference levels to compare the performance of two types of correlated channels with uncorrelated channel in each cell of Wyner cellular setup across each zone[11]. However, the impact of $\Omega \in \left(0,1\right)$ i.e. over entire range of interference levels is presented in the next sub-Section 5.6.8.

A. **zone #3**

Figure 5-17a and Figure 5-17b shows the BER curves offered by V-BLAST MMSE and ZF-DPC transmission schemes when both inter-cell interfering transmitters are offering low level of interference with 16-QAM. The transmission is designed by exploiting V-BLAST MMSE and ZF-DPC in combination with GMD over uncorrelated and correlated Wyner channel. The correlated channels are

[11] Recall from Chapter 3 that entire cell in C-GCMAC is spitted into three zones. The details of cell splitting are summarized in Table 3-2.

modelled as defined in Section 5.3 and Section 5.4. It is observed that the BER performance of Hadamard correlated fading channel and Hadamard Permuted channel is approximately identical. The performance is compared with the performance curves obtained over uncorrelated channel. From Figure 5-17a and Figure 5-17b, it is found that the performance of correlated and uncorrelated channels are approximately equivalent. When the inter-cell interference between the transmitters and the receivers is low i.e. the transmitters are locaters in zone #3, the receiver is still able to decode the transmitted symbols independently.

B. zone #2

Figure 5-18a and Figure 5-18b shows the scenario when both inter-cell interfering transmitters are offering medium level of interference i.e. they are located in zone #2$(\Omega = 0.4)$; The BER offered by V-BLAST MMSE and ZF-DPC transmission schemes shows that the performance of uncorrelated channel is superior as compare with correlated channel, when both inter-cell transmitters are offering medium level of inter-cell interference. The degraded BER performance over correlated channel is due to the fact that the possibility of recovering the transmitted symbols correctly is lower as compare to the previous correlated scenario where at low level of interference the, the receiver is still able to decode the transmitted data independently over correlated channel and the performance of both correlated and uncorrelated channel is almost identical.

C. zone #1

Figure 5-19a and Figure 5-19b shows the scenario when both inter-cell interfering transmitters are offering high level of interference i.e. they are located in zone #1 $(\Omega = 0.9)$; It has been shown that the relative BER performance of the correlated channels is compromised with respect to BER performance of uncorrelated channel due to the fact that the correlation between the transmission links is pronounced, when inter-cell interference level is high (both transmitters are located in zone #1 and offering high channel slow gain). Furthermore, the BER performance of Rayleigh faded uncorrelated channel is superior and shows improved diversity as compared with respect to the previous scenarios. Therefore, it is

concluded that the BER performance of uncorrelated channel is improved with an increase in channel slow gain; On the contrary, the BER performance of correlated channels is degraded with the increase in channel slow gain. It can be seen from the eigenvalue analysis that at high level of inter-cell interference (channel slow gain), there are effective numbers of distinct paths between the transmission links in case of uncorrelated Rayleigh channel. Moreover, there is a higher possibility of recovering the transmitted data streams independently, when the channel is fully uncorrelated.

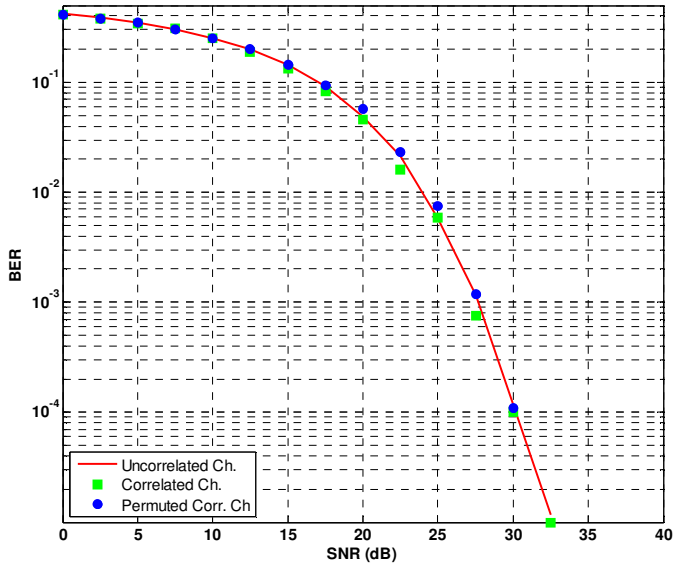

(a) V-BLAST MMSE

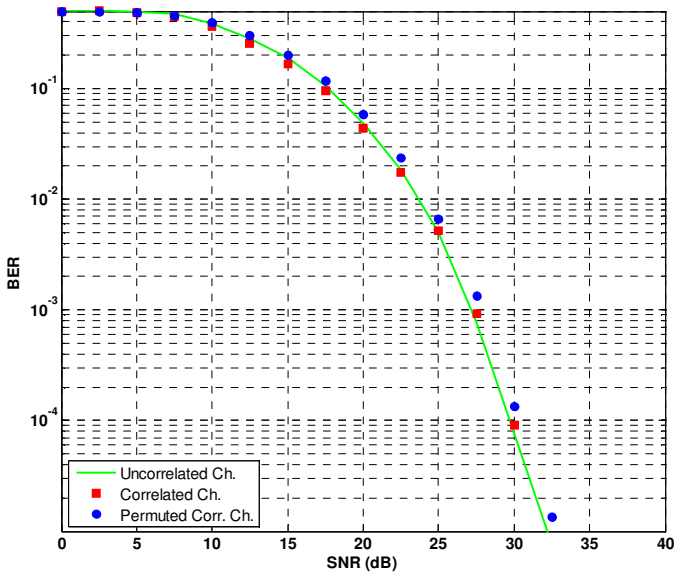

(b) ZF-DPC

Figure 5-17: Comparison of BER over Uncorrelated and Correlated Wyner structures, with $K = 1,\ N = 6$ and $\Omega = 0.2$ (i.e. both MTs are located in zone #3 and offering low level of interference) and 16-QAM.

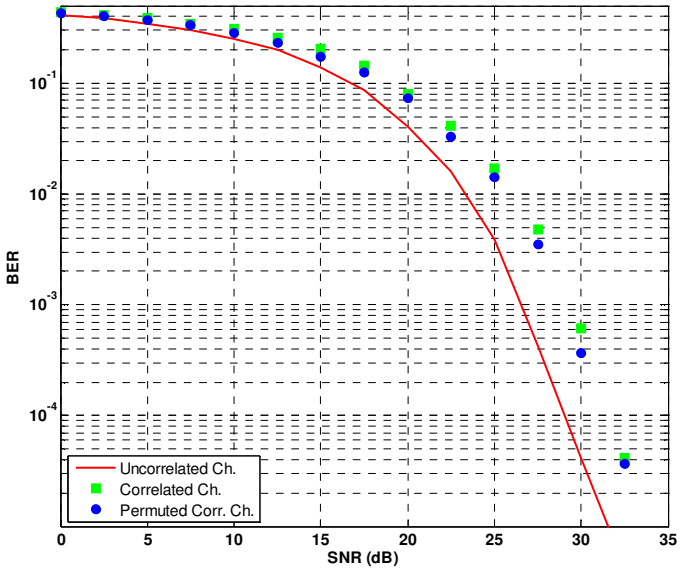

(a) V-BLAST MMSE

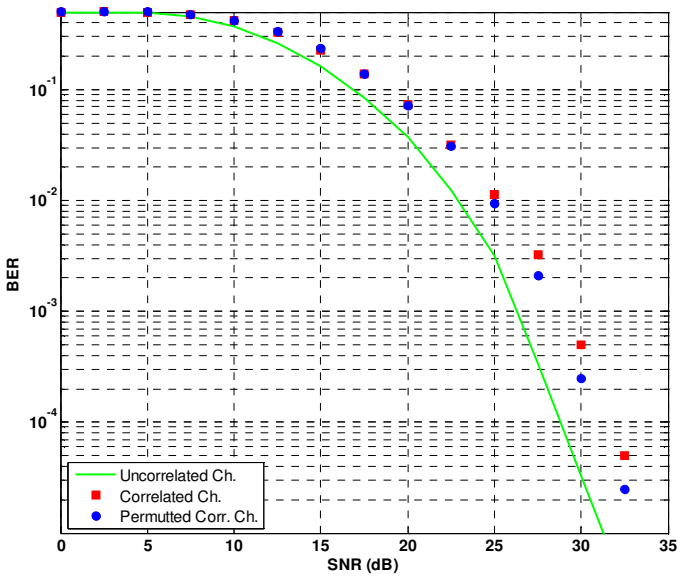

(b) ZF-DPC

Figure 5-18: Comparison of BER over Uncorrelated and Correlated Wyner structures, with $K = 1$, $N = 6$ and $\Omega = 0.4$ (i.e. both MTs are located in zone #2 and offering medium level of interference) and 16-QAM.

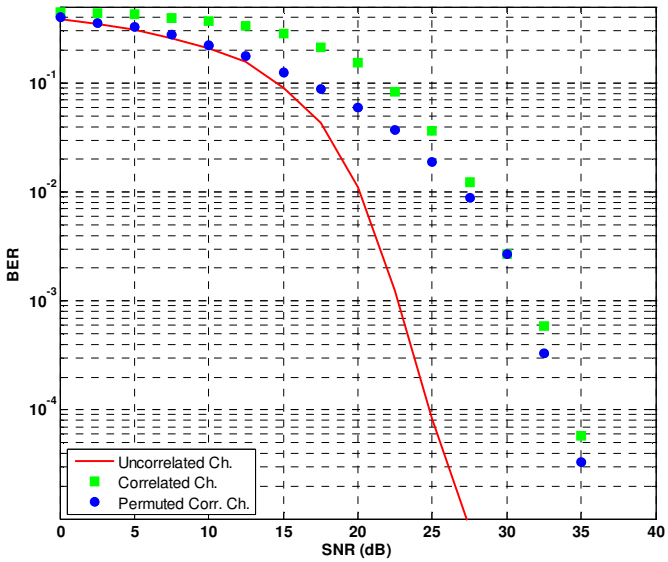

(a) V-BLAST MMSE

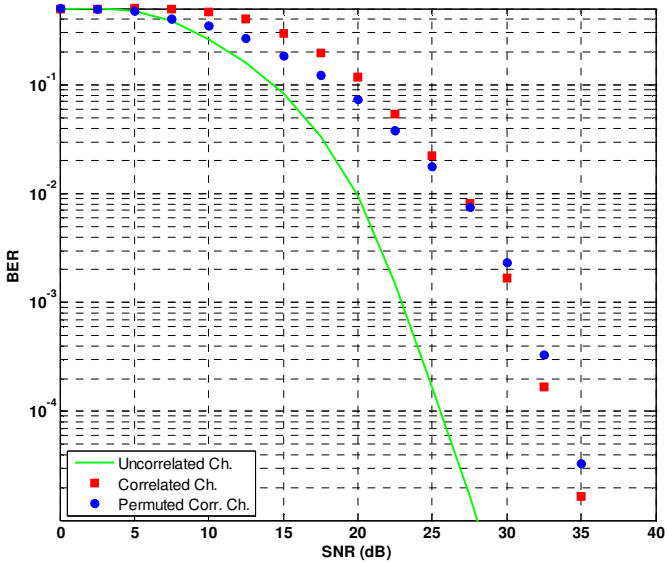

(b) ZF-DPC

Figure 5-19: Comparison of BER over Uncorrelated and Correlated Wyner structures, with $K = 1$, $N = 6$ and $\Omega = 0.9$ (i.e. both MTs are located in zone #1 and offering high level of interference) and 16-QAM.

5.6.5 Impact of Inter-Cell Interference on BER Performance of Correlated Channel

Figure 5-20a and Figure 5-20b shows the performance of V-BLAST MMSE and ZF-DPC over the entire range of $\Omega \in (0,1)$ with 16-QAM and 64-QAM respectively. The BER performance is degraded with the increase in inter-cell interference over correlated channels. As suspected, it is shown that BER performance of both transmission schemes over uncorrelated channel is superior as compared with the performance over correlated channel. The BER over uncorrelated channel decreases with the increase in inter-cell interference (see Figure 5-12 and Figure 5-13). It is observed that the performance of ZF-DPC outperforms the performance of V-BLAST MMSE significantly at higher SNR over correlated channel (see green curves in Figure 5-20a and Figure 5-20b).

Moreover, significant degradation in BER performance of V-BLAST MMSE and ZF-DPC over correlated channels is observed when the inter-cell interference level over the transmission link is $\Omega = 0.5$ and $\Omega = 1$. To present the insight of this typical behaviour of the channel, investigation based on eigenvalue analysis is included in the next Section. Afterwards, the channel model incorporating the regularization of channel gain matrix is also illustrated.

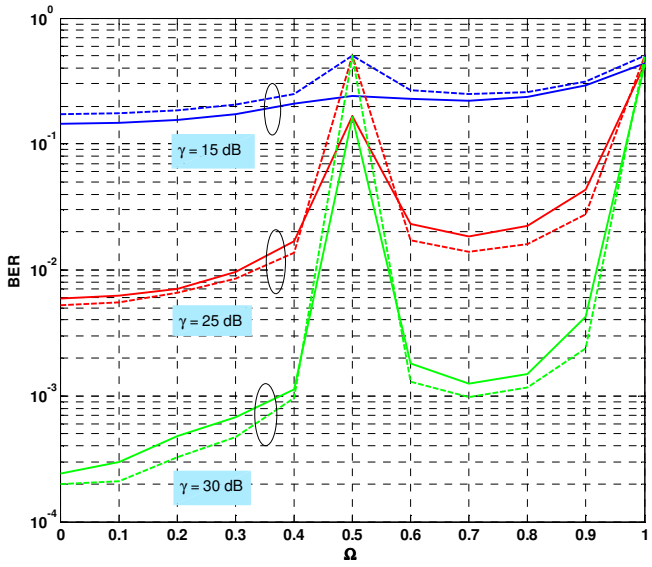

(a)

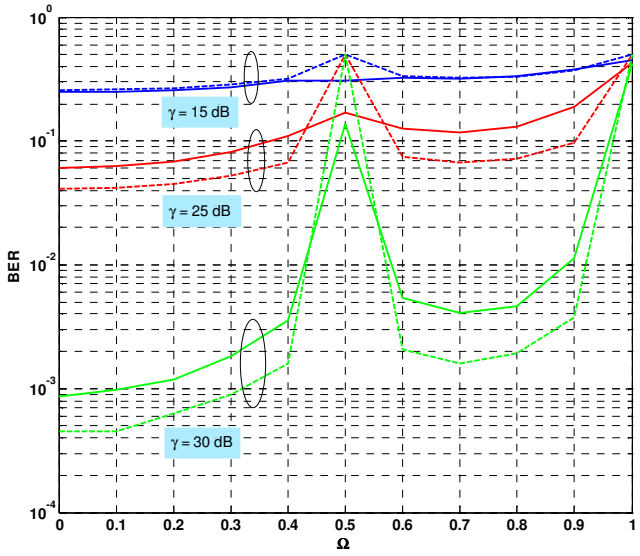

(b)

Figure 5-20: Comparison summary of BER reliance on inter-cell interference levels over C-GCMAC with $K = 1$, $N = 6$: Solid lines shows V-BLAST MMSE and dotted lines shows ZF-DPC transmission schemes: (a) 16-QAM; (b) 64-QAM.

5.6.6 Rank Reduction and Regularization of Ω

Recall from lemma 3.9.1, the channel slow gain matrix in Wyner's circular cellular setup is expressed as (3.15). Let us define $\Omega_{B_jT_{j+1}} = \Omega_{B_jT_{j-1}} = \Omega$ as a channel slow gain over the transmission link between the MTs and the BS. The resultant empirical form in (3.15) is now reduced to

$$\begin{aligned} \boldsymbol{\Omega}_{N,1} &= \mathbf{I} + \Omega\left(\boldsymbol{\mathcal{S}} + \boldsymbol{\mathcal{S}}^T\right) \\ &= \mathbf{I} + \Omega\tilde{\boldsymbol{\mathcal{S}}} \end{aligned} \tag{5-51}$$

In matrix form, we can express the channel slow gain matrix as

$$\boldsymbol{\Omega}_{N,1} = \begin{pmatrix} 1 & \Omega & 0 & \cdots & \Omega \\ \Omega & 1 & \Omega & & 0 \\ 0 & \ddots & \ddots & \ddots & \vdots \\ \vdots & & \Omega & 1 & \Omega \\ \Omega & 0 & \cdots & \Omega & 1 \end{pmatrix} \tag{5-52}$$

where $\Omega \in \left(0,1\right)$. It is well known that the eigenvalues of a circulant matrix are obtainable by evaluating the Discrete Fourier Transform (DFT) of its first row [94]. Hence, the columns of the Fourier matrix are the eigenvectors of $\boldsymbol{\Omega}$ and the eigenvalues of $\boldsymbol{\Omega}$ in (5-52) may be expressed as

$$\lambda_k = \sum_{p=0}^{N-1} \Omega_k \, \rho_k^p \qquad k = 0,1,2,\cdots,N-1 \tag{5-53}$$

where $\rho_k = \exp\left(\frac{2\pi \mathrm{i} k}{N}\right) = \cos\left(\frac{2\pi k}{N}\right) + \mathrm{i}\sin\left(\frac{2\pi k}{N}\right)$

$$\lambda_k = \Omega_0 + \Omega_1\rho_k^1 + \Omega_2\rho_k^2 + \cdots + \Omega_{N-1}\rho_k^{N-1} \tag{5-54}$$

In the case of a typical circulant channel slow gain matrix (5-52), we have

$$\lambda_k = 1+\Omega\left(\rho_k^1+\rho_k^{N-1}\right) \tag{5-55}$$

$$= 1+\Omega\left(\cos\left(\frac{2\pi k}{N}\right)+\cos\left(\frac{2\pi k(N-1)}{N}\right)\right)$$

$$= 1+2\Omega\cos\left(\frac{2\pi k}{N}\right)$$

We know that, $\lambda_k = 0$ exactly when

$$-\frac{1}{2\Omega} = \cos\left(\frac{2\pi k}{N}\right) \tag{5-56}$$

When $N = 6,\ \Omega = 1/2$,one of the eigenvalue $\lambda_{k=3} = 0$ and when $N = 6,$ $\Omega = 1,$ two eigenvalues $\lambda_{k=2} = \lambda_{k=4} = 0$. The eigenvalues of the channel slow gain matrix approached zero due to the fact that the channel is correlated and rank deficient. This phenomenon is further investigated with the help of graphical interpretation. Figure 5-21 shows the graphs of $y(k) = \cos\left(\frac{2\pi k}{N}\right)\ \ \forall k$ and $y(k) = -\frac{1}{2\Omega}\ \ \forall k$. It can be seen that the line $y(k) = -\frac{1}{2\Omega}\ \ \forall k$ interests the $y(k) = \cos\left(\frac{2\pi k}{N}\right)\ \ \forall k$ at: only one point i.e. $k = 3\ (\lambda_{k=3} = 0)$, when $\Omega = 1/2$; and at two points i.e. $k = 2,4\ (\lambda_{k=2} = \lambda_{k=4} = 0)$, when $\Omega = 1$.

The number of intersection points is the dimension of the null space of $\mathbf{\Omega}$, and the reduced rank of $\mathbf{\Omega}$ is given by

$$\text{rank}\left(\mathbf{\Omega}_{\lambda_k=0}\right) = N - \dim \text{Null Space}(\mathbf{\Omega}).$$

It is observed that the rank of $\mathbf{\Omega}$ reduced to 5 and 4 when $\Omega = 1/2$ and $\Omega = 1$ respectively. The influence of rank reduction at $\Omega = 1/2$ and $\Omega = 1$ on the performance of the V-BLAST MMSE and the ZF-DPC schemes over the correlated channel can be seen from Figure 5-20a and Figure 5-20b.

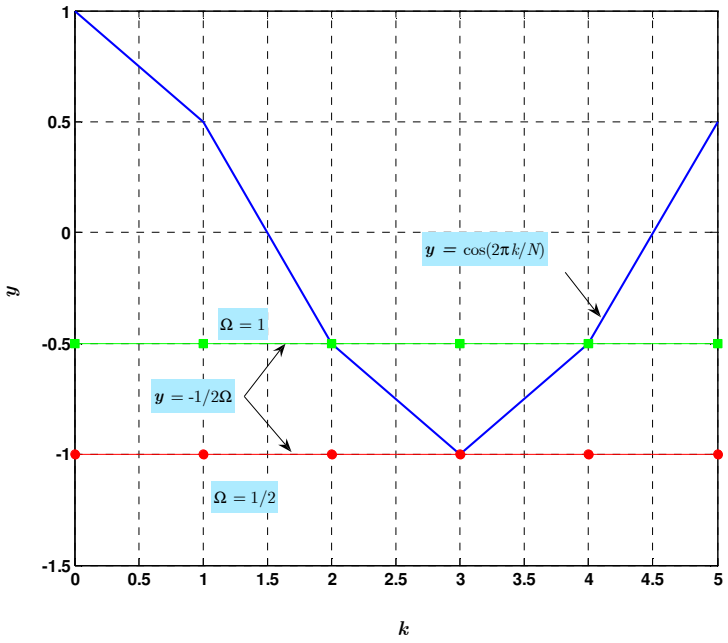

Figure 5-21: Graphical interpretation of rank reduction of circulant channel gain matrix; when $\Omega = 1/2$ at $k = 3$ and when $\Omega = 1$ at $k = 2, 4$.

Regularization of Ω [12]

Let us introduce a regularization parameter $\varepsilon \ll \Omega$. The purpose of introduction of regularization parameter is to regularize the channel gain matrix $\left(\boldsymbol{\Omega}\right)$ to avoid the rank reduction and subsequently, the degradation in channel BER performance curves as observed in Figure 5-20. The degradation in performance is mainly due to the fact that the eigenvalues of the channel gain matrix $\left(\boldsymbol{\Omega}\right)$ are zero at more than one instance. The dependency of rank of on channel regularization parameter is shown in Figure 5-22.

In order to recover the rank of channel slow gain matrix, we represent the channel model in (5.51) as

[12] Regularization is a numerical treatment applied to the not well-posed problem by introducing an additional parameter which causes smoothness in solutions. We introduced a simple method to avoid rank deficiency; however there are more precise regularization methods which can be applied. One of the well known regularization method is Tikhonov regularization [90].

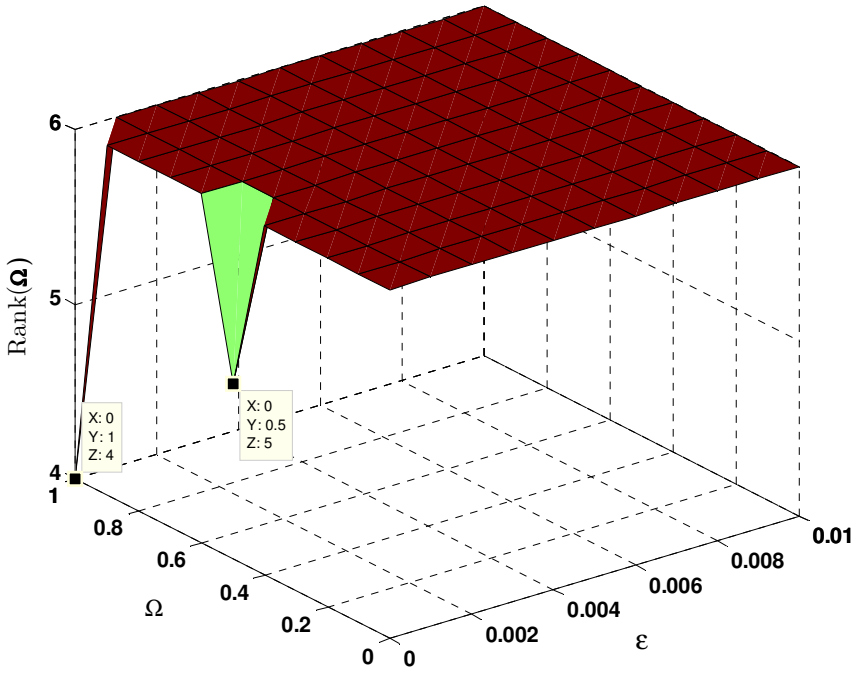

Figure 5-22: Dependency of rank of channel gain matrix $(\boldsymbol{\Omega})$ on the regularization parameter(ε). The figure also shows the rank reduction phenomena at$\varepsilon = 0$.

$$\boldsymbol{\Omega}_{Reg} = \mathbf{I} + \Omega\left(\boldsymbol{\mathcal{S}} + \boldsymbol{\mathcal{S}}^T\right) + \varepsilon\left(\boldsymbol{\mathcal{S}} + \boldsymbol{\mathcal{S}}^T\right) \quad (5\text{-}57)$$

$$= \mathbf{I} + \Omega\,\tilde{\boldsymbol{\mathcal{S}}} + \varepsilon\,\tilde{\boldsymbol{\mathcal{S}}} \quad (5\text{-}58)$$

Subsequently, the resultant regularized Wyner channel model can be expressed as

$$\mathbf{H}_{Reg} = \mathbf{G} \circ \boldsymbol{\Omega}_{Reg} \quad (5\text{-}59)$$

Now, we examine the performance of transmission design with respect to range of $\Omega(0,1)$ incorporating the $\boldsymbol{\Omega}_{Reg}$ in the channel model (3-5). Figure 5-23a and Figure 5-23b shows the BER reliance of V-BLAST MMSE and ZF-DPC when 16-QAM and 64-QAM is employed respectively. On comparison of Figure 5-23a and Figure 5-23b with Figure 5-20a and Figure 5-20b respectively, it is found that the degradation in BER performance of V-BLAST MMSE and ZF-DPC at $\Omega = 1/2$ and $\Omega = 1$ is stable due to the regularization of channel slow gain matrix $\boldsymbol{\Omega}$.

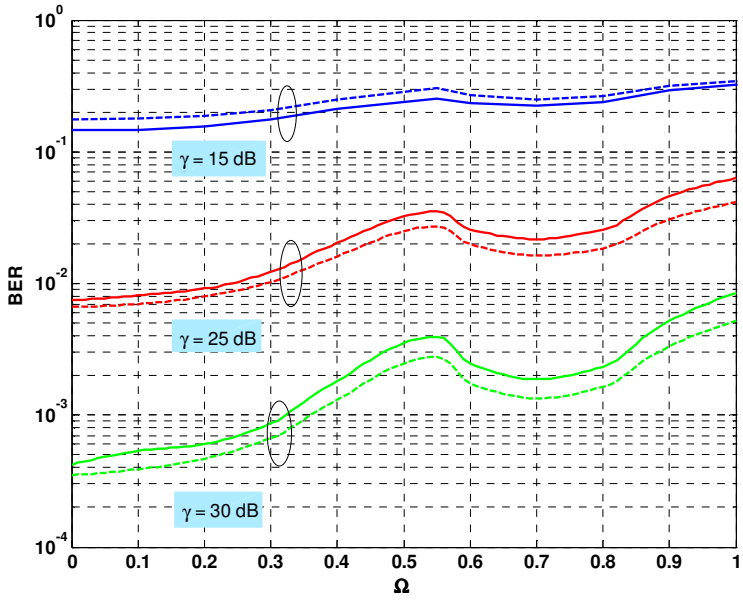

(a)

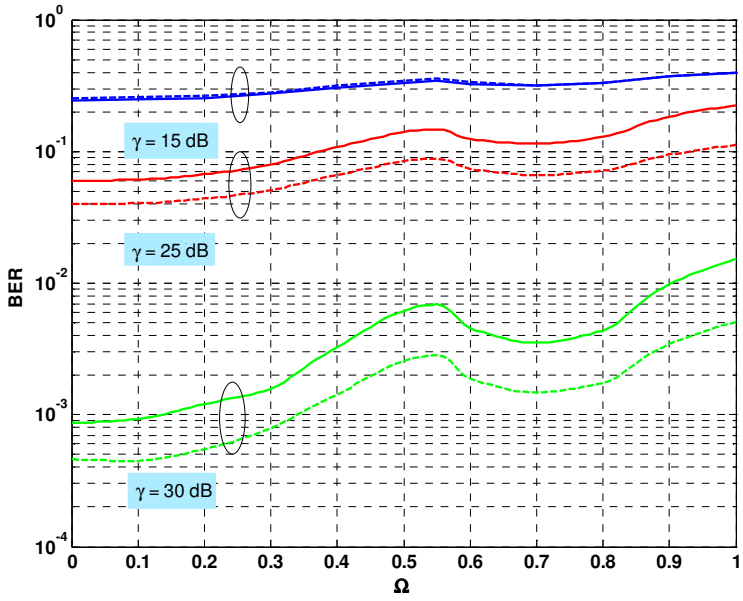

(b)

Figure 5-23: Comparison summary of BER reliance on inter-cell interference levels over regularized C-GCMAC ($\mathbf{H}_{Reg}$) with $K=1$, $N=6$: Solid lines shows V-BLAST MMSE and dotted lines shows ZF-DPC transmission schemes: (a) 16-QAM; (b) 64-QAM.

5.7 Final Remarks on Simulation Results: Diversity vs. Inter-Cell Interference

Final remarks on simulation results are now in order:

- It is observed that for the uncorrelated channel the diversity of cellular system increases with the increase in inter-cell interference (compare Figure 5-17 - Figure 5-19). On the contrary, the diversity decreases with the increase in inter-cell interference for correlated channels. The behaviour of channel is based on the mean power of the eigenvalues of the channel. The mean power of eigenvalues of the uncorrelated and the correlated channels is shown in Figure 5-24.

- It can be seen from the Figure 5-24 that at low level of inter-cell interference the performance of the uncorrelated and the correlated channels is almost same. However, for $\Omega > 0.2$ the performance of uncorrelated channel outperforms the performance of correlated channel. The same can be seen from Figure 5-17a and Figure 5-17b.

- The diversity of the Cellular MIMO Networks (CeMNets) over the uncorrelated channel model increases by exploiting the inter-cell interference among the mobile terminals and the base stations independently in each of the adjacent cells across the three zones (compare Figure 5-14 - Figure 5-16).

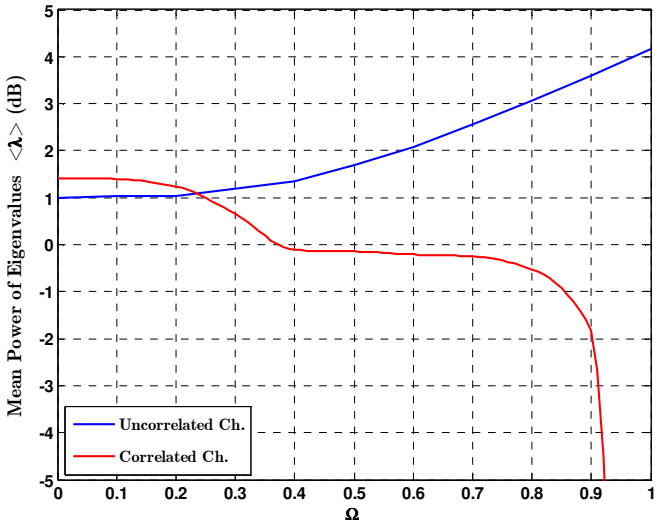

Figure 5-24: Summary of performance reliance of uncorrelated and correlated channels as a measure of mean power of eigenvalues of channel matrix over the range of $\Omega \in (0,1)$.

5.8 Conclusions

This chapter presented the simulation and derivation perspectives of transmission designs over the Wyner C-GCMAC exploiting the inter-cell interference of the transmission links. The BER performances of V-BLAST and ZF-DPC for uncorrelated and correlated fading scenarios have been presented. The BER offered by uncorrelated channel is inversely proportional to the inter-cell interference. The increase in inter-cell interference levels caused an improvement in the BER performance of uncorrelated channel. On the contrary, for the correlated channel, the BER performance is directly proportional to the inter-cell interference. The BER is degraded with the increase in inter-cell interference levels. The performance of ZF-DPC is superior to the V-BLAST MMSE over high levels of SNR and entire range of channel slow gain. However, the increase is distinct when the higher constellation is employed to symbols (like 64-QAM as shown in Figure 5-20 and Figure 5-23). The behaviour of uncorrelated and correlated channels for

Wyner circular cellular set up is almost same as $\Omega \to 0$. The same has been shown in Figure 5-17a and Figure 5-17b.

A new correlated channel model has been proposed based on random matrix theory and the circular nature of Wyner like model. The BER performance of the transmission schemes over conventional correlated channel and the proposed channel model shows that the correlated scenario in Wyner circular cellular setup can be approximated by unsystematic correlated channel which is referred to as the Hadamard Permuted channel (HPC) (see Figure 5-18 and Figure 5-19).

Chapter 6

Conclusion and Future work

6.1 Channel Modelling Perspective

Wireless communication systems in general and cellular communication systems in particular are of major interest as they allow the provision of continuous services to mobile users. In recent years, considerable research effort has been devoted to the development of new technologies for providing better services and extending system coverage. In this context, numerous cellular channel models have been formulated and analyzed using information theoretic principles to succinctly identify the impact of system constraints and design parameters on performance. The analytical framework of this thesis is inspired by analytically tractable model for the multi-cell processing as proposed by Wyner [29]. The circular version of the Wyner GCMAC referred to as C-GCMAC is the focus of this thesis. The existence of such model in realistic cellular setup is one of the major findings of this research. Later, we exploited the principle of introducing variable inter-cell interference levels among the BSs and the MTs. It has been revealed during the experimental trials carried out in Glasgow city centre around the circular cellular ring that the inter-cell interference among the users and the BSs is variable and by exploiting the inter-cell interference, new dimensions of cellular channel modelling has been introduced. This thesis is an attempt to alleviate the basic assumption that Wyner cellular model imposed to analyze the cellular networks i.e. every user is offering equal level of inter-cell interference. It was shown that by splitting the entire cell into three zones, namely, zone #1 where MTs are offering high level of interference to the BSs as if they are located in close vicinity of the BS of interest; zone #2 where MTs are offering medium level of interference to the BSs and lastly, zone #3 where MTs are offering low level of interference to the BSs as if they are located too far from the BS of interest. New empirical channel model for a single and the multi-user Cellular MIMO Networks (CeMNets) were introduced which incorporate the realistic gains among the BSs and the MTs (see Section 3.6).

6.2 Channel Decomposition Perspective

In Chapter 2, the unique MIMO channel decomposition technique referred to as GMD was introduced. By exploiting the GMD, the multi-user/multi-antenna channel was decomposed into parallel, identical and independent transmission pipes for data transmission at higher rates. The transmission design based on the GMD offers minimum BER as compared to transmission design based on the SVD. It was shown that GMD was also an optimal solution to the equal power allocation. This Identical Eigenmode Transmission Systems (IETS) brings much more convenience in modulation/demodulation and coding/decoding processes. Later, in Chapter 5, the IETS is designed for Wyner C-GCMACs. By assuming full BS cooperation and conferencing among the MTs (MTs cooperation), the resultant circular cellular setup was considered as a virtual MIMO cellular network. The GMD was employed to decompose the cellular channel into identical, parallel and independent transmission pipes. The GMD ensured Identical Mean Square Error (IMSE) across the each parallel sub-channels and subsequently, minimum overall BER performance. The transmission was designed by employing V-BLAST MMSE and ZF-DPC schemes.

The simulation perspectives of these two transmission design over the Wyner C-GCMAC exploiting the inter-cell interference gain was investigated in depth in Chapter 5. The BER performance of V-BLAST and ZF-DPC was analyzed for uncorrelated and correlated fading statistics. It was also shown that the BER performance of uncorrelated channel was superior as compared to correlated channel. The reliance of BER performance on the inter-cell interference over uncorrelated and correlated fading statistics was evaluated (refer to Figure 5-12, Figure 5-13, and Figure 5-20). It was found that BER performance of the uncorrelated channel is improved with the increase in inter-cell interference levels among the MTs and the BSs and BER performance of the correlated channel is degraded. However, further improvement in BER performance was also investigated by exploiting the inter-cell interference separately in each of the adjacent cells. The transmission schemes were also investigated to incorporate the realistic cellular scenario which was introduced in Chapter 3. As an example, when $K = 1$ (two inter-cell interfering MTs for each BS), the inter-cell interfering gain of each of the interfering MT was varied separately to minimize the BER performance (see Figure 5-14, Figure 5-15, and Figure 5-16).

A new correlated channel model was proposed by exploiting the concepts of Random Matrix Theory (RMT) and the circular nature of the Wyner model. The resultant

channel was a Permuted version of random i.i.d channel matrix. The Wyner cellular model with such correlation statistics was referred to as Hadamard Permuted Channel (HPC). The BER performance of transmission schemes like V-BLAST MMSE and ZF-DPC over simple correlated channel and the proposed Permuted channel shows that the correlated scenario in Wyner circular cellular setup can be approximated by our proposed HPC.

The BER offered by the two transmission schemes over uncorrelated channel significantly outperforms the BER performance of correlated channel at high levels of interference (refer to Figure 5-17, Figure 5-18, and Figure 5-19). It was observed that the performance was depending on the mean power distribution of eigenvalues of Wyner cellular channels. It was also observed that at low level of inter-cell interference the mean power distribution of eigenvalues of Wyner uncorrelated and correlated channels are close to each other. The same has been shown in Figure 5-17a and Figure 5-17b. Moreover, the mean power distribution of eigenvalues of uncorrelated channel increases as compared with correlated channel beyond $\Omega \approx 0.2$ which subsequently contributed to improve the BER performance of transmission schemes.

6.3 Information Theory Perspective

In Chapter 4, the fundamental principles from information theory were introduced, which have been used recently in the literature to gain insight into the performance of multi-access and multi-antenna cellular communication systems. The information theory perspective of the Wyner's cellular channel by employing the optimum joint decoding, cell optimum decoding, single user decoding and single user with intra-cell TDMA decoding was investigated and numerous simulation examples were included in Section 4.8. The important results are summarized as follows:

- The multi-user decoding strategies are distinctly advantageous over single user decoding (with not intra-cell TDMA) for all levels of inter-cell interference (see Figure 4-5).
- For low levels of inter-cell interference there is no observable distinct advantage of one multi-user decoding strategy over another. Therefore for this scenario, since $\mathbf{C}_{\text{cell}} = \mathbf{C}_{\text{sud}}^{\text{tdma}}$, the best strategy in terms of complexity is to employ intra-cell TDMA with single user decoding. However, for high levels of inter-cell interference since cell optimum decoding is interference limited it offers the lowest capacity of the multi-user decoding strategies (see Figure 4-7).

- Optimum joint decoding is the best strategy in terms of capacity; however, its exponential complexity with N renders it impractical in any realistic cellular system. At high level of inter-cell interference, intra-cell TDMA used in conjunction with linear MMSE filtering followed by single user decoding offers substantial capacity gain over cell optimum and single user decoding strategies (see Figure 4-6 Figure 4-5)
- The capacity expressions were derived to incorporate the variable inter-cell interference levels among the MTs and BSs. It was shown that by exploiting the slow gain of inter-cell interfering users in both adjacent cells separately the cell optimum decoding and linear MMSE filtering capacities were sub-optimal at moderate level of inter-cell interference. Several simulation scenarios are created to observe the capacity when the slow gain among the users and BS was variable. The advantage of exploiting variable sow gain is significant over both fading and AWGN channels (see Figure 4-11 - Figure 4-13 for non-fading case and Figure 4-19 - Figure 4-19 for fading case).

- The capacity behaviour for $N \to \infty$ over linear and circular Wyner GCMAC was also covered in Chapter 4. The summary was shown in Figure 4-10. It was shown that at low range of SNR, capacity offered by finite order channel matrix e.g. $N = 6$ follows capacity offered by channel matrix where $N \to \infty$ till medium range of interference $\Omega \approx 0.6$ (see Figure 4-10a) where as at high SNR this threshold increases to $\Omega \approx 0.7$. Thus, at low level of interference the information theoretic performance of linear-GCMAC and circular-GCMAC were approximately same.

6.4 Impact of Hadamard Operation on the Performance of Wyner C-GCMAC

Since the resultant MIMO wireless channel is the Hadamard product of the channel slow gain matrix $\mathbf{\Omega}$ and channel fading matrix $\mathbf{G}$ (3.5). We investigated the strong properties of the Hadamard operator to reveal the new dimensions with respect to information theory, and channel decomposition. We derived a novel application of the Hadamard inequality in Section 4.8 as Theorem 4.8.3. It was shown that by exploiting the Hadamard inequality a few more Bits can be offered by the Wyner's cellular channel. It was also shown in Section 4.8.4a, that when there was no inter-cell interference the new upper

bound on optimum joint decoding capacity is identical to the Shannon capacity definition and holds equal results.

It has also been demonstrated that in the multi-user case when inter-cell TDMA is employed, the gain in capacity is $\log_2(K)$ (see Figure 4-26). By exploiting the Hadamard inequality we can deterministically calculate the gain in optimum joint capacity with inter-cell and intra-cell TDMA schemes. In Chapter 5, we developed very useful aspects of the Hadamard operator, particularly when the channel fading statistics were semi or fully correlated. It was found that the resultant channel matrix **H** was rank deficient due to ill conditioned channel slow gain matrix $\boldsymbol{\Omega}$. The BER performance of cellular system with correlated fading statistics showed abrupt changes whenever the channel slow gain matrix was ill conditioned (see Theorem 5.3.2, § 5.3). This leads to degradation in the system's overall BER performance (see Figure 5-20). The rank regularization method was introduced to recover the BER performance of correlated channel. However, the ill conditioned channel slow gain matrix $\boldsymbol{\Omega}$ does not affect the BER performance of uncorrelated fading channel.

6.5 Future Work

This Section provides some directions in which the work in this thesis can be extended.

- **Frequency Selective Scenario for Wyner Cellular Channels**

This thesis focused on linear C-GCMAC and although the planar GCMAC (two dimensional cellular model) has been investigated in [27] and [28]. The transmission design, channel decomposition and information theoretic perspectives of planar model incorporating the variable inter-cell interference among MTs and BSs is yet to be done. Throughout the thesis, we assumed that the cellular channel is Rayleigh flat fading. However, one of the possible extensions of this research is to investigate the frequency selective channel statistics. It is suggested to employ Orthogonal Frequency Division Multiplexing (OFDM) to decompose the frequency selective channel into flat fading channels. Therefore, the GMD technique can be applied to achieve the optimal BER performance. However, the main problem is to find explicit expressions for the capacity which is a very challenging task in these scenarios.

Hadamard Channel Decomposition for Wyner Channels

Throughout the thesis, some very important properties of the Hadamard operator have been revealed. In Chapter 3 and Chapter 4 the very useful contribution of the Hadamard product has been presented. However, it is expected that the Hadamard product of channel fading matrix and channel slow gain matrix would play an important role if one is able to derive the Hadamard inequality by exploiting the GMD of $\mathbf{G}$ and $\mathbf{\Omega}$ individually. The GMD of the Hadamard product may be expressed as

$$\mathbf{G} \circ \mathbf{\Omega} = \left(\mathbf{Q}_{\mathbf{G}}\mathbf{R}_{\mathbf{G}}\mathbf{P}_{\mathbf{G}}^{H}\right) \circ \left(\mathbf{Q}_{\mathbf{\Omega}}\mathbf{R}_{\mathbf{\Omega}}\mathbf{P}_{\mathbf{\Omega}}^{H}\right) \tag{6-1}$$

It is found that, numerically we have

$$\left(\mathbf{Q}_{\mathbf{G}}\mathbf{R}_{\mathbf{G}}\mathbf{P}_{\mathbf{G}}^{H}\right) \circ \left(\mathbf{Q}_{\mathbf{\Omega}}\mathbf{R}_{\mathbf{\Omega}}\mathbf{P}_{\mathbf{\Omega}}^{H}\right) > \left(\mathbf{Q}_{\mathbf{G}} \circ \mathbf{Q}_{\mathbf{\Omega}}\right)\left(\mathbf{R}_{\mathbf{G}} \circ \mathbf{R}_{\mathbf{\Omega}}\right)\left(\mathbf{P}_{\mathbf{G}}^{H} \circ \mathbf{P}_{\mathbf{\Omega}}^{H}\right) \tag{6-2}$$

However, up to now, the equivalent conditions for inequality in (6.2) to hold equal are not known. Moreover, the application of the Hadamard inequalities based on GMD is one of the possible extensions for similar kind of analysis presented in Chapter 5.

Realistic Channel Modelling by Using Pilot Walk Tour

In Chapter 3, we used Net-monitor software to monitor the received power level and subsequently, to calculate the distance between the MTs and BSs. The software can only be used with GMS systems. However, there are (Universal Mobile Telecommunication System) UMTS BSs which were neglected during the trials and analysis. The software we used does not support post processing analysis e.g. Storage of data files for tests. There are other networks monitoring software which are available to perform the trials efficiently. One of the candidates to be used for future Modelling is Pilot Walk Tour by Dingli Communications Ltd. [132]. Dingli Pilot WalkTour is the most convenient portable derive test tool for measuring or monitoring the air interface of GSM/GPRS/EDGE/UMTS/HSDPA wireless networks based on Symbian intelligent operation system. Its small size and powerful application testing features make it a favorable tool, currently supporting indoor test, as well as field test (GPS) with no essential need to connect external devices. Compared to traditional test tool, Walktour can effectively collect measurements even in special locations and buildings where traditional tool cannot function well. It records a comprehensive set of accurate measurement information, which greatly helps network evaluation and analysis by exporting log data to Dingli's post-processing system.

- **Multi-antenna Array at Both Side of Communication Link**

In this thesis each user and base station were assumed to have only a single antenna. It would be interesting to observe the effects on system performance when each user and base station employs multi-antennas. Increasing the number of antennas effectively increases the number of degree of freedom, which should result in an increase in capacity, like in standard MIMO communication system [127]. However, affect of inter-cell interference, timesharing protocols, transmits CSI and optimum input covariance matrix for such an antenna array is unknown and is subject of future work. The analysis may be extended for large system using random matrix theory.

- **Information Theoretic Analysis for Cooperative Cellular MIMO Networks (CeMNets):**

In Chapter 5, we presented information theoretic perspectives of the MIMO cellular network with only base stations cooperation. The information theoretic analysis can be extended when mobile terminals also cooperates. Our analysis has been limited to the uplink of cellular networks. With recent results in information theory, the downlink has also gained importance and the evaluation of the downlink capacity of MIMO cellular networks is an important aspect for the future design of such networks (see e.g. [135] and [136]). The analytical characterization of the results has used simplified assumptions to provide explicit expressions. In addition, the work in this thesis characterizes only the fundamental scaling limits of the cooperating base station architecture and does not take into account the practical implementation constraints.

Bibliography

[1] T. Kaiser, A. Bourdoux, and H. Boche, et al., *Smart antennas - state of the art*. Hindawi Publishing Corp., USA, 2005.

[2] Y. Jiang, J. Li, and W. Hager, "The geometric mean decomposition," *in Elsevier Jour. Linear Algebra and its Application*, vol. 396, pp. 373-384, Feb. 2005.

[3] Y. Jiang, W. W. Hager, and J. Li, "The geometric mean decomposition and generalized triangular decomposition," *presented at the SIAM Annu. Meeting*, Portland, OR, USA, Jul. 16, 2004.

[4] B. W. Silverman, *Density estimation for statistics and data analysis*, Chapman and Hall, London, 1986.

[5] P. W. Wolniansky, G. J. Foschini, and G. D. Golden, et al., "V-BLAST: an architecture for realizing high data rates over the rich scattering wireless channels," *in Proc. Intl. symp. on Signals, Systems and Electronics*, pp. 295-300, Pisa, Italy, Sep. 1998.

[6] G. J. Foschini, and M. J. Gans, "On limits of wireless communications in a fading environment when using multiple antennas," *in Springer Jour. on Wireless Personal Communs.*, vol. 6, no. 3, pp. 311–335, 1998.

[7] G. J. Foschini, "Layered space time architecture for wireless communication in a fading environment when using multiple antennas," *in Bell Labs. Tech. Jour.*, vol. 1, no. 2, pp. 41-59, 1996.

[8] G. Tsoulos, *MIMO system technology for wireless communications*, CRC Press, 2006.

[9] G. G. Raleigh, and J. M. Coiffi, "Spatio-temporal coding for wireless communications," in *IEEE Trans. on Communs.*, vol. 46, no. 3, pp-357-366, Mar. 1998.

[10] S. M. Alamouti, "Space time block coding: A simple transmitter diversity technique for wireless communications," *IEEE Journal on Selected Area in Communications*. Vol.16, pp.1451–1458, 1998.

[11] D. Wubben, R. Bohnke, V. Kuhn, and K. D. Kammeyer, "MMSE extension of V-BLAST based on sorter QR decomposition," *in Proc. IEEE 58th Vehicular Technology Conf.*, vol. 1, pp. 508-512, Orlando, Fla, USA, Oct. 2003.

[12] V. Kuhn, *Wireless communications over MIMO channels: application to CDMA and multiple antenna systems*, John Wiley & Sons Ltd, England, 2006.

[13] E. Telatar, "Capacity of Multi-antenna Gaussian Channels," *Technical Memorandum, AT&T Bell Laboratories*, 1995.

[14] G. Lebrun, T. Ying, and M. Faulkner, "MIMO transmission over a time varying TDD channel using SVD," *in IEE Electronics Let.*, vol. 37, no. 22, pp. 1363-1364, 2001.

[15] G. Lebrun, J. Gao, and M. Faulkner, "MIMO transmission over a time varying TDD channel using SVD," *in Proc. IEEE Conf. on Global Communs., GLOBCOM* 2002, Oct. 2002.

[16] T. S. Rappaport, "*Wireless communications - principles and practice*," Prentice Hall, Upper Saddle River, New Jersy, 1996.

[17] P. J. Smith, and M. Shafi, "Waterfilling methods for MIMO systems," *in Proc. 3rd Aus. Workshop on Commun. Theory, AusCTW 2002, Australian National University*, Feb. 2002.

[18] H. Bolcskei, and A. J. Paulraj, *The communications handbook, Chapter: Multiple-input multiple-output (MIMO) wireless systems*, pp. 90.1–90.14, J. Gibson, Ed. CRC Press, 2nd ed., 2002.

[19] V. Tarokh, H. Jafharkani, and A. R. Calderbank, "Space-time block codes from orthogonal designs," *in IEEE Trans. on Inform. Theory*, vol. 45, no. 5, pp. 1456–1467, Jul. 1999.

[20] L. Zheng, and D. N. C. Tse, "Diversity and multiplexing: A fundamental trade off in multiple antenna channels," *in IEEE Trans. on Inform. Theory*, vol. 49, no. 5, pp. 1073–1096, May 2003.

[21] M. Tulino, and S. Verdu, *Random Matrix Theory and Wireless Communications*, Now Publishers Inc., Hanover, USA, 2004.

[22] T. M. Cover, and J. A. Thomas, *Elements of information theory*, John Wiley & Sons Ltd, New York, 1991.

[23] J. R. Schott, Matrix *analysis for statistics*, John Wiley & Sons Ltd, New York, 1996.

[24] R. A. Horn, and C. R. Johnson, *Matrix analysis*, Cambridge University Press, Cambridge, U.K., 1985.

[25] S. Haykin, *Communication systems*, John Wiley & Sons Ltd, New York, 2001.

[26] J. G. Proakis, *Digital communications*, McGraw-Hill, New York, 2001.

[27] S. Shamai, and A. D. Wyner, "Information-theoretic considerations for symmetric, cellular, multiple-access fading channels - part I," *in IEEE Trans. on Inform. Theory*, vol. 43, no. 6, pp. 1877–1894, Nov. 1997.

[28] S. Shamai, and A. D. Wyner, "Information-theoretic considerations for symmetric, cellular, multiple-access fading channels - part II," *in IEEE Trans. on Inform. Theory*, vol. 43, no. 6, pp. 1895–1911, Nov. 1997.

[29] D. Wyner, "Shannon-theoretic approach to a Gaussian cellular multiple-access channel," *in IEEE Trans. on Inform. Theory*, pp. 1713–1727, 1994.

[30] D. Tse, and P. Viswanath, *Fundamentals of Wireless Communication*, Cambridge University Press, (Dec. 2005), Online available at: http://www.eecs.berkeley.edu/ dtse/book.html.

[31] O. Somekh, B. M. Zaidel, and S. Shamai, "Spectral efficiency of joint multiple cell-site processors for randomly spread DS-CDMA systems," *in IEEE Intl. Symp. on Inform. Theory*, Chicago, Jun. 2004.

[32] O. Somekh, B. M. Zaidel, and S. Shamai, "Sum-rate characterization of multi-cell processing," *in Proc. Canadian Workshop on Inform. Theory*, McGill University, Montreal, Quebec, Canada, Jun. 2005.

[33] D. Aktas, M. N. Bacha, J. Evans, and S. Hanly, "On the sum capacity of mult-iuser MIMO channels," *in Proc. Intl. Symp. on Inform. Theory and its Application, ISITA 2004*, pp. 1013-1018, Oct. 2004.

[34] U. Grenander, and G. Szego, *Toeplitz Forms And Their Applications*, Cambridge University Press, 1958.

[35] Z. Ni, and D. Li, "Impact of fading correlation and power allocation on capacity of distributed MIMO," *in IEEE Proc. 6th CAS Symp. on Emerging Technologies: Mobile and Wireless Communs*., Shanghai, China, May 2004, pp. 697-700.

[36] J. Quirke, "*Nokia Net-Monitor manual version 0.80.1 Beta*," (revised 2004), Online available at: http://www.mt-box.org/mtbox_free/nokia_net_monitor_guide_v0_80_1.pdf

[37] O. Somekh, B.M. Zaidel, and S. Shamai, "Sum rate characterization of joint multiple cell-site processing," *in IEEE Trans. on Inform. Theory*, vol. 53, no. 12, pp. 4473-4497, Dec. 2007.

[38] R. M. Gray, *Toeplitz and circulant matrices: A review,* (Aug. 2002), Online available at: http://ee.stanford.edu/~gray/toeplitz.pdf

[39] R. Goodman, *Finite Fourier transforms circulant matrices and fast Fourier transform,* (Oct. 30, 2007), Online available at: http://www.math.rutgers.edu/courses/550A/550-f07/fftnotes.pdf

[40] D. Guo, S. Shamai, and S. Verdu, "Mutual information and MMSE in Gaussian channels," *in IEEE Intl. Symp. on Inform. Theory*, Chicago, p. 347, Jun. 2004.

[41] D. Guo, S. Shamai, and S. Verdu, "Mutual information and minimum mean-square error in Gaussian channels," *in IEEE Trans. Inform. Theory*, vol. 51, no. 4, pp. 1261–1282, 2005.

[42] S. Verdu, *Multiuser Detection*, Cambridge University Press, 1998.

[43] Z. Xie, R. T. Short, and C. K. Rushforth, "A family of suboptimal detectors for coherent multi-user communications," *in IEEE Jour. on Selected Areas in Commun*., vol. 8, no. 4, pp. 683–690, May 1990.

[44] H. V. Poor, *An Introduction to Signal Detection and Estimations*, Springer-Verlag, New York, 1988.

[45] S. M. Kay, *Fundamentals of statistical processing: estimation theory*, Prentice Hall International, Englewood Cliffs, 1993.

[46] A. M. Tulino, and S. Verdu, *Random Matrix Theory and Wireless Communications*, now Publishers Inc., Hanover, USA, 2004.

[47] D. P. Palomar, and S. Verd´u, "Gradient of mutual information in linear vector Gaussian channels," *in IEEE Intl. Symp. on Inform. Theory, ISIT 2005*, Adelaide, Australia, Sep. 2005.

[48] D. Guo, S. Verdu, and S. Shamai, "Additive non-Gaussian noise channels: Mutual information and conditional mean estimation," *in IEEE Intl. Symp. on Inform. Theory*, Adelaide, Australia, Sep. 2005.

[49] A. V. Fiacco, and G. P. McCormick, *Nonlinear Programming: Sequential Unconstrained Minimization Techniques*, Res. Anal. Corp., USA, 1968.

[50] A. J. Grant, S. Hanly, J. Evans, and R. Muller, "Distributed decoding for Wyner cellular systems," *in Proc. 5th Aust. Commun. Theory Workshop, AusCTW 2004*, Newcastle, Feb. 2004, pp. 77–81.

[51] C. Berrou, A. Glavieux, and P. Thitimajshima, "Near Shannon limit error –correcting coding and decoding: Turbo codes," *in Proc. IEEE Intl. Conf. on Commun*., pp. 1064 – 1070. May, 1993.

[52] L. R. Bahl, J. Cocke, F. Jelinek, and J. Raviv, "Optimal decoding of linear codes for minimizing symbol error rate," *in IEEE Trans. on Inform. Theory*, vol. 20, pp. 284 – 287, Mar. 1974.

[53] B. L. Ng, J. Evans, S. Hanly, and A. J. Grant, "Distributed linear multiuser detection in cellular networks," *in Proc. 5th Aust. Commun. Theory Workshop, AusCTW 2004*, Newcastle, Feb. 2004, pp. 127–132.

[54] S. Verdu, "Computational complexity of optimum multiuser detection," *Algorithmica*, pp. 303–312, May 1989.

[55] L. K. Rasmussen, A. J. Grant, and P. D. Alexander, "An extrinsic Kalman filter for iterative multiuser decoding," *in IEEE Trans. on Inform. Theory*, vol. 50, no. 4, pp. 642–648, Apr. 2004.

[56] M. Abramowitz, and I. A. Stegun, *Handbook of mathematical functions, graphs and mathematical tables*, Dover Publications, New York, 1965.

[57] J. G. Proakis, *Digital Communications*, McGraw-Hill, New York, 1995.

[58] R. M. Gray, "On the asymptotic eigenvalue distribution of Toeplitz matrices," *in IEEE Trans. on Inform. Theory*, vol. 18, pp. 725–730, 1972.

[59] M. C. Reed, C. B. Schlegel, P. D. Alexander, and J. A. Asenstorfer, "Iterative multiuser detection for CDMA with FEC: Near-single-user performance," *in IEEE Trans. on Commun.*, vol. 46, no. 12, pp. 1693–1699, Dec. 1998.

[60] P. D. Alexander, A. J. Grant, and M. C. Reed, "Iterative detection in code-division multiple-access with error control coding," *in Europe. Trans. on Telecommun.*, vol. 9, no. 5, pp. 419–426, Sept.-Oct. 1998.

[61] P. D. Alexander, M. C. Reed, J. A. Asenstorfer, and Schlegel C. B., "Iterative multiuser interference reduction: Turbo CDMA," *in IEEE Tran. on Commun.*, vol. 47, no. 7, pp. 1008–1014, Jul. 1999.

[62] M. L. Moher, "An iterative multiuser decoder for near-capacity communications," *in IEEE Trans. on Commun.*, vol. 46, pp. 870–880, Jul. 1998.

[63] O. Somekh, and S. Shamai, "Shannon-theoretic approach to a Gaussian cellular multiple-access channel with fading," *in IEEE Trans. on Inform. Theory*, vol. 46, no. 4, pp. 1401–1425, 2000.

[64] M. L. Moher, "Multiuser decoding for multi-beam systems," *in IEEE Trans. Inform. Theory*, vol. 49, no. 4, pp. 1226–1234, 2000.

[65] P. J. Davis, *Circulant Matrices*, Wiley-Interscience, 1979.

[66] R. R. Muller, "*Random matrices*," (Sep. 2000), Online available at http://lthiwww.epfl.ch/~levequ/Matrix/muller.pdf

[67] A. Edelman, *Eigenvalues and Condition Number of Random Matrices*, Ph.D. thesis, Dept. Mathematics, MIT, Cambridge, MA, 1989.

[68] G. Visick, "A quantitative version of the observation that the Hadamard product is a principal sub-matrix of the Kronecker product," *Elsevier Jour. on Linear Algebra and its Applications*, vol. 304, pp. 45-68, 2000.

[69] T. Amemiya, "*Advanced Econometrics*," Harvard University Press, Cambridge, USA, 1985.

[70] Y. Liang, and A. Goldsmith, "Symmetric rate capacity of cellular systems with cooperative base stations," *in Proc. IEEE Conf. on Global Telecommuns., GLOBCOM 2006*, Nov. 2006.

[71] Y. Liang, T. Yoo, and A. Goldsmith, "Coverage spectral efficiency of cellular systems with cooperative base stations," *in Proc. 40th Asilomar Conf. on Signals, Systems and Computers, ACSSC 2006*, pp. 349-353, Oct. 2006.

[72] Y. Jiang, J. Li, and W. Hager, "Joint transceiver design for MIMO communications using geometric mean decomposition," *in IEEE Trans. on Signal Processing*, vol. 53, no. 10, pp. 3791-3803, Oct. 2005.

[73] D. Wubben, R. Bohnke, V. Kuhn, and K. D. Kammeyer, "Efficient algorithm for decoding layered space time codes," *in IEE Electronic Let.*, vol. 37, no. 22, pp. 1348-1350, 2001.

[74] R. B. Wubben, V. Kuhn, and K. D. Kammeyer, "MMSE extension of V-BLAST based on sorter QR decomposition," *in Proc. IEEE 58th Vehicular Technology Conf.*, vol. 1, pp. 508-512, Orlando, Fla, USA, Oct. 2003.

[75] N. B. Getu, and J. B. Andersen, "MIMO systems in random uncorrelated, correlated and deterministic radio channels," *in Springer Jour. on Wireless Personal Communs.*, vol. 30, no. 1, pp. 27-61, Jul. 2004.

[76] G. J. Foschini, G. D. Golden, R. A. Valenzuela, and P. W. Wolniansky, "Simplified processing for high spectral efficiency wireless communication employing multiple-element arrays," *in* Springer Jour. on *Wireless Personal Communs.*, vol. 6, pp. 311–335, Mar. 1999.

[77] G. Ginis, and J. M. Cioffi, "Vectored transmission for digital subscriber line systems," *in IEEE Jour. on Selected Areas Communs.*, vol. 20, pp. 1085–1104, Jun. 2002.

[78] G. Caire, and S. Shamai, "On the achievable throughput of a multi-antenna Gaussian broadcast channel," *in IEEE Trans. on Inform. Theory*, vol. 49, no. 7, pp. 1691–1706, Jul. 2003.

[79] G. Ginis, and J. M. Cioffi, "A multi-user precoding scheme achieving crosstalk cancellation with application to DSL systems," *in Proc. 34th Asilomar Conf. on Signals, System, Computers*, vol. 2, Asilomar, CA, pp. 1627–1631, Oct.–Nov., 2000,

[80] M. Costa, "Writing on dirty paper," *in IEEE Trans. on Inform. Theory*, vol. IT–29, pp. 439–441, May 1983.

[81] M. Tomlinson, "New automatic equalizer employing modulo arithmetic," *in IEE Electronic. Let.*, vol. 7, pp. 138–139, Mar. 1971.

[82] H. Harashima, and H. Miyakawa, "Matched-transmission technique for channels with inter-symbol interference," *in IEEE Trans. on Commun.*, vol. 20, pp. 774–780, Aug. 1972.

[83] W. Yu, and J. M. Cioffi, "Trellis precoding for the broadcast channel," *in Proc. IEEE Conf. on Global Telecommuns.*, *GLOBCOM 2001*, vol. 2, Nov. 2001, pp. 1344–1348.

[84] G. Ginis, and J. M. Cioffi, "On the relationship between V-BLAST and the GDFE," *in IEEE Commun. Let.,* vol. 5, no. 9, pp. 364–366, Sep. 2001.

[85] G. Fascine, K. Karakayali, and R. Valenzuela, "Coordinating multiple antenna cellular networks to achieve enormous spectral efficiency," *in IEE Proc. on Commun.*, vol.153, no 4, pp. 548–555, Aug. 2006.

[86] H. Weingarten, Y. Steinberg, and S. Shamai, "The capacity region of the Gaussian MIMO broadcast channel," *in Proc. IEEE Intl. Symp. on Inform. Theory, ISIT 2004*, p. 174, Chicago IL, Jun. 2004.

[87] P. Viswanath, and D. Tse, "Sum capacity of the vector Gaussian broadcast channel and uplink-downlink duality," *in IEEE Trans. on Inform. Theory*, vol. 49, no. 8, pp. 1912–1921, Aug. 2003.

[88] S. Vishwanath, N. Jindal, and A. Goldsmith, "Duality, achievable rates, and sum-rate capacity of Gaussian MIMO broadcast channels," *in IEEE Trans. on Inform. Theory*, vol. 49, no. 10, pp. 2658–2668, Oct. 2003.

[89] K. Erdman, and M. J. Wildon, *Chapter: Solvable lie algebras and a rough classification, Introduction to lie Algebras*, Springer London, Sep. 2006.

[90] R. A. Beezer, A *first course in linear algebra*, version 2.20, (Aug. 17, 2009), Online available at: http://linear.ups.edu/download/fcla-electric-2.20.pdf

[91] A. Sanderovich, O. Somekh, and S. Shamai (Shitz), "Uplink macro diversity with limited backhaul capacity," *in Proc. IEEE Intl. Symp. on Inform. Theory, ISIT 2007*, Nice, France, Jun. 24-29, 2007.

[92] O. Simeone, O. Somekh, Y. Bar-Ness, and U. Spagnolini, "Uplink throughput of TDMA cellular systems with multi-cell processing and Amplify-and-Forward cooperation between mobiles," *in IEEE Trans. on Wireless Commun.,* vol. 6, no. 8, pp. 2942-2951, Aug. 2007.

[93] O. Somekh, O. Simeone, H. V. Poor, and S. Shamai, "Cellular systems with full-duplex Amplify-and-Forward relaying and cooperative base stations," *in Proc. IEEE Intl. Symp. on Inform. Theory, ISIT 2007,* Nice, France, Jun. 24-29, 2007.

[94] O. Simeone, O. Somekh, Y. Bar-Ness, and U. Spagnolini, "Throughput of low-power cellular systems with collaborative base stations and relaying," *in IEEE Trans. on Inform. Theory*, vol. 54, no. 1, pp. 459-467 2008.

[95] O. Simeone, O. Somekh, Y. Bar-Ness, H. V. Poor, and S. Shamai (Shitz), "Capacity of linear two-hop mesh networks with rate splitting, decode-and-forward relaying and cooperation," *in Proc. 45th Annual Allerton Conf. on Commun., Control, and Computing*, Monticello, Illinois, Sept. 26-28, 2007.

[96] O. Somekh, O. Simeone, H.V. Poor, and S. Shamai (Shitz), "Throughput of cellular uplink with dynamic user activity and cooperative base-stations," *in Proc. IEEE Inform. Theory Workshop, ITW 2009, Taormina, Italy*, Oct. 11-16, 2009.

[97] S. Shamai (Shitz), O. Somekh, and B. M. Zaidel, "Multi-cell communications: An information theoretic perspective," *in Proc. Joint Workshop on Commun. and Coding, JWCC'04*, Donnini, Florence, Italy, Oct.14–17, 2004.

[98] O. Somekh, O. Simeone, Y. Bar-Ness, A. M. Haimovich, U. Spagnolini, and S. Shamai (Shitz), *Distributed Antenna Systems: Open Architecture for Future Wireless Communications*, *Chapter: An Information Theoretic View of Distributed Antenna Processing in Cellular Systems*, Auerbach Publications, CRC Press, May 2007.

[99] R. Pabst, B. H. Walke, D. C. Schultz, P. Herhold, and H. Yanikomeroglu, et al., "Relay-based deployment concepts for wireless and mobile broadband radio," *in IEEE Commun. Magazine*, pp. 80-89, Sep. 2004.

[100] O. Somekh, B. M. Zaidel and S. Shamai (Shitz), "Spectral efficiency of joint multiple cell-site processors for randomly spread DS-CDMA systems," *in IEEE Trans. on Inform. Theory*, vol. 52, no. 7, pp. 2625-2637, Jul. 2007.

[101] P. Marsch, S. Khattak, and G. Fettweis, "A framework for determining realistic capacity bounds for distributed antenna systems," *in Proc. IEEE Inform. Theory Workshop, ITW 2006*, China, Oct. 2006.

[102] P. Marsch, and G. Fettweis, "A framework for optimizing the downlink performance of distributed antenna systems under a constrained backhaul," *in Proc. European Wireless Conf., EW 2007*, Apr. 1-4, Paris, France, 2007.

[103] P. Marsch, and G. Fettweis, "A framework for optimizing the uplink performance of distributed antenna systems under a constrained backhaul," *in Proc. IEEE Intl. Conf. on Communs., ICC 2007*, Jun. 24-28, Glasgow, Scotland, 2007.

[104] E. Atkas, J. Evans, and S. Hanly, "Distributed decoding in a cellular multiple access channels," *in Proc. IEEE Intl. Symp. on Inform. Theory, ISIT 2004*, p. 484, Jun. 27-Jul. 2, Chicago, Illinois, 2004.

[105] O. Shental, A. J. Weiss, N. Shental, and Y. Weiss, "Generalized belief propagation receiver for near optimal detection of two-dimensional channels with memory," *in Proc. Inform. Theory Workshop, ITW 2004*, San Antonio, Texas, Oct. 24-29, 2004.

[106] O. Simeone, O. Somekh, Y. Bar-Ness, and U. Spagnolini, "Uplink throughput of TDMA cellular systems with multicell processing and Amplify-and-Forward cooperation between mobiles," *in IEEE Trans. on Wireless Commun.,* vol. 6, no. 8, pp. 2942-2951, Aug. 2007.

[107] O. Somekh, O. Simeone, H. V. Poor, and S. Shamai, "Cellular systems with full-duplex Amplify-and-Forward relaying and cooperative base stations," *in Proc. IEEE Intl. Symp. on Inform. Theory, ISIT 2007,* Nice, France, Jun. 24-29, 2007.

[108] G. Kramer, I. Maric, and R. D. Yates, *Cooperative Communications*, *Foundations and Trends in Networking (FnT),* Now Publishers, Jun. 2007.

[109] S. V. Hanly, and P. A. Whiting, "Information-theoretic capacity of multi-receiver networks," *Telecommun. Syst.*, vol. 1, pp. 1–42, 1993.

[110] Y. Lifang, and A. Goldsmith, "Symmetric Rate Capacity of Cellular Systems with Cooperative Base Stations," *in Proc. IEEE Conf. on Global Telecommuns., GLOBCOM 2006*, San Francisco, California, Nov. 27- Dec. 1, 2006.

[111] Y. Lifang, T. Yoo, and A. Goldsmith, "Coverage Spectral Efficiency of Cellular Systems with Cooperative Base Stations," *in Proc. IEEE Conf. on Global Telecommuns., GLOBCOM 2006*, San Francisco, California, Nov. 27- Dec. 1, 2006.

[112] R. Dabora, and S. Servetto, "Broadcast channels with cooperating decoders," *in IEEE Trans. on Inform. Theory*, vol. 52, no.12, pp. 5438-5454, Dec. 2006.

[113] S. C. Draper, B. J. Frey, and F. R. Kschischang, "Interactive decoding of a broadcast message," *in Proc. 41st Annual Allerton Conf. on Commun., Control, and Computing*, Monticello, Illinois, 2003.

[114] Y. Liang, and V. V. Veeravalli, "Cooperative relay broadcast channels," *in IEEE Trans. on Inform. Theory*, vol. 53, no. 3, pp. 900-928, Mar. 2007.

[115] F. M. J. Willems, *Information theoretical Results for the Discrete Memoryless Multiple Access Channel*, Ph.D. thesis, Katholieke Universiteit Leuven, 1982.

[116] I. Maric, R. D. Yates, and G. Kramer, "The discrete memoryless compound multiple access channel with conferencing encoders," *in Proc. Intl. Symp. on Inform. Theory, ISIT 2005*, pp. 407-410, Adelaide, Australia, Sept. 4-9, 2005.

[117] C. T. K. Ng, I. Maric, A. J. Goldsmith, S. Shamai (Shitz), and R. D. Yates, "Iterative and one-shot conferencing in relay channels," *in Proc. IEEE Inform. Theory Workshop, ITW 2006*, Punta del Este, Uruguay, Mar. 13-17, 2006.

[118] A. Lapidoth, S. Shamai (Shitz), and M. Wigger, "A linear interference network with local side-information," *in Proc. Intl. Sym. on Inform. Theory, ISIT 2007*, Nice, France, Jun. 24-29, 2007.

[119] D. Slepian, and J. K. Wolf, "A coding theorem for multiple access channels with correlated sources," *Bell Systems Tech. Jour.*, vol. 52, pp. 1037-1076, Sep. 1973.

[120] T. E Hunter, and A. Nosratinia, "Cooperative diversity through coding," *in Proc. Intl. Sym. on Inform. Theory, ISIT 2002*, Lausanne, Switzerland, p. 220, June 2002.

[121] J. N. Lanemane, and G.W. Wornell, "Distributed space-time coded protocols for exploiting cooperative diversity in wireless network," *in IEEE Trans. on Inform. Theory*, vol. 49, no. 10, pp. 2415-2425, Oct. 2003.

[122] A. Sendonaris, E. Erkip, and B. Aazhang, "User cooperation diversity - Part I: System description," *in IEEE Trans. on Commun*., vol. 51, no. 11, pp. 1927-1938, Nov. 2003.

[123] A. Sendonaris, E. Erkip, and B. Aazhang, "User cooperation diversity - Part II: Implementation aspects and performance analysis," *in IEEE Trans. on Commun*., vol. 51, no. 11, pp. 1939-1948, Nov. 2003.

[124] A. Stefanov, and E. Erkip, "Cooperative coding for wireless networks," *in Proc. Intl. Workshop on Mobile and Wireless Commun. Networks*, Stockholm, Sweden, pp. 273-277, Sep 2002.

[125] B. Suard, G. Xu, and T. Kailath, "Uplink channel capacity of space division multiple access schemes," *in IEEE Trans. on Inform. Theory*, vol. 44, no. 4, pp. 1468-1476, Jul. 1998.

[126] W. Yu, and J. M. Cioffi, "Trellis precoding for the broadcast channel," *in Proc. IEEE Conf. on Global Telecommuns., GLOBCOM 2001*, San Antonio, TX, vol. 2, pp. 1338-1344, Nov. 2001.

[127] E. Biglieri, R. Calderbank, and A. Constantinides et al., "*MIMO wireless communications*," Cambridge University Press, 2007.

[128] M. L. Mehta, "*Random matrices*, Revised and Enlarged," Academic Press Limited, London, second edition, 1991.

[129] F. Hiai, and D. Petz, "*The semicircle law, free random variables and entropy*," American Mathematical Society, USA, 2000.

[130] J. Hoydis, M. Kobayashi, and M. Debbah, "On the optimal number of cooperative base stations in network MIMO," *to be appear in Intl. Sym. on Inform. Theory, ISIT 2010*, Austin, Jul. 2010.

[131] O. Simeone, O. Somekh, and H. V. Poor, et al., "Local base station cooperation via finte capacity links for the uplink of linear cellular networks," *in IEEE Trans. on Inform. Theory*, vol. 55, no 1, pp. 190-204, Jan. 2009.

[132] Dingli Communications Ltd., website: http://www.rdtest.co.il/

[133] O. Somekh, O. Simeone, H.V. Poor, and S. Shamai (Shitz), "Throughput of cellular uplink with dynamic user activity and cooperative base-stations," *in Proc. IEEE Inform. Theory Workshop, ITW 2009*, Taormina, Italy, Oct. 11-16, 2009.

[134] J. P. Kermoal, L. Schumacher, P. E. Mogensen, and K. I. Pedersen, "Experimental Investigation of Correlation Properties of MIMO Radio Channels for Indoor Picocell Scenarios", *in Proc. IEEE Conf. on Vehicular Techgy., VTC2000*, pp.14-21, 2000.

[135] S. Shamai (Shitz), O. Simeone, O. Somekh, and H. V. Poor, "Joint multi-cell processing for downlink with limited-capacity backhaul," *in Proc. Inform. Theory and Applications Workshop, ITAW 2008*, San Diego, CA, Jan. 27- Feb. 1, 2008.

[136] O. Somekh, O. Simeone, Y. Bar-Ness, A. M. Haimovich, and S. Shamai (Shitz), "Cooperative multi-cell zero-forcing beamforming in cellular downlink", *in IEEE Trans. on Inform. Theory*, vol. 55, no. 7, pp. 3206-3219, Jul. 2009.

[137] A. Goldsmith, S. A. Jafar. N. Jindal, and S. Vishwanath, "Capacity limits of MIMO channels," *in IEEE Jour. on Selected Areas commun.*, vol. 21, no. 5, pp. 684-702, Jun. 2003.

[138] M. Wigger, A. Lapidoth, N. Levy, and S. Shamai (Shitz), "Receivers-Transmitters side-information duality in linear interference networks," *Inform. Theory and Application workshop*, *ITAW 2009*, Invited Talk, California, San Diego, USA, Feb. 2009.

[139] A. Sanderovich, O. Somekh, and S. Shamai, "Uplink macro diversity with limited backhaul capacity*," in Proc. IEEE Intl. Symp. on Inform. Theory, ISIT 2007*, PP. 11-15, 2007.

[140] Ofcom regulation authority, website: http://www.sitefinder.ofcom.org.uk/

[141] M. Z. Shakir, T. S. Durrani and M-Slim Alouini, "New upper bound on the optimum joint decoding capacity of Wyner Circular-GCMAC by exploiting Hadamard inequality," *IEEE ITW'10, Dublin, Sep. 2010, [to be submitted].*

[142] M. Z. Shakir, and T. S. Durrani, "Information theoretic analyses of Wyner Circular-GCMAC (C-GCMAC) with variable inter-cell interfering gain," *ISWCS'10, York*, Sep. 2010 *[to be submitted].*

[143] M. Z. Shakir, and T. S. Durrani, "Identical eigenmode transmission systems (IETS) – A channel decomposition perspective," *in Proc. 15th EUSIPCO'07*, Poznan, pp. 916-920, Sep. 2007.

[144] M. Z. Shakir, and T. S. Durrani, "On the upper bound of optimum joint decoding capacity of Wyner C-GCMAC by exploiting Hadamard inequality," *in IEEE Trans. on Inform. Theory*, *[to be submitted].*

[145] J. K. Zhang, A. Kavcic, and K. M. Wong, "Equal-diagonal QR decomposition and its application to precoder design for successive-cancellation detection," *in IEEE Trans. on Inform. Thoery*, vol. 51, pp. 154-172, Jan. 2005.

[146] S. Loyka, and F. S. Gagnon, "V-BLAST without optimal ordering: analytical performance evaluation for Rayleigh fading channels," *in IEEE Trans. on Communs.*, vol. 54, pp. 1109-1120, Jan. 2006.

[147] S. Chatzinotas, S. M. Imran, and C. Tzaras, "On the Capacity of Variable Density Cellular Systems under Multicell Decoding*," in IEEE Let., on Communs.*, vol 12, pp. 496-498, Jul. 2008.

Appendix A Proof of Waterfiling Algorithm

Though the waterfilling algorithm is well known in MIMO literarure [1] and [6], the original derivation of the algorithm is not easily available in most of the text. We derived the algorithm during the initial study of MIMO systems as follows.

Proof of (2.21):

The power allocation problem may be expressed as

$$\text{maximize } \mathrm{C} = \sum_{i=1}^{M} \log_2 \left(1 + \frac{\gamma_i \lambda_i}{\sigma_n^2}\right) \quad \text{subject to} \quad \sum_{i=1}^{M} \gamma_i = P_t$$

Introducing Lagrange multiplier λ, *the cost function becomes*

$$J = \sum_{i=1}^{M} \log_2 \left(1 + \frac{\gamma_i \lambda_i}{\sigma_z^2}\right) + \lambda \left(\sum_{i=1}^{M} \gamma_i - P\right)$$

$$\frac{\partial J}{\partial \gamma_i} = \frac{1}{\left(1 + \frac{\gamma_i \lambda_i}{\sigma_z^2}\right)} \frac{\lambda_i}{\sigma_z^2} \frac{1}{\ln(2)} + \lambda = 0$$

$$\frac{1}{\left(1 + \frac{\gamma_i \lambda_i}{\sigma_z^2}\right)} = \frac{-\lambda \ln(2)}{\frac{\lambda_i}{\sigma_z^2}}$$

$$\gamma_i = \left(\frac{1}{-\lambda \ln(2)} - \frac{\sigma_z^2}{\lambda_i}\right) = \left(\mu - \frac{\sigma_z^2}{\lambda_i}\right)$$

Since γ_i *should be positive*,

$$\gamma_i = \left(\mu - \frac{\sigma_z^2}{\lambda_i}\right)^+ \qquad \square$$

where μ is chosen to satisfy the total power constraint $\sum_{i=1}^{M} \gamma_i = P_t$

Appendix B Additional Figures of Section 2.10.1

In this Appendix, we present supplementary figures of Section 2.10.1. Figure B-1 and Figure B-2 shows capacity CDF curves when Equal power allocation and adaptive power allocation transmission schemes are employed for $\mathbf{H}\left(N,M\right)=\left(2,2\right)$ at $\gamma=0$ dB and $\gamma=-10$ dB respectively. In each of the figures the red curve shows the capacity offered by the identical eigenmode schemes. The numerical values of the capacity offered by each of the transmission schemes are summarized in Table 2-1. It can be seen from Figure B-2b that CDF curve for the first eigenmode $L=1$ crosses the vertical axis at a value less than one, which means that the worst channel corresponding to the smallest singular value of channel matrix $\mathbf{H}$ is sometimes discarded by waterfilling power allocation process. Again, the capacity obtained via GMD is more than the capacity offered by $L=1$. Hence, both eigenmodes are capable of offering identical Bits/sec/Hz. Similarly, we repeat the simulation scenarios for $\mathbf{H}\left(N,M\right)=\left(4,4\right)$ independent Rayleigh flat-fading channel. Figure B-3 and Figure B-4 shows the CDF curves for $\gamma=0$ dB and $\gamma=-10$ dB respectively. The numerical values of outage capacity are summarized in Table 2-2. It is recognized that the identical eigenmode transmission scheme is offered comparable capacity as compared to the adaptive power allocation and the equal power allocation transmission schemes.

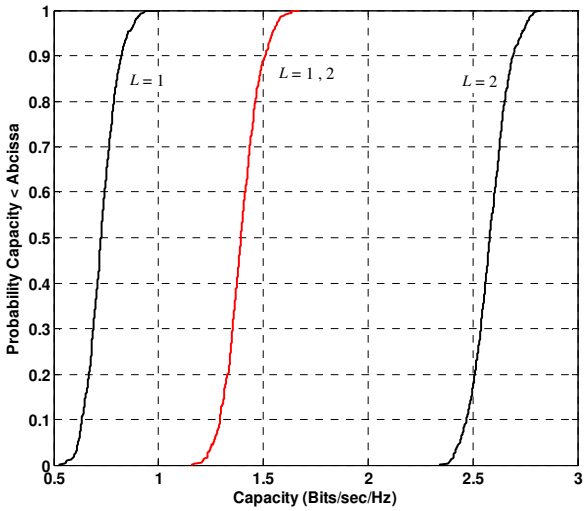

(a) EPA

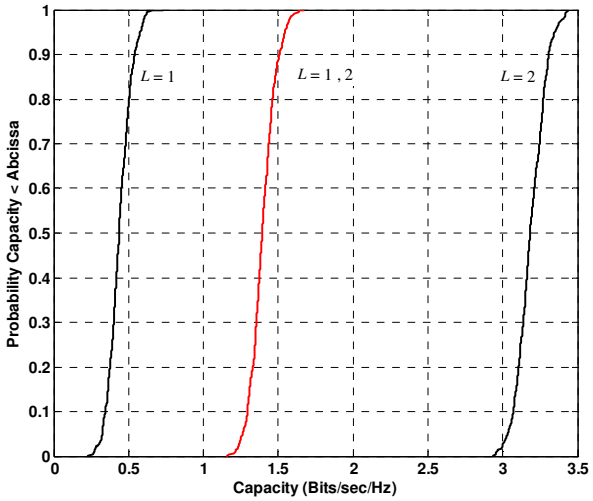

(b) APA

Figure B-1: Capacity offered by $\mathbf{H}\left(N,M\right)=\left(2,2\right)$MIMO wireless system with $\gamma = 0$ dB : (a) Equal Power Allocation (EPA) (b) Adaptive Power Allocation (APA) (employing waterfilling scheme to pour desirable power into sub-channels); red curve shows the capacity offered Identical Eigenmode (IE) using GMD.

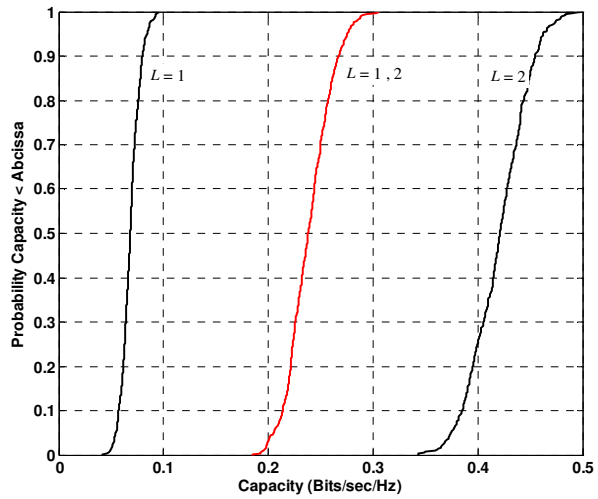

(a) EPA

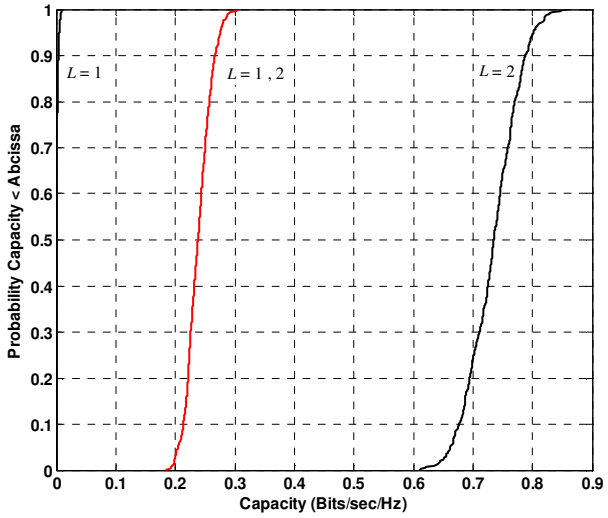

(b) APA

Figure B-2: Capacity offered by $\mathbf{H}\left(N,M\right)=\left(2,2\right)$ MIMO wireless system with $\gamma=-10$ dB: (a) Equal Power Allocation (EPA) (b) Adaptive Power Allocation (APA) (employing waterfilling scheme to pour desirable power into sub-channels); red curve shows the capacity offered Identical Eigenmode (IE) using GMD.

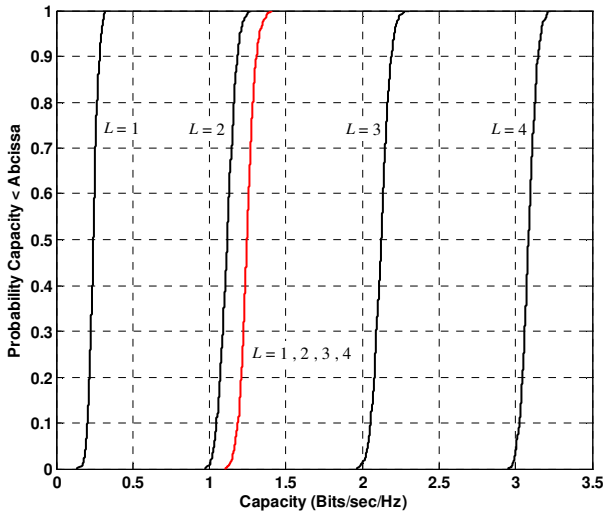

(a) EPA

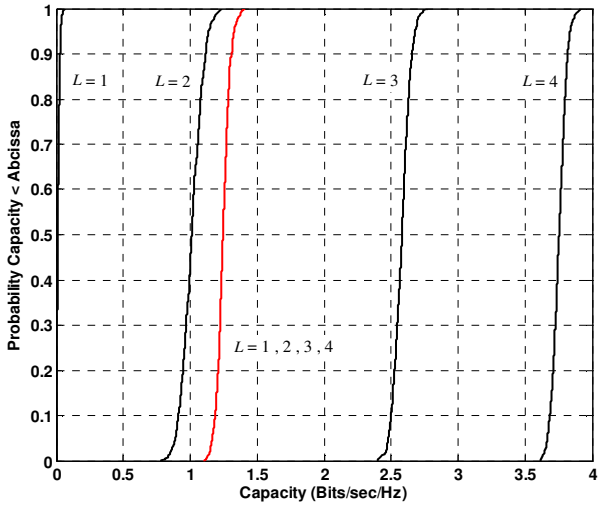

(b) APA

Figure B-3: Capacity offered by $(N,M) = (4,4)$ MIMO wireless system with $\gamma = 0$ dB : (a) Equal Power Allocation (EPA) (b) Adaptive Power Allocation (APA) (employing waterfilling scheme to pour desirable power into sub-channels); red curve shows the capacity offered Identical Eigenmode (IE) using GMD.

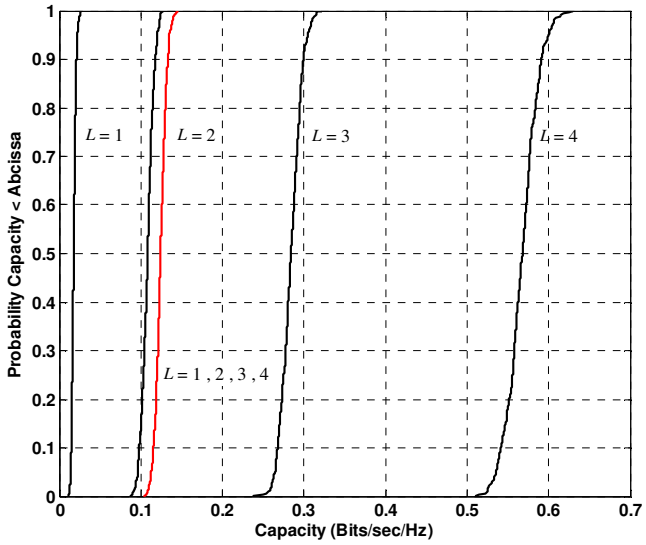

(a) EPA

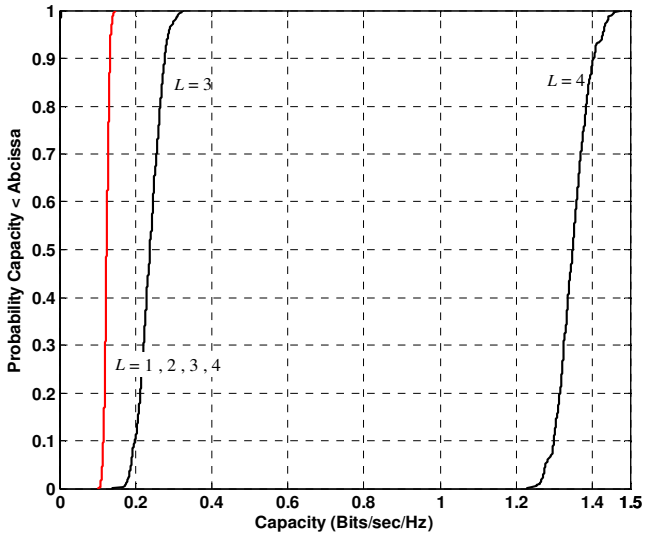

(b) APA

Figure B-4: Capacity offered by $\left(N,M\right)=\left(4,4\right)$ MIMO wireless system with $\gamma=-10$ dB: (a) Equal Power Allocation (EPA) (b) Adaptive Power Allocation (APA) (employing waterfilling scheme to pour desirable power into sub-channels); red curve shows the capacity offered Identical Eigenmode (IE) using GMD.

Appendix C Circular Setup in Other Cities of UK

In this Appendix, we include the snap shot of city centres of different cities in UK to the existence of circular cellular setup. The information about the each base stations are provided by Ofcom[1]. The images are the courtesy of Google Earth.

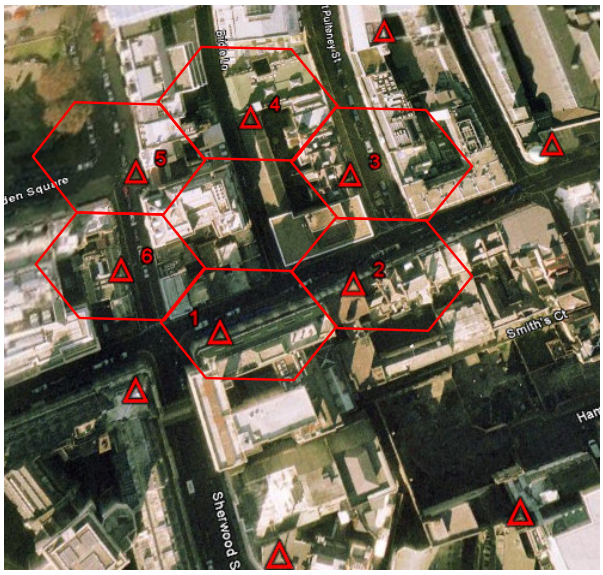

Figure C-1: Snap shot of London city centre showing circular cellular setup. Each cell at least has one base station to cover the entire region.

Table C-1: Details of BS arranged in circle in London city centre [140].

BS No.	h_b (m)	f_c (MHz)	Transmitter power (dBm)
1	4	1800	15.2
2	4	1800	10
3	5	1800	24
4	5	1800	10
5	6	1800	20.6
6	3	1800	5

[1] Ofcom is the independent regulator and competition authority for the communication industries in the United Kingdom.

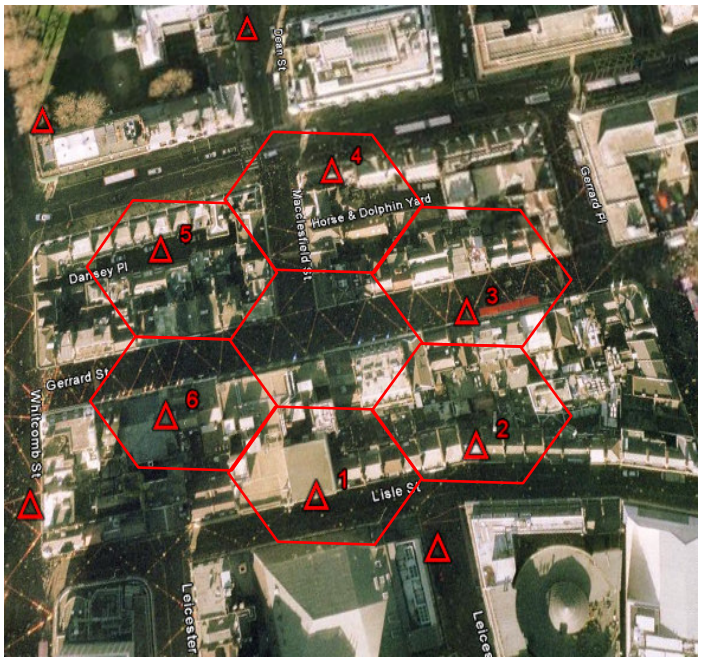

Figure C-2: Snap shot of London city near Leicester square showing circular cellular setup. Each cell at least has one base station to cover the entire region.

Table C-2: Details of BS arranged in circle in London city near Leicester square [140].

BS No.	h_b (m)	f_c (MHz)	Transmitter power (dBm)
1	6	900	39
2	8	1800	40.8
3	8	1800	35.7
4	8	1800	46.1
5	7	1800	39
6	6	900	36.8

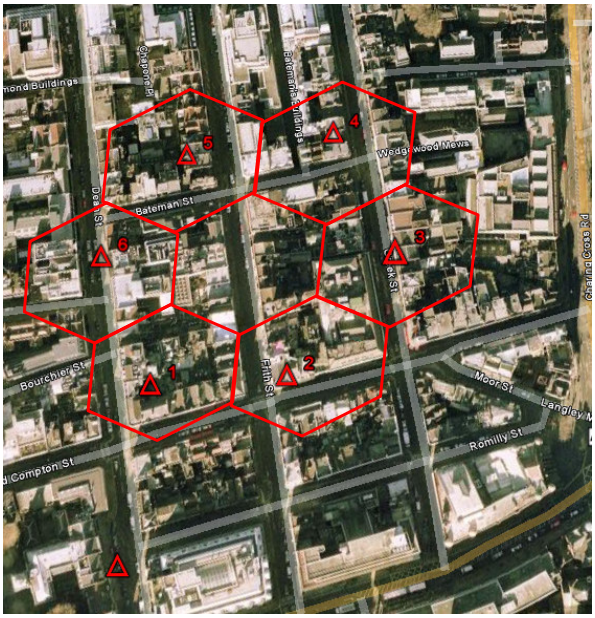

Figure C-3: Snap shot of London city near Soho square showing circular cellular setup. Each cell at least has one base station to cover the entire region.

Table C-3: Details of BS arranged in circle in London city Soho square [140].

BS No.	h_b (m)	f_c (MHz)	Transmitter power (dBm)
1	4	1800	10
2	4	1800	10
3	5	1800	15
4	4	900	7.1
5	4	1800	10
6	3	1800	10

Figure C-4: Snap shot of Edinburgh city centre showing circular cellular setup. Each cell at least has one base station to cover the entire region.

Table C-4: Details of BS arranged in circle in Edinburgh city centre [140].

BS No.	h_b (m)	f_c (MHz)	Transmitter power (dBm)
1	5	900	2
2	4	900	5.65
3	5	900	6.2
4	5	900	2.2
5	5	900	4.2
6	4	900	7.5

Appendix D Net-Monitor Tests

Following are the test which we used during the experimental trials carried out in Glasgow city centre.

Test 01 – Serving Cell Information

Test 01 displays the information about signal, selection characteristics and communication with the serving BS. It is continued in Test 03 – Neighbouring Cell Information. The graphical interpretation of the Test 01 screen is shown in Figure D-1. Following are the details of Test 01[36]:

CH: Serving cell's radio frequency channel. In idle mode, this displays the channel of the BCCH carrier. In dedicated mode, this displays the channel the MT is using for communication. This may be preceded by an 'H' to indicate frequency hopping in dedicated mode. The display will cycle through the channels being hopped. The radio frequency channel's number also indicates what band it is in.

RxL: Received signal strength of the serving cell in dBm. If the value is less than -100 dBm, the '-' sign will not be displayed.

TxPwr: This value displays the output power of the transmitter. A '*' character precedes this value if the transmitter is active (which it always is if this value is displayed). If the transmitter is not active, "xxx" is displayed.

TS: The current radio timeslot. When idle, this value displays the timeslot containing the CCCH/BCCH (always 0), otherwise, in dedicated mode a value from 0-7 indicating timeslot for communication.

TA: The timing advance value, used by the MT to indicate how early to send bursts (packets) so that they arrive in time and don't overwrite somebody else's timeslot. Units are in symbol-periods, which are 3.69 microseconds. This parameter can allow calculating approximate distance to the BS. Maximum value is 63 (35km), except for GSM400, which is 219. Since the timing advance can only be calculated after a transmission with the network, in idle mode you will need to update it by initiating a transmission, such as quickly starting a call and hanging up.

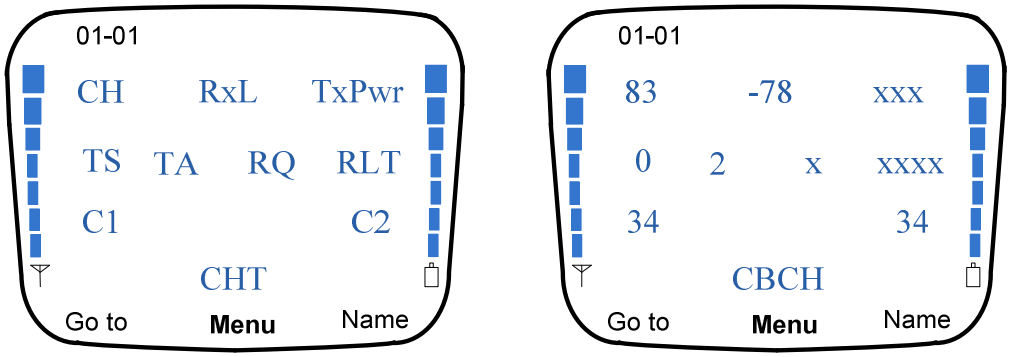

Figure D-1: Graphical interpretation of Test screen 01 - Serving cell information.

RQ: This value represents the received signal quality, when the phone is communicating with the BS, calculated from the Bit Error Rate (BER). It displays 'x' when in idle mode. The RQ value ranges from 0 to 7, where 0 shows the least errors (BER < 0.2%) and 7 shows the most errors (BER > 12.8%). The higher the value, the poorer quality signal and the more likely communication will fail. This value is only displayed in dedicated mode.

RLT: The Radio Link Timeout value. This value controls whether the connection will be abandoned. It starts at a value assigned by the network (on BCCH), and is decreased by 1 every time an SACCH message is incorrectly decoded (corrupt), and increased by 2 every time an SACCH message is correctly decoded (intact). The counter never exceeds the initial value, and if the counter reaches 0, the connection is terminated. The maximum initial value of the counter is 64, and the minimum is 4, and is a multiple of 4. SACCH message are sent/received usually about 2 times a second (half each 51-multiframe, which is about 235ms). This value is only displayed in dedicated mode.

C1: C1 value (path loss criterion). The C1 value is calculated primarily based on signal strength, but also transmitter capability. This value is used to decide whether a cell is suitable to camp on in idle mode. It is also used in the calculation of C2 values. If the C1 value falls below 0, cell reselection takes place. C1 value is between -99 and 999.

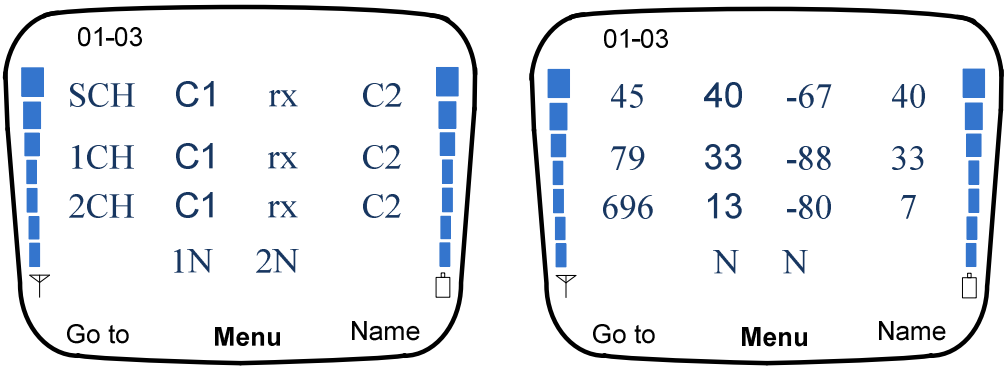

Figure D-2: Graphical interpretations of Test screen 03 showing selection characteristics of serving cell and neighbour cell #1 and cell #2.

C2: C2 value (reselection criterion). This is used to determine whether to select a new cell for camping on. If a cell's C2 value is higher than the current cell's C2 value for at least 5 seconds, the new cell is usually chosen. If C2 values are not supported or the phone is in dedicated mode, the C1 value is displayed.

CHT : The type of logical channel or sub-channel the phone is currently using.

Test 03 – Selection characteristics of Serving cell and neighbour cell #1 and cell #2

Test 03 displays summary of the serving cell, and the 1st and 2nd neighbour cells. Information about each cell is allocated at its own line in the test display screen. The format of each line is identical. The graphical interpretation of the Test 03 screen is shown in Figure D-2. Following are the details of Test 03 [36]:

SCH: The radio channel number (ARFCN) of the serving cell. See "Test 01 – Serving Cell Information".

C1: The C1 value of the serving cell in idle mode. See "Test 01 – Serving Cell Information". In dedicated mode, the BSIC value used to distinguish between multiple cells using the same channel is shown, in the form of a 2-digit value from 0-63 preceded by a 'B'.

rx: The received signal strength of the serving cell. This value is in dBm, but if the value is -100 dBm or less, in order to fit the 3 digits, the '-' sign is not shown. In dedicated mode, this value will be used to calculate the receive signal level.

C2: The C2 value of the serving cell in idle mode. See "Test 01 – Serving Cell Information". If C2 values are not supported, the C1 value is displayed. Even if C2 values are supported, the C2 on many cells will equal the C1 value. In dedicated mode (i.e. call), the information here is meaningless (in particular for neighbour cells, since the MT may not have received the cell reselection criteria to calculate the C1/C2 values).

The second and third line in Test 03 shows the summary of information about the 1st and 2nd neighbour cell respectively. The format is exactly the same as the serving cell information (explain above).

1N: '1' indicates whether the 1st neighbour cell is in a forbidden location. It displays 'F' if it is, otherwise it displays nothing. 'N' indicates the selection priority of the 1st neighbour cell. It can be 'N' (normal), 'L' (low), 'B' (barred).

2N: '2' indicates whether the 2nd neighbour cell is in a forbidden location. It displays 'F' if it is, otherwise it displays nothing. 'N' indicates the selection priority of the 2nd neighbour cell. This can be 'N' (normal), 'L' (low), 'B' (barred).

There are situations when the 1st and 2nd neighbour cell lines may not be displayed, if there are no neighbours found to be measured, or the BTS Test ("Test 12 – BTS Test") is enabled. Any line not displayed is shown as 'x's, including its corresponding priority and forbidden indicator. The first line (serving cell) will always be displayed, if there is no coverage on the home network, it will show information about another network. If there are no networks found, it will show the last stored values from when a network was found.

These Tests (03-05) are useful for observing the number of cells detected in the area. The measurement report is sent by the MT to the network in order for the network to make decisions for handover.

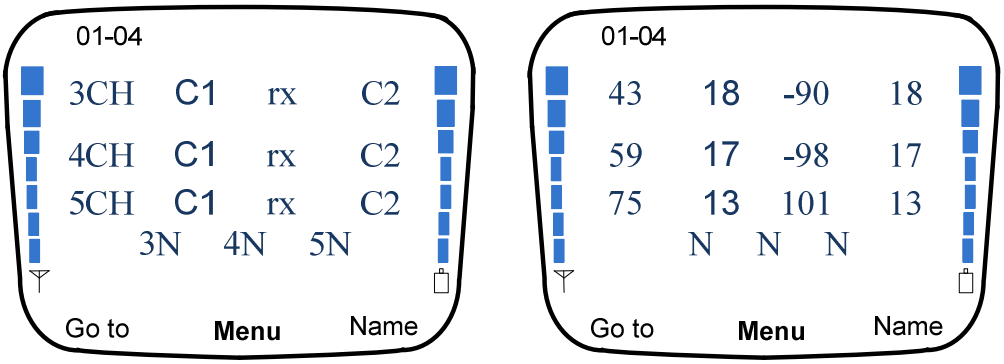

Figure D-3: Graphical interpretations of Test screen 04 showing selection characteristics of serving cell and neighbour cell #3, cell #4 and cell #5.

Test 04 – Selection characteristics of Neighbour 3, 4 and 5

Test 04 displays a selection summary of the serving cell, and the 3rd , 4th and 5th neighbour cells. Each cell has its own line. The format of each line is exactly the same as that of the serving cell (see "Test 03 – Selection characteristics of Serving Cell and Neighbour cell #1 and cell #2"). The graphical interpretation of the Test 04 screen is shown in Figure D-3.

Test 05 – Selection characteristics of Neighbour 6, 7, and 8

Test 05 displays a selection summary of the serving cell, and the 6th , 7th and 8th neighbour cells. Each cell has its own line. The format of each line is exactly the same as that of the serving cell (see "Test 03 – Selection characteristics of Serving Cell and Neighbour cell #1 and cell #2").

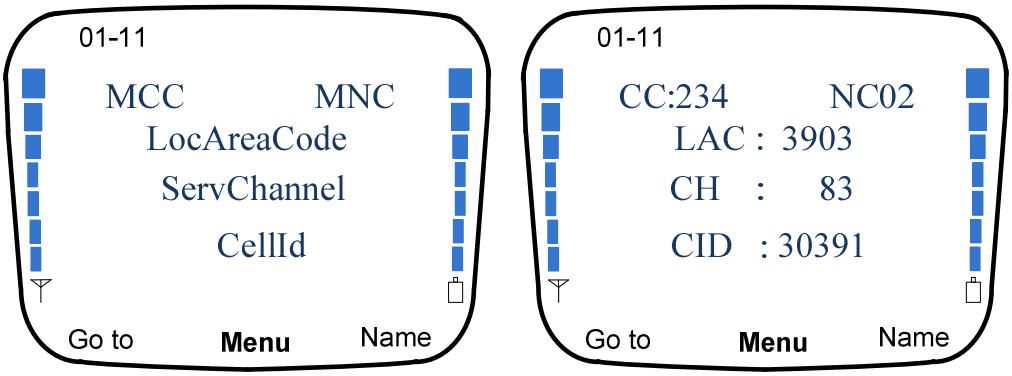

Figure D-4: Graphical interpretations of Test screen 11 showing cell and local area information.

Test 11 – Cell and Local Area Information

Test 11 displays basic information about the current cell and local area. The graphical interpretation of the Test 11 screen is shown in Figure D-4. Following are the details of Test 11 [36]:

MCC: Country Code - 3 digit country code of the current country.

MNC: Network Code - Up to 3 digit network code of the current GSM network in country. (3 digits for GSM1900, otherwise 2 digits).

LocAreaCode (LAC): Location Area Code – 16-bit code (in decimal) of the current location.

ServChannel (CH): This is 4 digit code of the current cell's RF channel (ARFCN) of BCCH. If hopping is enabled, 'H' will appear in front of the channel number.

CellID (CID): This is 16-bit code of cell, unique within local area. It is displayed in decimal. This test is useful for distinguishing the identity of the current cell. Since channels are reused many times across the GSM network, only the LAC and the Cell ID will allow you to confirm the identity of a cell. This test will also determine current LAC, it is useful to see how far a LAC extends. LACs with denser coverage and mobile usage tend to be smaller.

When the phone cannot contact the home network, it will start monitoring other GSM networks. When the phone is in Search mode (See "Test 01 – Current Cell Information"), this test will display the MCC, MNC, LAC, CH and CID of the monitored cell on the foreign GSM network. As a side note, various network

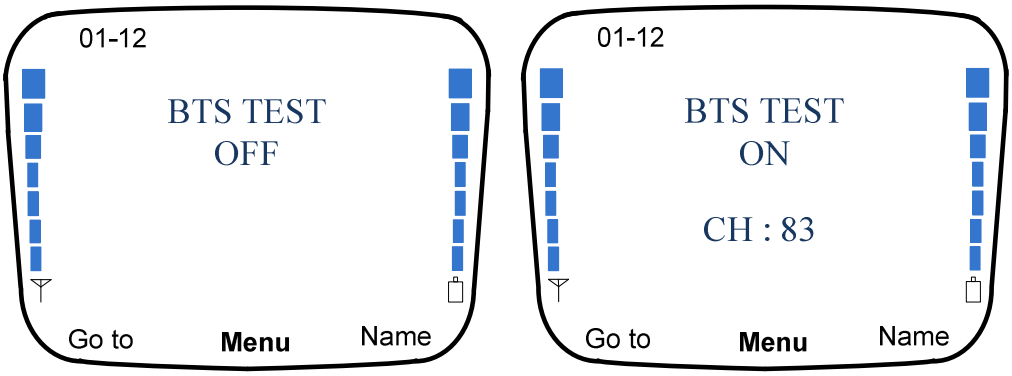

Figure D-5: Graphical interpretation of Test screen 12 showing BTS Test.

operators use conventions when defining LACs and CellIDs. For example, first digit of the CellID is used to indicate the city and the last digit to indicate the sector.

Test 12 – BTS (Base Transceiver Station)

Test 12 allows locking the phone to a BS of choice, or more specifically, a radio channel of choice. BTS Test allows the user to specify a channel for testing. The graphical interpretation of the Test 12 screen is shown in Figure D-5. Once the BTS mode is engaged, only that channel is used for idle mode and active mode (although the phone is allowed to frequency hop). The phone ignores neighbour information broadcast by the tested BS, and will not handover during call to another cell. If the phone moves out of range of the tested BS, the phone will show no coverage and will enter NSPS (No Serve Power Save) mode until it finds another BS using the specified channel for its BCCH. Obviously, the channel requested must be a BCCH carrier (the carrier on which information about the cell is broadcast, which phones listen to in idle mode).

To use the BTS Test mode, the radio channel to test must be entered in SIM memory location number 33. The name can be set to anything. However, something like “BS Test” would be appropriate. Then, jump to this test. The display will change from “BTS TEST OFF” to “BTS TEST REQUESTED”. The channel number should display the chosen channel number [36].

If the channel number displayed is “xxxx”, it means the entered channel number is an invalid channel number. It also could mean the SIM card could not be read (which seems to happen sometimes after a power on). If this is the case, jump to this test to cancel the BTS Test, wait a few minutes for SIM to respond (i.e. check the phonebook for the BTS TEST entry), and then retry the test. When the BTS test is activate, the test screen 12 shows “BTS TEST ON” and the channel number. One can see that the BTS Test is active by viewing “Test 03 – Information about Serving Cells and Neighbours”, and observing that only the serving cell entry (the top line) is present and the neighbour cells information line shows all ‘x’s.

Disable BTS Test: To disable the BTS Test, simply let the phone lose coverage, since it is locked to a channel, it probably will at some stage. When this does happen, the phone will search for other channels and return to normal operation. Alternatively, you can power the phone on and then off. When the BTS Test is off again, it will display “BS TEST OFF” and the channel number currently saved in the SIM memory. BTS Test mode is a very powerful test, and can sometimes help in a number of situations [36].

Appendix E Formation of Permutation matrix

In this Appendix, we present the two examples of the multi-user channel modelling using (3.19).

Case I: When $K = 2$ and $N = 6$, the resultant channel matrix can be expressed as

$$\boldsymbol{\Omega}_{N=6,K=2} = \begin{pmatrix} \boldsymbol{\Omega}_{N,1}^{(1)} & \boldsymbol{\Omega}_{N,1}^{(2)} \end{pmatrix} \breve{\boldsymbol{\mathcal{P}}}_{N=6,K=2} \tag{E-1}$$

The channel slow gain matrices $\boldsymbol{\Omega}_{N,1}^{(1)}$ and $\boldsymbol{\Omega}_{N,1}^{(2)}$ for user 1 and user 2 respectively can be modelled by using (3.16) and $\breve{\boldsymbol{\mathcal{P}}}_{N=6,K=2} \in \mathbb{P}^{12\times 12}$ is a permutation matrix. The permutation matrix $\breve{\boldsymbol{\mathcal{P}}}_{N=6,K=2} \in \mathbb{P}^{12\times 12}$ can be partitioned into K^2 $N \times N$ block matrices, such that we have

$$= \begin{pmatrix} \boldsymbol{\Omega}_{N,1}^{(1)} & \boldsymbol{\Omega}_{N,1}^{(2)} \end{pmatrix} \begin{pmatrix} \breve{\boldsymbol{\mathcal{P}}}_{11} & \breve{\boldsymbol{\mathcal{P}}}_{12} \\ \breve{\boldsymbol{\mathcal{P}}}_{21} & \breve{\boldsymbol{\mathcal{P}}}_{22} \end{pmatrix}$$

Where $\breve{\mathcal{P}}_{ij} \in \mathbb{P}^{6\times 6}$ and can be constructed as below

Let us first define $\breve{\boldsymbol{\mathcal{P}}}_{11}$ as

$$\breve{\boldsymbol{\mathcal{P}}}_{11} \triangleq \begin{pmatrix} 1 & 0 & 0 & 0 & 0 & 0 \\ 0 & 0 & 1 & 0 & 0 & 0 \\ 0 & 0 & 0 & 0 & 1 & 0 \\ 0 & 0 & 0 & 0 & 0 & 0 \\ 0 & 0 & 0 & 0 & 0 & 0 \\ 0 & 0 & 0 & 0 & 0 & 0 \end{pmatrix} \tag{E-1}$$

Now, $\breve{\boldsymbol{\mathcal{P}}}_{21}$ is the shifted version of block matrix $\breve{\boldsymbol{\mathcal{P}}}_{11}$ such that

$$\breve{\boldsymbol{\mathcal{P}}}_{21} \triangleq \breve{\boldsymbol{\mathcal{P}}}_{11} \boldsymbol{\mathcal{S}} \tag{E-2}$$

$$= \underbrace{\begin{pmatrix} 1 & 0 & 0 & 0 & 0 & 0 \\ 0 & 0 & 1 & 0 & 0 & 0 \\ 0 & 0 & 0 & 0 & 1 & 0 \\ 0 & 0 & 0 & 0 & 0 & 0 \\ 0 & 0 & 0 & 0 & 0 & 0 \\ 0 & 0 & 0 & 0 & 0 & 0 \end{pmatrix}}_{\breve{\mathcal{P}}_{11}} \underbrace{\begin{pmatrix} 0 & 1 & 0 & 0 & 0 & 0 \\ 1 & 0 & 0 & 0 & 0 & 0 \\ 0 & 0 & 0 & 1 & 0 & 0 \\ 0 & 0 & 1 & 0 & 0 & 0 \\ 0 & 0 & 0 & 0 & 0 & 1 \\ 0 & 0 & 0 & 0 & 1 & 0 \end{pmatrix}}_{\mathcal{S}}$$

$$\breve{\mathcal{P}}_{21} = \begin{pmatrix} 0 & 1 & 0 & 0 & 0 & 0 \\ 0 & 0 & 0 & 1 & 0 & 0 \\ 0 & 0 & 0 & 0 & 0 & 1 \\ 0 & 0 & 0 & 0 & 0 & 0 \\ 0 & 0 & 0 & 0 & 0 & 0 \\ 0 & 0 & 0 & 0 & 0 & 0 \end{pmatrix}$$

where $\mathcal{S}$ is the shift operator. The matrix $\breve{\mathcal{P}}_{12}$ is the flipped version of matrix $\breve{\mathcal{P}}_{21}$ whereas the matrix $\breve{\mathcal{P}}_{22}$ is the flipped version of the matrix $\breve{\mathcal{P}}_{11}$. The construction of these matrices is define as

$$\Upsilon_v : \breve{\mathcal{P}}_{21} \rightarrow \breve{\mathcal{P}}_t \quad \text{and} \quad \Upsilon_h : \breve{\mathcal{P}}_t \rightarrow \breve{\mathcal{P}}_{12} \tag{E-3}$$

where Υ_v and Υ_h are the vertical and horizontal flip operators respectively and $\breve{\mathcal{P}}_t$ is the transition matrix which is transformed to $\breve{\mathcal{P}}_{12}$ in the end. Eq. (E-4) can also be expressed as [2]

$$\Upsilon_h \bullet \Upsilon_v : \breve{\mathcal{P}}_{21} \rightarrow \breve{\mathcal{P}}_{12} \text{ or equivalently}$$

$$\breve{\mathcal{P}}_{12} = \left(\Upsilon_h \bullet \Upsilon_v\right)\left(\breve{\mathcal{P}}_{21}\right) = \Upsilon_h\left(\Upsilon_v\left(\breve{\mathcal{P}}_{21}\right)\right) \tag{E-4}$$

where the notation $\Upsilon_h \bullet \Upsilon_v$ is a composite function and can be read as Υ_h circle Υ_v or Υ_h following Υ_v [3].

[2] In mathematics, function composition is the application of one function to the results of another. For instance, the functions $f : X \rightarrow Y$ and $g : Y \rightarrow Z$ can be composed by computing the output of g when it has an argument of $f(x)$ instead of x.

$$\breve{\mathcal{P}}_{12} = \begin{pmatrix} 0 & 0 & 0 & 0 & 0 & 0 \\ 0 & 0 & 0 & 0 & 0 & 0 \\ 0 & 0 & 0 & 0 & 0 & 0 \\ 1 & 0 & 0 & 0 & 0 & 0 \\ 0 & 0 & 1 & 0 & 0 & 0 \\ 0 & 0 & 0 & 0 & 1 & 0 \end{pmatrix}$$

Similarly, the flipped version of matrix $\breve{\mathcal{P}}_{11}$ can be obtained by

$$\breve{\mathcal{P}}_{22} = \left(\Upsilon_h \bullet \Upsilon_v\right)\left(\breve{\mathcal{P}}_{11}\right) = \Upsilon_h\left(\Upsilon_v\left(\breve{\mathcal{P}}_{11}\right)\right) \qquad \text{(E-5)}$$

$$\breve{\mathcal{P}}_{22} = \begin{pmatrix} 0 & 0 & 0 & 0 & 0 & 0 \\ 0 & 0 & 0 & 0 & 0 & 0 \\ 0 & 0 & 0 & 0 & 0 & 0 \\ 0 & 1 & 0 & 0 & 0 & 0 \\ 0 & 0 & 0 & 1 & 0 & 0 \\ 0 & 0 & 0 & 0 & 0 & 1 \end{pmatrix}$$

Finally, the resultant permutation matrix $\breve{\mathcal{P}}_{N=6,K=2}$ constitutes of block matrices $\breve{\mathcal{P}}_{11}$, $\breve{\mathcal{P}}_{21}$, $\breve{\mathcal{P}}_{12}$ and $\breve{\mathcal{P}}_{22}$ is given by [4]

$$\breve{\mathcal{P}}_{N,K} = \begin{pmatrix} \breve{\mathcal{P}}_{11} & \left(\Upsilon_h \bullet \Upsilon_v\right)\left(\breve{\mathcal{P}}_{11}\mathcal{S}\right) \\ \breve{\mathcal{P}}_{11}\mathcal{S} & \left(\Upsilon_h \bullet \Upsilon_v\right)\left(\breve{\mathcal{P}}_{11}\right) \end{pmatrix} \qquad \text{(E-6)}$$

In matrix notation, (E-6) is shown as (3-20).

[3] The function $\left(\Upsilon_h \bullet \Upsilon_v\right)$ is developed in MATLAB using commands "fliplr" (horizontal-flip: returns a matrix with columns flipped in the left-right direction, that is, about a vertical axis) and "flipud" (vertical-flip: returns a matrix with rows flipped in the up-down direction, that is, about a horizontal axis).

[4] The composition of functions is always associative [90].

Case II: When $K = 3$ and $N = 6$, the resultant channel matrix can be expressed as

$$\boldsymbol{\Omega}_{N=6,K=3} = \begin{pmatrix} \boldsymbol{\Omega}_{N,1}^{(1)} & \boldsymbol{\Omega}_{N,1}^{(2)} & \boldsymbol{\Omega}_{N,1}^{(3)} \end{pmatrix} \breve{\boldsymbol{\mathcal{P}}}_{N=6,K=3} \tag{E-7}$$

The matrix $\breve{\boldsymbol{\mathcal{P}}}_{N=6,K=3} \in \mathbb{P}^{18\times 18}$ can be partitioned into K^2 $N \times N$ block matrices, likewise we have 9 6×6 blocks such that (E-7) becomes

$$= \begin{pmatrix} \boldsymbol{\Omega}_{N,1}^{(1)} & \boldsymbol{\Omega}_{N,1}^{(2)} & \boldsymbol{\Omega}_{N,1}^{(3)} \end{pmatrix} \begin{pmatrix} \breve{\boldsymbol{\mathcal{P}}}_{11} & \breve{\boldsymbol{\mathcal{P}}}_{12} & \breve{\boldsymbol{\mathcal{P}}}_{13} \\ \breve{\boldsymbol{\mathcal{P}}}_{21} & \breve{\boldsymbol{\mathcal{P}}}_{22} & \breve{\boldsymbol{\mathcal{P}}}_{23} \\ \breve{\boldsymbol{\mathcal{P}}}_{31} & \breve{\boldsymbol{\mathcal{P}}}_{32} & \breve{\boldsymbol{\mathcal{P}}}_{33} \end{pmatrix}$$

where $\breve{\mathcal{P}}_{ij} \in \mathbb{P}^{6\times 6}$ and can be constructed as below

Let us first define $\breve{\boldsymbol{\mathcal{P}}}_{11}$ as

$$\breve{\boldsymbol{\mathcal{P}}}_{11} \triangleq \begin{pmatrix} 1 & 0 & 0 & 0 & 0 & 0 \\ 0 & 0 & 0 & 1 & 0 & 0 \\ 0 & 0 & 0 & 0 & 0 & 0 \\ 0 & 0 & 0 & 0 & 0 & 0 \\ 0 & 0 & 0 & 0 & 0 & 0 \\ 0 & 0 & 0 & 0 & 0 & 0 \end{pmatrix} \tag{E-8}$$

Now, $\breve{\boldsymbol{\mathcal{P}}}_{21}$ is the shifted version of block matrix $\breve{\boldsymbol{\mathcal{P}}}_{11}$ such that

$$\breve{\boldsymbol{\mathcal{P}}}_{21} \triangleq \breve{\boldsymbol{\mathcal{P}}}_{11}\, \boldsymbol{\mathcal{S}}_0 \tag{E-9}$$

$$\triangleq \underbrace{\begin{pmatrix} 1 & 0 & 0 & 0 & 0 & 0 \\ 0 & 0 & 0 & 1 & 0 & 0 \\ 0 & 0 & 0 & 0 & 0 & 0 \\ 0 & 0 & 0 & 0 & 0 & 0 \\ 0 & 0 & 0 & 0 & 0 & 0 \\ 0 & 0 & 0 & 0 & 0 & 0 \end{pmatrix}}_{\breve{\boldsymbol{\mathcal{P}}}_{11}} \underbrace{\begin{pmatrix} 0 & 1 & 0 & 0 & 0 & 0 \\ 1 & 0 & 0 & 0 & 0 & 0 \\ 0 & 0 & 1 & 0 & 0 & 0 \\ 0 & 0 & 0 & 0 & 1 & 0 \\ 0 & 0 & 0 & 1 & 0 & 0 \\ 0 & 0 & 0 & 0 & 0 & 1 \end{pmatrix}}_{\boldsymbol{\mathcal{S}}_0}$$

$$\breve{\mathcal{P}}_{21} = \begin{pmatrix} 0 & 1 & 0 & 0 & 0 & 0 \\ 0 & 0 & 0 & 0 & 1 & 0 \\ 0 & 0 & 0 & 0 & 0 & 0 \\ 0 & 0 & 0 & 0 & 0 & 0 \\ 0 & 0 & 0 & 0 & 0 & 0 \\ 0 & 0 & 0 & 0 & 0 & 0 \end{pmatrix}$$

where $\mathcal{S}_0$ is the horizontal shift operator. Similarly, the matrix $\breve{\mathcal{P}}_{31}$ is given by

$$\breve{\mathcal{P}}_{31} \triangleq \breve{\mathcal{P}}_{21}\,\mathcal{S}_1 \tag{E-7}$$

$$\triangleq \underbrace{\begin{pmatrix} 0 & 1 & 0 & 0 & 0 & 0 \\ 0 & 0 & 0 & 0 & 1 & 0 \\ 0 & 0 & 0 & 0 & 0 & 0 \\ 0 & 0 & 0 & 0 & 0 & 0 \\ 0 & 0 & 0 & 0 & 0 & 0 \\ 0 & 0 & 0 & 0 & 0 & 0 \end{pmatrix}}_{\breve{\mathcal{P}}_{21}} \underbrace{\begin{pmatrix} 1 & 0 & 0 & 0 & 0 & 0 \\ 0 & 0 & 1 & 0 & 0 & 0 \\ 0 & 1 & 0 & 0 & 0 & 0 \\ 0 & 0 & 0 & 1 & 0 & 0 \\ 0 & 0 & 0 & 0 & 0 & 1 \\ 0 & 0 & 0 & 0 & 1 & 0 \end{pmatrix}}_{\mathcal{S}_1}$$

$$\breve{\mathcal{P}}_{31} = \begin{pmatrix} 0 & 0 & 1 & 0 & 0 & 0 \\ 0 & 0 & 0 & 0 & 0 & 1 \\ 0 & 0 & 0 & 0 & 0 & 0 \\ 0 & 0 & 0 & 0 & 0 & 0 \\ 0 & 0 & 0 & 0 & 0 & 0 \\ 0 & 0 & 0 & 0 & 0 & 0 \end{pmatrix}$$

where $\mathcal{S}_1$ is the horizontal shift operator.

The matrix $\breve{\mathcal{P}}_{12}$ is the vertical shift version of matrix $\breve{\mathcal{P}}_{11}$, i.e.,

$$\breve{\mathcal{P}}_{12} \triangleq \mathcal{S}_2\,\breve{\mathcal{P}}_{11} \tag{E-8}$$

$$\triangleq \underbrace{\begin{pmatrix} 0 & 0 & 1 & 0 & 0 & 0 \\ 0 & 0 & 0 & 1 & 0 & 0 \\ 1 & 0 & 0 & 0 & 0 & 0 \\ 0 & 1 & 0 & 0 & 0 & 0 \\ 0 & 0 & 0 & 0 & 1 & 0 \\ 0 & 0 & 0 & 0 & 0 & 1 \end{pmatrix}}_{\mathcal{S}_2} \underbrace{\begin{pmatrix} 1 & 0 & 0 & 0 & 0 & 0 \\ 0 & 0 & 0 & 1 & 0 & 0 \\ 0 & 0 & 0 & 0 & 0 & 0 \\ 0 & 0 & 0 & 0 & 0 & 0 \\ 0 & 0 & 0 & 0 & 0 & 0 \\ 0 & 0 & 0 & 0 & 0 & 0 \end{pmatrix}}_{\breve{\mathcal{P}}_{11}}$$

$$\breve{\mathcal{P}}_{12} = \begin{pmatrix} 0 & 0 & 0 & 0 & 0 & 0 \\ 0 & 0 & 0 & 0 & 0 & 0 \\ 1 & 0 & 0 & 0 & 0 & 0 \\ 0 & 0 & 0 & 1 & 0 & 0 \\ 0 & 0 & 0 & 0 & 0 & 0 \\ 0 & 0 & 0 & 0 & 0 & 0 \end{pmatrix}$$

Similarly, the matrix $\breve{\mathcal{P}}_{22}$ and $\breve{\mathcal{P}}_{32}$ are vertical shift version of matrices $\breve{\mathcal{P}}_{21}$ and $\breve{\mathcal{P}}_{31}$ respectively and can be defined as follow

$$\breve{\mathcal{P}}_{22} \triangleq \mathcal{S}_2 \breve{\mathcal{P}}_{21} \tag{E-9}$$

$$\triangleq \underbrace{\begin{pmatrix} 0 & 0 & 1 & 0 & 0 & 0 \\ 0 & 0 & 0 & 1 & 0 & 0 \\ 1 & 0 & 0 & 0 & 0 & 0 \\ 0 & 1 & 0 & 0 & 0 & 0 \\ 0 & 0 & 0 & 0 & 1 & 0 \\ 0 & 0 & 0 & 0 & 0 & 1 \end{pmatrix}}_{\mathcal{S}_2} \underbrace{\begin{pmatrix} 0 & 1 & 0 & 0 & 0 & 0 \\ 0 & 0 & 0 & 0 & 1 & 0 \\ 0 & 0 & 0 & 0 & 0 & 0 \\ 0 & 0 & 0 & 0 & 0 & 0 \\ 0 & 0 & 0 & 0 & 0 & 0 \\ 0 & 0 & 0 & 0 & 0 & 0 \end{pmatrix}}_{\breve{\mathcal{P}}_{21}}$$

$$\breve{\mathcal{P}}_{22} = \begin{pmatrix} 0 & 0 & 0 & 0 & 0 & 0 \\ 0 & 0 & 0 & 0 & 0 & 0 \\ 0 & 1 & 0 & 0 & 0 & 0 \\ 0 & 0 & 0 & 0 & 1 & 0 \\ 0 & 0 & 0 & 0 & 0 & 0 \\ 0 & 0 & 0 & 0 & 0 & 0 \end{pmatrix}$$

$$\breve{\mathcal{P}}_{32} \triangleq \mathcal{S}_2 \breve{\mathcal{P}}_{31} \tag{E-10}$$

$$\triangleq \underbrace{\begin{pmatrix} 0 & 0 & 1 & 0 & 0 & 0 \\ 0 & 0 & 0 & 1 & 0 & 0 \\ 1 & 0 & 0 & 0 & 0 & 0 \\ 0 & 1 & 0 & 0 & 0 & 0 \\ 0 & 0 & 0 & 0 & 1 & 0 \\ 0 & 0 & 0 & 0 & 0 & 1 \end{pmatrix}}_{\mathcal{S}_2} \underbrace{\begin{pmatrix} 0 & 0 & 1 & 0 & 0 & 0 \\ 0 & 0 & 0 & 0 & 0 & 1 \\ 0 & 0 & 0 & 0 & 0 & 0 \\ 0 & 0 & 0 & 0 & 0 & 0 \\ 0 & 0 & 0 & 0 & 0 & 0 \\ 0 & 0 & 0 & 0 & 0 & 0 \end{pmatrix}}_{\breve{\mathcal{P}}_{31}}$$

$$\breve{\mathcal{P}}_{32} = \begin{pmatrix} 0 & 0 & 0 & 0 & 0 & 0 \\ 0 & 0 & 0 & 0 & 0 & 0 \\ 0 & 0 & 1 & 0 & 0 & 0 \\ 0 & 0 & 0 & 0 & 0 & 1 \\ 0 & 0 & 0 & 0 & 0 & 0 \\ 0 & 0 & 0 & 0 & 0 & 0 \end{pmatrix}$$

The block matrices $\breve{\mathcal{P}}_{13}$, $\breve{\mathcal{P}}_{23}$ and $\breve{\mathcal{P}}_{33}$ are the flipped version of matrices $\breve{\mathcal{P}}_{31}$, $\breve{\mathcal{P}}_{21}$ and $\breve{\mathcal{P}}_{11}$ respectively. The construction of these matrices is define as

$$\breve{\mathcal{P}}_{13} = \left(\Upsilon_h \bullet \Upsilon_v\right)\left(\breve{\mathcal{P}}_{31}\right) = \Upsilon_h\left(\Upsilon_v\left(\breve{\mathcal{P}}_{31}\right)\right) \tag{E-11}$$

where the function $\left(\Upsilon_h \bullet \Upsilon_v\right)$ is defined to perform horizontal flip following vertical flip on the matrix $\breve{\mathcal{P}}_{31}$.

$$\breve{\mathcal{P}}_{31} = \begin{pmatrix} 0 & 0 & 0 & 0 & 0 & 0 \\ 0 & 0 & 0 & 0 & 0 & 0 \\ 0 & 0 & 0 & 0 & 0 & 0 \\ 0 & 0 & 0 & 0 & 0 & 0 \\ 1 & 0 & 0 & 0 & 0 & 0 \\ 0 & 0 & 0 & 1 & 0 & 0 \end{pmatrix}$$

Similarly, the flipped version of matrix $\breve{\mathcal{P}}_{21}$ and $\breve{\mathcal{P}}_{11}$ can be obtained respectively as shown below

$$\breve{\boldsymbol{\mathcal{P}}}_{23} = \left(\Upsilon_h \bullet \Upsilon_v\right)\left(\breve{\boldsymbol{\mathcal{P}}}_{21}\right) = \Upsilon_h\left(\Upsilon_v\left(\breve{\boldsymbol{\mathcal{P}}}_{21}\right)\right) \tag{E-12}$$

$$\breve{\boldsymbol{\mathcal{P}}}_{23} = \begin{pmatrix} 0 & 0 & 0 & 0 & 0 & 0 \\ 0 & 0 & 0 & 0 & 0 & 0 \\ 0 & 0 & 0 & 0 & 0 & 0 \\ 0 & 0 & 0 & 0 & 0 & 0 \\ 0 & 1 & 0 & 0 & 0 & 0 \\ 0 & 0 & 0 & 0 & 1 & 0 \end{pmatrix}$$

$$\breve{\boldsymbol{\mathcal{P}}}_{33} = \left(\Upsilon_h \bullet \Upsilon_v\right)\left(\breve{\boldsymbol{\mathcal{P}}}_{11}\right) = \Upsilon_h\left(\Upsilon_v\left(\breve{\boldsymbol{\mathcal{P}}}_{11}\right)\right) \tag{E-13}$$

$$\breve{\boldsymbol{\mathcal{P}}}_{33} = \begin{pmatrix} 0 & 0 & 0 & 0 & 0 & 0 \\ 0 & 0 & 0 & 0 & 0 & 0 \\ 0 & 0 & 0 & 0 & 0 & 0 \\ 0 & 0 & 0 & 0 & 0 & 0 \\ 0 & 0 & 1 & 0 & 0 & 0 \\ 0 & 0 & 0 & 0 & 0 & 1 \end{pmatrix}$$

Finally, the resultant permutation matrix $\breve{\boldsymbol{\mathcal{P}}}_{N,K}$ constitutes of 9 6×6 block matrices can be expressed as

$$\breve{\boldsymbol{\mathcal{P}}}_{N=6,K=3} = \begin{pmatrix} \breve{\mathcal{P}}_{11} & \boldsymbol{\mathcal{S}}_2\breve{\mathcal{P}}_{11} & \left(\Upsilon_h \bullet \Upsilon_v\right)\left(\breve{\mathcal{P}}_{11}\boldsymbol{\mathcal{S}}_1\right) \\ \breve{\mathcal{P}}_{11}\boldsymbol{\mathcal{S}}_0 & \boldsymbol{\mathcal{S}}_2\breve{\mathcal{P}}_{11}\boldsymbol{\mathcal{S}}_0 & \left(\Upsilon_h \bullet \Upsilon_v\right)\left(\breve{\mathcal{P}}_{11}\boldsymbol{\mathcal{S}}_0\right) \\ \breve{\mathcal{P}}_{11}\boldsymbol{\mathcal{S}}_1 & \boldsymbol{\mathcal{S}}_2\breve{\mathcal{P}}_{11}\boldsymbol{\mathcal{S}}_1 & \left(\Upsilon_h \bullet \Upsilon_v\right)\left(\breve{\mathcal{P}}_{11}\right) \end{pmatrix} \tag{E-14}$$

In matrix notation (E-14) is shown as (3-22).

Appendix F Permutation Matrices $\mathcal{P}$ and $\mathcal{Q}$

In this Appendix, we present the permutation matrices $\mathcal{P} \in \mathbb{P}^{36\times 6}$ and $\mathcal{Q} \in \mathbb{P}^{36\times 30}$ for Wyner C-CMAC, when $N = M = 6$ i.e. single user case $(K = 1)$. However, with the increase in number of users, the size of permutation matrices renders it impossible to include them in this Appendix.

$$\mathcal{P} = \underbrace{\begin{pmatrix}
1 & 0 & 0 & 0 & 0 & 0 \\
0 & 0 & 0 & 0 & 0 & 0 \\
0 & 0 & 0 & 0 & 0 & 0 \\
0 & 0 & 0 & 0 & 0 & 0 \\
0 & 0 & 0 & 0 & 0 & 0 \\
0 & 0 & 0 & 0 & 0 & 0 \\
0 & 0 & 0 & 0 & 0 & 0 \\
0 & 1 & 0 & 0 & 0 & 0 \\
0 & 0 & 0 & 0 & 0 & 0 \\
0 & 0 & 0 & 0 & 0 & 0 \\
0 & 0 & 0 & 0 & 0 & 0 \\
0 & 0 & 0 & 0 & 0 & 0 \\
0 & 0 & 0 & 0 & 0 & 0 \\
0 & 0 & 0 & 0 & 0 & 0 \\
0 & 0 & 1 & 0 & 0 & 0 \\
0 & 0 & 0 & 0 & 0 & 0 \\
0 & 0 & 0 & 0 & 0 & 0 \\
0 & 0 & 0 & 0 & 0 & 0 \\
0 & 0 & 0 & 0 & 0 & 0 \\
0 & 0 & 0 & 0 & 0 & 0 \\
0 & 0 & 0 & 0 & 0 & 0 \\
0 & 0 & 0 & 1 & 0 & 0 \\
0 & 0 & 0 & 0 & 0 & 0 \\
0 & 0 & 0 & 0 & 0 & 0 \\
0 & 0 & 0 & 0 & 0 & 0 \\
0 & 0 & 0 & 0 & 0 & 0 \\
0 & 0 & 0 & 0 & 0 & 0 \\
0 & 0 & 0 & 0 & 0 & 0 \\
0 & 0 & 0 & 0 & 1 & 0 \\
0 & 0 & 0 & 0 & 0 & 0 \\
0 & 0 & 0 & 0 & 0 & 0 \\
0 & 0 & 0 & 0 & 0 & 0 \\
0 & 0 & 0 & 0 & 0 & 0 \\
0 & 0 & 0 & 0 & 0 & 0 \\
0 & 0 & 0 & 0 & 0 & 0 \\
0 & 0 & 0 & 0 & 0 & 1
\end{pmatrix}}_{n^2\times n}$$

$$
\mathcal{Q} = \underbrace{\begin{pmatrix}
0&0&0&0&0&0&0&0&0&0&0&0&0&0&0&0&0&0&0&0&0&0&0&0&0&0&0&0&0&0&0&0&0&0&0&0\\
0&1&0&0&0&0&0&0&0&0&0&0&0&0&0&0&0&0&0&0&0&0&0&0&0&0&0&0&0&0&0&0&0&0&0&0\\
0&0&1&0&0&0&0&0&0&0&0&0&0&0&0&0&0&0&0&0&0&0&0&0&0&0&0&0&0&0&0&0&0&0&0&0\\
0&0&0&1&0&0&0&0&0&0&0&0&0&0&0&0&0&0&0&0&0&0&0&0&0&0&0&0&0&0&0&0&0&0&0&0\\
0&0&0&0&1&0&0&0&0&0&0&0&0&0&0&0&0&0&0&0&0&0&0&0&0&0&0&0&0&0&0&0&0&0&0&0\\
0&0&0&0&0&1&0&0&0&0&0&0&0&0&0&0&0&0&0&0&0&0&0&0&0&0&0&0&0&0&0&0&0&0&0&0\\
0&0&0&0&0&0&1&0&0&0&0&0&0&0&0&0&0&0&0&0&0&0&0&0&0&0&0&0&0&0&0&0&0&0&0&0\\
0&0&0&0&0&0&0&0&0&0&0&0&0&0&0&0&0&0&0&0&0&0&0&0&0&0&0&0&0&0&0&0&0&0&0&0\\
0&0&0&0&0&0&0&0&1&0&0&0&0&0&0&0&0&0&0&0&0&0&0&0&0&0&0&0&0&0&0&0&0&0&0&0\\
0&0&0&0&0&0&0&0&0&1&0&0&0&0&0&0&0&0&0&0&0&0&0&0&0&0&0&0&0&0&0&0&0&0&0&0\\
0&0&0&0&0&0&0&0&0&0&1&0&0&0&0&0&0&0&0&0&0&0&0&0&0&0&0&0&0&0&0&0&0&0&0&0\\
0&0&0&0&0&0&0&0&0&0&0&1&0&0&0&0&0&0&0&0&0&0&0&0&0&0&0&0&0&0&0&0&0&0&0&0\\
0&0&0&0&0&0&0&0&0&0&0&0&1&0&0&0&0&0&0&0&0&0&0&0&0&0&0&0&0&0&0&0&0&0&0&0\\
0&0&0&0&0&0&0&0&0&0&0&0&0&1&0&0&0&0&0&0&0&0&0&0&0&0&0&0&0&0&0&0&0&0&0&0\\
0&0&0&0&0&0&0&0&0&0&0&0&0&0&0&0&0&0&0&0&0&0&0&0&0&0&0&0&0&0&0&0&0&0&0&0\\
0&0&0&0&0&0&0&0&0&0&0&0&0&0&0&1&0&0&0&0&0&0&0&0&0&0&0&0&0&0&0&0&0&0&0&0\\
0&0&0&0&0&0&0&0&0&0&0&0&0&0&0&0&1&0&0&0&0&0&0&0&0&0&0&0&0&0&0&0&0&0&0&0\\
0&0&0&0&0&0&0&0&0&0&0&0&0&0&0&0&0&1&0&0&0&0&0&0&0&0&0&0&0&0&0&0&0&0&0&0\\
0&0&0&0&0&0&0&0&0&0&0&0&0&0&0&0&0&0&1&0&0&0&0&0&0&0&0&0&0&0&0&0&0&0&0&0\\
0&0&0&0&0&0&0&0&0&0&0&0&0&0&0&0&0&0&0&1&0&0&0&0&0&0&0&0&0&0&0&0&0&0&0&0\\
0&0&0&0&0&0&0&0&0&0&0&0&0&0&0&0&0&0&0&0&1&0&0&0&0&0&0&0&0&0&0&0&0&0&0&0\\
0&0&0&0&0&0&0&0&0&0&0&0&0&0&0&0&0&0&0&0&0&0&0&0&0&0&0&0&0&0&0&0&0&0&0&0\\
0&0&0&0&0&0&0&0&0&0&0&0&0&0&0&0&0&0&0&0&0&0&1&0&0&0&0&0&0&0&0&0&0&0&0&0\\
0&0&0&0&0&0&0&0&0&0&0&0&0&0&0&0&0&0&0&0&0&0&0&1&0&0&0&0&0&0&0&0&0&0&0&0\\
0&0&0&0&0&0&0&0&0&0&0&0&0&0&0&0&0&0&0&0&0&0&0&0&1&0&0&0&0&0&0&0&0&0&0&0\\
0&0&0&0&0&0&0&0&0&0&0&0&0&0&0&0&0&0&0&0&0&0&0&0&0&1&0&0&0&0&0&0&0&0&0&0\\
0&0&0&0&0&0&0&0&0&0&0&0&0&0&0&0&0&0&0&0&0&0&0&0&0&0&1&0&0&0&0&0&0&0&0&0\\
0&0&0&0&0&0&0&0&0&0&0&0&0&0&0&0&0&0&0&0&0&0&0&0&0&0&0&1&0&0&0&0&0&0&0&0\\
0&0&0&0&0&0&0&0&0&0&0&0&0&0&0&0&0&0&0&0&0&0&0&0&0&0&0&0&0&0&0&0&0&0&0&0\\
0&0&0&0&0&0&0&0&0&0&0&0&0&0&0&0&0&0&0&0&0&0&0&0&0&0&0&0&0&1&0&0&0&0&0&0\\
0&0&0&0&0&0&0&0&0&0&0&0&0&0&0&0&0&0&0&0&0&0&0&0&0&0&0&0&0&0&1&0&0&0&0&0\\
0&0&0&0&0&0&0&0&0&0&0&0&0&0&0&0&0&0&0&0&0&0&0&0&0&0&0&0&0&0&0&1&0&0&0&0\\
0&0&0&0&0&0&0&0&0&0&0&0&0&0&0&0&0&0&0&0&0&0&0&0&0&0&0&0&0&0&0&0&1&0&0&0\\
0&0&0&0&0&0&0&0&0&0&0&0&0&0&0&0&0&0&0&0&0&0&0&0&0&0&0&0&0&0&0&0&0&1&0&0\\
0&0&0&0&0&0&0&0&0&0&0&0&0&0&0&0&0&0&0&0&0&0&0&0&0&0&0&0&0&0&0&0&0&0&1&0\\
0&0&0&0&0&0&0&0&0&0&0&0&0&0&0&0&0&0&0&0&0&0&0&0&0&0&0&0&0&0&0&0&0&0&0&0
\end{pmatrix}}_{n^2\times\left(n^2-n\right)}
$$

Appendix G Proof of Theorem 5.3.2

Proof of Theorem 5.3.2:

Let us define $\mathbf{A} = u\,v^H$ *where* u, *and* v *are non-zero complex* $N \times 1$ *and* $M \times 1$ *column vectors respectively such that* $r_A = 1$.

$$u = \begin{pmatrix} u_1 \\ u_2 \\ \vdots \\ u_N \end{pmatrix} \text{ and } v = \begin{pmatrix} v_1 \\ v_2 \\ \vdots \\ v_M \end{pmatrix}$$

The Hadamard product of $\mathbf{A} \circ \mathbf{B}$ *in terms of vectors* u, *and* v *may be expressed as*

$$\left(\mathbf{A} \circ \mathbf{B}\right) = \underbrace{\left(\begin{pmatrix} u_1 \\ u_2 \\ \vdots \\ u_N \end{pmatrix}\begin{pmatrix} v_1 & v_2 & \cdots & v_M \end{pmatrix}\right)}_{\mathbf{A}} \circ \underbrace{\begin{pmatrix} B_{1,1} & B_{1,2} & \cdots & B_{1,M} \\ B_{1,2} & B_{2,2} & \ddots & B_{1,1} \\ \vdots & \ddots & \ddots & \vdots \\ B_{1,N} & B_{1,1} & \cdots & B_{N,M} \end{pmatrix}}_{\mathbf{B}}$$

Let Λ_u *and* Λ_v *are the non-singular diagonal matrices whose diagonal entries are the respective entries of the vector* u *and* v *respectively. In component wise notation, we may have*

$$\Lambda_u = \begin{pmatrix} u_1 & 0 & \cdots & 0 \\ 0 & u_2 & \ddots & \vdots \\ \vdots & \ddots & \ddots & 0 \\ 0 & \cdots & 0 & u_N \end{pmatrix} \text{ and ;}$$

$$\Lambda_v = \begin{pmatrix} v_1 & 0 & \cdots & 0 \\ 0 & v_2 & \ddots & \vdots \\ \vdots & \ddots & \ddots & 0 \\ 0 & \cdots & 0 & v_M \end{pmatrix}$$

The Hadamard product $\mathbf{A} \circ \mathbf{B}$ *can also be expressed as*

$$\left(\mathbf{A} \circ \mathbf{B}\right) = \underbrace{\begin{pmatrix} u_1 & 0 & \cdots & 0 \\ 0 & u_2 & \ddots & \vdots \\ \vdots & \ddots & \ddots & 0 \\ 0 & \cdots & 0 & u_N \end{pmatrix}}_{N \times N} \underbrace{\begin{pmatrix} B_{1,1} & B_{1,2} & \cdots & B_{1,M} \\ B_{1,2} & B_{2,2} & \ddots & B_{1,1} \\ \vdots & \ddots & \ddots & \vdots \\ B_{1,N} & B_{1,1} & \cdots & B_{N,M} \end{pmatrix}}_{N \times M} \underbrace{\begin{pmatrix} v_1 & 0 & \cdots & 0 \\ 0 & v_2 & \ddots & \vdots \\ \vdots & \ddots & \ddots & 0 \\ 0 & \cdots & 0 & v_M \end{pmatrix}}_{M \times M}$$

$$= \Lambda_u \, \mathbf{B} \, \Lambda_v$$

which has same rank as rank of $\mathbf{B}$. *Hence, this proves that*

$$\text{Rank}\left(\mathbf{A} \circ \mathbf{B}\right) = \text{Rank}\left(\mathbf{B}\right)$$

Summary of Rank of Hadamard Operator

- If $\mathbf{A}$ and $\mathbf{B}$ are complex $N \times M$ matrices with arbitrary ranks r_A and r_B respectively. Then the rank of $\left(\mathbf{A} \circ \mathbf{B}\right)$ denoted by $r_{A \circ B}$, can be expressed as $r_{A \circ B} \geq \max\left\{r_A, r_B\right\}$

- If $\mathbf{A}$ is full rank matrix such that $r_A \geq r_B$, then $r_{A \circ B} = r_A$. Or if $\mathbf{B}$ is full rank matrix such that $r_B \geq r_A$, then $r_{A \circ B} = r_B$.

- If $\mathbf{A}$ is a $N \times M$ positive definite matrix (with positive diagonal entries) then $r_{A \circ B} \geq r_B$.

- If $r_A = 1$, then $r_{A \circ B} = r_B$.

Appendix H Matrix Notations

Matrix analysis techniques are employed extensively throughout this thesis. For consistency the same matrix notation is employed in each chapter and described as follows.

Throughout this thesis $\mathbb{R}^{N\times 1}$ and $\mathbb{C}^{N\times 1}$ denote N dimensional real and complex vector spaces respectively. Moreover, $\mathbb{P}^{N\times M}$ denotes a $N\times M$ permutation matrix which has 1 at its particular position and zero elsewhere. In complex vector spaces, $\mathrm{i}\triangleq\sqrt{-1}$ denotes the imaginary unit. The real and imaginary parts of a complex scalar $z=x+\mathrm{i}\,y$ are denoted by $\Re\left(z\right)=x$ and $\Im\left(z\right)=y$ respectively. The conjugate of a complex scalar $z=x+\mathrm{i}\,y$ is denoted by $z^{*}=x-\mathrm{i}\,y$.

Matrices are represented by uppercase boldface letters, as an example, the $N\times M$ matrix $\mathbf{A}$ with N rows and M columns are represented as $\mathbf{A}^{N\times M}$. The sub-matrix with only k columns extracted from original matrix $\mathbf{A}$ is presented by $\mathbf{A}_k$. Vectors are represented by lowercase boldface and italic version of the original matrix, as an example, a $N\times 1$ column vector $\boldsymbol{a}$ is represented as $\boldsymbol{a}^{N\times 1}$. Also, the k^{th} column vector of original matrix is represented as $\boldsymbol{a}_k$. An element of matrix or a vector is represented by the non-boldface letter representing the respective vector structure with subscripted row and column indices, as an example, $a_{n,m}$ refers to the element referenced by row n at column m of matrix $\mathbf{A}^{N\times M}$. Similarly, a_k refers to element k of the vector $\boldsymbol{a}^{N\times 1}$. Scalar variables are always represented by non-boldface characters. If the individual elements of a matrix depend on parameters $\theta_1,\cdots,\theta_N$, the dependent parameters are listed in square brackets, e.g. $\mathbf{A}\left[\boldsymbol{\theta}\right]=\mathbf{A}\left[\theta_1,\cdots,\theta_N\right]$.

The following special matrix constructs are defined as follows: $\mathbf{I}_N$ denotes the $N \times N$ identity matrix; $1_K = \left(1 \cdots\cdots 1\right)$ denotes the $1 \times K$ row vector with all entries equal to one; the function $\mathrm{diag}\left(\cdot\right)$ converts N-dimensional vector to an $N \times N$ diagonal matrix, e.g. $\mathbf{D} = \mathrm{diag}\left(\boldsymbol{d}\right)$ is a diagonal matrix with diagonal elements $\mathrm{D}_{k,k} = d_k$; the function $\mathrm{circ}\left(\cdot\right)$ converts an N-dimensional vector to an $N \times N$ circulant matrix, $\mathbf{C} = \mathrm{circ}\left(\boldsymbol{c}\right)$ is a circulant matrix whose first row is equal to the vector $\boldsymbol{c}$.